Terms and Conditions of Use of Digitised Theses from Trinity College Library Dublin

Copyright statement

All material supplied by Trinity College Library is protected by copyright (under the Copyright and Related Rights Act, 2000 as amended) and other relevant Intellectual Property Rights. By accessing and using a Digitised Thesis from Trinity College Library you acknowledge that all Intellectual Property Rights in any Works supplied are the sole and exclusive property of the copyright and/or other IPR holder. Specific copyright holders may not be explicitly identified. Use of materials from other sources within a thesis should not be construed as a claim over them.

A non-exclusive, non-transferable licence is hereby granted to those using or reproducing, in whole or in part, the material for valid purposes, providing the copyright owners are acknowledged using the normal conventions. Where specific permission to use material is required, this is identified and such permission must be sought from the copyright holder or agency cited.

Liability statement

By using a Digitised Thesis, I accept that Trinity College Dublin bears no legal responsibility for the accuracy, legality or comprehensiveness of materials contained within the thesis, and that Trinity College Dublin accepts no liability for indirect, consequential, or incidental, damages or losses arising from use of the thesis for whatever reason. Information located in a thesis may be subject to specific use constraints, details of which may not be explicitly described. It is the responsibility of potential and actual users to be aware of such constraints and to abide by them. By making use of material from a digitised thesis, you accept these copyright and disclaimer provisions. Where it is brought to the attention of Trinity College Library that there may be a breach of copyright or other restraint, it is the policy to withdraw or take down access to a thesis while the issue is being resolved.

Access Agreement

By using a Digitised Thesis from Trinity College Library you are bound by the following Terms & Conditions. Please read them carefully.

I have read and I understand the following statement: All material supplied via a Digitised Thesis from Trinity College Library is protected by copyright and other intellectual property rights, and duplication or sale of all or part of any of a thesis is not permitted, except that material may be duplicated by you for your research use or for educational purposes in electronic or print form providing the copyright owners are acknowledged using the normal conventions. You must obtain permission for any other use. Electronic or print copies may not be offered, whether for sale or otherwise to anyone. This copy has been supplied on the understanding that it is copyright material and that no quotation from the thesis may be published without proper acknowledgement.

DEVELOPMENT OF ACCURATE METHODS OF WEIGHING TRUCKS IN MOTION

Two Volumes

II

by

Arturo González

Thesis submitted to the University of Dublin, Trinity College,
for the Degree of Doctor of Philosophy

2001

CONTENTS

VOLUME II

7

THE DEVELOPMENT OF A DYNAMIC ALGORITHM

7.1 INTRODUCTION

The traditional B-WIM approaches have limitations when the dynamic behaviour of the bridge-truck structural system does not follow a periodical oscillating pattern around the static response. These dynamic sources of inaccuracy are related to the excitation of the dynamic wheel forces by the bridge joint or a bump in the approach (Lutzenberger & Baumgärtner 1999). Inaccuracy can be high when measurement duration covers only a small number of natural periods of vibration (Peters 1984), or bridges have low first natural frequencies, or where significant dynamic amplification occurs. Low-pass filtering of the signal can be used to remove the effects of bridge vibration, but a significant part of the static response can be removed inadvertently (i.e., in the case of bridges with low natural frequencies, closely spaced axles and/or high vehicle speeds as seen in Section 3.5.1). This chapter describes the theoretical background of new B-WIM algorithms which allows for dynamics. The formulation of these algorithms is based on mathematical models described in Chapters 3 and 5. Their accuracy will be further tested in Chapters 8 and 9.

An algorithm based on spectral analysis of the strain signal has been developed by the author (González & O'Brien 1998) to reduce errors introduced through comparison of theoretical models and reality. The main novelties of this algorithm are the resolution of the problem in the frequency domain and the fully experimental calibration of the system (no theoretical reference to the bridge structural behaviour is required). However, the spectra are limited by the time the load is on the bridge and low frequency components could not be defined accurately in every case. Accordingly, while effective for vehicles with a low number of axles, this frequency domain approach failed to accurately predict the weights of a high number of axles.

Other research has focused on the development of dynamic algorithms in the time domain. These approaches try to correct the deviation from the static value that bridge and truck

dynamics could introduce in the measured strain (Dempsey et al. 1998b, O'Connor & Chan 1988a, 1988b). A new dynamic B-WIM algorithm that compares the measured strain to the theoretical total strain (instead of just the static) is presented. The equations of the total strain are made up of static and dynamic components. They can be derived from the mechanical characteristics of the bridge and the variables representing its general dynamic behaviour: natural frequencies, mode shapes and damping. Further dynamic modelling can be introduced through the application of optimisation techniques.

Most of these procedures yield a unique average load as a result of using the whole strain record at one longitudinal sensor location. This assumption could induce significant errors due to the varying applied force. Kealy and O'Brien (1998) extended the traditional static algorithm based on one sensor location to the use of several sensors along the length of the bridge. This approach has the advantage of providing the complete distribution of varying axle forces as the truck traverses the bridge and appears to reduce the effect of truck bouncing and rocking motions overall. However, it does not address the issue of bridge vibration which can result in significant errors for bridges with low natural frequencies. A dynamic multiple-sensor algorithm is developed here to overcome this problem (González et al. 1999). Finally, the multiple-sensor algorithm is extended to deal with simultaneous traffic events.

7.2 AN ALGORITHM BASED ON SPECTRUM ANALYSIS

All the B-WIM approaches to date calculate the weights in the time domain, this is, strain measurements from each scan are compared to corresponding theoretical values. As a result, final results are highly sensitive to truck location. In addition, a B-WIM algorithm based on a time-domain analysis depends on an accurate knowledge of the influence line and will tend to be sensitive to the dynamic characteristics of the trucks which are unknown. In this section, an alternative dynamic B-WIM system is presented based on a frequency spectrum approach. It utilises the frequency components of the strain signal and requires no prior knowledge of the influence line. The frequency domain representation of the signal, although entirely equivalent to the time domain representation, facilitates the suppression of high frequency effects and tends to reduce errors induced by speed measurement (this problem appears to have been overcome recently with optimisation techniques as described in Section 3.5).

7.2.1 Principle

This spectral algorithm is based on some properties of the Fourier Transform. If the measured strain at each scan n is $\varepsilon[n]$, the Fourier transform a_k for a frequency $(2*\pi*k/N)$ is given by:

$$a_k = \frac{1}{N}\sum_{n=0}^{N-1} \varepsilon[n] * e^{-j2\pi Kn/N} \tag{7.1}$$

where N is the sample size, k the harmonic order and $j = \sqrt{-1}$. The bridge response due to a moving unit load can be represented in time or frequency domains as shown in Figure 7.1.

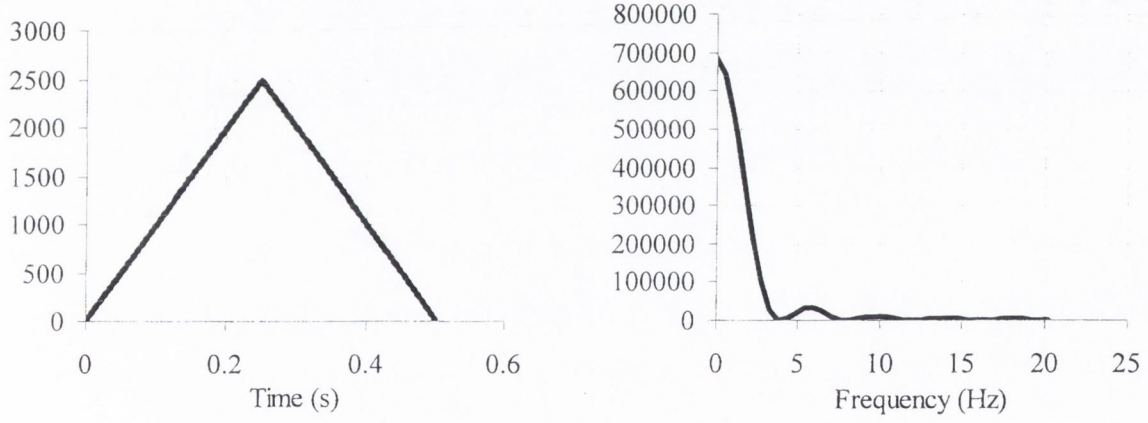

(a) Time Domain ($\varepsilon[t]$) (b) Magnitude in Frequency Domain ($|a_k|$)

Figure 7.1 – Bridge response due to a unit moving load

This transform has the property of linearity. If a load C times bigger acts on the bridge, the static strain response will be $C*\varepsilon[n]$, and then, the new magnitude of the Fourier transform for the k^{th} harmonic will be $C*a_k$. The phase component of the Fourier transform will remain the same.

If a signal is shifted by n_0 scans ($\varepsilon[n-n_0]$), the magnitude of the spectrum does not change, but the phase is different. The relationship between the transform of the shifted signal (b_k) and the original signal (a_k) is expressed by Equation 7.2.

$$b_k = a_k e^{-j\frac{2\pi k n_0}{N}} \tag{7.2}$$

Spectral energy can be expected to be concentrated around a period corresponding to the time it takes for a truck to cross the span. If the static response to two or more axles is considered, the total spectrum is a linear combination of their individual spectra.

The algorithm operates on the frequency-domain response of the bridge in free vibration and the frequency components of the strain signal, specifying which frequency range in the measured strain is to be suppressed. It compares results in the lowest frequency range, where most of the total energy of the signal is concentrated. Ideally this is far from the influence of the bridge's first natural frequency. When that frequency is excessively low, there will be spectral leakage that will have to be filtered out. Although there could be 'sidelobes' above the lowest frequencies containing significant energy due to the static response, this does not affect the algorithm's performance as the formulation operates in the frequency rather than the time domain. Accuracy depends on having a high definition of the response spectrum. Long flexible bridges allow for the collection of a lot of readings and a good definition of low frequency components, while short stiff bridges allow the extension of the algorithm to a wider range of frequencies.

7.2.2 Calibration

According to linearity and the time-shifting properties of Fourier transforms of digital signals, the total spectrum of the bridge response due to a calibration truck can be expressed as:

$$\overline{H_y}(f) = \overline{H_x}(f)[W_1 + W_2 e^{(-jfn_1)} + \ldots + W_i e^{(-jfn_{i-1})} + \ldots + W_r e^{(-jfn_{r-1})}] \tag{7.3}$$

where

$\overline{H}_y(f)$: Spectrum of total strain,

$\overline{H}_x(f)$: Spectrum of the strain response due to a moving unit load,

W_i : Weight corresponding to axle i,

j : Imaginary number, i.e., $\sqrt{-1}$,

r : Number of axles,

n_i : Number of readings between the first axle and axle $(i+1)$,

f : Frequency, as $f = 2\pi k/N$, where k (0,1,2,..) represents the k^{th} harmonic of the sample,

N : Number of strain readings induced by a vehicle crossing the bridge.

Figure 7.2 illustrates Equation 7.3 for a two-axle truck.

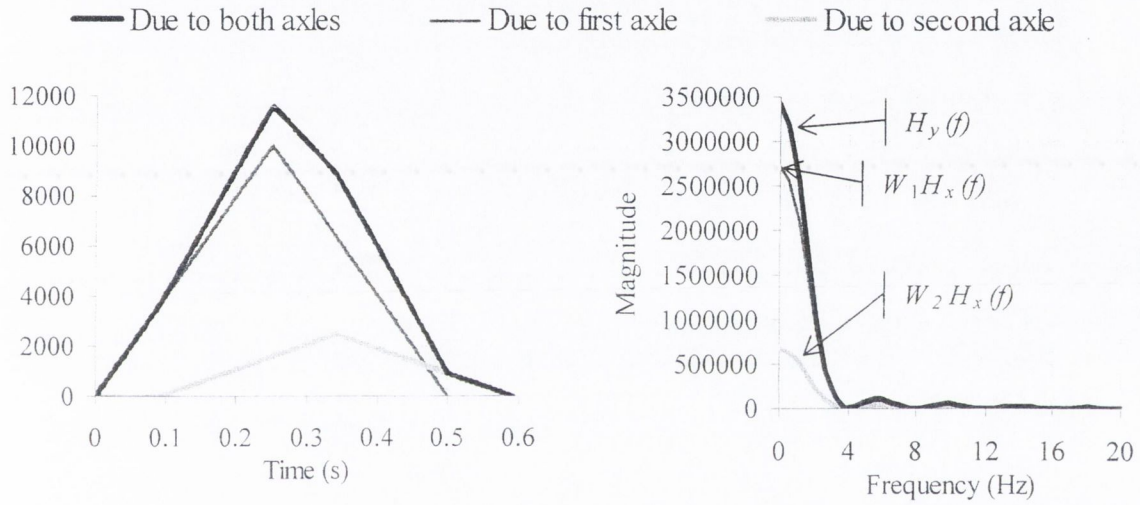

(a) Strain due to a two-axle truck (b) Spectra of (a)

Figure 7.2 – Calibration in frequency domain

As bridge frequencies and spectral leakage due to their components take place for relatively high frequencies, it is possible to assume for the lowest frequencies:

$$\overline{H}_y(f) \approx \overline{H}_m(f) \tag{7.4}$$

where $\overline{H}_m(f)$ is the spectrum of the measured strain.

Substituting Equation 7.4 in Equation 7.3, the spectrum corresponding to the pass of a single unit load can be obtained for the lowest frequencies by Equation 7.5:

$$\overline{H_x}(f) = \overline{H_m}(f)/[W_1 + W_2\, e^{(-jfn_1)} + \ldots + W_i e^{(-jfn_{i-1})} + \ldots + W_r e^{(-jfn_{r-1})}] \tag{7.5}$$

Very low speeds of the calibration truck allow for the collection of a lot of readings, and a good definition of low frequency components. A variety of speeds is necessary to evaluate the magnitude component of the fundamental harmonics for different sizes of the sample. Therefore, the scanning frequency should be quite high to reduce spectral leakage due to non-harmonic components. Some dispersion in spectra calculated through Equation 7.5 will occur due to truck dynamics.

7.2.3 Weight calculation

Once the spectrum of the bridge response due to a unit load is known, axles weights can be calculated by minimising an error function defined as the sum of squares of differences between the expected spectrum and the measured one, as follows:

Find W_i to minimise:

$$\sum_{f=0}^{f_c} [\overline{H_x}(f) \sum_{i=1}^{r} (W_i e^{(-jfn_{i-1})}) - \overline{H_m}(f)]^2 \tag{7.6}$$

where f_c is the limit frequency where spectra are compared. The spectrum $\overline{H_x}(f)$, taken as reference, must be the one corresponding to the speed of the traffic event being analysed. This spectrum can be calculated through inverse transform and interpolation from the calibration spectra obtained using Equation 7.5.

The error function is minimised by differentiating with respect to the weight of the k^{th} axle, W_k, which leads to the following expression:

$$\sum_{f=0}^{f_c} [\sum_{i=1}^{r} [W_i e^{(-j2fn_{i-1})} \overline{H_x}(f)] e^{(-jfn_{k-1})} \overline{H_x}(f)] = \sum_{f=0}^{f_c} [\overline{H_m}(f) \overline{H_x}(f) e^{(-jfn_{k-1})}] \tag{7.7}$$

In matrix form, the axle weights are given by Equation 7.8:

$$\{W\}_{rx1} = [H]_{rxr}^{-1} \{M\}_{rx1} \tag{7.8}$$

where the elements of the matrix of coefficients $[H]$ are given by Equation 7.9 and the vector of independent terms $\{M\}$ by Equation 7.10.

$$[H_{ik}] = \sum_{f=0}^{f_c} [e^{(-jf(n_{i-1}+n_{k-1}))} \overline{H_x}^2(f)] \tag{7.9}$$

$$\{M_k\} = \sum_{f=0}^{f_c} [\overline{H_m}(f)\overline{H_x}(f)e^{(-jfn_{k-1})}] \tag{7.10}$$

Spectra $\overline{H}(f)$ are composed of real and imaginary parts (or magnitude and phase). Axle weights are obtained from Equation 7.8 using complex arithmetic.

7.2.4 Theoretical Testing

A different number of trucks and road surface roughnesses are simulated to generate strains and the theoretical results used to check the validity of the algorithm. Pitch, bounce and roll of the truck body are taken into consideration. A beam model is used to represent the bridge. Road surface irregularities are idealised as a stochastic process and generated from power spectral density functions for 'very good', 'good', 'average' and 'poor' conditions (Wong 1993).

Results obtained by the new Spectral Bridge WIM approaches are compared to the conventional static approach, as described by Moses (1979). If a static bridge simulation is used to generate input strains, both algorithms are totally accurate. Further, if a bridge dynamic model consisting of constant forces moving at uniform speed is used, the spectral algorithm is still 100% accurate, unlike the static algorithm, where dynamics is a source of inaccuracy (even when this dynamic behaviour is linear).

Bridge-truck interaction model

The truck is represented by a planar 2-axle body, and implemented with the numerical methods proposed in Section 5.5. This planar model is represented in Figure 7.3. The bridge structure is modelled as a simply supported beam with surface irregularities. Bending strains are assumed to be measured at midspan.

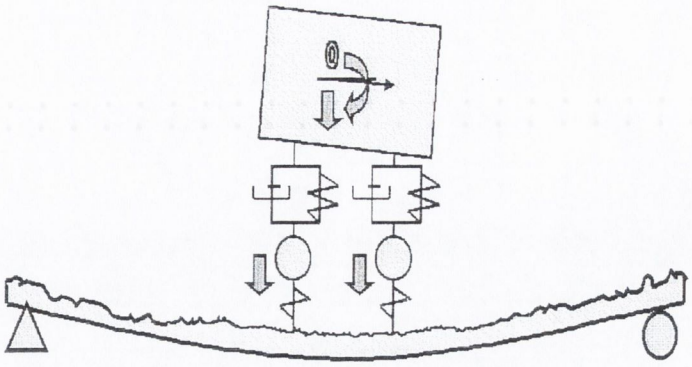

Figure 7.3 – Numerical approach

The features of the calibration truck, taken as reference, are: 50×10^3 kg.m^2 body inertia, 10×10^3 kg body mass equally distributed between axles, 4 m axle spacing, 20 m/s speed, and axle characteristics of: 1000 kg axle mass, 7×10^3 N.s/m suspension damping, 80×10^3 N/m suspension stiffness and 700×10^3 N/m tyre stiffness. The road conditions are taken as 'good'. The characteristics of the bridge model are: span 10 m, mass 12×10^3 kg/m, flexural rigidity 2.7×10^9 Nm^2, first natural frequency of the bridge in flexure 7.45 Hz and critical damping 5%. The road conditions are considered 'very good', unless otherwise specified.

Effect of different parameters

For any Bridge WIM system, based on static or dynamic principles, there is a difficulty in obtaining an accurate system calibration. In static terms, the calibration consists of determining an accurate influence line for the bridge. This is often determined by scaling and/or adjusting a theoretical influence line to give a best fit of measured to theoretical results for the calibration vehicle. For a dynamic algorithm, an attempt can be made to characterise the bridge in a similar way. However, the characteristics thus found tend to be highly dependent on the properties of the truck used for the calibration process. In this section, the sensitivity of the results to the differences in the properties of the truck being weighed and those of the calibration vehicle are investigated.

Influence of road conditions

There are clearly greater amplitudes of dynamic wheel forces in poor road conditions than in good conditions. Therefore, truck initial conditions have a strong influence on final results and the average axle load on the bridge could have an important deviation from the

static value. The dynamic algorithm is less sensitive to this variation than the static one. If the truck was calibrated in average road conditions, the maximum error in axle weight when half loaded is 2.75% if adopting the traditional approach compared to 1.47% with the dynamic one. However, this finding is based on a stochastic representation of the profile and does not take account of any biases that might be introduced by such phenomena as spatial repeatability (O'Connor et al. 1999).

Influence of bridge parameters

If inertia is decreased or span length/mass increased, the value of the natural frequencies will be reduced, and bridge-truck interaction will take place at lower frequencies. The difference between the total and static answers then becomes greater, and the dynamic algorithm is less sensitive to this variation than the static one.

Influence of vehicle parameters

Figure 7.4 shows the relationship between bending moment and truck position for a two-axle truck and the corresponding Fourier transform for the static and total (static + dynamic) cases. The response spectrum for frequencies below 5 Hz is very close for the two cases. By applying the new algorithm in this frequency range, the increasing deviation due to truck and bridge interaction at higher frequencies is avoided. The results of Figure 7.4 have been used to calibrate both systems for the comparisons described in this section.

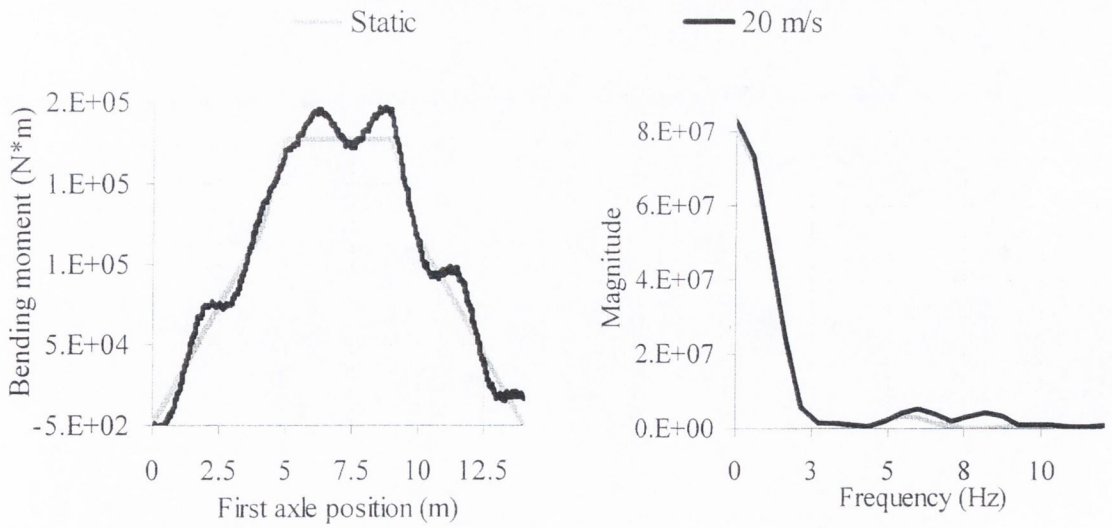

(a) Moment versus vehicle position (b) Spectra response

Figure 7.4 – Static and total bending moment for a two-axle truck

For the new system, values of the 'measured' spectra corresponding to a moving unit load can be obtained through Equation 7.5. Then, weights are calculated using Equation 7.8. There is an increasing deviation between the static and the total bending moment response with increasing speed but this increase ends at a certain speed.

Figure 7.5(a) gives the maximum relative error in individual axle weights for both the static and the new algorithms due to differences in the axle spacing and the position of the centroid of the body mass between sample truck and calibration truck. Figure 7.5(b) compares this maximum error when there are differences in the sprung and unsprung masses. The relative error due to a difference in the position of the sprung mass between the calibration truck and the truck being weighed is quite significant as illustrated in Figure 7.5(a). A difference in axle spacing can be seen to be an important source of inaccuracy for the spectral algorithm. Accuracy is also sensitive to mass differences as can be seen in Figure 7.5(b). This sensitivity has been found to be greater when the sprung or unsprung frequency is lower. Although the new algorithm gives an improvement in the accuracy of individual axle weights over the conventional static bridge WIM algorithm, the degree of uncertainty introduced by vehicle parameters is still important and truck low frequencies might yield an average value far from the static one in short span bridges.

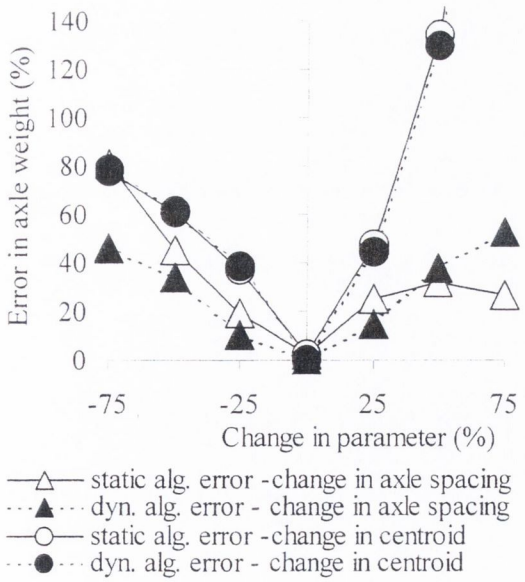

(a) Relative error due to change in axle spacing or centroid of sprung mass

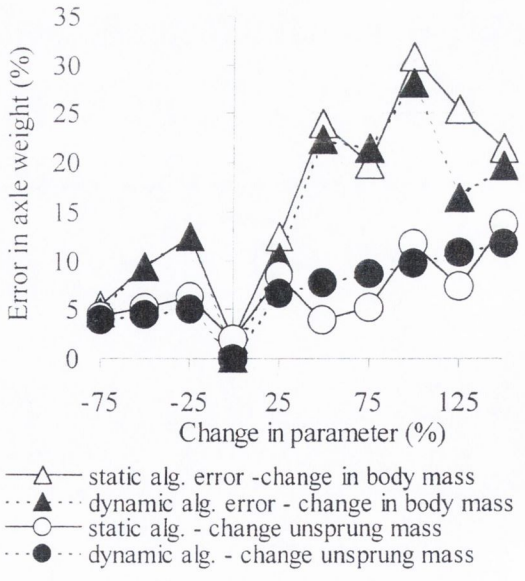

(b) Relative error due to change in vehicle masses

Figure 7.5 - Effect on accuracy of the change of vehicle masses and distances

In the same way, the influence on accuracy of vehicle mechanics is illustrated in Figure 7.6. Figure 7.6(a) shows the effect of a difference in pitch inertia or suspension damping while Figure 7.6(b) shows the effect of a difference in tyre or suspension stiffness. In these figures the dynamic algorithm is generally better than the static algorithm.

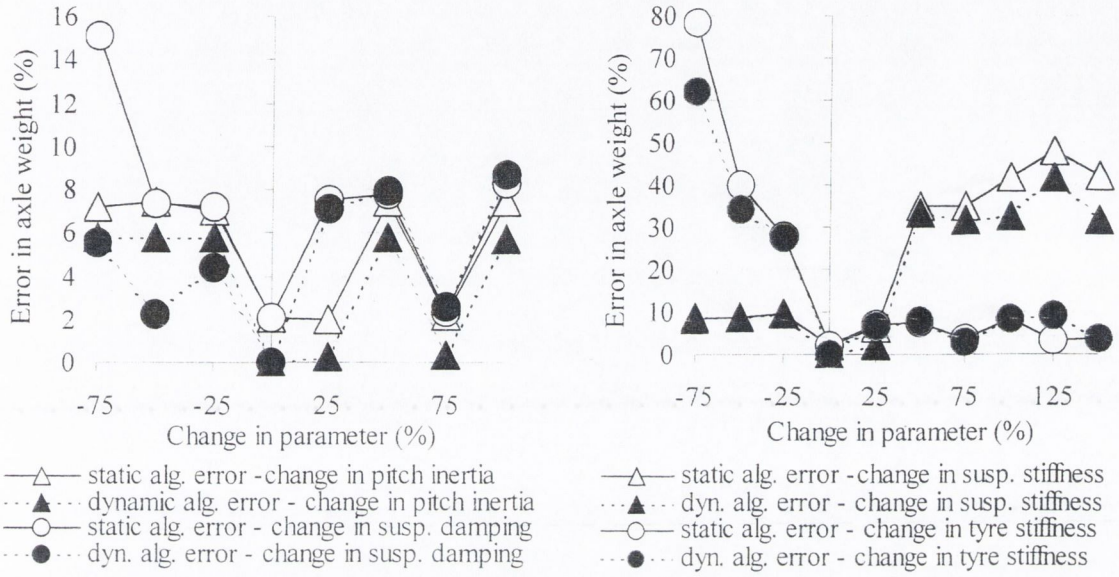

(a) Relative error due to change in pitch inertia/Damping

(b) Relative error due to change in tyre/suspension stiffness

Figure 7.6 – Effect on accuracy of the change of suspension and tyre characteristics

7.2.5 Advantages and Disadvantages

A Bridge WIM system gives a continuous reading that allows for a frequency domain analysis. In addition,

- Sources of inaccuracy in traditional static approaches are: (a) The determination of the real influence line; (b) An exact location of the truck on the bridge at each instant, (c) dynamics of bridge and truck introducing a deviation from the static response and (d) Low-pass filtering leads to errors in bridges with a low first natural frequency. In these bridges, filtering can inadvertently remove a significant part of the static response. In particular, it can be difficult to distinguish the effects of individual closely-spaced axles and filtering can lead to a reduction in the clarity of the individual effects.
- Compared to the problems mentioned before, a spectral Bridge WIM algorithm has the advantages: (a) No theoretical knowledge of the influence line is required; (b) Strain

measurements from each scan are not compared to corresponding theoretical values, but the contribution of each harmonic in frequency terms. This tends to reduce errors induced by inaccurate truck location (speed), (c) The frequency domain representation of the signal facilitates the suppression of high frequency effects and (d) The signal to work with is in a sense the 'true' one (No filtering or windowing effect that could have modified it, have been used).

However, the algorithm failed to accurately predict the weights of a lot of axles simultaneously. As a very good definition of low frequency components is not generally possible (due to the limited time the load is on the bridge), a high number of axles requires the use of equations for high frequency components of the signal. Higher frequency components generally have a smaller magnitude and their sensitivity to effects other than static response (i.e. dynamics) leads to unacceptable errors.

7.3 AN ALGORITHM BASED ON A BRIDGE DYNAMIC MODEL

The total strain response from a bridge due to a truck crossing can be modelled with a dynamic model based on constant loads. The total theoretical strain $\varepsilon(t)$ can be approximated as a function of the applied axle weights and the total (static + dynamic) strain response due to a unit moving load:

$$\varepsilon(t) = \sum_{i=1}^{no\_axles} W_i \varepsilon_{i1}(t) \tag{7.11}$$

where W_i is the axle weight corresponding to axle i, and $\varepsilon_{i1}(t)$ is the total strain due to a unit load moving at the vehicle speed and located at the position of axle i (Theoretical expressions for $\varepsilon_{i1}(t)$ are given in Section 5.3). The difference from Moses's approach would be the use of the dynamic response due to a unit load instead of the influence line. Variation in W_i is not taken into account.

The assumption of linearity and superposition involved in this formulation has been proven to match more realistic approaches (Dempsey & Brady 1999), even though the solution to the bridge-truck dynamic problem is non-linear. The theoretical model is also generated

with constant loads, so interaction between bridge and truck masses is neglected. This simplification allows a calculation in real time and a significant improvement in accuracy compared to the static algorithm based on the influence line. A more sophisticated model such as a quarter car could be considered instead of constant loads, but the difference in accuracy might not be justifiable due to the introduction of new unknown parameters.

The formulation for this dynamic B-WIM (DB-WIM) algorithm is derived by minimising an error function defined by the squared difference between measured and theoretical strains. The error function is:

$$\Psi = \sum_{t=1}^{no\_records} (\widetilde{\varepsilon}(t) - \varepsilon(t))^2 \tag{7.12}$$

where $\widetilde{\varepsilon}(t)$ is measured strain and $\varepsilon(t)$ is the total theoretical strain at a certain instant t given by 7.11.

By substituting Equation 7.11 into Equation 7.12, it is found that:

$$\Psi = \sum_{t=1}^{no\_records} (\widetilde{\varepsilon}(t) - \sum_{i=1}^{no\_axles} W_i \varepsilon_{i1}(t))^2 \tag{7.13}$$

Ψ is minimised by differentiating and setting to zero.

$$\frac{\partial \Psi}{\partial W_i} = 0 \quad ; \quad i = 1, 2, \ldots, \text{no. axles} \tag{7.14}$$

which gives,

$$\sum_{t=1}^{no\_records} [\widetilde{\varepsilon}(t) - \sum_{i=1}^{no\_axles} W_i \varepsilon_{i1}(t)] \varepsilon_{i1}(t) = 0 \quad ; \quad i = 1, 2, \ldots, \text{no. axles} \tag{7.15}$$

Re-arranging Equation 7.15 gives:

$$\sum_{t=1}^{no\_records} [\sum_{i=1}^{no\_axles} W_i \varepsilon_{i1}(t)]\varepsilon_{i1}(t) = \sum_{t=1}^{no\_records} \tilde{\varepsilon}(t)\varepsilon_{i1}(t) \tag{7.16}$$

or, in matrix form:

$$[T]\{W\} = \{H\} \tag{7.17}$$

where *[T]* is a matrix whose elements depend only on the total answer due to a unit load, axle spacings and speed,

$$[T_{ij}] = \sum_{t=1}^{no\_records} \varepsilon_{i1}(t)\varepsilon_{j1}(t) \tag{7.18}$$

{W} is a column vector composed of the unknown axle weights, and *{H}* is a column vector that depends on the measured strain as well as the total answer due to a unit load, axle spacing and speed.

$$\{H_i\} = \sum_{t=1}^{no\_records} \tilde{\varepsilon}(t)\varepsilon_{i1}(t) \tag{7.19}$$

Finally, axle weights are calculated as:

$$\{W\} = [T]^{-1}\{H\} \tag{7.20}$$

Gross Vehicle Weight (GVW) is obtained by summing the individual axle weights:

$$GVW = \sum_{i=1}^{no\_axles} W_i \tag{7.21}$$

Figure 7.7 illustrates the quality of the approximation obtained by DB-WIM to the simulated strains. The total strain and the static strain are obtained from numerical simulations (four degree of freedom model with mechanical characteristics described in Section 7.2.4). Another curve represents the strains obtained using Equation 7.11 if

considering constant loads. The DB-WIM system will be more accurate, the closer its adjustment is to the total strain.

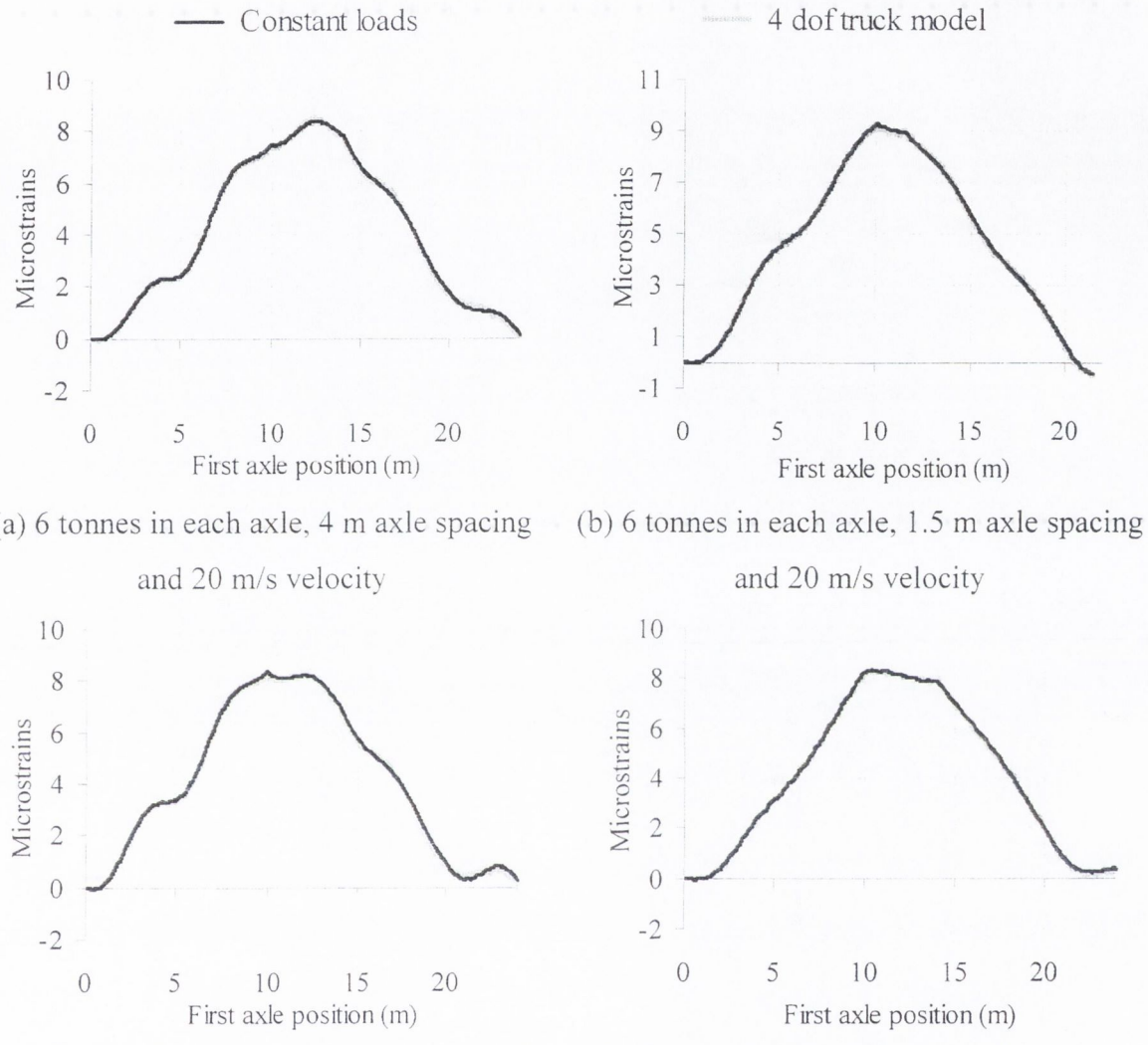

(a) 6 tonnes in each axle, 4 m axle spacing and 20 m/s velocity

(b) 6 tonnes in each axle, 1.5 m axle spacing and 20 m/s velocity

(c) 8.5 and 3.5 tonnes in each axle, 4 m axle spacing and 20 m/s velocity

(d) 6 tonnes in each axle, 4 m axle spacing and 30 m/s velocity

Figure 7.7 – Strain at midspan induced by a 2-axle vehicle and approximation by DB-WIM algorithm for different cases

Figure 7.8 shows the quality of the adjustment obtained by a static algorithm as proposed by Moses in comparison to the simulated static strain. In the case of Figure 7.8(d), it is possible to notice how the static approach overestimates the weight of both axles when trying to adjust the static answer to the total strain (the real static strain is unknown in measurements).

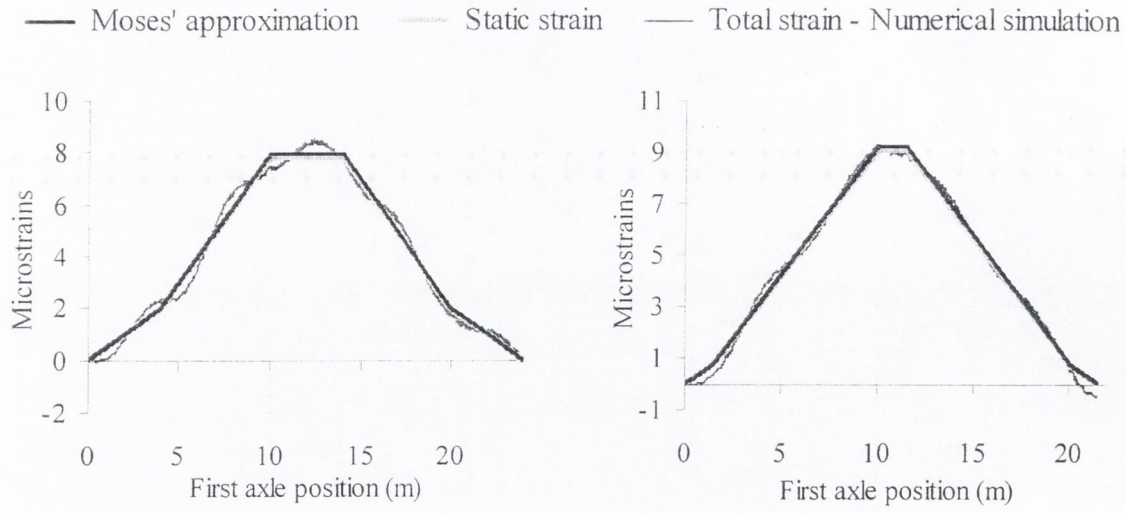

(a) 6 tonnes in each axle, 4 m axle spacing and 20 m/s velocity

(b) 6 tonnes in each axle, 1.5 m axle spacing and 20 m/s velocity

(c) 8.5 and 3.5 tonnes in each axle, 4 m axle spacing and 20 m/s velocity

(d) 6 tonnes in each axle, 4 m axle spacing and 30 m/s velocity

Figure 7.8 – Strain at midspan induced by a 2-axle vehicle and approximation by static algorithm for different cases

The results in Figures 7.7 and 7.8 correspond to a road profile in 'good' condition. In this case, the dynamic model based on constant loads achieves a solution very close to that obtained by a four degree of freedom vehicle model. Although a good road surface considerably increases the accuracy, other factors such as the presence of a bump at the expansion joint must also be taken into account. Some road classifications do not cater for this unevenness, which is responsible for high truck dynamic forces on the bridge (Section 3.5.1). The improvement of the dynamic algorithm over the static is especially important in the cases of frequency matching presented in the following subsection.

Influence of speed – frequency matching on B-WIM accuracy

When a load traverses a bridge, there is a pseudo-frequency associated with this passing given by:

$$frequency_{moving\_load} = Speed / Bridge\_Length \tag{7.22}$$

When this frequency is close to twice the natural frequency of the bridge, a static B-WIM algorithm could give significant errors in GVW due to the difference between the static and total strain. For a normal range of speeds and bridge dynamic behaviour (first natural frequency of the bridge decreasing as the bridge length increases), this frequency matching is more likely to happen in bridges over 30 m.

Figure 7.9 illustrates the influence on the accuracy of Moses' static algorithm when considering a two-axle vehicle at different speeds over a 40-m bridge (first natural frequencies: 1.06 and 4.26 Hz, strong damping 5%). The vehicle model is shown in Figure 7.3 (mechanical characteristics in Section 7.2.4). Solutions provided by Moses for simulations at three vehicle speeds 20, 25 and 30 m/s (equivalent to frequencies 0.5, 0.625 and 0.75 Hz respectively) are represented. The bridge response does not have a sufficient number of dynamic oscillations and Moses' adjustment differs from the simulated static strain (which should be symmetric in Figures 7.9(a) and (c)). Error in axle weights is significant.

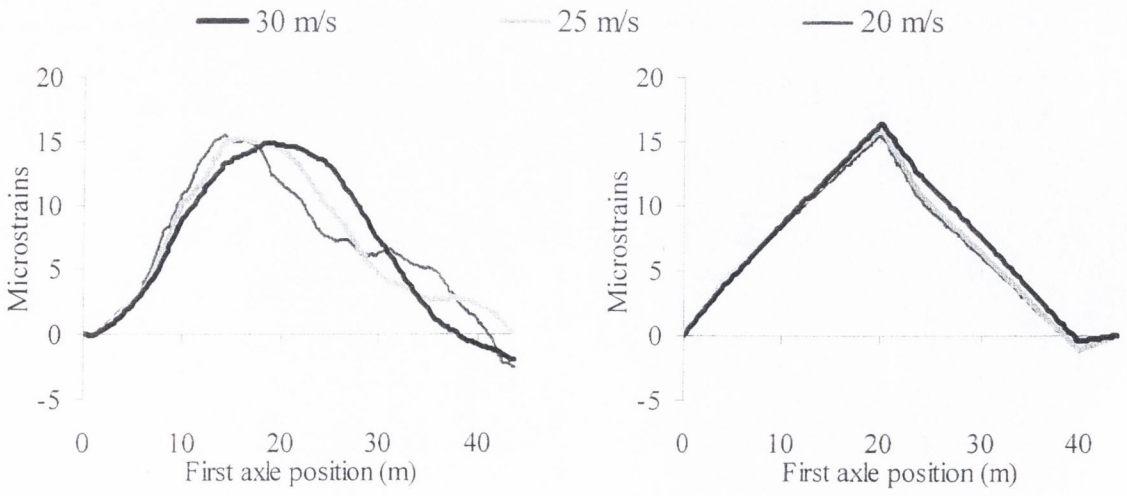

(a) Total strain due to weights: 6 + 6 t (b) Moses's solution to (a)

Figure 7.9 (continued on following page)

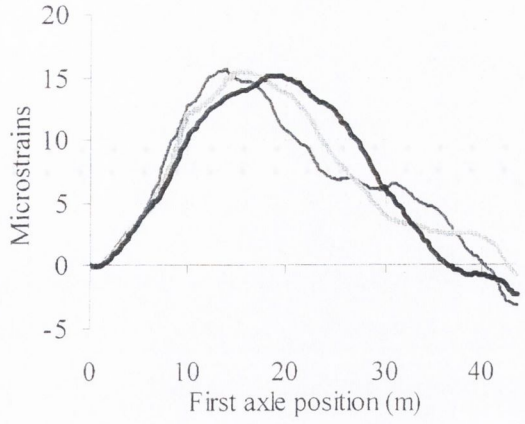

(c) Total strain due to weights: 8.5 + 3.5 t

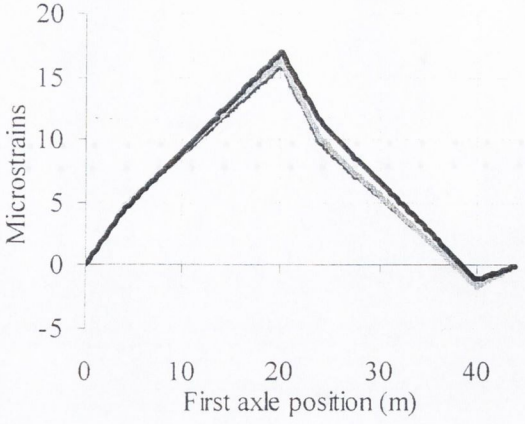

(d) Moses's solution to (c)

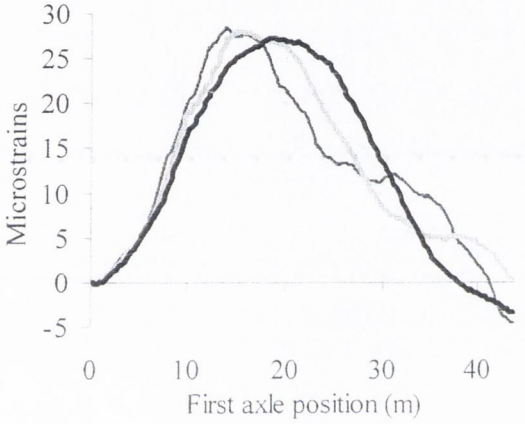

(e) Total strain due to weights: 11 + 11 t

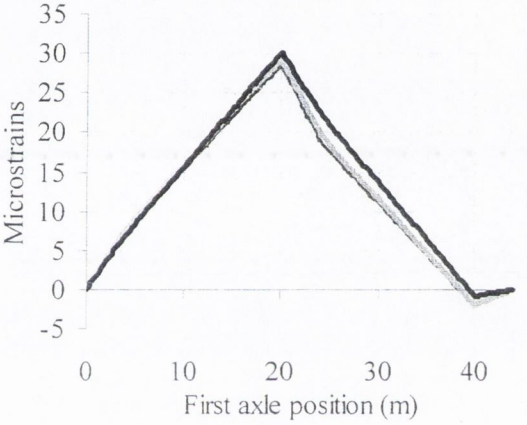

(f) Moses's solution to (e)

Figure 7.9 – Static adjustment for different axle weights in a 40-m bridge

Figure 7.10 shows the ideal calibration factor for this bridge at different vehicle speeds. This static calibration factor was obtained dividing the real GVW by the estimated GVW. The calibration factor is the same for the two vehicles of weight equally distributed between axles (6+6 and 11+11), but changes when the axle weight distribution is different. There is a tendency to overweigh vehicles as the speed increases.

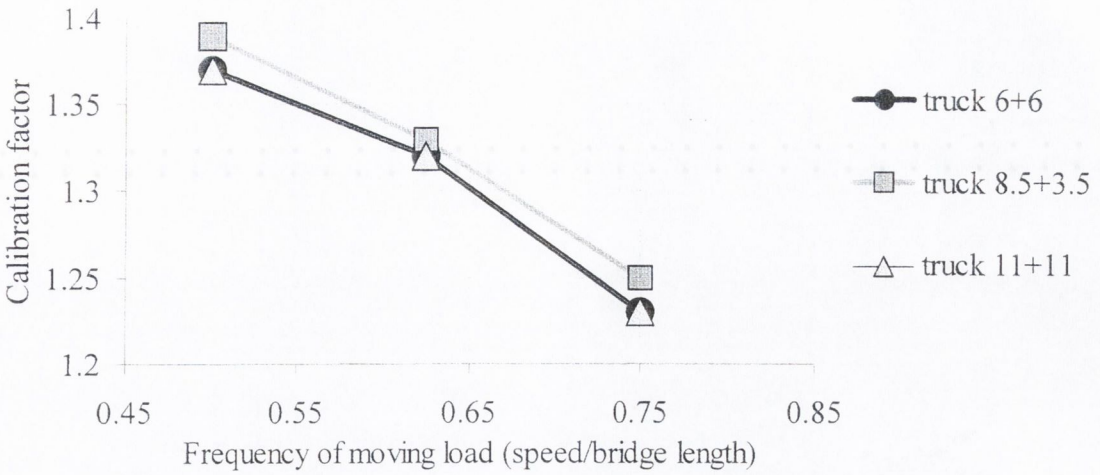

Figure 7.10 - Calibration factors obtained for the 40-m bridge

The dynamic approach gave the following results:

- The preceding cases with a small number of oscillation periods are solved satisfactorily.
- Truck dynamics are removed through a least square fitting of all the readings along the bridge. The value that is obtained for static weight should be very close to the correct value.
- Bridge mass/inertia is taken into account in the formulation. No filtering techniques that rely on a sufficient number of vibration periods for a safe removal of bridge dynamics are necessary.

As a conclusion, a DB-WIM algorithm looks to be a more satisfactory solution that caters accurately for more bridge and truck types than traditional static B-WIM algorithms. It caters better for those cases with a low first natural frequency that could not be smoothed properly by static B-WIM, or records where vehicles travel at high speed, and in general, situations where the induced dynamic effects are large. A good solution can be identified in the field when the theoretical strain generated by the bridge dynamic model of DB-WIM matches the measured strain. This algorithm is based on one longitudinal sensor location, though it will be further extended to multiple sensors in Section 7.5.1. The performance of DB-WIM will be tested in Chapter 9.

7.4 AN ALGORITHM BASED ON A TRUCK DYNAMIC MODEL

The non-linear approach described in this section is based on the application of optimisation techniques to allow for the dynamic modelling introduced in Chapter 5. The bridge-car structural system has an infinite number of degrees of freedom and only a limited number of them given by the strain readings are available (apart from strains, some dynamic characteristics of the bridge such as first natural frequencies and damping can be obtained experimentally). The first limitation is the fact that it is strains that are measured, as dynamic equations are related to displacements, velocities and accelerations of the deformed shape. To convert strains into displacements or vice versa, it is necessary to make assumptions on the bridge dynamic behaviour.

7.4.1 Optimisation Process

The objective function is given by the sum of squared differences between the measured and theoretical strains for each record in time. The optimisation process is summarised in Figure 7.11. The iteration process requires:

- Initial conditions given by a static B-WIM system. These initial conditions (i.e. speed, axle spacing, axle weights) play a very important role in the achievement of the correct solution,
- Optimising results given by the dynamic simulation of the truck on the bridge. In every case, the bridge is modelled as described in Section 5.2. The equation of motion corresponding to the bridge is:

$$EI\frac{\partial^4 z(x,t)}{\partial x^4}+\mu\frac{\partial^2 z(x,t)}{\partial t^2}+2\mu\omega_b\frac{\partial z(x,t)}{\partial t}=\sum_{i=1}^{n}\varepsilon_i\delta(x-x_i)R_i(t) \tag{7.23}$$

where :

$z(x,t)$: displacement of the bridge at position x and time t,

E, μ and I : Young's modulus, mass per unit length, and second moment of area of the bridge respectively,

δ : Dirac function,

ε_i = 1 when axle i is on the bridge (otherwise zero),

ω_b = $\xi\omega_n$ is damping frequency, where ξ is damping and ω_n is natural frequency of the bridge,

n : number of axles,

$R_i(t)$: the interaction force between the bridge and the applied axle load i,

x_i = $vt - a_i$, is the position of axle i (the position of first axle is $x_1 = vt$), where a_i is spacing between first axle and axle i, and v is velocity.

- Truck modelling that can have different parameters: (a) Consider axles as constant loads, (b) Consider axles as masses or (c) Consider axles as sprung masses. The introduction of truck models based on more degrees of freedom does not result in a more accurate solution necessarily as new parameters can lead to an iterative process that does not converge.

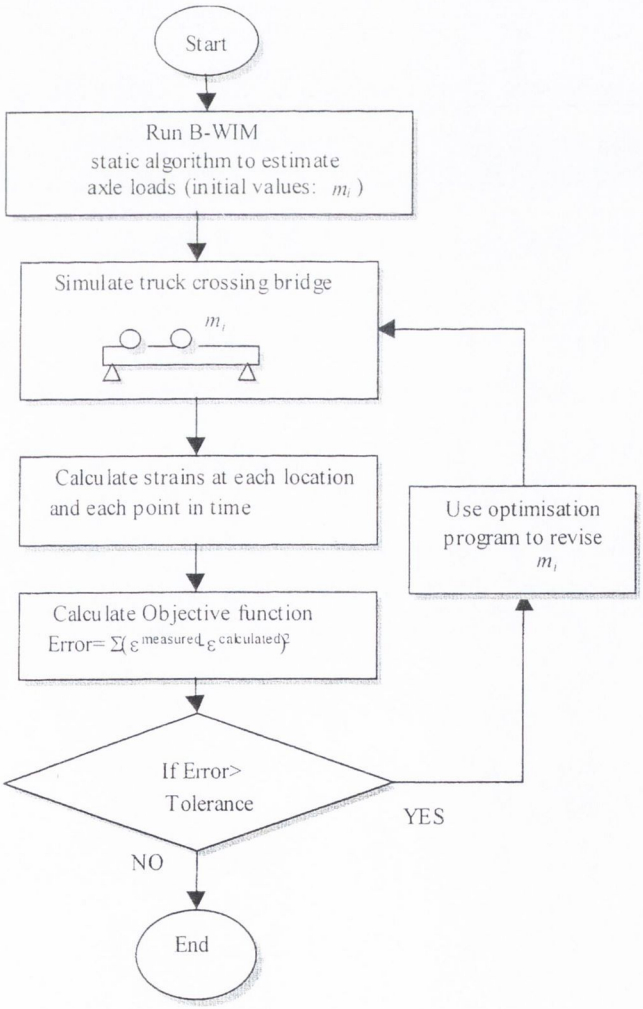

Figure 7.11 – Optimisation process

(a) Consider axle loads as constant loads

Axle loads are assumed to be constant and equal to the static weights. This assumption can be acceptable in long span bridges where the vehicle mass is negligible compared to the bridge mass. Parameters to optimise: R_i, axle force.

When vehicle axles are modelled as constant loads, speed (v), axle spacing (a_i) and loads ($m_i g$) for each axle define the vehicle parameters to be optimised. Equations 7.24 represent the applied forces in this simplified model.

$$m_i g = R_i \qquad ; \quad i = 1,2,...n \tag{7.24}$$

where n is number of axles.

(b) Consider axle loads as moving masses

Inertial effects of the axle mass are taken into account. It is assumed there is no redistribution of load between axles. Compared to the dynamic model based on constant loads, this modelling can improve accuracy in short span bridges.

Speed (v), axle spacing (a_i) and masses (m_i) for each axle define the parameters to be optimised. Mass is optimised until the difference between one value and the next one is sufficiently small. The iteration will stop when the difference between the value of the parameters for an iteration and the preceding one is within a given threshold.

The moving mass has one degree of freedom that represents vertical displacement. Equations 7.25 represent the vertical motion (z_i) of the moving masses (m_i),

$$m_i g - \frac{m_i d^2 z_i(t)}{dt^2} = R_i(t) \qquad i = 1,2,...n \tag{7.25}$$

where n is number of axles. The systems of differential Equations 7.23 and 7.25 can be solved with the method of Runge-Kutta (Appendix E).

(c) Consider axle loads as moving masses with stiffness elements (sprung masses)

The mass and stiffness of the axle force are taken into account in the axle modelling. An instantaneous interaction force R_i can be obtained at each instant by optimising strain at a number of sensors. The objective function for this process is given by the sum of the squared differences between measured strain and theoretical strain for each sensor. This interaction force takes account of the road irregularities. A second iterative process (Figure 7.10) optimises speed (v), and masses (m_i) and axle spacings (a_i) for each axle.

Each moving mass is allowed to move in the vertical direction. Equations 7.26 represent the vertical motion (z_i) of the moving masses (m_i),

$$m_i g - \frac{m_i d^2 z_i(t)}{dt^2} - R_i(z_i,t) = 0 \qquad i = 1,2,...n \tag{7.26}$$

where n is number of axles.

Equation 7.27 represents the interaction force $R_i(z_i,t)$ between the bridge and the wheel at the contact point.

$$R_i(z_i,t) = K_i\left[z(x_i,t) - r(x_i)\right] \tag{7.27}$$

where $r(x_i)$ is the road profile.

The Runge-Kutta method can be used to solve Equations 7.23, 7.26 and 7.27. If the masses m_i are known (i.e. calibration vehicle), interaction forces can be calculated accurately at each instant. This information can be useful to analyse dynamic wheel forces.

While truck models (a) and (b) assume a smooth road profile, approach (c) tries to take account of the road irregularities by allowing for an assumed tyre stiffness at each instant. This optimisation at each instant is only feasible if there are a sufficient number of sensors.

7.4.2 Objective Function

The objective function for the numerical simulation of a 12 tonne two-axle rigid body running over a 20-m bridge (4.26 Hz first natural frequency) is analysed for both the static and dynamic algorithms based on constant loads. The characteristics of the truck are given in section 7.2.4. The results of the simulation and adjustment based on bridge dynamic model are shown in Figure 7.12.

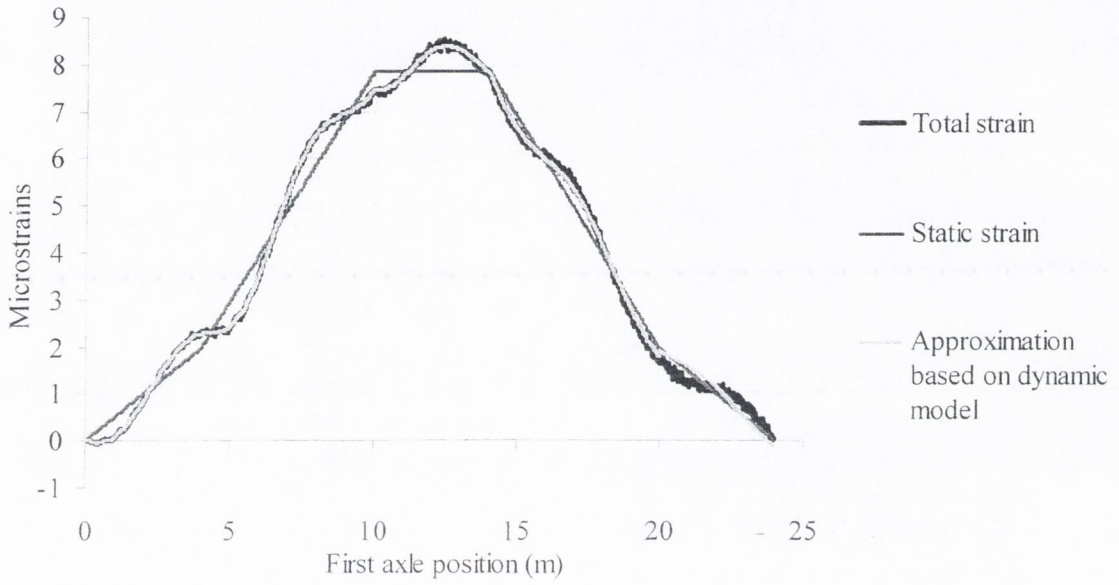

Figure 7.12 – Simulation of a two-axle rigid body

Axle weights are obtained using the static and dynamic algorithms. All variables are fixed, except front and rear axle weight. The contours of the objective function for front and rear axle weight are represented in Figure 7.13. The objective function has a minimum. For the dynamic approach, the solution fits in the centre of the central area in Figure 7.13(f). For the static approach, the solution is not perfectly symmetric, and the rear axle tends to be overweighed due to dynamics. Appendix G illustrates the values of the objective function for other combinations of parameters (speed, axle spacing and axle weights).

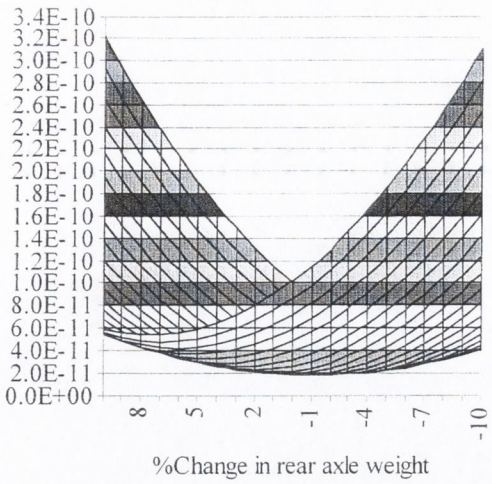

(a) Linear static approach (-10% to 10%)

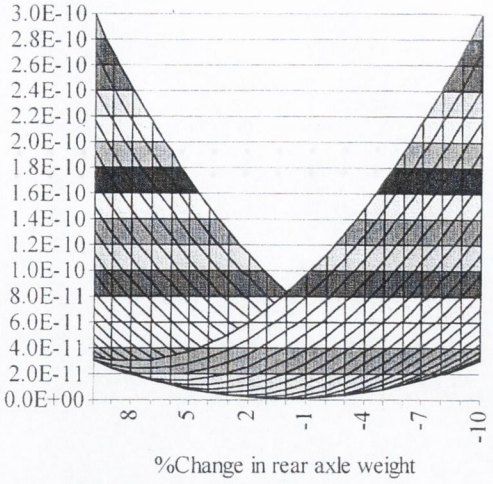

(b) Linear dynamic approach (-10% to 10%)

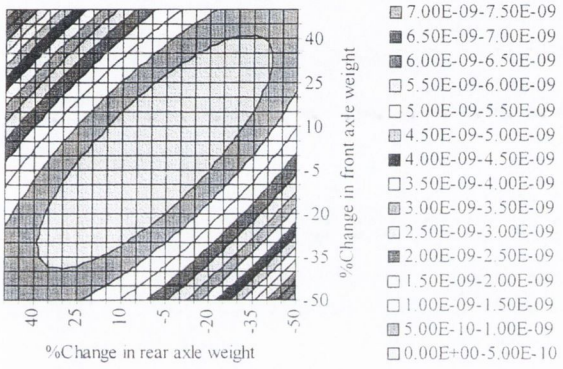

(c) Linear static approach (-50% to 50%)

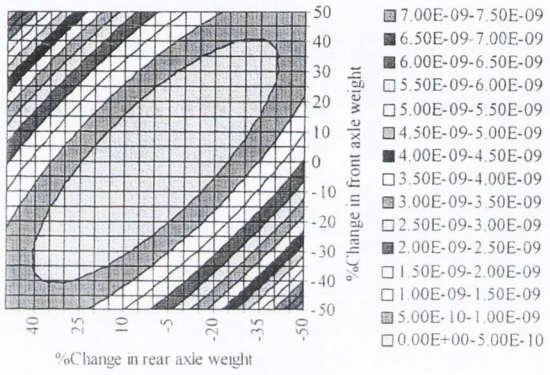

(d) Linear dynamic approach (-50% to 50%)

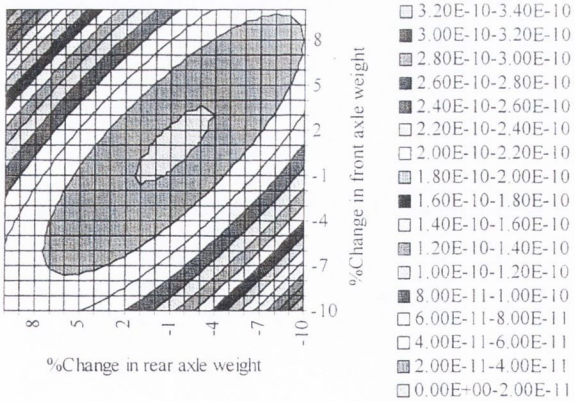

(e) Linear static approach (-10% to 10%)

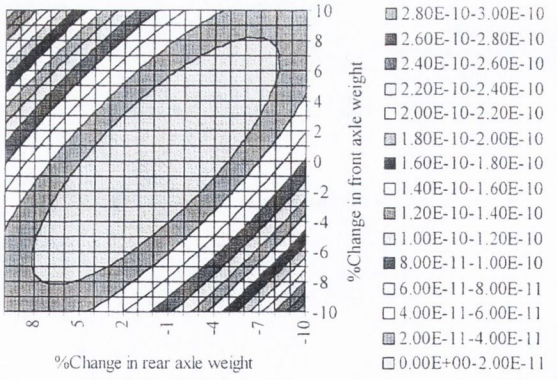

(f) Linear dynamic approach (-10% to 10%)

Figure 7.13 – Objective function for variables: Front and Rear axle weight

A vehicle of the same mechanical characteristics but different redistribution of weight between axles (8.5 tonnes in the front and 3.5 in the rear axle) is also used to test the objective function. The dynamic algorithm based on constant loads was used to generate

the theoretical strain. Figure 7.14 represents this function when allowing axle weight to change while fixing the rest of the parameters.

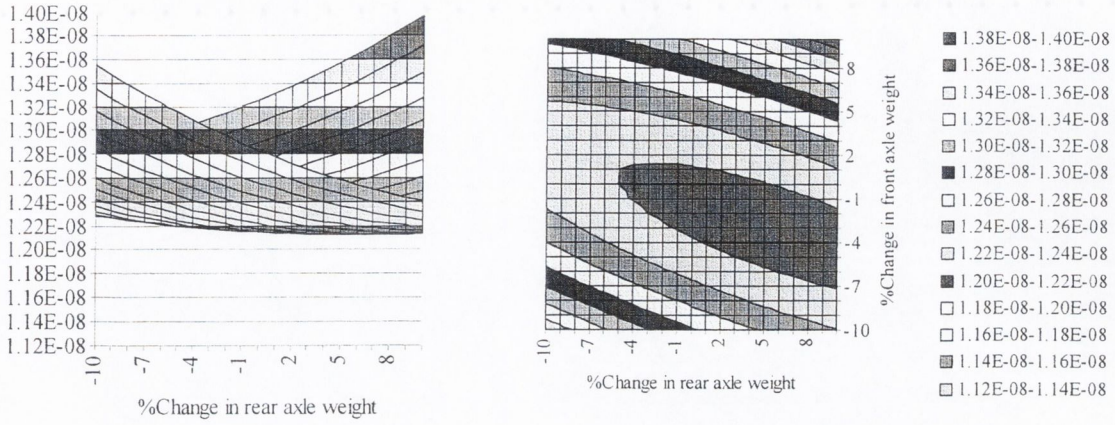

(a) SideView (-10% to 10%) (b) PlanView (-10% to 10%)

Figure 7.14 – Objective Function for different weight distribution (Dynamic algorithm)

The same dynamic algorithm (based on constant loads) is applied to nine different locations simultaneously (simulated strain at all locations is added together). The objective function is defined as the sum of the differences between predicted and simulated strain at every location. Figure 7.15 shows the values of the objective function (variables: front and rear axle weights) if using the sum of nine sensors equally distributed along the bridge instead of one sensor at midspan (Figure 7.14). In this case, there is not significant improvement in the estimation of static weights by increasing the number of sensors.

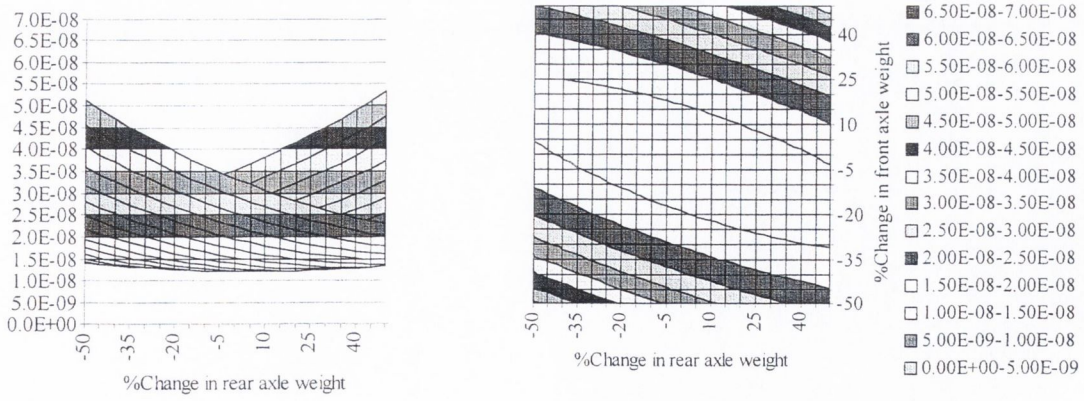

(a) SideView (-50% to 50%) (b) PlanView (-50% to 50%)

Figure 7.15 – Objective Function for different number of sensors

7.5 ONE-DIMENSIONAL MULTIPLE-SENSOR ALGORITHMS

The multiple-sensor static algorithm introduced in Section 3.5.4 (Kealy & O'Brien 1998) tries to find the applied force applied along the bridge using multiple longitudinal sensor locations. This results in a number of strain records for each point in time, permitting the possibility of instantaneous axle and gross vehicle weight calculation. An equation based on the influence line for each location can be formulated for each sensor at each instant. However, the static approach has limitations resulting from the dependency of the equations. The system can be solved for a fixed number of axles related to the degree of indeterminacy of the structure: 2 axles in a single span, 3 in a continuous two span-bridge, etc... The algorithm introduced in this section overcomes this limitation by using a high number of sensors and applying a least square fitting technique. The dynamic response can also be adopted as a reference in a multiple-sensor algorithm. In another words, the measured strain is compared to the theoretical total strain instead of the static strain (given by influence lines).

7.5.1 Dynamic Multiple-sensor Algorithm

A dynamic algorithm capable of calculating instantaneous values of axle force as the truck travels across the bridge is introduced. This algorithm is based on measurements at multiple sensor locations in the longitudinal direction. The axle load at each instant can be calculated from the theoretical dynamic strain response at these locations due to a single load. The static value is given by the root mean square of axle forces from the force history. The advantages of this new approach is that bridge dynamics are removed from the experimental strain record without the need for filtering that could remove some significant static component. Additional information will stem from knowing the complete history of dynamic axle forces applied to the bridge: dynamic amplification factors, data for fatigues studies and spatial repeatability and collection of truck dynamic characteristics through spectrum analysis of the applied load.

Formulation

This multiple-sensor system is based on the accurate determination of the theoretical strain response due to a moving constant load at different bridge locations. This is obtained by a) experimental determination of the natural frequencies and damping of the bridge, b)

calculation of the mode shapes based on the bridge geometry, and c) adjustment of the unit response curves to give a best fit to the known loads applied by the calibration vehicle. Each sensor location is calibrated differently. The axle weights are considered to be moving loads, and the effect of their mass is neglected compared to the mass of the bridge. This approach assumes linearity and the principle of superposition when several loads are applied to the bridge at the same time.

The total strain response ε_k from a bridge due to a truck crossing can be modelled with a dynamic model based on constant loads. The total theoretical strain $\widetilde{\varepsilon}_k(t)$ at a certain location k can be approximated as a function of the applied axle weights W_i and the total (static + dynamic) strain response due to a unit moving load, $\varepsilon_{ki}(t)$ (Section 5.3) as follows:

$$\widetilde{\varepsilon}_k(t) = \sum_{i=1}^{n} \varepsilon_{ki}(t) W_i \tag{7.28}$$

where n is the number of axles. In matrix form,

$$\{\widetilde{\varepsilon}\}_{kx1} = [\varepsilon]_{kxn} \{W\}_{nx1} \tag{7.29}$$

If there are a number of sensors, k, equal to the number of axles n, it is possible to formulate the following system of equations at each instant, t:

$$\{W\}_{nx1} = [\varepsilon]_{nxn}^{-1} * \{\widetilde{\varepsilon}\}_{nx1} \tag{7.30}$$

where:

$\{\widetilde{\varepsilon}\}_i$: measured strain due to the total applied load at longitudinal location i,

$[\varepsilon]_{ij}$: theoretical strain at sensor location i due to a unit moving load located at j,

$\{W\}_j$: applied load at location j,

n : total number of axles on the bridge.

The system of equations 7.30 is limited by the vehicle length and weight, which is assumed to be negligible compared to the corresponding length and weight of the bridge (long span bridges). It is therefore invalid for shorter bridges. However, the simulations described in this section would suggest that it gives results that are useful, being more accurate than existing static methods. On this basis, the method is being investigated further, despite the fact that it is theoretically unproven at this time.

There are certain critical locations: i.e., at the start and end of the bridge where small strains introduce rounding errors (these locations should not be considered in the calculations). If the determinant of the influence line matrix, $|\varepsilon|$ is null for a combination of sensors, it is necessary to choose a different location. The value of this determinant will be analysed in Section 7.3.2.

The spectrum of the calculated axle loads $\{W\}$ can be obtained. The static value is the component of zero frequency of this spectrum. In practice, the static value is obtained through the root mean square of all instantaneous axle values.

Theoretical testing

Theoretical bridge-truck interaction models are used to generate strains at different locations along the bridge that allow the feasibility of the multiple-sensor system to be studied. Road surface irregularities are idealised as a stochastic process and generated from power spectral density functions as suggested by the International Standards Organisation. The bridge modelled is a simply supported 20 m single span with a first natural frequency of 4.26 Hz and 1% damping. Bending strains are obtained numerically at 9 different locations equally spaced along the bridge length. A 2-axle vehicle is modelled numerically (Figure 7.3) to analyse the influence of truck parameters during calibration. The data for the vehicle is given in Section 7.2.4. The performance of the dynamic multiple-sensor Bridge WIM algorithm is compared to a static approach (Moses 1979) for each simulation.

Figure 7.16 shows the information on strains required for the application of the algorithm. Referring to Equation 7.30, Figures 7.16(a), (c) and (e) give the components of the influence line matrix $[\varepsilon]$ for each sensor and load position. Figures 7.16(b), (d) and (f)

present the variation in the components of $\{\widetilde{\varepsilon}\}$, the simulated strains at different fixed points, with distance travelled by the moving load.

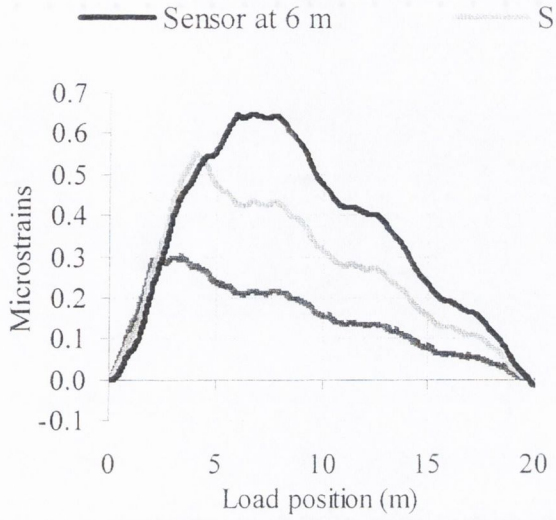

(a) Total strain due to a moving unit load at sensor locations: 2, 4 and 6 m

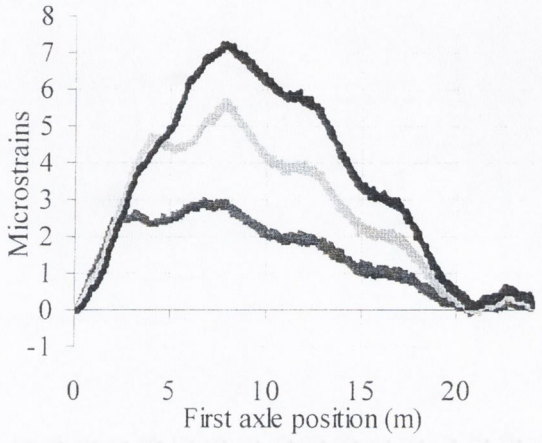

(b) Total strain due to a 2-moving axle body at sensor locations: 2, 4 and 6 m

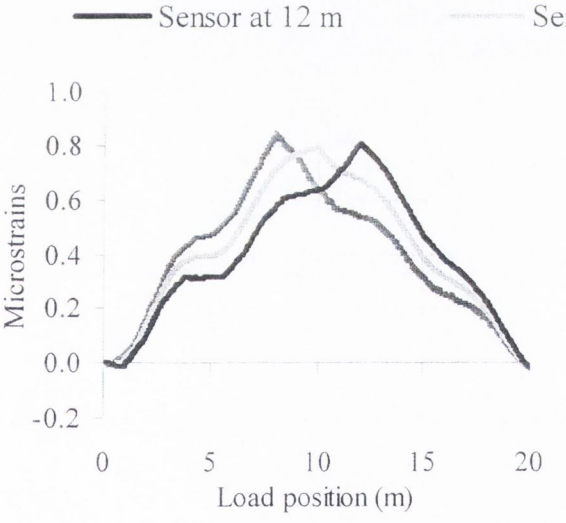

(c) Total strain due to a moving unit load at sensor locations: 8, 10 and 12 m

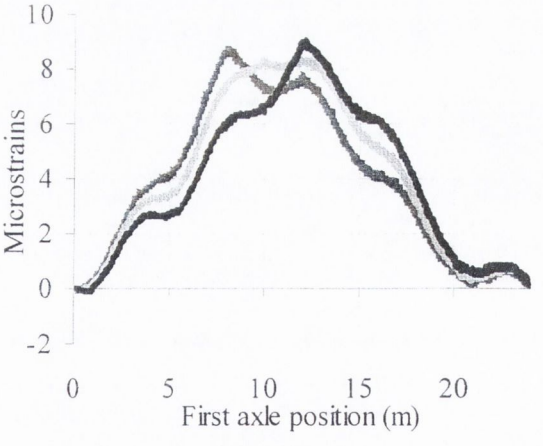

(d) Total strain due to a 2-moving axle body at sensor locations: 8, 10 and 12 m

Figure 7.16 (continued on following page)

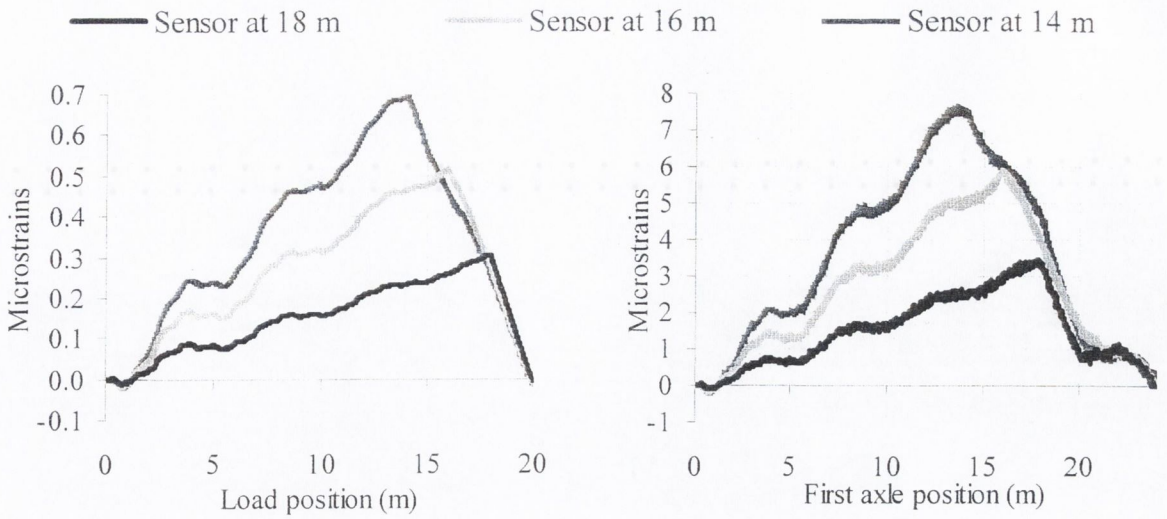

(e) Total strain due to a moving unit load at sensor locations: 14, 16 and 18 m

(f) Total strain due to a 2-moving axle body at sensor locations: 14, 16 and 18 m

Figure 7.16 – Total strain in different sensor locations

Figure 7.17(a) presents the variation of a calculated axle load, one component of $\{W\}$, with distance along 2 meters of the bridge. The corresponding applied axle load used for the simulation is included for comparison. Figure 7.17(b) is the spectrum of the predicted load variation for the first axle. From this spectrum an accurate static value of 6 tonnes can be obtained, in excellent agreement with the actual weight. A root mean square of all instantaneous axle values is generally preferred to obtain the static value.

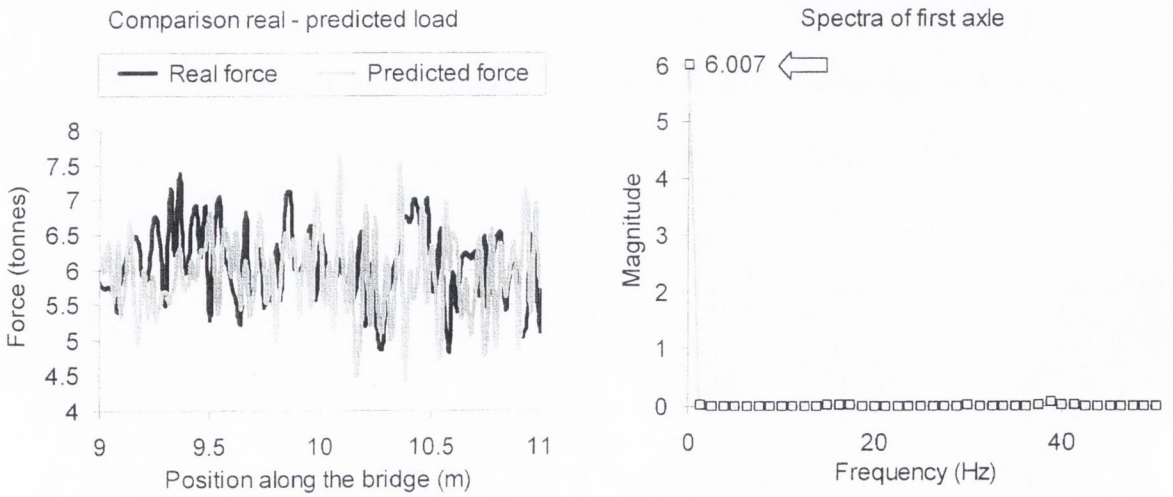

(c) Determination of instantaneous force

(d) Spectra of axle load history

Figure 7.17 – Short-term calculation

The accuracy of BWIM algorithms is sensitive to changes in some truck mechanical characteristics as compared to those used during calibration. The effect of altering certain vehicle parameters on the dynamic algorithm is studied by modifying its value by a percentage while leaving the rest of the parameters unaltered. Some of these parameters are a distribution of load between axles, axle spacing and tyre stiffness. The gross vehicle weight is the same in each case. The performance of the dynamic multiple-sensor Bridge WIM algorithm is compared to a static approach (Moses 1979). Figures 7.18(a) and (b) give the maximum relative error in weights for both the static and the new algorithms due to differences in the axle spacing and the position of the centroid of the body mass. Both algorithms are very accurate when there is only a change in axle spacing of the calibration truck. While the static algorithm gets more inaccurate when both axles are very closely spaced (tandem configurations), the new algorithm achieves the same degree of accuracy. When the body weight distribution between the axles changes, the dynamic algorithm is generally more accurate and shows a smaller standard deviation.

In the same way, the influence on accuracy of a difference in tyre stiffness is illustrated in Figure 7.18(c). A significant error appears for a decrease of 25% in the tyre stiffness as a result of a lower axle hop frequency. This very low frequency yields an average value far from the static weight. Figure 7.18(d) represents the applied load against axle position for this case. The inaccuracy is a consequence of the reduced number of available cycles of strain readings due to bridge length and speed. This limitation prevents the removal of that low frequency component in the spectrum. However, the 0.2 Hz frequency of this example is only a theoretical case, not a realistic one. In practice, these truck frequencies will be around 2 Hz, which correspond to an increase of the tyre stiffness in the graph. For these cases, the performance of both algorithms is good. The results show an improvement in the estimation of axle weights and a significantly smaller standard deviation when applying the multiple-sensor algorithm.

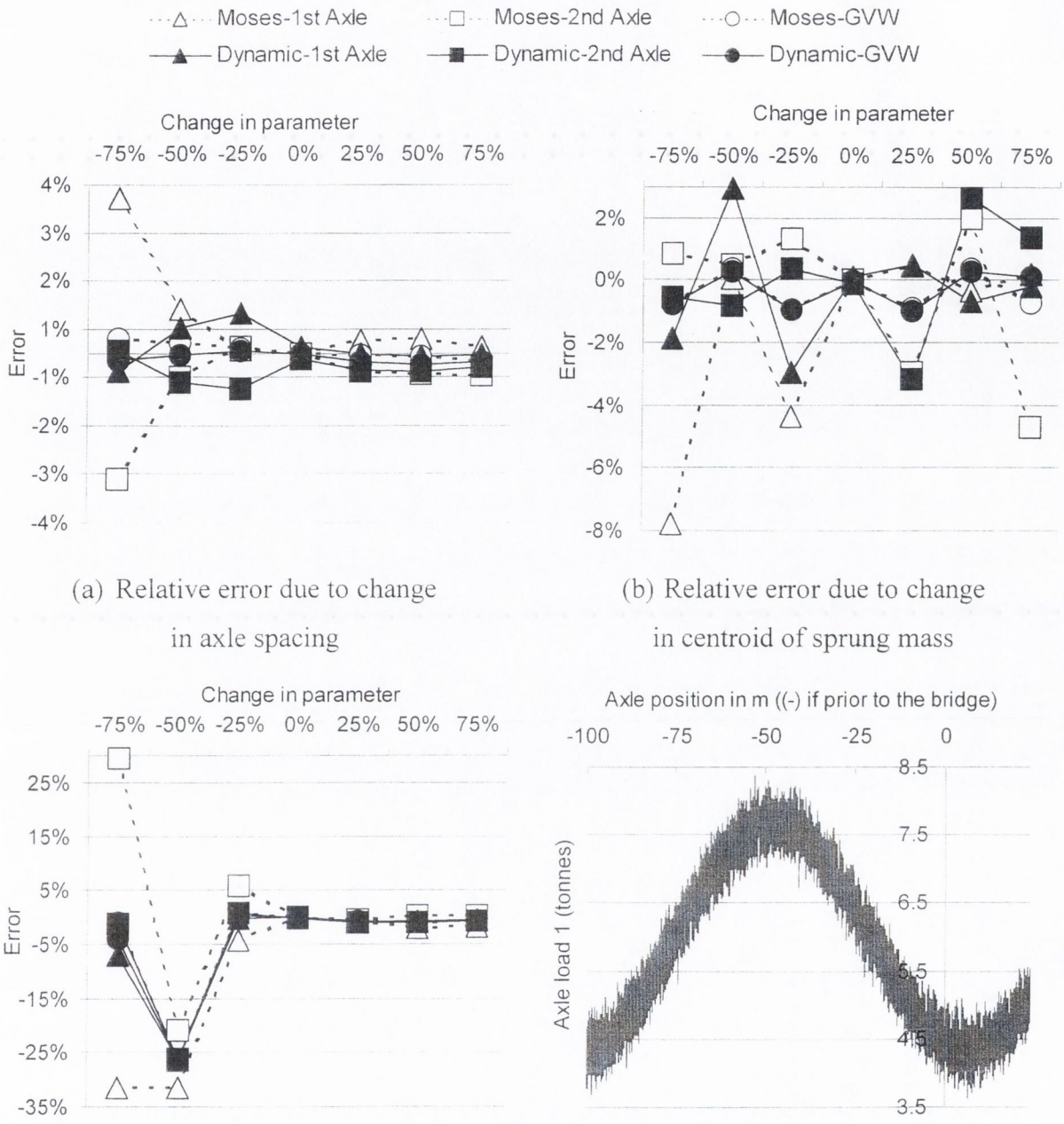

(a) Relative error due to change in axle spacing

(b) Relative error due to change in centroid of sprung mass

(c) Relative error due to change in tyre stiffness

(d) Applied load in the case of a decrement of 25% in tyre stiffness

Figure 7.18 – Effect on accuracy of the change of vehicle mechanics

Advantages and Disadvantages

The new algorithm achieves a considerable reduction in errors for individual axle weights. It is also less sensitive to truck mechanical characteristics than the traditional static approach. The traditional static algorithm is still very competitive for GVW. Some improvements introduced by the new approach are:

- There is always an error in the evaluation of a static axle load derived from the limitation in the definition of the applied load with time (Small samples are too sensitive to road profile, truck mechanics, etc.). This problem is significantly reduced with bridges where load can be defined for most of the bridge length based on the new approach introduced herein. Low speeds benefit this calculation. From spectral analysis of the varying axle loads, other frequency components can also be studied and mechanical characteristics of the truck collected depending on the road surface.
- No filtering of the strain signal is required. Bridge dynamics are removed during application of the dynamic equations of the algorithm. After applying the algorithm, the behaviour of the truck loads remains. Hence, the danger is removed of suppressing a significant static component through filtering over a relatively low first natural frequency of the bridge, especially if the vehicle speed is high and/or the axle spacings are small.

7.5.2 A Least Squares Fitting Multiple-sensor Algorithm

This section presents a further development on the approach initiated by Kealy & O'Brien. The algorithm formulates a system of static equations at each instant. Each of these equations is based on the influence line for each sensor location at each instant. However, this static approach has limitations due to the dependency of the equations, which relate applied load to measured strain. The equations can be solved for a limited number of axles related to the degree of indeterminacy of the structure: 2 axles in a single span, 3 in a continuous 2-span bridge, etc. The procedure that follows overcomes the limitations of the original approach by using a lot of sensors and applying an optimisation technique. The same technique can be applied to the dynamic multiple-sensor algorithm from the previous section.

The coefficients of the matrix $[\varepsilon]$ in Equation 7.30 can be calculated taking as reference the total answer due to a single load (dynamic multiple-sensor B-WIM) or the influence lines (static multiple-sensor B-WIM). If the determinant $|\varepsilon|$ is null, there will not be solution. The influence lines corresponding to the example in Figure 7.16 are represented in Figures 7.19(a), (c) and (e). The static strain depends directly on the applied load, its location on the bridge, the Young's modulus and section modulus at the sensor location. This static strain is directly proportional to the applied load. The differences between the

theoretical static and dynamic strain due to a unit moving load are shown in Figures 7.19(b), (d) and (f). As expected, the dynamic deviation is higher for the locations near midspan. This dynamic strain corresponds to a moving load travelling at 20 m/s. Unlike the static component, the total strain for a given load depends on its speed, so there is a different reference for each speed.

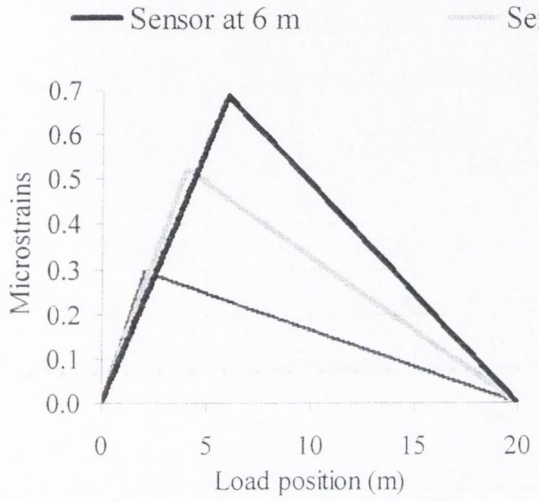

(a) Influence lines at 2, 4 and 6 m

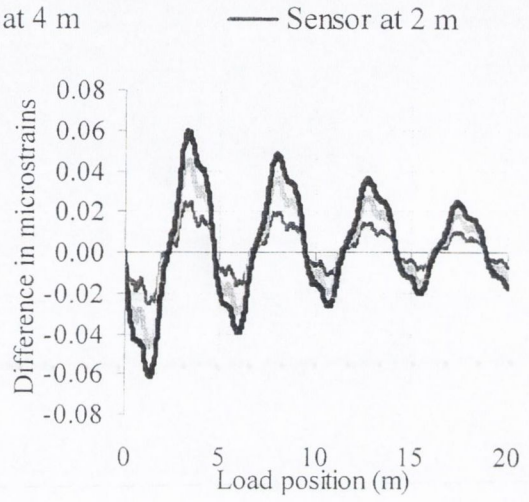

(b) Difference between dynamic answer due to a unit load and influence lines of (a)

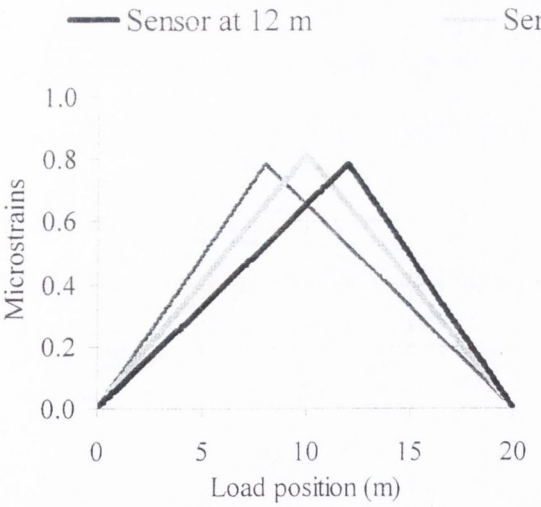

(c) Influence lines at 8, 10 and 12 m

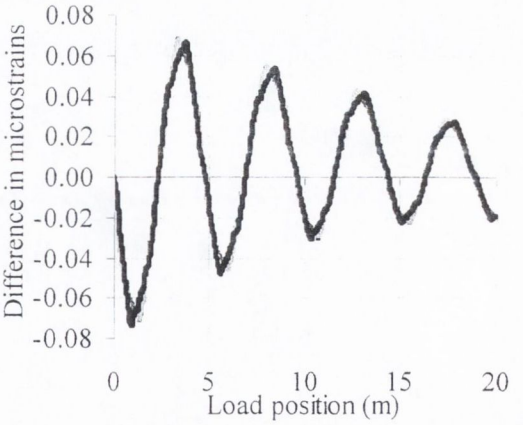

(d) Difference between dynamic answer due to a unit load and influence lines of (c)

Figure 7.19 (continued on following page)

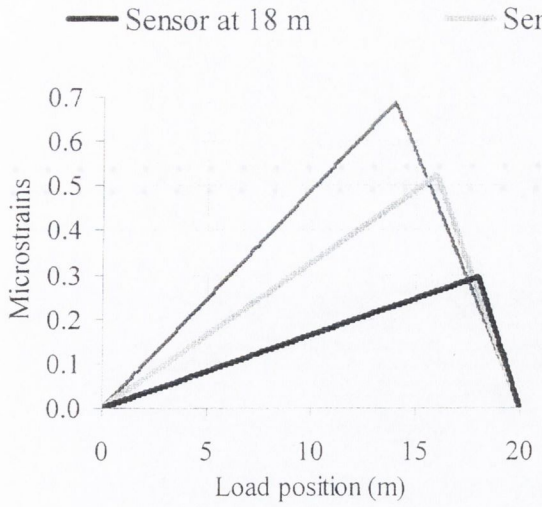

(e) Influence lines at 14, 16 and 18 m

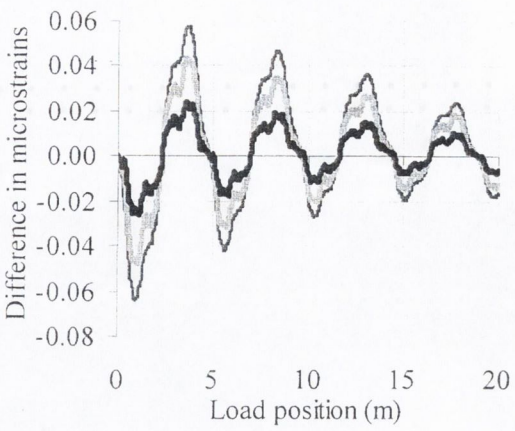

(f) Difference between dynamic answer due to a unit load and influence lines of (e)

Figure 7.19 – Static response for 9 different locations equally spaced along the bridge

The value of the determinant obtained by applying the static and dynamic multiple-sensor B-WIM systems are compared in Figure 7.20. The static and total responses due to a unit load represented in Figures 7.19 and 7.16 respectively are used to generate the determinant for different combination of sensors. The values of the determinant are given since the first axle is at 4 m from the bridge support. This is the vehicle axle spacing and the position where simultaneous calculation of the two axles start.

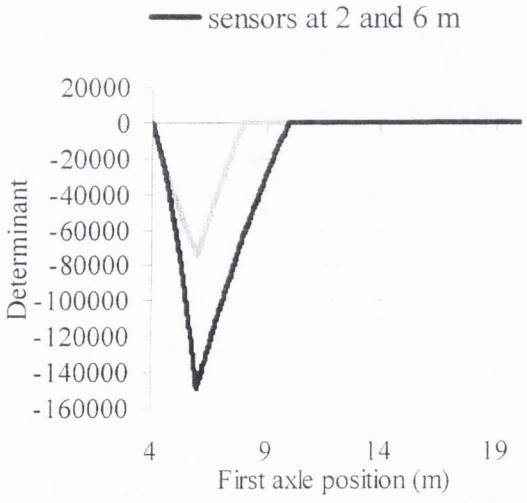

(a) Determinant by static MS-BWIM

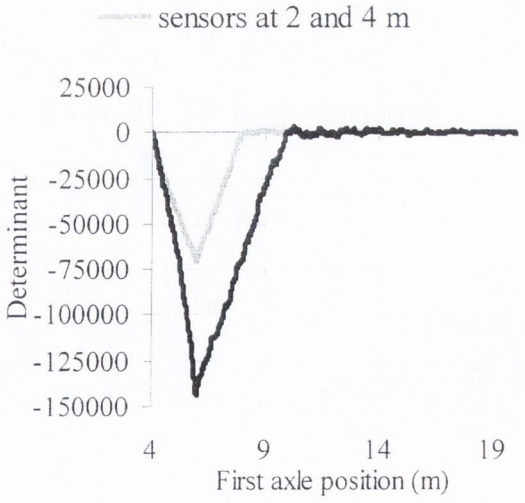

(b) Determinant by dynamic MS-BWIM

Figure 7.20 (continued on following page)

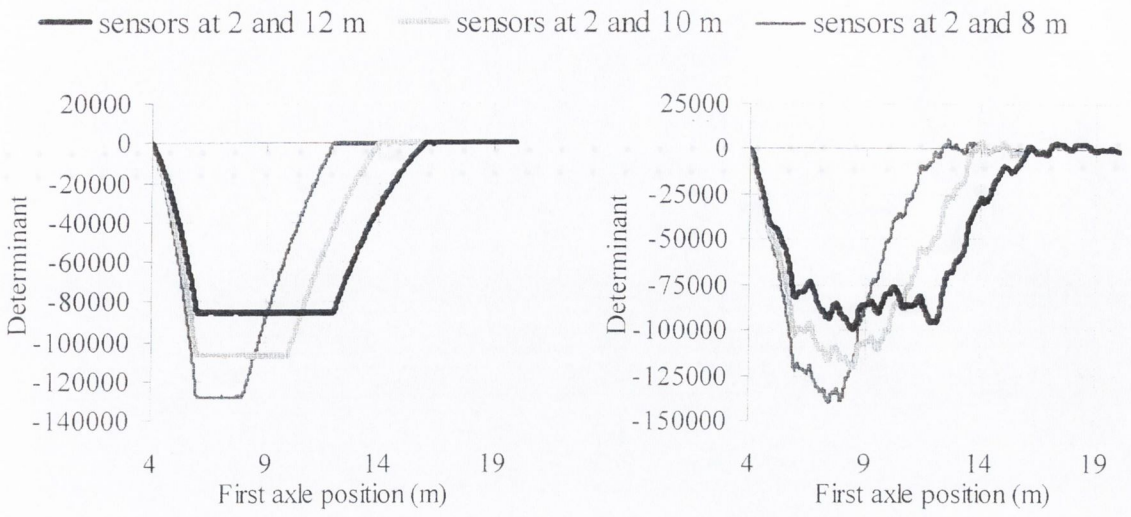

(c) Determinant by static MS-BWIM (d) Determinant by dynamic MS-BWIM

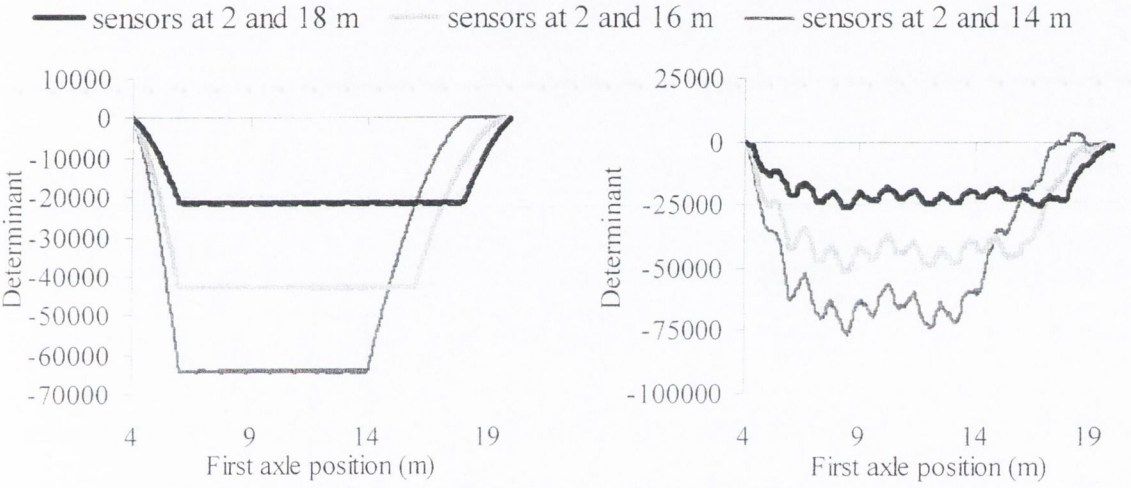

(e) Determinant by static MS-BWIM (f) Determinant by dynamic MS-BWIM

Figure 7.20 – Values of determinant for different combinations of two sensors

If a minimum number of sensors is chosen (this is, same as number of axles: 2 in this case), solution is only possible in a fixed portion of the bridge. Instantaneous axle calculations by a static and dynamic MS-BWIM are represented in Figures 7.21 and 7.22 for the front and rear axles respectively. If using two sensors, instantaneous calculation is feasible in those sections of the bridge where the determinant is high enough. The maximum value of this determinant generally takes place when the vehicle is between both sensors (the exact location depends on the influence line and the axle spacing) and it becomes zero when the vehicle moves away from this space between them. Thus, when using sensors at 2 and 4 m, instantaneous axle values can only be obtained before the first axle reaches 7 m from the start of the bridge. If using sensors at 2 and 6 m, calculations can be further extended to 9 m.

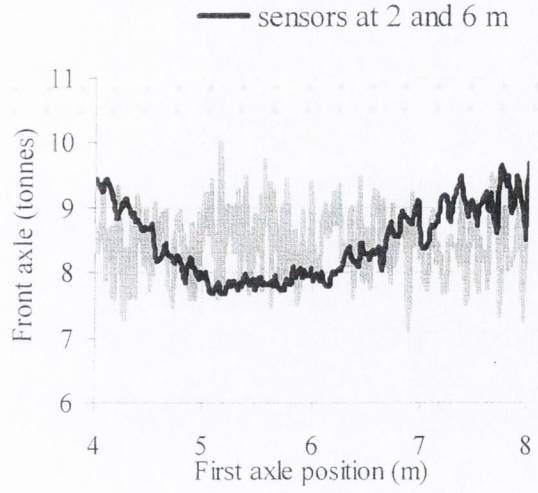

(a) Static MS-BWIM (at 2 and 6 m)

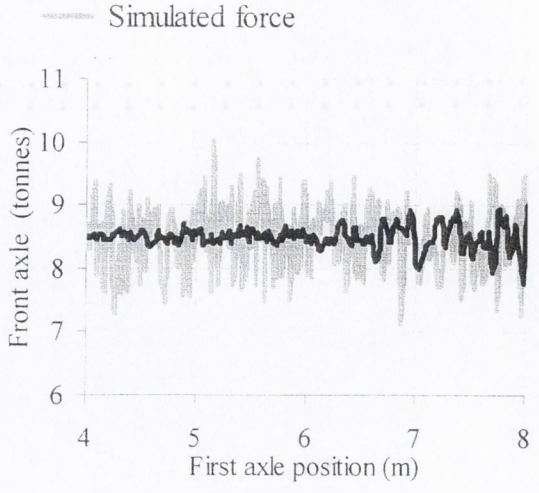

(b) Dynamic MS-BWIM (at 2 and 6 m)

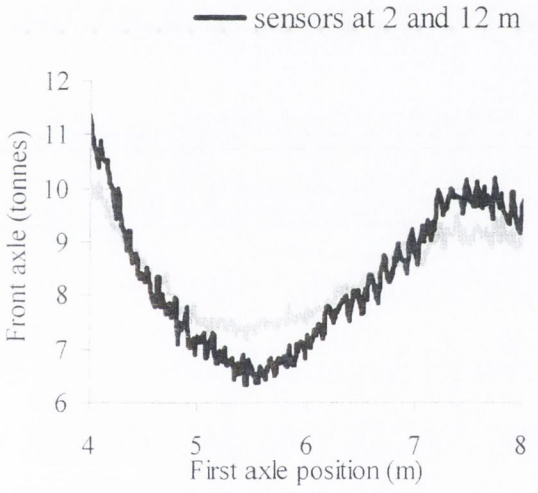

(c) Static MS-BWIM (at 2, 8 and 12 m)

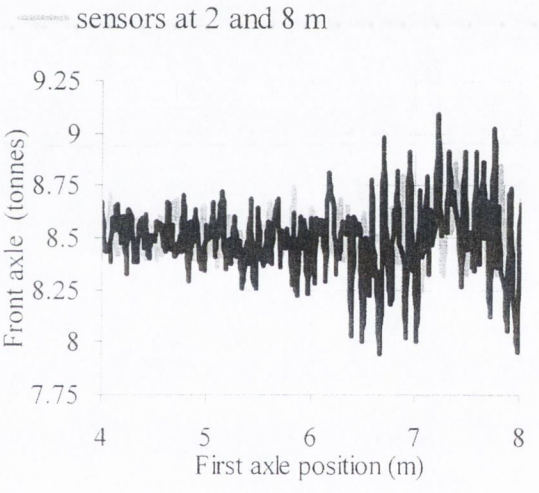

(d) Dynamic MS-BWIM (at 2, 8 and 12 m)

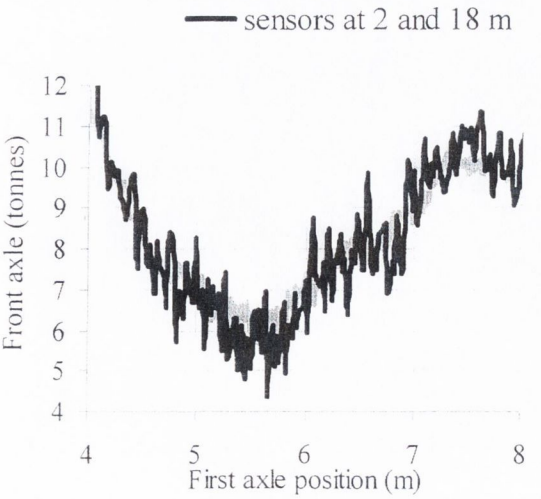

(e) Static MS-BWIM (at 2, 14 and 18 m)

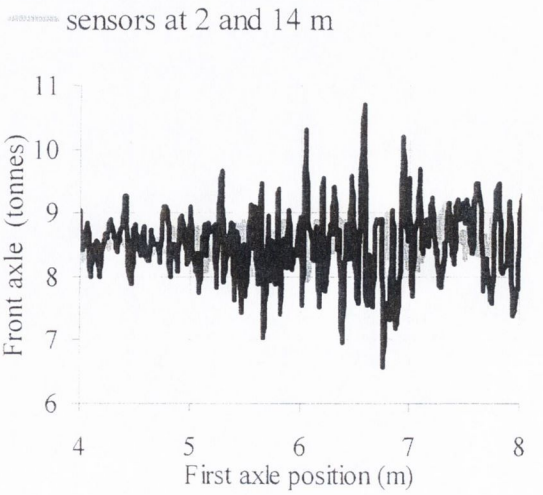

(f) Dynamic MS-BWIM (at 2, 14 and 18 m)

Figure 7.21 – Instantaneous calculation of front axle weight for combinations of 2 sensors

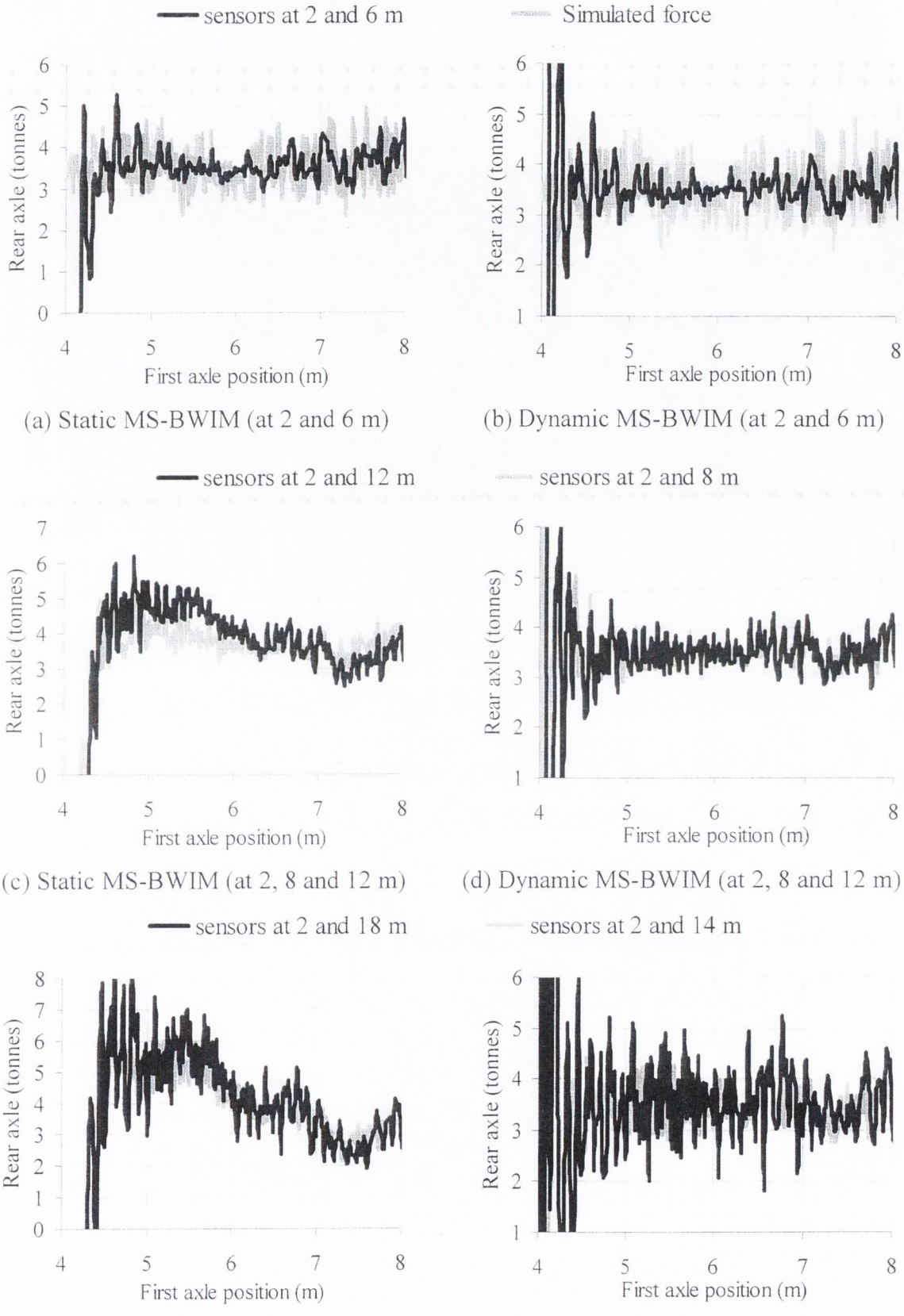

(a) Static MS-BWIM (at 2 and 6 m)

(b) Dynamic MS-BWIM (at 2 and 6 m)

(c) Static MS-BWIM (at 2, 8 and 12 m)

(d) Dynamic MS-BWIM (at 2, 8 and 12 m)

(e) Static MS-BWIM (at 2, 14 and 18 m)

(f) Dynamic MS-BWIM (at 2, 14 and 18 m)

Figure 7.22 – Instantaneous calculation of rear axle weight for combinations of 2 sensors

The criterion to stop calculations can be established by the instant when the root mean square of the axle history tends towards infinity. Figure 7.23 represents the root mean square of accumulated instantaneous calculations by the dynamic MS-BWIM algorithm in Figure 7.21.

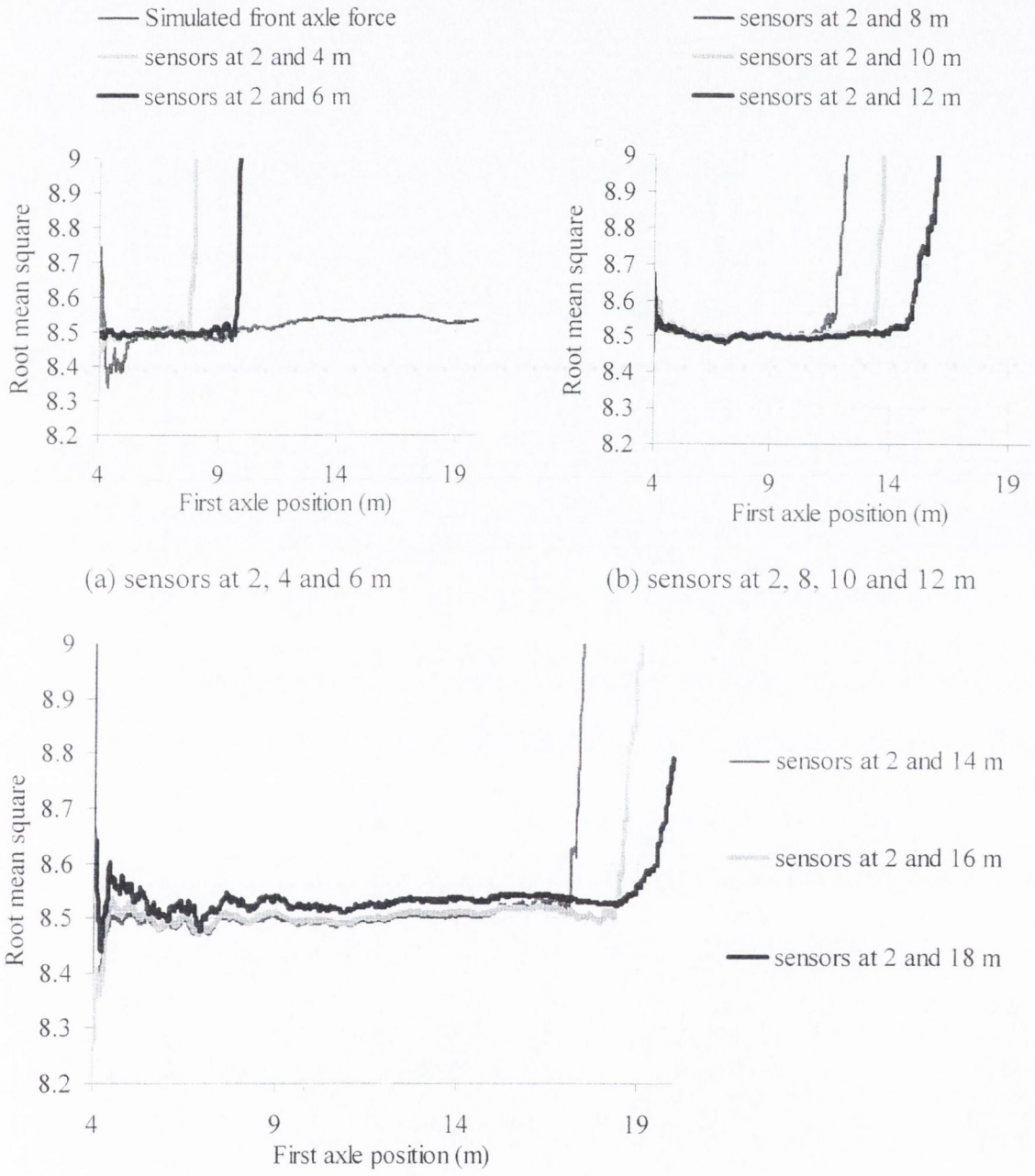

(a) sensors at 2, 4 and 6 m

(b) sensors at 2, 8, 10 and 12 m

(c) sensors at 2, 14, 16 and 18 m

Figure 7.23 – Values of root mean square for front axle and combinations of 2 sensors

A longer force-time history could be obtained by using sensors at both ends of the bridge. However, for a simply supported bridge, strain in locations close to the bridge supports is

small and hence, it is not very sensitive to changes in traffic loads. Some combinations of sensors give null determinant or very small values (prone to numerical instability) as shown in Figure 7.24. Sensors at 6 and 16 m could achieve a reasonable result along most of the bridge length.

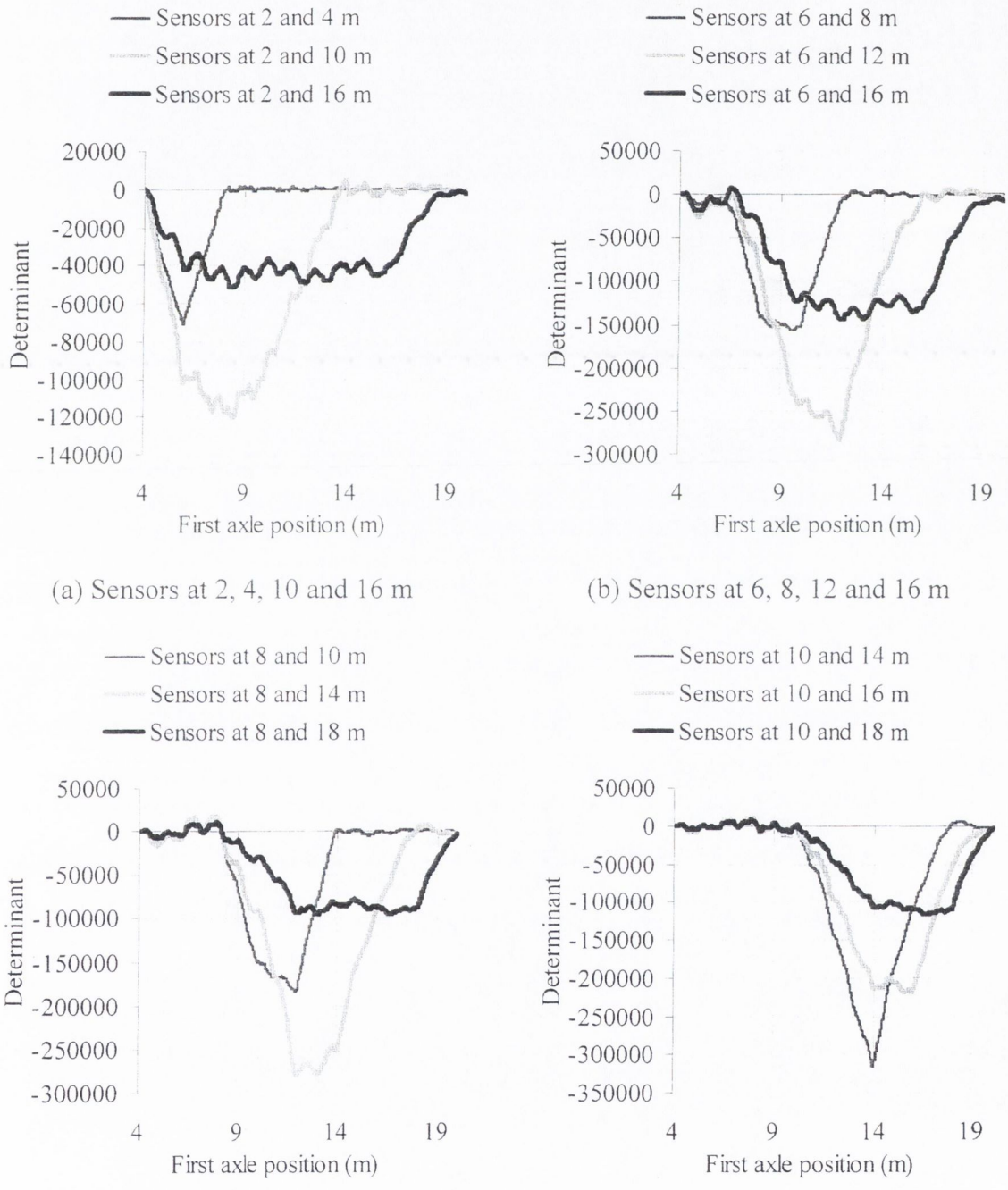

(a) Sensors at 2, 4, 10 and 16 m

(b) Sensors at 6, 8, 12 and 16 m

(c) Sensors at 8, 10, 14 and 18 m

(d) Sensors at 10, 14, 16 and 18 m

Figure 7.24 – Values of determinant for different combination of two sensors and dynamic MS-BWIM algorithm

The main shortcoming of this approach arises from considering truck configurations of 3 or more axles. Then, the determinant becomes zero along most of the bridge, regardless of the combination of sensors used for the calculation. Figure 7.25 illustrates the value of the determinant obtained by the static MS-BWIM algorithm if using combinations of 3 sensors (this is the minimum number required to solve a 3-axle truck).

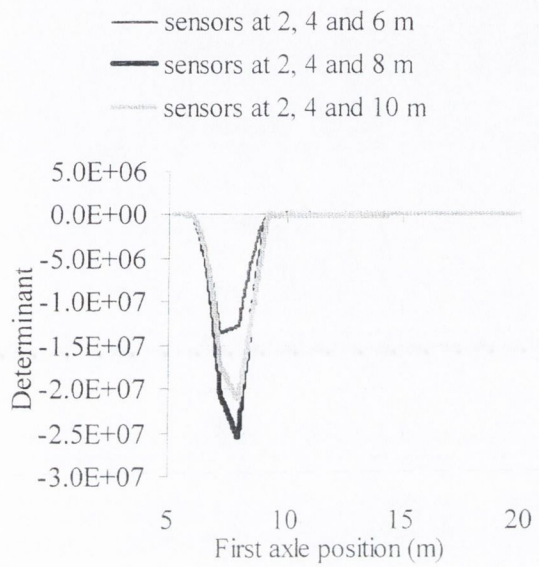

(a) sensors at 2, 4, 6, 8 and 10 m

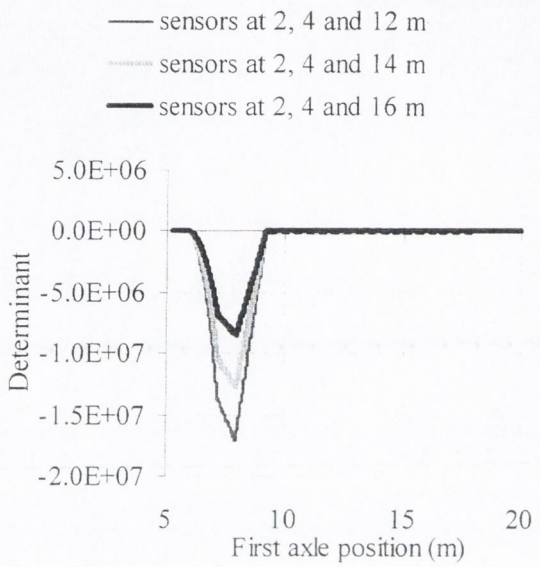

(b) sensors at 2, 4, 12, 14 and 16 m

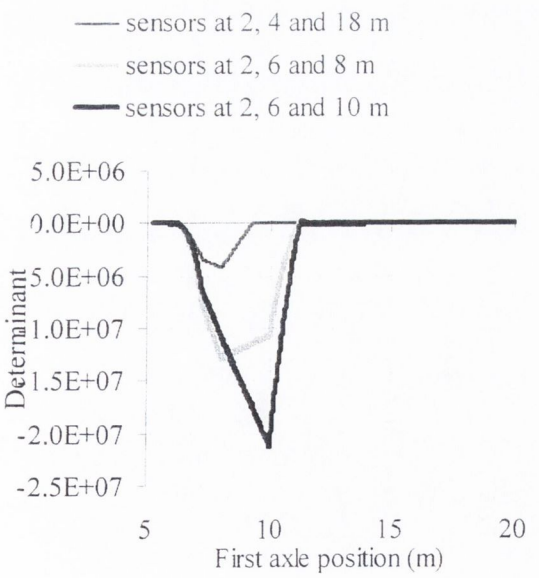

(c) sensors at 2, 4, 6, 8, 10 and 18 m

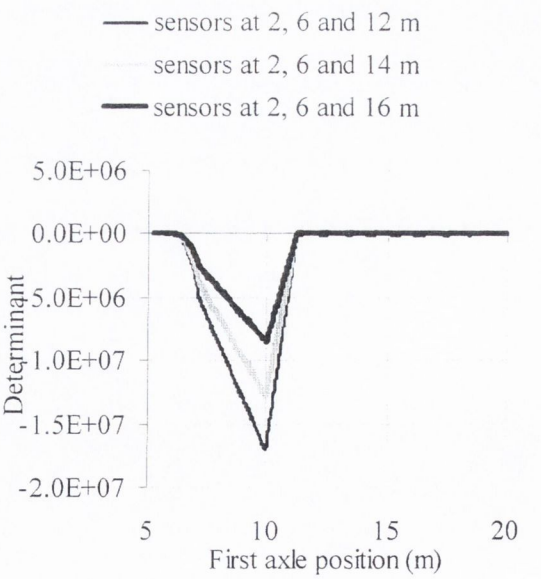

(c) sensors at 2, 6, 12, 14 and 16 m

Figure 7.25 – Values of determinant for combinations of 3 sensors

Figure 7.26 shows the value of the determinant obtained by the static and dynamic MS-BWIM algorithms if using combinations of 4 sensors (minimum number to solve the presence of 4 axles on the bridge). In either case, as the number of axles increases, the bridge length where solution is feasible, decreases.

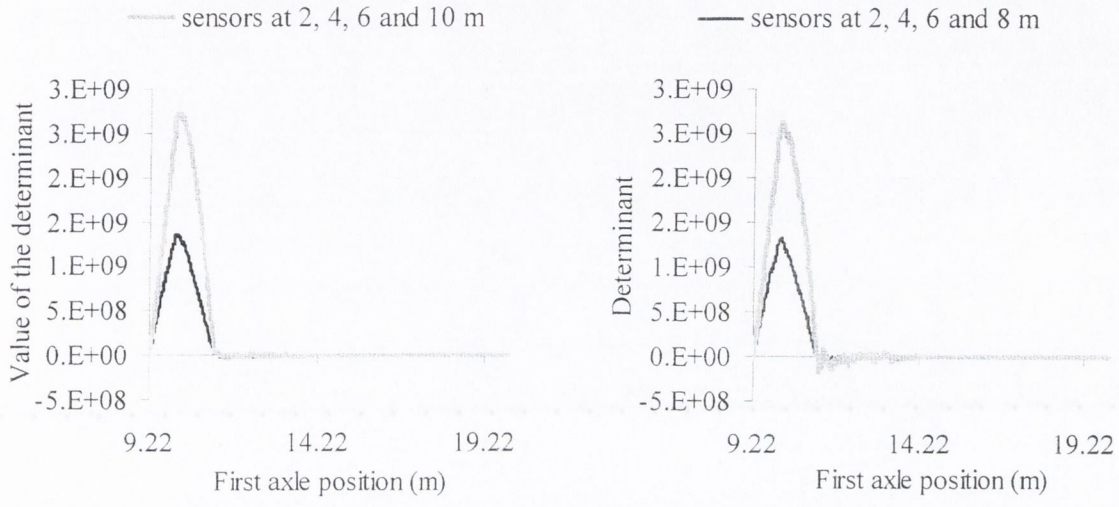

(a) Static MS-BWIM (b) Dynamic MS-BWIM

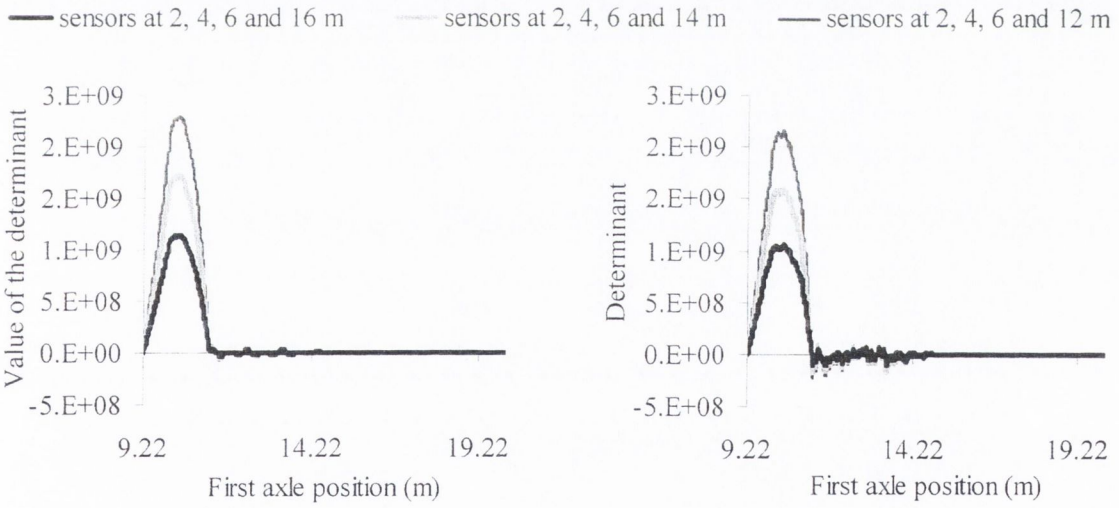

(a) Static MS-BWIM (b) Dynamic MS-BWIM

Figure 7.26 (continued on following page)

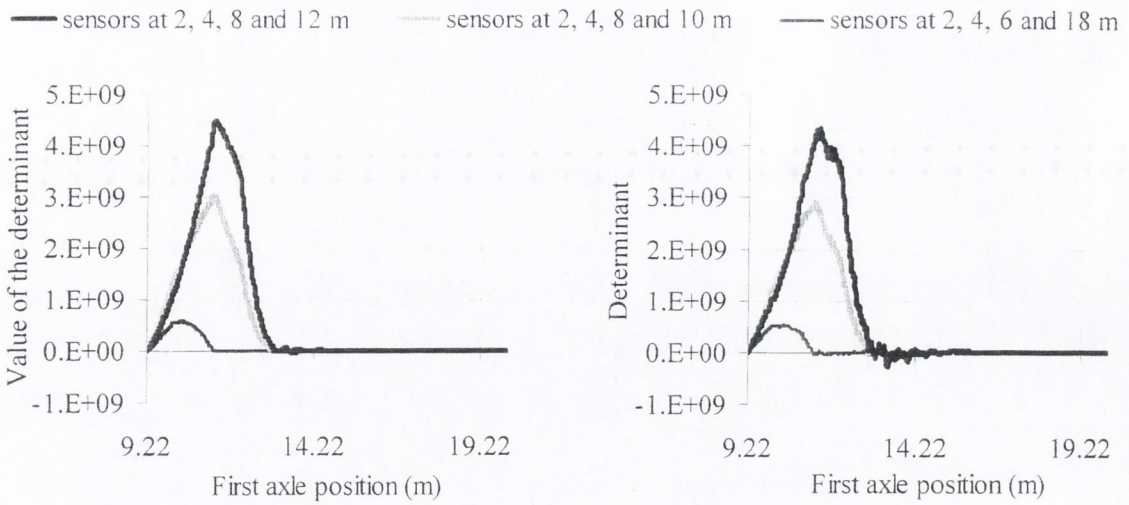

(a) Static MS-BWIM (b) Dynamic MS-BWIM

Figure 7.26 – Values of determinant for combinations of 4 sensors

If using more sensors and a least squares fitting technique, it is possible to solve for a higher number of axles and the length where solution is possible increases. This instantaneous calculation along the length of the bridge requires a lot of sensors, well in excess of the number of axles. If there are a number of sensors, m, equal or greater than the number of axles n, it is possible to minimise the error function defined in Equation 7.31:

$$f = \sum_{k=1}^{k=m} (\varepsilon_k - \widetilde{\varepsilon}_k)^2 \quad \text{at each instant } t \tag{7.31}$$

where ε_k is the theoretical total strain due to the applied load at location k and $\widetilde{\varepsilon}_k$ is the measured strain due to the applied load at location k.

By assuming linearity and applying the principle of superposition, it is possible to express the strain at each sensor as:

$$\varepsilon_k = \varepsilon_{k1} W_1 + \varepsilon_{k2} W_2 + \ldots + \varepsilon_{kn} W_n \tag{7.32}$$

By combining Equations 7.31 and 7.32:

$$f = \sum_{k=1}^{k=m} (\varepsilon_{k1} W_1 + \varepsilon_{k2} W_2 + ... + \varepsilon_{kn} W_n - \widetilde{\varepsilon}_k)^2 \text{ at each instant } t \tag{7.33}$$

Differentiating Equation 7.33 with respect to the axle weight, W_i and setting it equal to zero gives:

$$\frac{df}{dW_i} = 2\sum_{k=1}^{k=m} (\varepsilon_{k1} W_1 + \varepsilon_{k2} W_2 + ... + \varepsilon_{kn} W_n - \widetilde{\varepsilon}_k)\varepsilon_{ki} = 0 \tag{7.34}$$

The full set of equations can be expressed in matrix form as:

$$\begin{bmatrix} \sum_{k=1}^{k=m} \varepsilon_{k1}\varepsilon_{k1} & \sum_{k=1}^{k=m} \varepsilon_{k2}\varepsilon_{k1} & \cdot & \sum_{k=1}^{k=m} \varepsilon_{kn}\varepsilon_{k1} \\ \sum_{k=1}^{k=m} \varepsilon_{k1}\varepsilon_{k2} & \sum_{k=1}^{k=m} \varepsilon_{k2}\varepsilon_{k2} & \cdot & \sum_{k=1}^{k=m} \varepsilon_{kn}\varepsilon_{k2} \\ \cdot & \cdot & \cdot & \cdot \\ \sum_{k=1}^{k=m} \varepsilon_{k1}\varepsilon_{kn} & \sum_{k=1}^{k=m} \varepsilon_{k2}\varepsilon_{kn} & \cdot & \sum_{k=1}^{k=m} \varepsilon_{kn}\varepsilon_{kn} \end{bmatrix} \begin{Bmatrix} W_1 \\ W_2 \\ \cdot \\ W_n \end{Bmatrix} = \begin{Bmatrix} \sum_{k=1}^{k=m} \widetilde{\varepsilon}_k\varepsilon_{k1} \\ \sum_{k=1}^{k=m} \widetilde{\varepsilon}_k\varepsilon_{k2} \\ \cdot \\ \sum_{k=1}^{k=m} \widetilde{\varepsilon}_k\varepsilon_{kn} \end{Bmatrix} \tag{7.35}$$

where:

$\widetilde{\varepsilon}_k$: measured strain due to the total applied load at sensor location k,

ε_{ij} : theoretical strain at sensor location i due to moving load located at j (influence line in the static approach, or dynamic response due to a unit load in the dynamic case),

W_j : applied load at location j,

n : total number of axles on the bridge.

Finally, applied loads (weights) can be calculated from Equation 7.36:

$$\{W\}_{nx1} = [\varepsilon]_{nxn}^{-1} \{\widetilde{\varepsilon}\}_{nx1} \tag{7.36}$$

If the number of strain sensor locations is high enough, Equation 7.36 provides a solution along most of the bridge. The static value can be obtained from the root mean square of the calculated instantaneous axle forces.

The value of the determinant $|\varepsilon|$ at each instant for a 2-axle truck on a 20 m simply supported bridge with sensors spaced every 2 m is shown in Figure 7.27. This determinant has been obtained using the static equations illustrated in Figure 7.19 and the dynamic reference of 7.16.

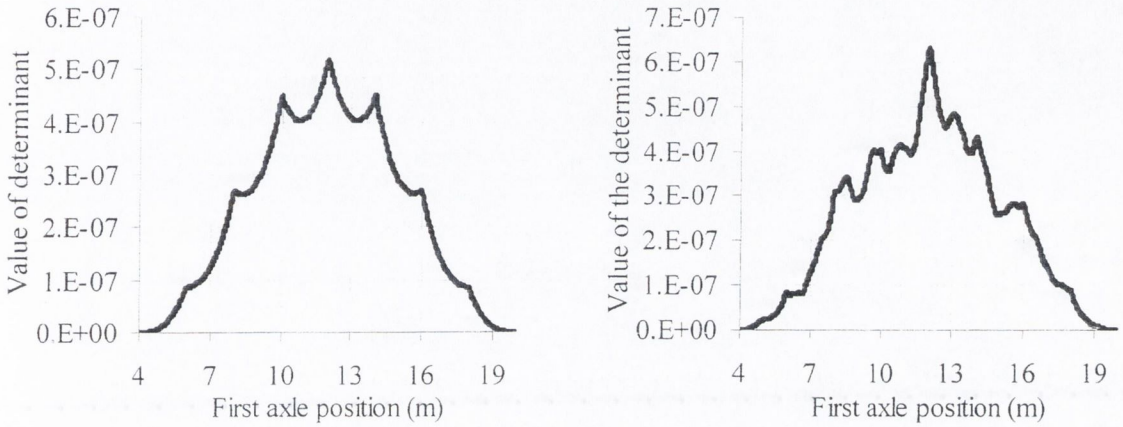

(a) Static MS-BWIM (b) Dynamic MS-BWIM

Figure 7.27 – Values of determinant $|\varepsilon|$ for each position of a 2-axle vehicle

Figure 7.28 shows the value of the determinant for a 3 and 4-axle truck respectively during the time all axles are on the bridge. Both static and dynamic multiple-sensor approaches (Figure 7.28) are able to achieve an instantaneous calculation for the time that the vehicle is on the bridge. Unlike the 'static' determinant, the 'dynamic' determinant is not symmetric.

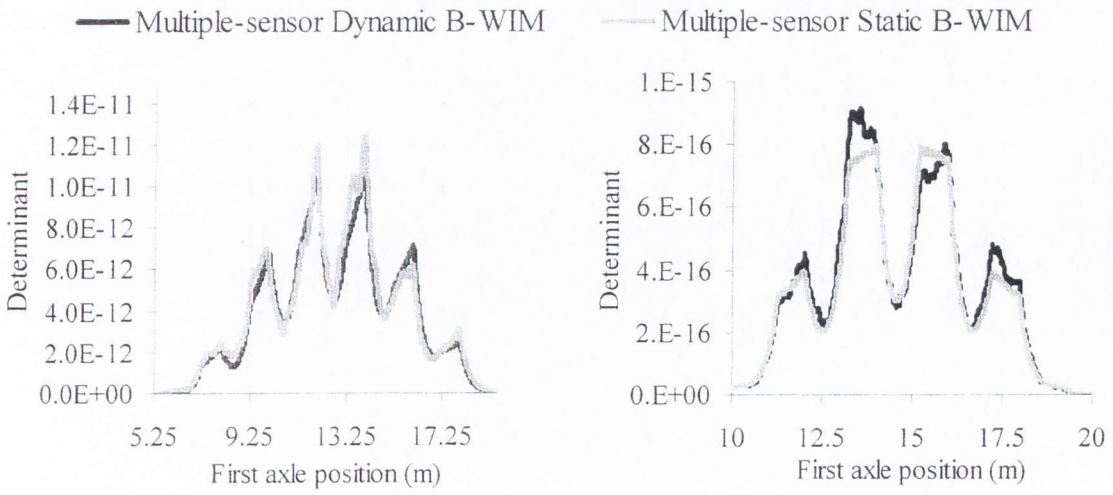

(a) 3-axle vehicle (b) 4-axle vehicle

Figure 7.28 – Values of determinant $|\varepsilon|$ for 3 and 4-axle vehicles

Figure 7.29 shows the differences between the representation of the axle load history obtained by the two multiple-sensor Bridge WIM algorithms in the case of the front axle of a moving 2-axle body vehicle. Equation 7.36 has been used for this instantaneous calculation.

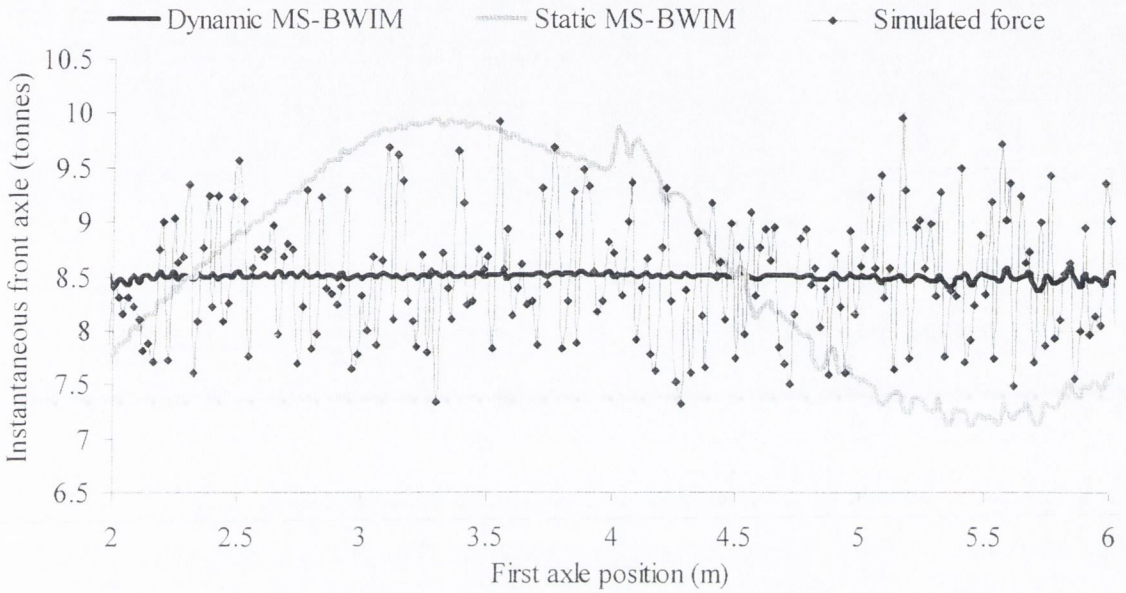

Figure 7.29 – Applied axle load calculated by 2 different multiple-sensor approaches using a least square fitting technique at each instant

The multiple-sensor systems are not able to reproduce the instantaneous applied axle forces accurately, but the dynamic system gives results around the real static weight of 8.5 tonnes along most of the bridge length. Figure 7.30 represents the whole load history of this front axle, the rear axle (static value = 3.5 tonnes) and the GVW (12 tonnes) by both multiple-sensor approaches. The estimation of instantaneous forces does not appear to be very accurate. However, the average value along the bridge can be very close to the static value if the number of readings is high enough (in particular for the static approach). The start and end of the instantaneous calculation should be avoided due to obvious rounding errors. A dynamic B-WIM algorithm based on one longitudinal location (as presented in Section 7.3) might be able to predict static weights as accurately as the multiple-sensor approach.

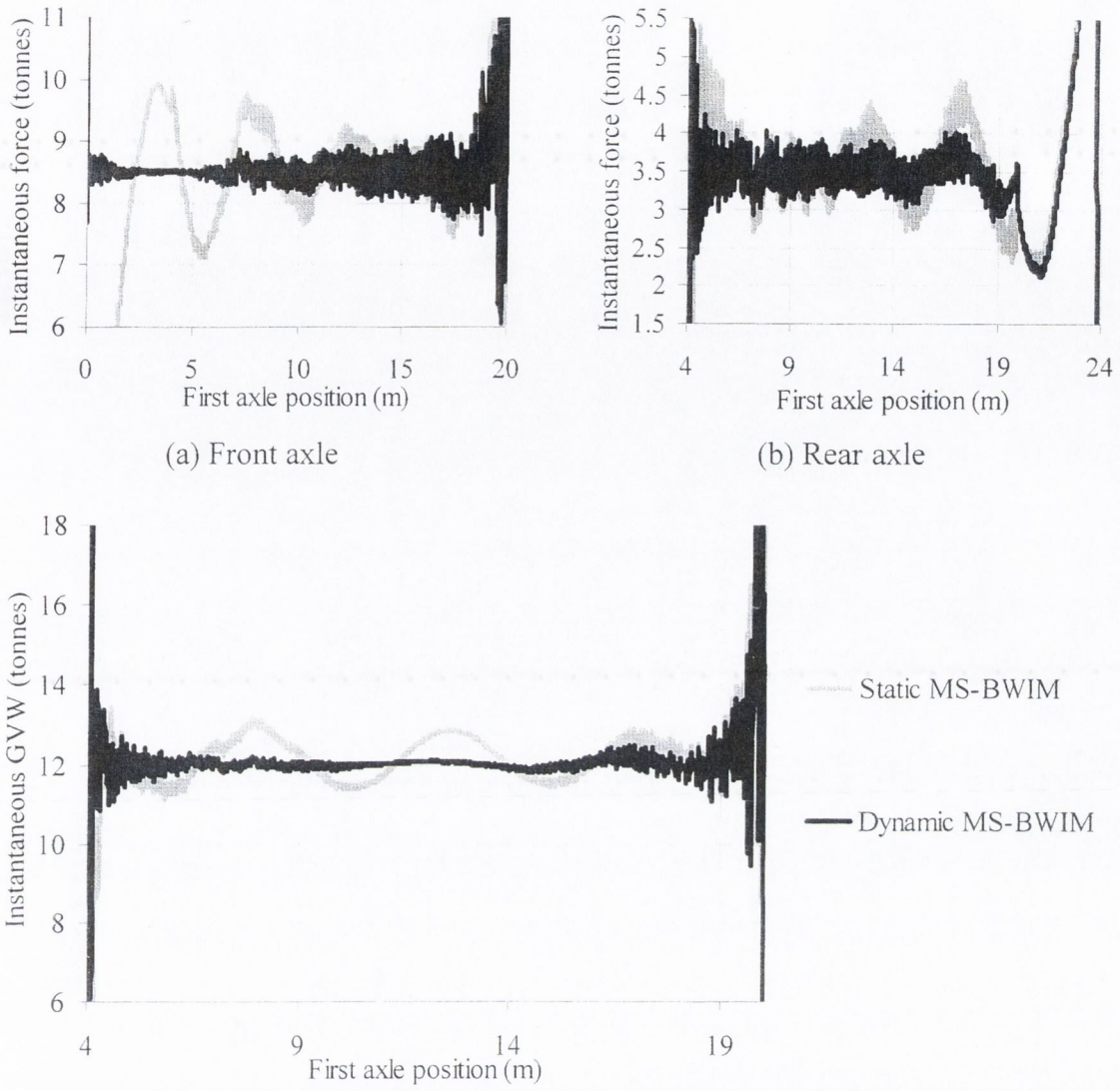

(a) Front axle

(b) Rear axle

(c) Gross Vehicle Weight

Figure 7.30 – Instantaneous forces by a multiple-sensor BWIM algorithm

7.5.3 An Algorithm based on Modal Decoupling

The approach described in this section uses strain gauges at different longitudinal locations to obtain a number of independent measurements of axle loads at each point in time. The steps involved in this dynamic algorithm based on modal decoupling are: (a) compute natural frequencies and mode shapes for the bridge, (b) calculate contribution of each mode shape from strain readings, (c) solve dynamic equation to obtain generalised load associated with each mode shape and finally (d) evaluate axle loads and gross vehicle weights from generalised load. Compared to the dynamic algorithm developed by Dempsey (Section 3.6.3), there are some improvements concerning:

- A better evaluation of the strain dynamics
- A greater number of mode shapes
- A description of the evolution of the axle load with time

(a) Compute mode shapes and frequencies

The beam displacements in a dynamic situation can be represented by:

$$z(x,t) = \sum_{i=1}^{\infty} \phi_i(x) Z_i(t) \tag{7.37}$$

where $\phi_i(x)$ represents the shape of the i^{th} mode shape, and $Z_i(t)$ represents the variation of amplitude with time of the i^{th} mode.

For a simply supported beam:

$$\phi_i(x) = \sin\left(\frac{i\pi x}{L}\right) \tag{7.38}$$

and then, the deflection is given by substituting 7.38 in 7.37:

$$z(x,t) = \sum_{i=1}^{\infty}\left[\sin\left(\frac{i\pi x}{L}\right) Z_i(t)\right] \tag{7.39}$$

And the bending moment is:

$$M(x,t) = EI\frac{\partial^2 z(x,t)}{\partial x^2} \tag{7.40}$$

By combining Equations 7.40 and 7.39:

$$M(x,t) = -EI\sum_{i=1}^{\infty}\left[\left(\frac{i\pi}{L}\right)^2 \sin\left(\frac{i\pi x}{L}\right) Z_i(t)\right] \tag{7.41}$$

Hence, bending moment can be expressed as a linear function of a series of mode shapes with amplitude $Z_i(t)$ that depends on time.

(b) Calculate contribution of each mode shape from strain readings

From Equation 7.41, measured bending strain in a particular location will be given by:

$$\varepsilon(x,t) = c\sum_{i=1}^{\infty}\left[\left(\frac{i\pi}{L}\right)^2 \sin\left(\frac{i\pi x}{L}\right)Z_i(t)\right] \tag{7.42}$$

where c is a constant. If there are strain sensors in m different longitudinal positions, it is possible to know the contribution Z_i of m mode shapes at each instant. A number of sensors higher than the number of mode shapes is required (solution through a least squares fitting technique).

The constants defining the contribution of each shape can be determined by positioning a stationary pre-weighed truck on the bridge: dynamic interaction is nil and the theoretical contribution of each mode shape can be obtained from the static bending moment diagram for that location. Once the constant for each sensor location is known, the amplitude Z_i for each shape ϕ can be derived from the strain readings for any truck at each point in time.

In matrix form:

$$\{\varepsilon\}_{mx1} = c\left[\frac{\partial^2\phi}{\partial x^2}\right]_{mxm}\{Z\}_{mx1} \tag{7.43}$$

$$\Rightarrow \{Z\}_{mx1} = \frac{1}{c}\left[\frac{\partial^2\phi}{\partial x^2}\right]^{-1}_{mxm}\{\varepsilon\}_{mx1} \tag{7.44}$$

(c) Solve dynamic equation to obtain generalised load

The values of amplitudes $Z_i(t)$ obtained in step (b) are substituted in the generalised equations of motion to obtain generalised loads. Hence, the dynamic equations for each mode shape are:

$$d^2Z_i(t)/dt^2 + 2\xi_i\omega_i(dZ_i(t)/dt) + \omega_i^2 Z_i(t) = P_i(t)/M_i \qquad (7.45)$$

where $M_i = \int \phi_i^2(x)\mu(x)dx$, and $\mu(x)$ is mass per unit length. $\mu(x)$ can be calculated during calibration if it can be assumed to be constant along the bridge. Natural frequencies (ω_i) and damping ratio (ξ_i) are determined through a Fourier analysis of a sample strain record in free vibration. Modal loads $P_i(t)$ are obtained from Equation 7.45. These generalised loads are a function of the magnitude and position of every axle load for each mode shape.

(d) Evaluate axle loads and Gross vehicle weight

The generalized load $P_i(t_1)$ (obtained in step (c)) associated with the mode shape $\phi_i(x)$ at a certain time t_1 is given by:

$$\begin{aligned} P_i(t_1) &= \int_0^L \phi_i(x)\ W(x^1,t_1)]dx \\ &= \Sigma_r[\phi_i(x_r)W_r(x_r^1,t_1)] \end{aligned} \qquad (7.46)$$

where $W_r(x_r^1,t_1)$ is the axle load r in the position x_r^1 at time t_1. That is, for a n-axle truck and m-mode shapes used in the calculation:

$$\begin{aligned} &\phi_1(x_1^1)\ W_1(x_1^1,t_1) + \phi_1(x_2^1)W_2(x_2^1,t_1) + \ldots + \phi_1(x_n^1)W_n(x_n^1,t_1) = P_1(t_1) \\ &\phi_2(x_1^1)\ W_1(x_1^1,t_1) + \phi_2(x_2^1)W_2(x_2^1,t_1) + \ldots + \phi_2(x_n^1)W_n(x_n^1,t_1) = P_2(t_1) \\ &\text{----------} \\ &\phi_m(x_1^1)\ W_1(x_1^1,t_1) + \phi_m(x_2^1)W_2(x_2^1,t_1) + \ldots + \phi_m(x_n^1)W_n(x_n^1,t_1) = P_m(t_1) \end{aligned} \qquad (7.47)$$

Adding the above equations gives:

$$[\Sigma\phi_i(x_1^1)]^* W_1(x_1^1,t_1) + [\Sigma\phi_i(x_2^1)]^*W_2(x_2^1,t_1) + \ldots + [\Sigma\phi_i(x_n^1)]^*W_n(x_n^1,t_1) = \Sigma P_i(t_1) \qquad (7.48)$$

The calculation of the applied dynamic axle load $W_r(t)$ requires a number of mode shapes equal or greater than the number of axles (those ones of greater contribution $P_i(t)$ to the total load). In matrix form:

$$[\phi]_{mxm}\{W\}_{mx1} = \{P\}_{mx1} \qquad (7.49)$$

where $n = m$ is number of axles. Weights are then obtained through:

$$\{W\}_{mx1} = [\phi]_{mxm}^{-1} \{P\}_{mx1} \tag{7.50}$$

For short span bridges, the average of the varying axle load could be far from the static value. Static axle loads can be derived from the dynamic variation of axle load with time.

A simpler approach is to solve Equation 7.45 for just one mode shape (or a small number of them) and applying a least squares fitting method. This latter approach is expressed by minimising an error function defined by the squared difference between the measured record $\Sigma[P_i(t)]$ (Equation 7.45) and the predicted record. By rearranging the result of this derivative:

$$\Sigma_T[\Sigma_r[[\Sigma\phi_i(x_r^t)]\ W_r(x_r^t,t)]\ \Sigma\phi_i(x_s^t)] = \Sigma_T[\Sigma P_i(t)\ \Sigma\phi_i(x_s^t)] \tag{7.51}$$

where $r = 1,2,..,m$ (number of axles), and $i = 1,2,...,n$ (number of mode shapes). $\Sigma\phi_i(x_s^t)$ is the value of the sum of the mode shapes corresponding to the position of the s^{th} axle at time t.

In matrix form:

$$[\Phi^*]_{mxm}\ \{W\}_{mx1} = \{P^*\}_{mx1} \tag{7.52}$$

where $\Phi^*_{rs} = \Sigma_T[\Sigma\phi_i(x_r^t)\Sigma\phi_i(x_s^t)]$, and $P_{s1}^* = \Sigma_T[\Sigma P_i(t)\Sigma\phi_i(x_s^t)]$. Then, axle weights are given by:

$$\{W\}_{mx1} = [\Phi^*]_{mxm}^{-1}\ \{P^*\}_{mx1} \tag{7.53}$$

If a number of mode shapes $n = 1$ is adopted, expressions 7.52 and 7.53 are as in Dempsey's algorithm (Section 3.6.3).

Finally, the gross vehicle weight would be given by:

$$GVW = W_1 + W_2 + \ldots + W_n \tag{7.54}$$

Even though a few mode shapes may define axle load accurately, when the contribution $Y_i(t)$ of each mode shape is calculated from measured strain in step (b), a much higher number of mode shapes is required; otherwise the results obtained in Equation 7.45 can be very poor. For a central dynamic loading, the first mode contribution provides over 98% of the central deflection, while 11 modes provide only about 97% of the total *bending moment* developed at midspan (Clough and Penzien 1975). In other words, accuracy in weight calculation increases when a higher number of longitudinal positions along the bridge is considered. This approach was the first attempt at a dynamic algorithm carried out by the author, but research was orientated in another direction due to the difficulties of implementation and testing on site (i.e. uncertainty in the modal components of the parameters, need for many sensors, etc...).

7.6 TWO-DIMENSIONAL MULTIPLE-SENSOR ALGORITHM

One-dimensional B-WIM algorithms generally add all strains obtained along the same longitudinal section to compensate for the influence of the transverse location of the truck. However, there will be differences in total strain for each path (Section 6.5.1). The magnitude of this difference will depend on the characteristics of the bridge. Even if the total bending of a bridge section is similar for different transverse locations, there is a need to deal with simultaneous traffic events. Though short span bridges might allow for one single vehicle at a time, there is always the possibility of another heavy vehicle travelling in the same or opposite direction in the adjacent lane. Hence, there is a need for a two-dimensional B-WIM algorithm. The algorithm presented in this section is a static algorithm that can be applied to simultaneous traffic events in the same or different lanes, at the same or different speeds.

The system uses influence lines due to a single wheel, instead of an axle weight. An advantage of predicting wheel weights is found in closely spaced axles. For instance, if all wheels have the same weight, the wheels closer to the strain sensor location will induce higher strain. This distinction is not possible if considering axle weights. The improvement in accuracy could be particularly significant in unbalanced trucks. The possibility of

representing the complete history of dynamic axle forces applied to the bridge can allow: the calculation of dynamic amplification factors, data for fatigue studies and data for investigations of spatial repeatability.

The algorithm is based on the same static equations as the multiple-sensor approach in Section 7.5.2 (Equations 7.31 to 7.35). This is an instantaneous calculation that allows a force-time history for each axle to be obtained. The difference is based on the definition of the influence line at each location. Hence, the bending moment ε_j at each sensor j due to p vehicles will be given by:

$$\varepsilon_j(x_j, y_j) = \frac{1}{E_j S_j} \sum_{i=1}^{p} W_{1i} I_j(x_i, y_i) + W_{2i} I_j(x_i \pm a_{1i}, y_i \pm d_i) + W_{3i} I_j(x_i \pm a_{1i} \pm a_{2i}, y_i \pm d_i) + \ldots \tag{7.55}$$

where W_{1i}, W_{2i}, ... and a_{1i}, a_{2i}, ... are wheel weights and axle spacings respectively corresponding to the i^{th} vehicle, d_i transverse distance between wheels, E_j and S_j the modulus of elasticity and section modulus at the sensor location j, I_j the influence line at sensor location j, (x_j, y_j) the position of the sensor j and (x_i, y_i) the position of the first axle of the vehicle.

An error function defined by the squared difference between measured $\tilde{\varepsilon}_j$ and theoretical strain ε_j at each sensor j is defined at each instant t:

$$f = \sum_{k=1}^{k=m} \left(\sum_{i=1}^{p} \sum_{j=1}^{n_i} \varepsilon_{kji} W_{ji} - \tilde{\varepsilon}_k \right)^2 \tag{7.56}$$

where n_i is the number of wheels of vehicle i, and ε_{kji} represents the value of the influence line at the sensor k for the location of wheel j in vehicle i.

By minimising Equation 7.56 with respect to the wheel weights:

$$\frac{df}{dW_{ji}} = 2 \sum_{k=1}^{k=m} \left(\sum_{i=1}^{p} \sum_{j=1}^{n_i} \varepsilon_{kji} W_{ji} - \tilde{\varepsilon}_k \right) \varepsilon_{kji} = 0 \tag{7.57}$$

In matrix form, wheel weights can be obtained at each instant from:

$$\{W\} = [\varepsilon]^{-1} * \{\widetilde{\varepsilon}\} \tag{7.58}$$

where:

$$[\varepsilon] = \begin{bmatrix} \sum_{k=1}^{k=m} \varepsilon_{k11}\varepsilon_{k11} & \sum_{k=1}^{k=m} \varepsilon_{k21}\varepsilon_{k11} & \cdot & \sum_{k=1}^{k=m} \varepsilon_{knp}\varepsilon_{k1p} \\ \sum_{k=1}^{k=m} \varepsilon_{k11}\varepsilon_{k21} & \sum_{k=1}^{k=m} \varepsilon_{k21}\varepsilon_{k21} & \cdot & \sum_{k=1}^{k=m} \varepsilon_{knp}\varepsilon_{k2p} \\ \cdot & \cdot & \cdot & \cdot \\ \sum_{k=1}^{k=m} \varepsilon_{k1p}\varepsilon_{kn_p p} & \sum_{k=1}^{k=m} \varepsilon_{k2p}\varepsilon_{kn_p p} & \cdot & \sum_{k=1}^{k=m} \varepsilon_{kn_p p}\varepsilon_{kn_p p} \end{bmatrix} \tag{7.59}$$

$$\{\widetilde{\varepsilon}_k\} = \begin{Bmatrix} \sum_{k=1}^{k=m} \widetilde{\varepsilon}_k \varepsilon_{k11} \\ \sum_{k=1}^{k=m} \widetilde{\varepsilon}_k \varepsilon_{k21} \\ \cdot \\ \sum_{k=1}^{k=m} \widetilde{\varepsilon}_k \varepsilon_{kn_p p} \end{Bmatrix} \tag{7.60}$$

It is also proposed to optimise vehicle position at each instant, instead of assuming a uniform speed along the bridge as in all previous algorithms. If a pair of axle detectors is placed prior to the bridge, the information on axle spacing and speed can be used as initial values in the optimisation process shown in Figure 7.31. Once the vehicle is initially located on the bridge, the transverse and longitudinal positions are optimised as an extra pair of parameters besides axle forces. Initial values for wheel weights can be obtained by using a one-dimensional B-WIM algorithm as defined in previous sections. Axle weights can be assumed to be equally distributed between wheels in a first approach. Velocity and transverse locations are not assumed to be constant. Further, velocity is not a parameter of the objective function, but transverse and longitudinal co-ordinates of one of the front wheels. Instantaneous velocity is updated in every incremental step from these two co-ordinates. From the previous truck location and instantaneous velocity (re-calculated in each time step), it is possible to obtain initial values of transverse and longitudinal positions for the next incremental step. The parameters of the objective function are

changed in an iterative process and the solution is found when the change in their values is less than a specified tolerance. The parameters for positioning the truck are constrained in a reasonable area around the initial transverse and longitudinal positions. This area will depend on the scanning frequency and the maximum likely vehicle acceleration/deceleration.

The objective function is given by Equation 7.56. The parameters to be estimated at each incremental step are: longitudinal, x_i, and transverse location, y_i, for each truck i and wheel weights W_{ji}. Axle spacings could also be among these parameters, but only if values provided by road axle detectors give insufficient accuracy.

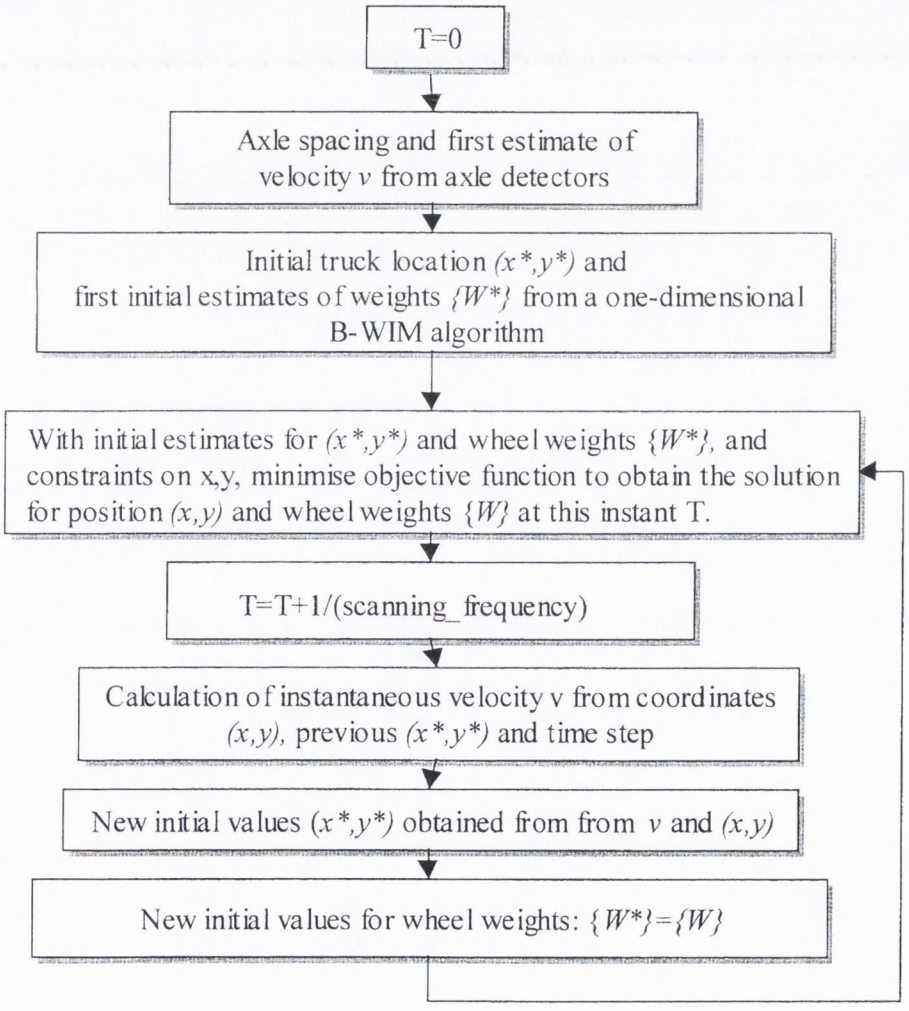

Figure 7.31 – Optimisation of two-dimensional instantaneous calculation

The disadvantage of this approach is the high number of sensors necessary to distinguish between the individual contribution of each wheel weight at each instant. The application of the algorithm is only recommended for short span bridges. A variant based on axle weights as parameters of the objective function (instead of using wheel weights) could be used for longer bridges. Compared to previous BWIM algorithms where an average speed parameter is optimised, the new algorithm optimises the vehicle position and re-calculate velocity in each time step.

7.7 SUMMARY

The search for a more accurate B-WIM algorithm has been focused on a consideration of dynamics. A new B-WIM algorithm that allows for bridge vibrations (natural frequencies, damping) has been presented (DB-WIM). More elaborate dynamic models can incorporate truck dynamics. The parameters of these models are determined by applying optimisation techniques to a number of measurement points. However, the randomness of these parameters (due to the high variety of truck and bridge mechanical characteristics) and the reduced information that can be obtained in the field, are a disincentive to using very refined dynamic models.

Static or dynamic equations can be formulated at more than one location. If the number of sensors is equal to or greater than the number of axles, the equations can be solved for the unknown axle weights for each instant in time. However, some of these equations could be dependent and a solution might not be achievable for all locations of the truck on the bridge. This is consistent with the original multiple-sensor B-WIM (MS-BWIM) system which was limited in the number of axles that could be weighed simultaneously (Kealy & O'Brien 1998). The author proposes a solution based on a least squares fitting technique that makes feasible the calculation of more axles.

An experimental algorithm based purely on the measured record is also introduced. This algorithm is based on the representation of the signal in the frequency domain. Weights are calculated from the spectrum. When the number of axles increases, the limiting frequency where spectra are compared might need to be increased and poor results have been obtained. However, the algorithm is calibrated in a way that can be directly applied to other algorithms based on the time domain. For instance, the method can be used

experimentally to obtain the influence line used in a static B-WIM algorithm or the dynamic answer due to a unit load used in DB-WIM.

The theoretical basis for a two-dimensional B-WIM algorithm has been established. This formulation takes into account the transverse location of the truck and the possibility of different trucks.

Finally, Table 7.1 identifies the main features of all the algorithms considered in this chapter. They all compare the measured strain to a theoretical strain. The difference lies in the theoretical strain used as reference.

Table 7.1 – B-WIM algorithms

Algorithm type	**Principle**
Spectral	Comparison of measured spectra at one sensor location to reference spectra in frequency domain.
Based on a bridge dynamic model	Comparison of measured strain at one sensor location to theoretical strain derived from a model that allows for bridge dynamics.
Based on a bridge + truck dynamic model	Comparison of measured strain at one or multiple bridge locations to theoretical strain derived from a model that allows for bridge-truck dynamic interaction.
Static multiple-sensor	Comparison of measured strains to theoretical static strain at different bridge locations.
Dynamic multiple-sensor	Comparison of measured strains at different bridge locations to theoretical strains derived from a model that allows for bridge dynamics.
Based on modal decoupling	Comparison of the estimation of the modal components of the applied force and the theoretical value derived from a bridge dynamic model.
Two-dimensional	Comparison of measured strains to theoretical static strain at different transverse and longitudinal bridge locations.

The first two algorithms (spectral and based on a bridge dynamic model) are based on measurements at only one longitudinal section. Average forces (assumed to be close to static weights) are calculated through a least squares fitting technique applied to all readings at the section location. The algorithm based on a bridge and truck dynamic model can be based on measurements at one or several sections. The solution is obtained through optimisation of an objective function in an iterative process. The other four algorithms (static multiple-sensor, dynamic multiple-sensor, based on modal decoupling and two-dimensional) are based on measurements at different sections. An instantaneous applied

force is obtained by applying a least squares fitting technique to the readings of all sensors at each instant. Then, static axle weights are derived from the corresponding load history.

8

EXPERIMENTAL TESTING

8.1 INTRODUCTION

Fieldwork has been carried out to validate theory developed in this thesis. Some of the algorithms described in Chapters 3 and 7 are tested. Four different B-WIM sites have been monitored with the techniques described in Chapter 4:

- The first site, Delgany (Ireland), was used to obtain data to calibrate the Eurocode (EC1.3) for Irish conditions. B-WIM data was recorded for two uninterrupted weeks for this purpose. An experimental procedure to calibrate a B-WIM system in the frequency domain is introduced. The effect of a change of speed on B-WIM accuracy is also discussed.
- The performance of a B-WIM system under harsh climatic conditions was tested in a bridge in Luleå (Northern Sweden). A major trial with a lot of different truck configurations took place as part of the Cold Environment Test (CET) programme coordinated by COST323 (Henau & Jacob 1998). Results obtained from two vehicles used for calibration are presented.
- A B-WIM system was installed in a bridge in Belleville (Eastern France). This is a long span bridge with substantial dynamics and a high traffic density. A fully instrumented truck participated in this experiment as part of the Continental Motorway Test (CMT) programme (Henau & Jacob 1998). The accuracy of a dynamic algorithm is assessed.
- Finally, a bridge in Slovenia was instrumented at different longitudinal and transverse sensor locations. The multiple-sensor B-WIM algorithm is tested with data obtained from this experiment.

The author has taken an active part in the installation of the B-WIM sites in Ireland, Sweden and France while the data from Slovenia was provided by Brady (University College Dublin, Ireland) and ZAG (Slovenian National Building and Civil Engineering

Institute). In Belleville, TUM (Technische Universität München) provided additional data on bridge strains and VTH (Technical Research Centre of Finland) on the wheel forces applied by the instrumented truck. All accuracy tables are based on the accuracy classification system of the COST323 WIM specification (Appendix B).

8.2 DELGANY, SKEWED SHORT SPAN (15 M) SIMPLY SUPPORTED BRIDGE

This bridge is known as the 'Barry Bridge' and is located near Delgany, on the N-11, the main Rosslare-Wexford-Dublin route (Southbound carriageway). Data was obtained from May to July 1997 as part of a contract with the Irish National Roads Authority for the calibration of the Eurocode for Irish Conditions. The bridge is a simply supported single span carrying a two lane road in the same direction (There is another two-lane bridge for the Wexford-Dublin direction). The site location is shown in Figure 8.1.

(a) General location (b) Detailed map

Figure 8.1 – Bridge Location (Delgany)

Reinforced concrete abutments retain embankments at each side. Figure 8.2 gives a general view of the bridge.

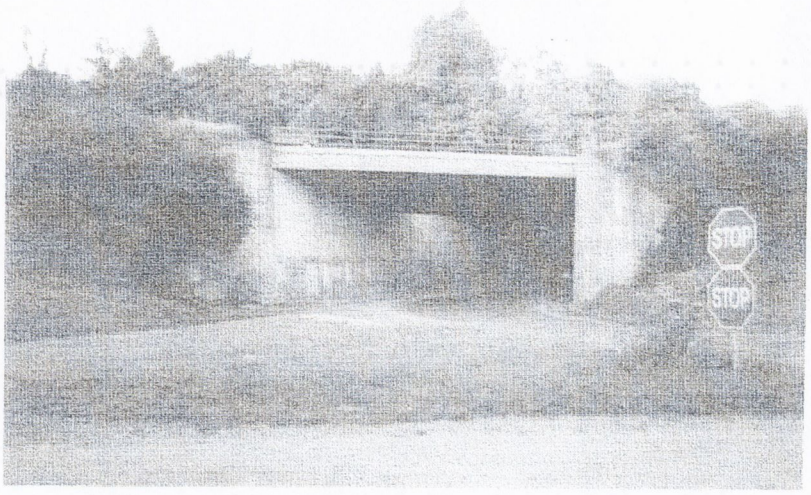

Figure 8.2 – Side View of Delgany Bridge

8.2.1 Installation

The bridge is a 16 meter long simply supported 'beam-and-slab' structure, composed of 28 precast concrete beams. It has a skew angle of approximately 30 degrees. The dimensions of the bridge are shown in Figure 8.3.

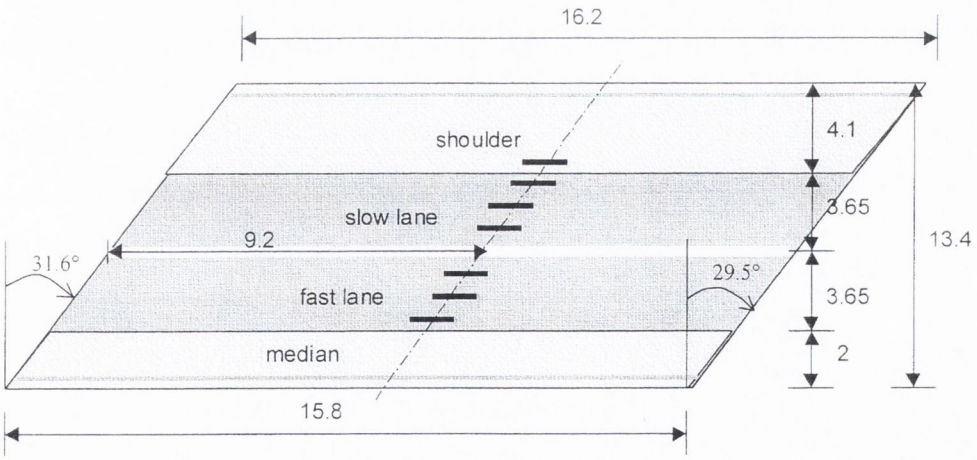

Figure 8.3 - Plan view of Barry Bridge (South-bound carriageway)

Mechanical Strain Amplifiers

The bridge WIM system was installed in one day. It consisted of seven mechanical strain amplifiers (Section 4.2.2) attached to the beams on the soffit and pneumatic axle detectors nailed to the road surface (Section 4.3.1). The amplifiers were used to amplify the strain

induced in the bridge approximately 13 times. This provided a more accurate strain signal by reducing the effects of noise. The amplifiers were placed at approximately mid-span in each beam where the bending moment is relatively large. The exact distance of each amplifier from the abutment is given in Table 8.1. The longitudinal distances were measured from the abutment on the Dublin (North) side of the bridge.

Table 8.1 - Distances of mechanical amplifiers from abutment (Delgany)

Mechanical strain amplifier No.	Beam No.	Longitudinal position (m)	Lane
1	7	9.39	Hard Shoulder
2	10	9.36	Slow
3	13	9.37	Slow
4	16	9.24	Slow
5	19	9.20	Fast
6	22	9.09	Fast
7	25	9.07	Fast

Axle Detectors

Two pneumatic axle detectors (rubber tubes), at a known distance apart, were fixed to each lane (22.827 m in slow lane and 22.657 m in fast lane). The tube before the bridge was placed an average distance of 3.86 m and 1.87 m from the nearest joints in the slow and fast lane respectively. This provided information regarding the speed of the vehicle and the vehicle classification. The axle detectors needed regular maintenance and would not be recommended by the author for long term use.

The rubber tubes were connected to pneumatic convertors which convert the air pulse into electrical analog signals (Figure 8.4(a)). These in turn were connected to the signal conditioning equipment, which conditions the incoming signal. The latter was connected to a portable computer which stored the data (Figure 8.4(b)). The system used to record the strain was developed by National Instruments and is known as the SCXI signal conditioning system which is combined with plug-in boards for data acquisition (Appendix C). The equipment was capable of operating unmanned, though periodic visits were made to the site to back-up data and release memory space from the hard drive as well as to fix the axle detectors, which tended to loosen due to the action of traffic loads. More details of the working of the system can be found in Chapter 4.

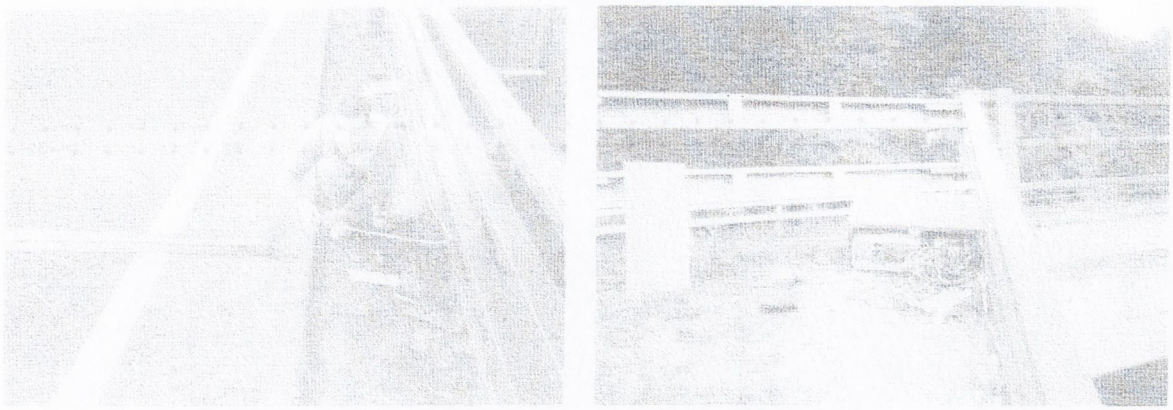

(a) Installation of axle detectors (b) Data Acquisition Equipment

Figure 8.4 – Installation of data collection devices (Delgany)

8.2.2 Testing

The calibration of the system was carried out on the 15th July, 1997 with a 3-axle rigid truck of GVW, 212.3 kN and distances between axles of 4.02 and 1.40 m. The vehicle is shown in Figure 8.5.

Figure 8.5 – Calibration truck used in Delgany

The front axle has a static axle weight of 59.21 kN and the rear tandem 153.09 kN as determined at a certified static scales. Ten significant runs were made at three different speed levels as specified by the European Specification on Weigh-In-Motion of Road Vehicles (2 runs about 55 km/h, 6 runs at 70 km/h and 2 runs at 85 km/h). Both lanes were calibrated although weights were subsequently calculated in only one. Results from a previous calibration of the slow lane on 20th May 1997 are also presented. Accuracy

analysis takes place under extended repeatability conditions (r2) according to the COST323 specification: One vehicle passes several times at different speeds with small variations in lateral position.

Calibration based on a theoretical beam model

The static scale gave only the total weight for the tandem of the calibration truck, so it was assumed that the weight of the individual tandem axles were evenly distributed between the two. Figure 8.6 shows the shape of the theoretical bending moment due to the static loads of the calibration truck according to beam theory. This theoretical response must be scaled down to the corresponding measured record by a calibration factor of 0.683 in order to achieve the correct GVW after applying Equation 3.12. It can be seen the theoretical model does not match well the shape or boundary conditions. The final calibration factor was calculated from all truck crossings.

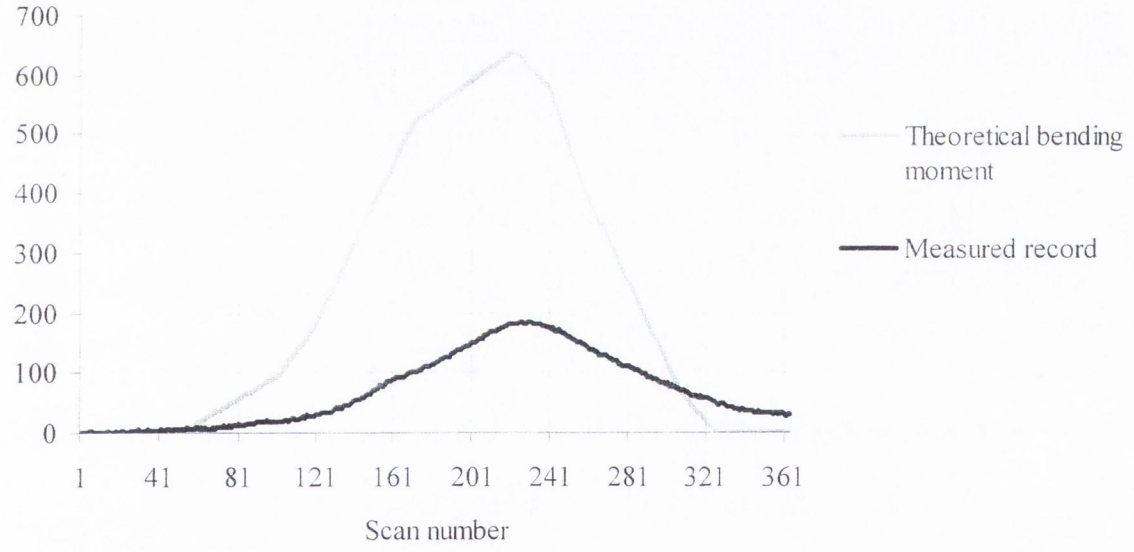

Figure 8.6 – Calibration of theoretical influence line (truck running at 69.48 km/h) (Delgany)

Tables 8.2, 8.3 and 8.4 give accuracy classes for different identities and three different tests: slow lane in May, and both lanes in July. Accuracy results for the slow lane differ between May and July. The failure of axle detectors and three mechanical strain amplifiers resulted in the installation of new sensors after the calibration in May and the system had to be re-calibrated in July. The most accurate results are obtained in May due to a better adjustment of the amplifiers to the bridge deck. In July, errors were higher in the fast lane

than in the slow lane. The accuracy was poor for axle weights and their values were not used for statistical studies at this site.

Table 8.2 – Accuracy classification by algorithm based on beam model (slow lane - May)

(**n**: Total number of vehicles; **m**: mean; **s**: Standard deviation; π_0: level of confidence; δ: tolerance of the retained accuracy class; δ_{min}: minimum width of the confidence interval for π_0; π: Level of confidence of the interval $[-\delta,\delta]$)

	Relative error statistics				Accuracy calculation				
Criterion	**n**	**m** (%)	**s** (%)	π_0 (%)	**Class**	δ (%)	δ_{min} (%)	π (%)	**Class Retained**
Single axle	10	-42.0	8.35	90.0	**E(55)**	66	59.6	97.0	**E(55)**
Group of axles	10	16.22	3.50	90.0	**D(25)**	28	23.6	98.7	
Gross Weight	10	-0.01	1.95	90.0	**A(5)**	5	5.0	90.2	

Table 8.3 – Accuracy classification by algorithm based on beam model (slow lane - July)

(**n**: Total number of vehicles; **m**: mean; **s**: Standard deviation; π_0: level of confidence; δ: tolerance of the retained accuracy class; δ_{min}: minimum width of the confidence interval for π_0; π: Level of confidence of the interval $[-\delta,\delta]$)

	Relative error statistics				Accuracy calculation				
Criterion	**n**	**m** (%)	**s** (%)	π_0 (%)	**Class**	δ (%)	δ_{min} (%)	π (%)	**Class Retained**
Single axle	10	-40.2	9.74	90.0	**E(60)**	72	60.7	98.4	**E(60)**
Group of axles	10	15.68	2.79	90.0	**D+(20)**	23	21.5	95.5	
Gross Weight	10	0.09	2.37	90.0	**B+(7)**	7	6.1	94.8	

Table 8.4 – Accuracy classification by algorithm based on beam model (fast lane - July)

(**n**: Total number of vehicles; **m**: mean; **s**: Standard deviation; π_0: level of confidence; δ: tolerance of the retained accuracy class; δ_{min}: minimum width of the confidence interval for π_0; π: Level of confidence of the interval $[-\delta,\delta]$)

	Relative error statistics				Accuracy calculation				
Criterion	**n**	**m** (%)	**s** (%)	π_0 (%)	**Class**	δ (%)	δ_{min} (%)	π (%)	**Class Retained**
Single axle	10	-62.3	9.75	90.0	**E(80)**	96	82.8	98.8	**E(80)**
Group of axles	10	21.50	9.08	90.0	**E(40)**	44	40.6	94.4	
Gross Weight	10	-1.89	7.62	90.0	**D+(20)**	20	19.8	90.5	

The errors in the estimation of static weights for all runs are illustrated in Figure 8.7. Front axle and rear tandem are underweighed and overweighed respectively.

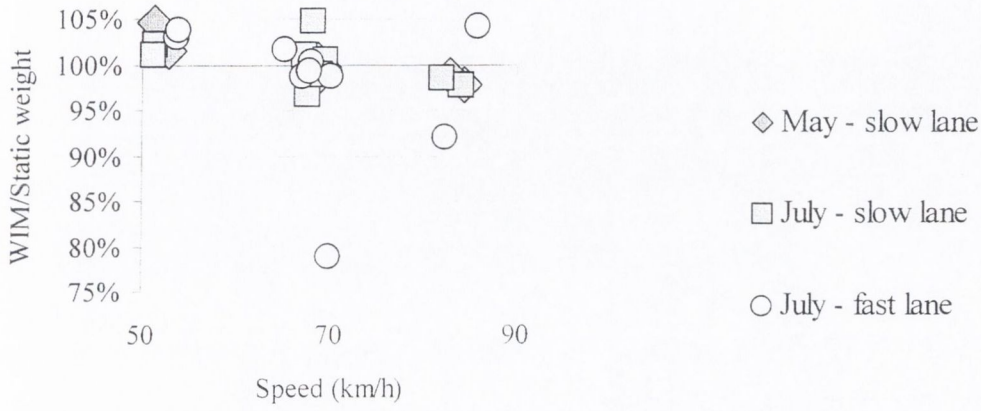

(a) Gross weight

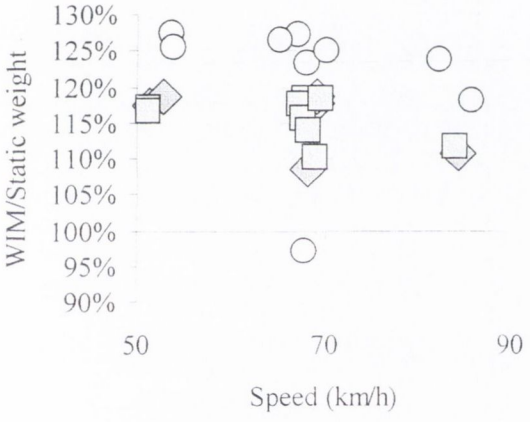

(b) Axle group

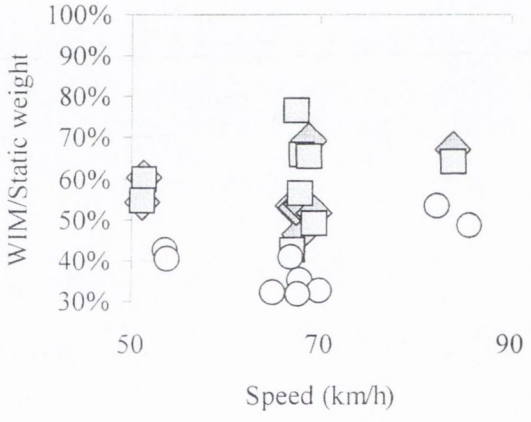

(c) Single axle

Figure 8.7 – Errors in weights by using a theoretical beam model (Delgany)

Calibration based on an experimental influence line

Accurate influence lines are very important in the overall accuracy of a B-WIM system. Ideally, it should be possible to make a direct calculation of the influence line in stiff bridges (high first natural frequency and low dynamic amplitudes). That is, when there is only one axle on the bridge, if the masses of the calibration truck are known, it is possible to know the value of the influence line from the measured strain record. Then, when a second axle appears on the bridge, the contribution of this second axle to the measured strain can be obtained from the known values of the influence line (already calculated when the first axle passed by that point). As the load effect caused by a second axle on the

bridge is known, the values of the influence line at the new locations of the first axle can be obtained readily by discounting the effect of the second axle. The same procedure could be applied to more axles entering the bridge. In practice, this procedure is very sensitive to the small magnitude of the strains at the start of the bridge and significant errors are introduced in the first steps of the calculation making this approach prone to error.

Hence, the search of the influence line is carried out in such a way that the sum of the effect of all axles matches the measured strains as close as possible. Generally, a theoretical influence line is tested initially and then modifications are done on this curve to improve accuracy (Section 3.5.1). The final adjustment might not be adequate for every single truck as deviations take place due to bridge and truck dynamics.

Alternatively, the author suggests calculating the influence line in the frequency domain as proposed in Section 7.2.2. The spectrum of the influence line is obtained by calculating the unit contribution of all readings to a given frequency. The limitations of a direct calculation in the time domain or the inconvenience of an experimental adjustment, point by point, are overcome. Accordingly, by applying complex arithmetic to Equation 7.5:

$$H_u(f) = \frac{H_m(f)}{\sqrt{(W_1 + W_2\cos(-fn_1) + ... + W_r\cos(-fn_{r-1}))^2 + (W_2\sin(-fn_1) + ... + W_r\sin(-fn_{r-1}))^2}} \tag{8.1}$$

$$\alpha_u(f) = \alpha_m(f) - \tan^{-1}\left(\frac{W_2\sin(-fn_1) + ... + W_r\sin(-fn_{r-1})}{W_1 + W_2\cos(-fn_1) + ... + W_r\cos(-fn_{r-1})}\right) \tag{8.2}$$

where

$H_m(f)$: Spectrum magnitude of total measured strain,

$H_u(f)$: Spectrum magnitude of the strain response due to a moving unit load,

$\alpha_m(f)$: Spectrum phase of total measured strain,

$\alpha_u(f)$: Spectrum phase of the strain response due to a moving unit load,

W_i : Weight corresponding to axle i,

r : Number of axles,

n_i : Number of readings between the first axle and axle $(i+1)$,

f : Frequency, as $f=2\pi k/N$, where k (0,1,2,..) represents the k^{th} harmonic of the sample.

N = Number of strain readings induced by a vehicle crossing the bridge.

Once the spectrum due to a unit load is obtained, the influence line can be obtained in the time domain through the real part of the inverse transform of $\overline{H}_u(f)$. The process is illustrated in Figures 8.8 and 8.9. Figure 8.8(a) shows the total strain measured for a three-axle truck travelling at 52.85 km/h, and Figure 8.8(b) the corresponding spectrum $\overline{H}_m(f)$.

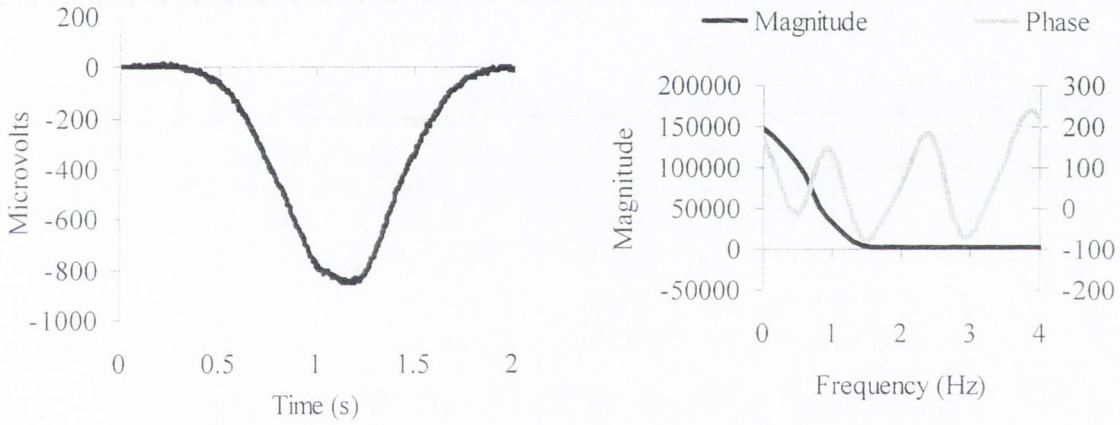

(a) Original record at 52.85 km/h (b) Spectra of record in (a)

Figure 8.8 – Calculation of DFT of the original record (Delgany)

The spectra due to a unit load, $\overline{H}_u(f)$ (Figure 8.9(a)), can be calculated from spectra in Figure 8.8(b) by applying Equations 8.1 and 8.2. The influence line in the time domain is given in Figure 8.9(b) and it is obtained by inverse transform of the spectrum $\overline{H}_u(f)$ in Figure 8.9(a).

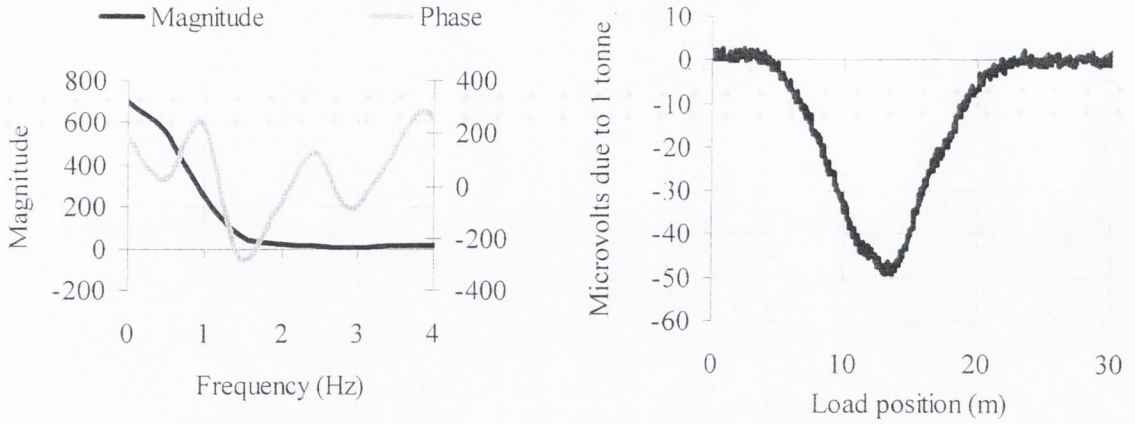

(a) Spectra due to a unit load (b) Experimental influence line

Figure 8.9 – Calculation of spectra due to a unit load and experimental influence line (Delgany, May 1997)

The levels of accuracy achieved with the influence line in Figure 8.9(b) are given in Table 8.5. Compared to the theoretical beam model, there is an improvement in overall accuracy from E(55) to C(15).

Table 8.5 – Accuracy classification (experimental influence line at 50 km/h) (May) (r2)

(**n**: Total number of vehicles; **m**: mean; **s**: Standard deviation; π_0: level of confidence; δ: tolerance of the retained accuracy class; δ_{min}: minimum width of the confidence interval for π_0; π: Level of confidence of the interval $[-\delta,\delta]$)

	Relative error statistics				Accuracy calculation				
Criterion	**n**	**m** (%)	**s** (%)	π_0 (%)	**Class**	δ (%)	δ_{min} (%)	π (%)	**Class Retained**
Single axle	10	-2.30	6.88	90.0	**C(15)**	20	18.1	93.6	**C(15)**
Group of axles	10	0.92	1.51	90.0	**A(5)**	7.14	4.2	99.6	
Gross Weight	10	0.02	1.50	90.0	**A(5)**	5	3.8	97.2	

Accuracy can be further improved by obtaining the final influence line through an average of all calibration runs. A low pass filter can also be used to remove noise interference (50 Hz) but an excessive 4 Hz hardware filter was applied while acquiring data in Delgany. This filter does not allow for a recovery of the original signal and undoubtedly it had a negative effect on accuracy by cutting off frequency components of the static response.

Due to the smoothing action of the filter, results are expected to improve if using a separate influence line for each range of speeds. The calibration of a run at 68.94 km/h results in the influence line shown in Figure 8.10.

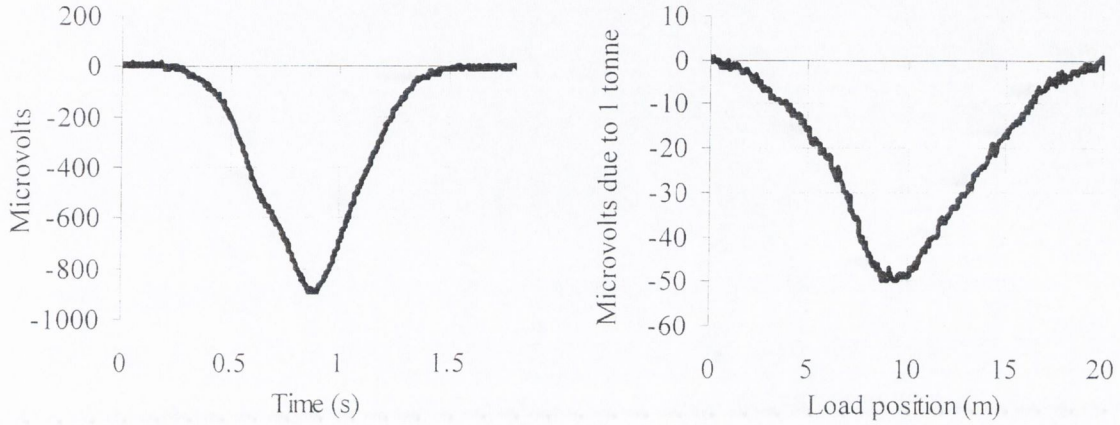

(a) Measurement at 68.94 km/h (b) Influence line

Figure 8.10 - Calibration of slow lane at 68.94 km/h (Delgany, May 1997)

Table 8.6 gives accuracy classes if the 6 runs at about 70 km/h are analysed in full repeatability conditions. The most accurate class, A(5), is obtained for every single criterion.

Table 8.6 – Accuracy classification (experimental influence line at 70 km/h) (May) (r1)

(**n**: Total number of vehicles; **m**: mean; **s**: Standard deviation; π_0: level of confidence; δ: tolerance of the retained accuracy class; δ_{min}: minimum width of the confidence interval for π_0; π: Level of confidence of the interval $[-\delta,\delta]$)

	Relative error statistics				Accuracy calculation				
Criterion	**n**	**m (%)**	**s (%)**	π_0 (%)	**Class**	δ (%)	δ_{min} (%)	π (%)	**Class Retained**
Single axle	6	-2.39	1.53	89.6	**A(5)**	8	6.2	97.5	**A(5)**
Group of axles	6	0.78	0.69	89.6	**A(5)**	7.14	2.5	100.	
Gross Weight	6	-0.10	0.56	89.6	**A(5)**	5	1.7	99.9	

If all runs are analysed with the influence line derived from calibration at 70 km/h (instead of the 50 km/h run from Figure 8.9(a) - both shapes will be slightly different due to the filter), accuracy classes are as shown in Table 8.7. The results are less accurate than in Table 8.6. The same influence line is used for calculations in Tables 8.6 and 8.7, but the

latter considers all runs, not only those at the speed that influence line has been obtained. Overall accuracy decreases to C(15) due to the poorer estimation of individual axle weights. Hence, it can be seen that results can be improved by using an influence line for each range of speeds when having data filtered at a low frequency.

Table 8.7 – Accuracy classification (experimental influence line at 70 km/h) (May) (r2)

(**n**: Total number of vehicles; **m**: mean; **s**: Standard deviation; π_0: level of confidence; δ: tolerance of the retained accuracy class; δ_{min}: minimum width of the confidence interval for π_0; π: Level of confidence of the interval $[-\delta,\delta]$)

	Relative error statistics				Accuracy calculation				
Criterion	**n**	**m** (%)	**s** (%)	π_0 (%)	**Class**	δ (%)	δ_{min} (%)	π (%)	**Class Retained**
Single axle	10	0.85	7.48	90.0	**C(15)**	20	19.1	91.7	**C(15)**
Group of axles	10	-0.30	1.56	90.0	**A(5)**	7.14	4.0	99.6	
Gross Weight	10	0.02	1.45	90.0	**A(5)**	5	3.7	97.7	

The calibration of the slow lane in July 1997 is shown in Figure 8.11.

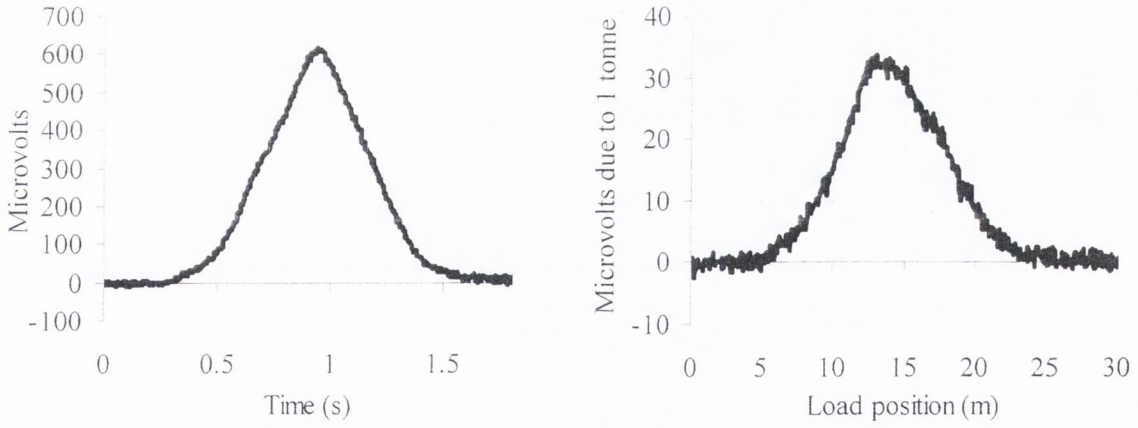

(a) One measured record at 67.9 km/h (b) Influence line

Figure 8.11 – Calibration of slow lane (Delgany, July 1997)

Accuracy classes when using the influence line of Figure 8.11(b) for calibrating the ten July runs are given in Table 8.8. Compared to the theoretical beam model, accuracy in single axles is improved from E(60) to E(40), and accuracy in group of axles from D+(20) to B+(7). Compared to the calibration in May, accuracy in July decreases due to a poorer

resolution for the installation in July. This can be seen in Figures 8.10 and 8.11 (signal to noise ratio lower in July).

Table 8.8 – Accuracy classification (experimental influence line) (slow lane) (July) (r2)

(**n**: Total number of vehicles; **m**: mean; **s**: Standard deviation; π_0: level of confidence; δ: tolerance of the retained accuracy class; δ_{min}: minimum width of the confidence interval for π_0; π: Level of confidence of the interval $[-\delta,\delta]$)

	Relative error statistics				Accuracy calculation				
Criterion	**n**	**m** (%)	**s** (%)	π_0 (%)	**Class**	δ (%)	δ_{min} (%)	π (%)	**Class Retained**
Single axle	10	9.17	14.55	90.0	**E(40)**	48	40.9	95.3	**E(40)**
Group of axles	10	-3.46	2.66	90.0	**B+(7)**	10	9.1	94.2	
Gross Weight	10	0.06	2.65	90.0	**B+(7)**	7	6.8	91.4	

The calibration of the passing lane in July 1997 is shown in Figure 8.12.

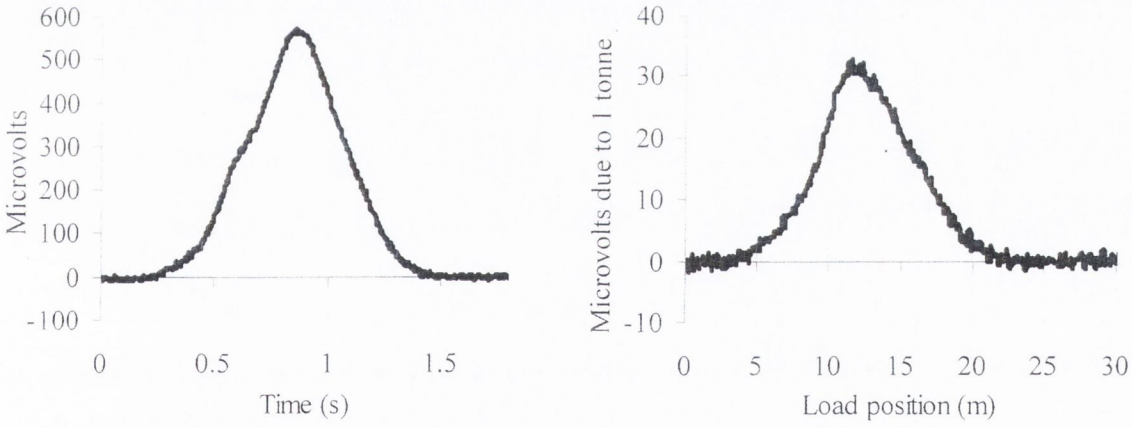

(a) Measured record at 67.75 km/h (b) Influence line

Figure 8.12 – Calibration of fast lane (Delgany, July 1997)

Table 8.9 gives the corresponding accuracy classes obtained for this lane. Accuracy for gross weight is in class B(10) while the calibration using a theoretical beam model only reaches D+(20).

Table 8.9 – Accuracy classification (experimental influence line) (passing lane) (July) (r2)

(**n**: Total number of vehicles; **m**: mean; **s**: Standard deviation; π_0: level of confidence; δ: tolerance of the retained accuracy class; δ_{min}: minimum width of the confidence interval for π_0; π: Level of confidence of the interval $[-\delta,\delta]$)

	Relative error statistics				Accuracy calculation				
Criterion	**n**	**m (%)**	**s (%)**	π_0 (%)	**Class**	δ (%)	δ_{min} (%)	π (%)	**Class Retained**
Single axle	10	0.62	19.75	90.0	**E(50)**	60	50.4	95.5	**E(50)**
Group of axles	10	-0.05	5.15	90.0	**C(15)**	18	13.1	97.9	
Gross Weight	10	0.14	3.78	90.0	**B(10)**	10	9.6	91.4	

All results are represented in Figure 8.13.

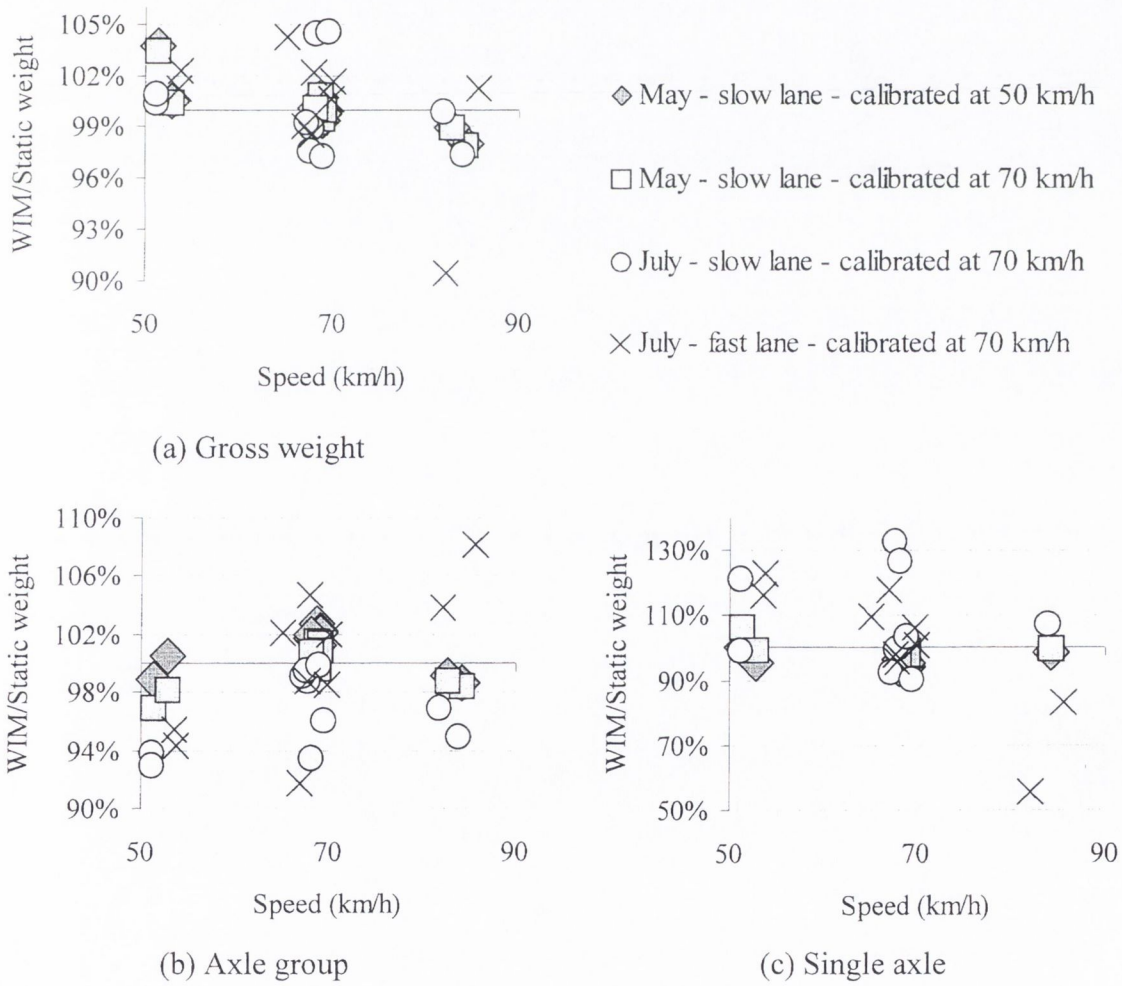

(a) Gross weight

(b) Axle group

(c) Single axle

Figure 8.13 – Errors in weights by using calibration in frequency domain (Delgany)

Inaccuracy generally increases when checking results in a speed different from the calibration speed (influenced by inappropriate filtering). The passing lane is the most sensitive to the changes of each run due to the smaller and narrower strain response obtained for this lane.

8.2.3 Traffic Statistics

Fourteen days of South-bound data was collected at the Delgany site between May 20th and July 3rd, 1997 in order to calibrate the Irish bridge load model. Voltage data was recorded continuously on site into 11 channels: 4 from the rubber tubes on the road, and 7 from the strain gauges on the bridge deck. Labview software was used during data acquisition while post-processing was carried out using purpose-written programs in the C language, converting the original voltage information into times and strains for both lanes (Section 4.4.3 and Appendix D). A time was stored for each axle at each tube, and strain was stored for the entire period that a vehicle was on the bridge. Some general statistics on the number of vehicles classified and weighed by the author in twelve days of recording are given in Figure 8.14.

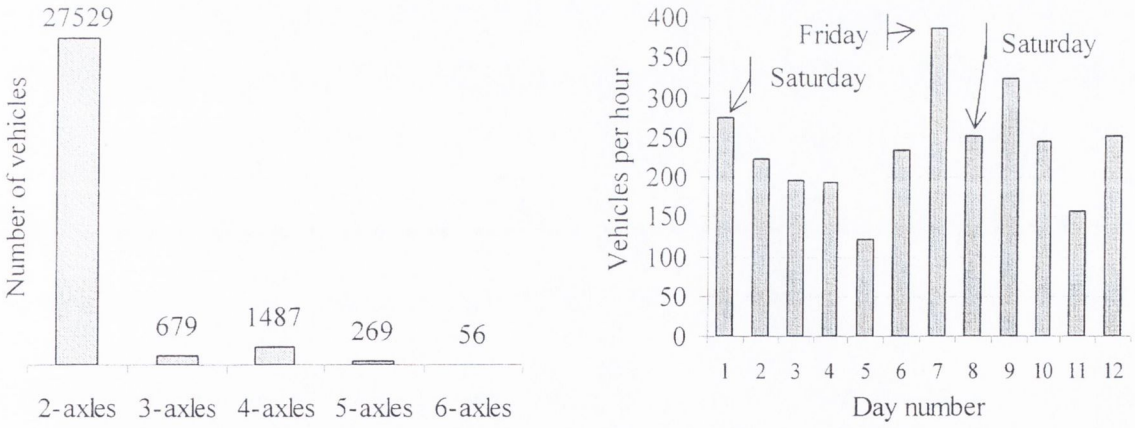

(a) Total number of vehicles (b) Average number vehicles per hour

Figure 8.14 – Statistics on the sample in the N11 (Delgany)

A distribution of the composition by class of Irish truck traffic at the three sites can be seen in Figure 8.15. Vehicles with gross weight less than 3500 kg (i.e., cars and light vans) are grouped in Class 1. In traffic flow modelling for bridges, such vehicles are considered important only for the spacing they represent between larger vehicles in traffic jam

situations (O'Brien et al. 1998b). It is clear that the largest proportion of traffic is made up of the rigid Class 2 vehicles.

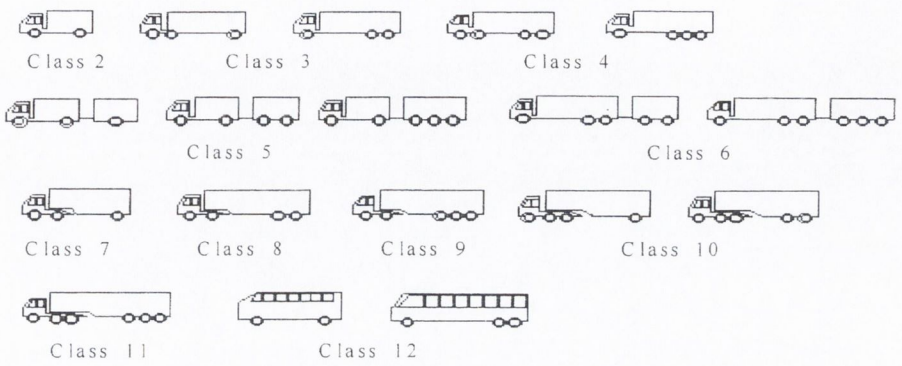

(a) Vehicle classification system

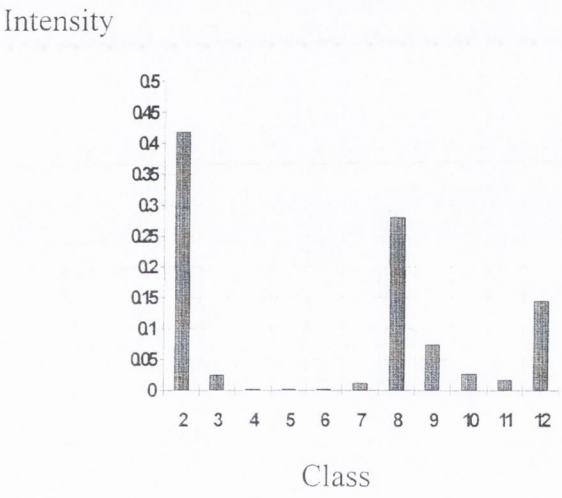

(b) Histogram for N11

Figure 8.15 - Irish truck traffic composition for sample periods (after O'Brien et al. 1998b)

The 'normal' load model specified in EC1.3 is illustrated in Figure 8.16. It consists of uniformly distributed loading and a bogie of four point loads in each lane. The intensities of load can be adjusted by the relevant national authority through 'alpha-factors' appropriate to local traffic conditions on given road classes. As result of the WIM data collected in Delgany and two other Irish sites, O'Brien et al (1998b) recommends an alpha factor of about 1.3 for all 1-lane bridges. No reduction below unity is recommended in the alpha factors for all 2, 3 and 4-lane bridges.

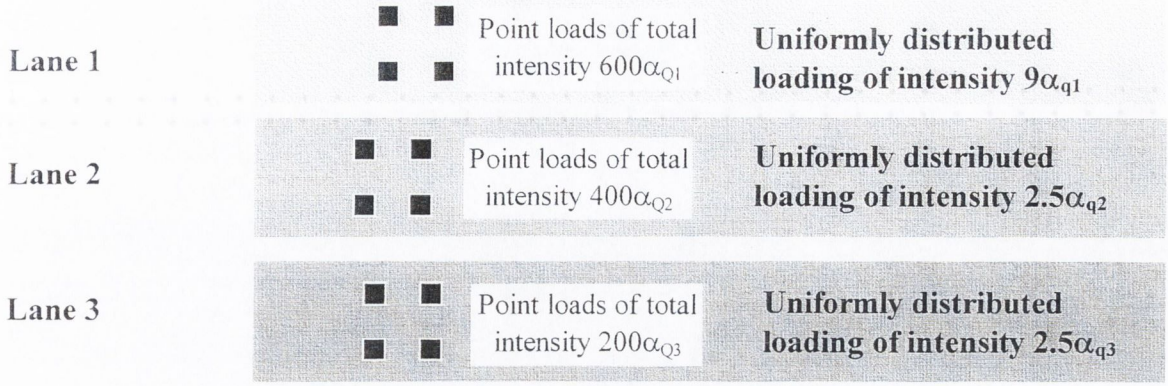

Figure 8.16 - EC1.3 Normal load model: plan view of loadings in each lane with intensities of loading expressed as a function of the alpha factors (O'Brien et al 1998b)

Individual axle weights by the B-WIM system installed in Delgany are not very accurate. According to O'Brien et al (1998b), while axle spacing can be important, the distribution of weights between axles is not considered to be a significant factor in the calculation of bridge load effects (bending moments and shear forces). At the N11 site, only the gross weights were used. For the purposes of the simulations to calculate 'alpha-factors', typical distributions of the gross weight between the axles were adopted based on those determined at the other Irish WIM sites. This approximation is considered by O'Brien et al (1998b) to not be of such inaccuracy as to invalidating the conclusions.

8.2.4 Influence of Braking Forces on Accuracy

Most B-WIM algorithms are based on an average speed along the bridge that is assumed to be constant. Sudden braking on a bridge can cause a dynamic amplification from 10 to 20% over a road in good condition or from 25 to 30% in poor condition (Major 1980). The Delgany bridge is at a turn on the road and hence the B-WIM site is tested for a strong change in speed along the bridge. Data was collected during September 1996 to analyse the maximum bending in abutments due to horizontal forces (González 1996). Strains were also collected from the bridge deck and the results are shown in Figure 8.17. Five mechanical strain amplifiers were installed about midspan and data was acquired at 60 Hz. A 4 Hz hardware filter was applied.

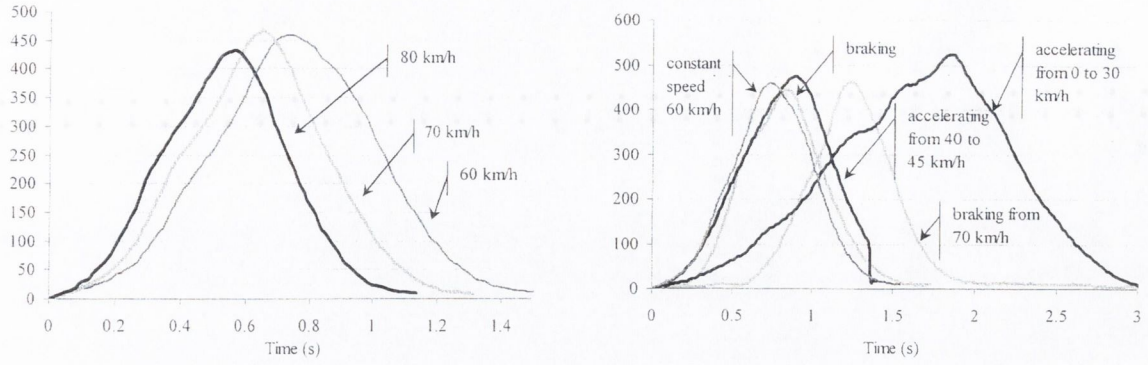

(a) Bridge response at constant speed (b) Bridge response at changing speed

Figure 8.17 – Bridge response in the presence of horizontal forces

Bridge response is smaller for higher speeds (80 km/h), while it is closer to the static response for speeds lower than 70 km/h (Section 5.3). Only when the vehicle is imposed a maximum acceleration from nearly null speed at the start of the bridge, a significant deviation from the other runs appears. Hence, the assumption of an average speed is acceptable for most traffic conditions in short span bridges such as Delgany, even in cases of sudden change in speed.

8.3 LULEÅ, TWO SPAN (15 m EACH) INTEGRAL BRIDGE

Tests on the durability of WIM systems in cold climates were organised by the Swedish National Road Administration (SNRA) as part of the CET programme that took place in Northern Sweden, 150 km south of the Arctic Circle (Figure 8.18(a)), from June 1997 to June 1998. The Irish B-WIM system was installed near Aleån, 20 km south of the city of Luleå, on the E4 route (Figure 8.18(b)). Traffic is carried by one lane in each direction with no central median. The speed limit for heavy vehicles is 80 km/h.

The B-WIM system only participated in the test periods of June 1997, March 1998 (Figure 8.19) and June 1998. The records of the first two periods were acquired with a 4 Hz hardware low-pass filter. Hallström (1999) emphasises B-WIM as a promising technology for cold climates. Accuracy of B-WIM systems is not as influenced by the fast deterioration of the road surface as road WIM sensors.

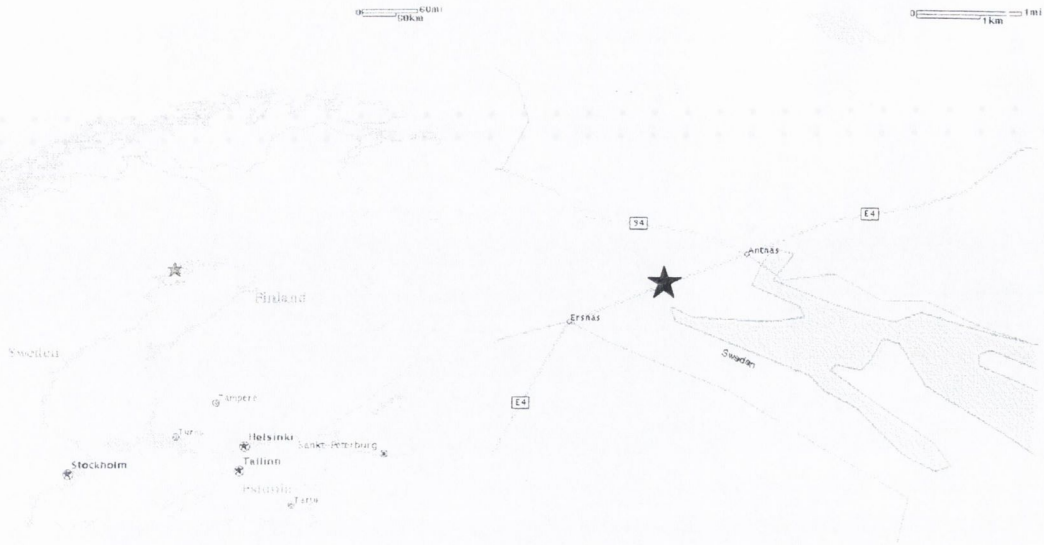

(a) General location (b) Detailed map

Figure 8.18 – Bridge Location (Luleå)

Figure 8.19 - Side View of Luleå Bridge

8.3.1 Installation

The installation carried out by the author in March 1998 is described. The bridge is a two span integral bridge with two equal spans of 14.6 m and is straight in plan (Figure 8.20). The bridge deck has a mid-span depth of 550 mm and is solid in cross-section.

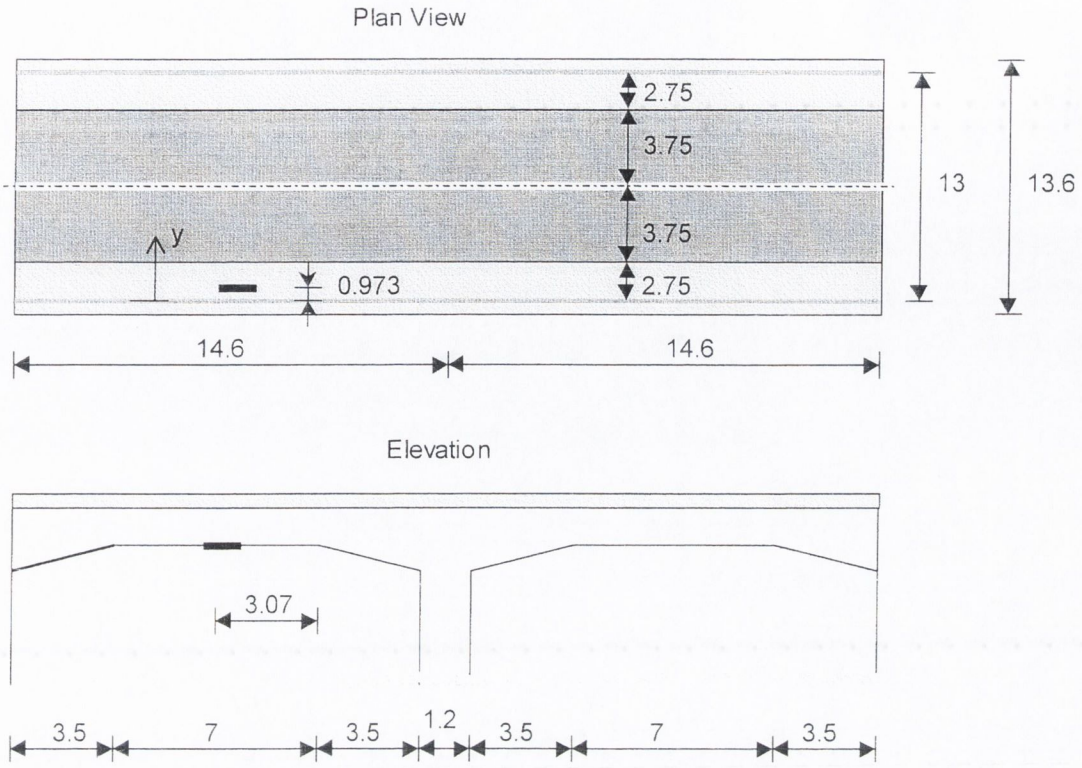

Figure 8.20 – Bridge layout (Luleå)

Mechanical strain amplifiers

Strain sensors were placed at the middle of the first span as represented in Figure 8.19. Eight mechanical strain amplifiers were bolted to the soffit of the bridge under the southbound carriageway of the first span (Figure 8.21). Cable connectors were placed on each of the cables, as these ones had to be removed for safety purposes at the end of each day's testing. In this way, mechanical strain amplifiers could be left on site for the duration of the test.

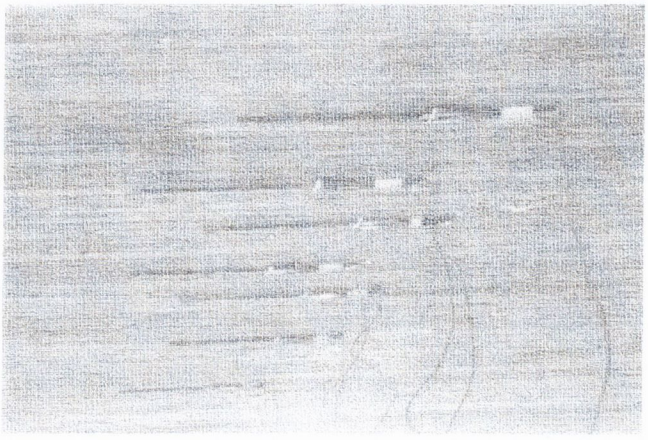

Figure 8.21 – Mechanical strain amplifiers (Luleå)

Table 8.10 gives the transverse position of the mechanical strain amplifiers, where transverse axis y is defined in Figure 8.20. Longitudinally, the amplifiers are about 7.17 m from the middle of the central column.

Table 8.10 - Distances of mechanical amplifiers (Luleå)

Mechanical strain amplifier no.	y (m)	Lane
1	0.973	Hard Shoulder
2	2.156	Hard Shoulder
3	2.973	Test lane
4	3.977	Test lane
5	4.97	Test lane
6	6.01	Test lane
7	7.507	Northbound lane
8	9.016	Northbound lane

Axle Detectors

Four pneumatic tubes were fixed across both lanes: one just before the bridge (at 15.70 m from the centre of the column between both spans), two immediately at the end of the first span (over the middle of the central column) and one after the bridge (Figure 8.22(a)). These tubes were fixed at the road edges with clamps. The pneumatic tubes were connected to the pneumatic converters in the middle of the bridge to minimise the lengths of tube required. These converters were inside a car to prevent them from freezing. The pneumatic converters and signal cables from the mechanical strain amplifiers were connected to the computer data acquisition equipment which was kept in the car (Figure 8.22(b)). The sampling rate for all channels was 250 Hz.

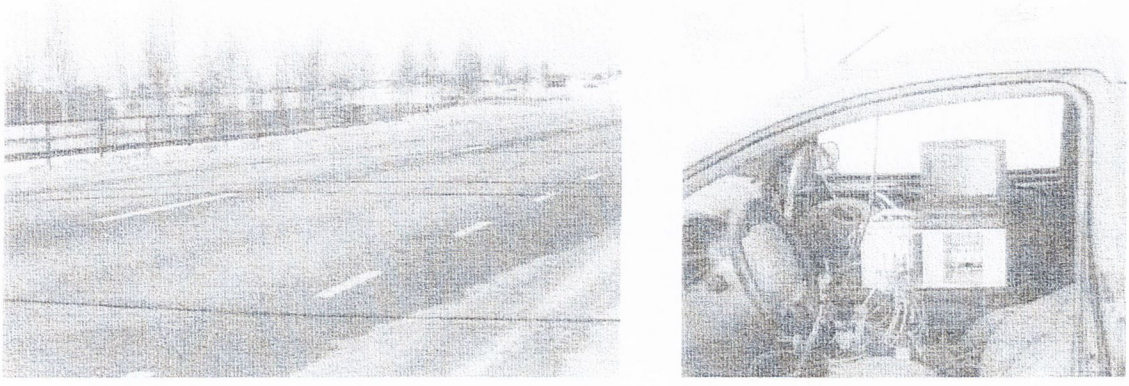

(a) Rubber tubes (b) Data Acquisition Equipment

Figure 8.22 – Measuring Devices (Luleå)

8.3.2 Testing

A 3-axle truck with a rear tandem (static axle weights: 6.25, 8 and 6.5 tonnes, with axle spacings: 4.20 and 1.30 m) and a 6-axle semi-trailer with a rear tridem (axle weights: 7.3, 10.95, 8.5, 7.8, 8.1 and 7.95 tonnes, with axle spacings 4.20, 1.35, 5.35, 1.35 and 1.35 m) were used to evaluate B-WIM accuracy. The axle loads of these calibration trucks were measured with portable static scales. The data used for the analysis belongs to the test period of June 1997.

Bridge dynamics were found to be negligible. A record of the unfiltered free vibration of the bridge due to a fully laden 6-axle truck is shown in Figure 8.23. There are not significant vibrations remaining once the truck has left the second span of the bridge.

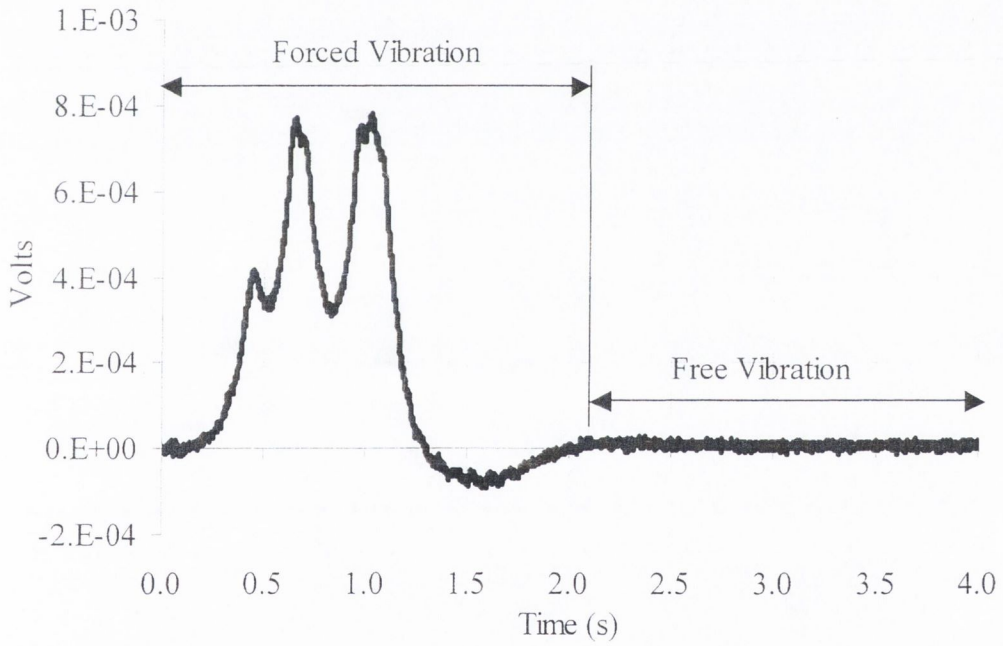

Figure 8.23 – Measured Record in Free Vibration (Luleå)

The determination of the influence line in this structure has been a tedious task, as the bridge behaviour appears to change for the different seasons where the test took place (Jacob et al 2000, McNulty 1999). These methods work in the time domain and they take a theoretical influence line as an initial starting point. However, the structural behaviour of this influence line could differ significantly from the bridge and the calculation of the 'real' influence line from experimental data can consume a considerable amount of time. These

difficulties are easily overcome by applying the calibration algorithm in the frequency domain suggested in Section 8.2. With this approach, the determination of boundary conditions is straightforward.

Figures 8.24(a) and (b) show the voltage-time history and the corresponding Fourier transform respectively, for the passing of a three-axle truck at 51.48 km/h.

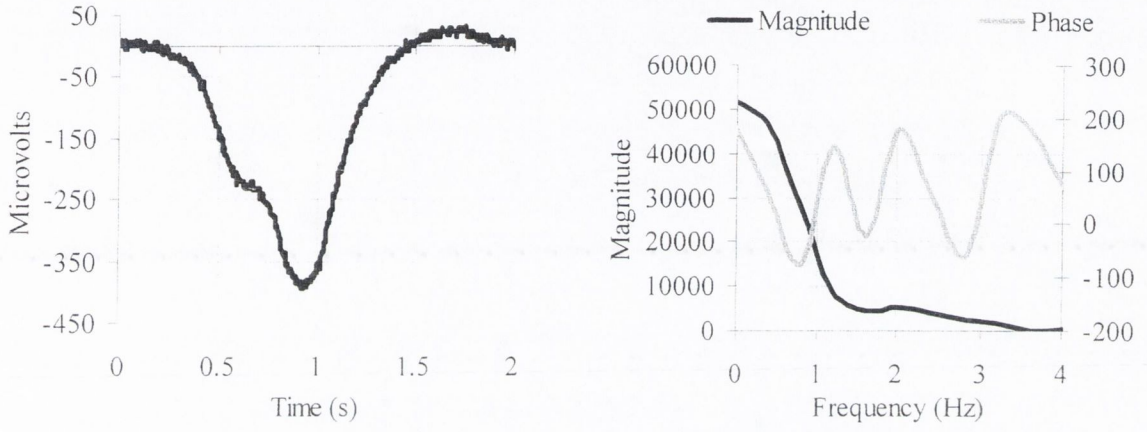

(a) Time domain (b) Frequency domain

Figure 8.24 – Strain due to three-axle truck at 51.48 km/h (Luleå)

Figures 8.25(a) and (b) show the transform and inverse transform respectively when applying Equations 8.1 and 8.2 to the spectrum represented in Figure 8.24(b). Figure 8.25(b) represents the experimental influence line for this particular run.

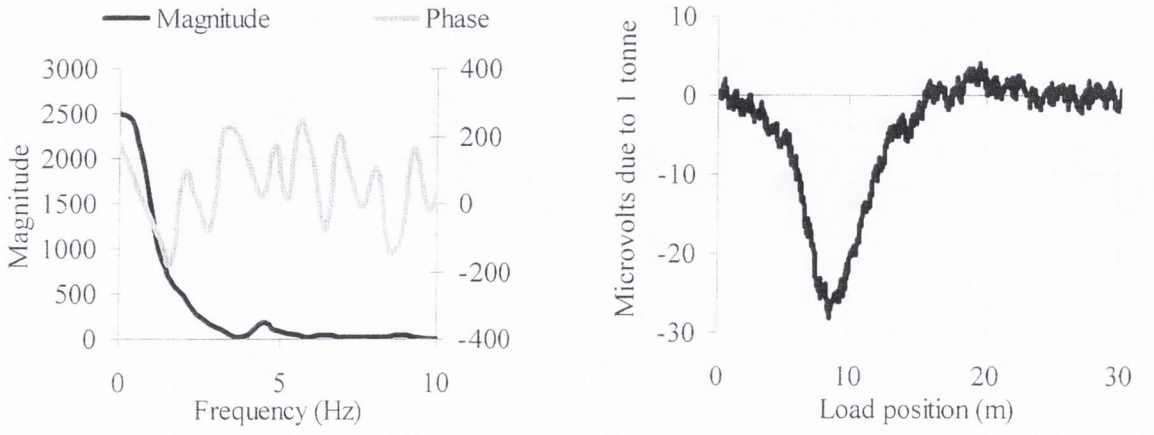

(a) Frequency domain (b) Influence line

Figure 8.25 – Bridge response due to a unit load (Luleå)

Accuracy analysis is done under limited reproducibility conditions (R1): two vehicles passing several times at different combinations of speed and with small variations in lateral position. The influence line from Figure 8.25(b) has been used for testing all runs, but a better approximation of the real influence line could have been obtained by averaging the experimental influence lines obtained for every calibration run. Table 8.11 shows the final result. Gross weight is not very accurate mainly due to the 4 Hz hardware filter. This filter smoothed out strain peaks and removed a significant static component from the total strain. The degree of accuracy achieved by other calibration methods based on adjustments in the time domain is one class better (Sections 3.5 and 3.7.4). However, these methods used a bigger number of runs for the same two calibration vehicles, but specially, two different influence lines depending on the vehicle speed.

Table 8.11 – Accuracy classification (Luleå) (R1)

(**n**: Total number of vehicles; **m**: mean; **s**: Standard deviation; π_0: level of confidence; δ: tolerance of the retained accuracy class; δ_{min}: minimum width of the confidence interval for π_0; π: Level of confidence of the interval $[-\delta,\delta]$)

	Relative error statistics				Accuracy calculation				
Criterion	**n**	**m** (%)	**s** (%)	π_0 (%)	**Class**	δ (%)	δ_{min} (%)	π (%)	**Class Retained**
Single axle	23	-2.83	10.66	91.5	**D+(20)**	25	24.4	92.3	**E(50)**
Axle of group	76	0.30	26.83	94.6	**E(50)**	65	58.6	96.9	
Group of axles	33	0.16	9.99	92.8	**D+(20)**	23	22.1	94.0	
Gross Weight	23	0.45	6.62	91.5	**C(15)**	15	14.8	91.9	

Strain responses are plotted versus vehicle position on the bridge in Figure 8.26. Significant differences in magnitude can be seen depending on the two ranges of speed (about 50 km/h and 80 km/h) and the truck configuration (three- or six-axle truck). Filtering is the main cause of this phenomenon. The bridge response due to the three-axle truck is smaller at 80 km/h than at 50 km/h as shown in Figure 8.26(a), unlike the response due to the six-axle truck which is smaller at 50 km/h.

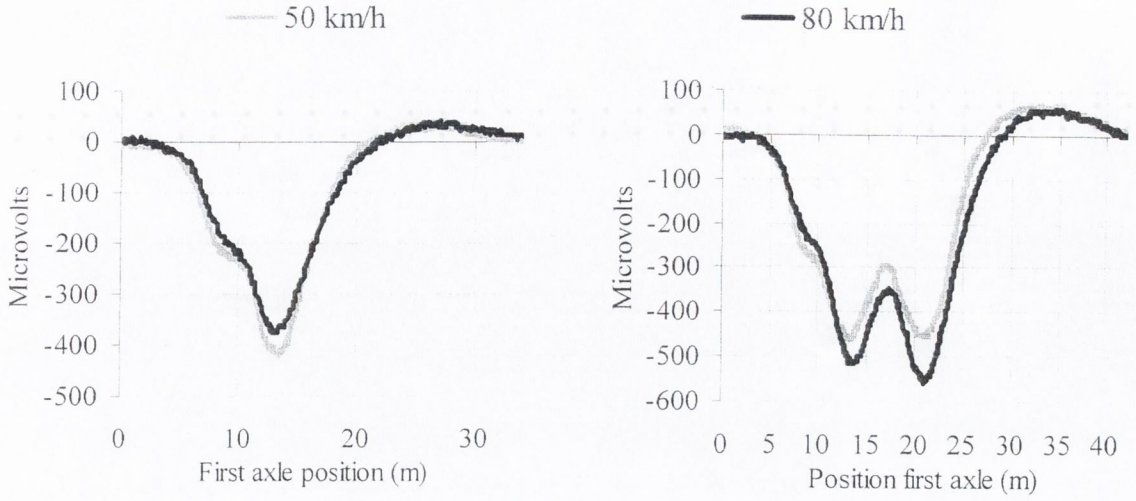

(a) Three-axle truck (b) Six-axle truck

Figure 8.26 – Influence of 4Hz hardware filter on the record (Luleå)

If the test took place in full repeatability conditions (several passes of one vehicle at the same speed and with the same load) for the three-axle truck travelling at about 50 km/h, the accuracy classes that result are given in Table 8.12. The improvement in prediction of single axle weights is noteworthy (from D+(20) to B+(7)), but the GVW and axle group criteria remain in class C(15) and D+(20) respectively.

Table 8.12 – Accuracy classification (Luleå) (r1) (3-axle truck at 50 km/h)

(**n**: Total number of vehicles; **m**: mean; **s**: Standard deviation; π_0: level of confidence; δ: tolerance of the retained accuracy class; δ_{min}: minimum width of the confidence interval for π_0; π: Level of confidence of the interval $[-\delta,\delta]$)

	Relative error statistics				Accuracy calculation				
Criterion	**n**	**m (%)**	**s (%)**	π_0 (%)	**Class**	δ (%)	δ_{min} (%)	π (%)	**Class Retained**
Single axle	8	-0.30	3.22	93.4	**B+(7)**	11	9.7	96.2	**E(30)**
Axle of group	16	-0.16	12.51	96.8	**E(30)**	41	36.2	98.5	
Group of axles	8	0.30	6.29	93.4	**D+(20)**	23	19.0	97.4	
Gross Weight	8	0.12	3.62	93.4	**C(15)**	15	10.9	98.7	

If the runs of the six-axle truck at 50 km/h are included in the testing, all accuracy classes are worse as shown in Table 8.13. This is motivated by the different smoothing effect of the hardware filter in different axle group configurations. The influence line in Figure 8.25(b) works best for that three-axle configuration, but it changes for other trucks. Axle of

group and group of axles criteria are the ones determining the overall accuracy class again. The mean error for the axle group is negative, this is, the axle group is being underweighed as a result of the loss of static component caused by filtering.

Table 8.13 – Accuracy classification (Luleå) (R1) (3 and 6-axle trucks at 50 km/h)

(**n**: Total number of vehicles; **m**: mean; **s**: Standard deviation; π_0: level of confidence; δ: tolerance of the retained accuracy class; δ_{min}: minimum width of the confidence interval for π_0; π: Level of confidence of the interval $[-\delta,\delta]$)

	Relative error statistics				Accuracy calculation				
Criterion	**n**	**m** (%)	**s** (%)	π_0 (%)	**Class**	δ (%)	δ_{min} (%)	π (%)	**Class Retained**
Single axle	13	7.07	4.11	87.9	**B(10)**	15	14.6	89.5	**E(60)**
Axle of group	41	-4.45	30.81	93.4	**E(60)**	77	68.6	96.3	
Group of axles	18	-3.44	11.38	90.3	**D(25)**	28	26.4	92.4	
Gross Weight	13	0.74	8.72	87.9	**D+(20)**	20	19.9	88.2	

If the calibration took place for the six-axle truck travelling at about 80 km/h, the results are shown in Figure 8.27. Compared to the influence line derived at 50 km/h (Figure 8.25(b)), the influence line at 80 km/h is very similar in the first span, but lightly bigger and smoother in the second span.

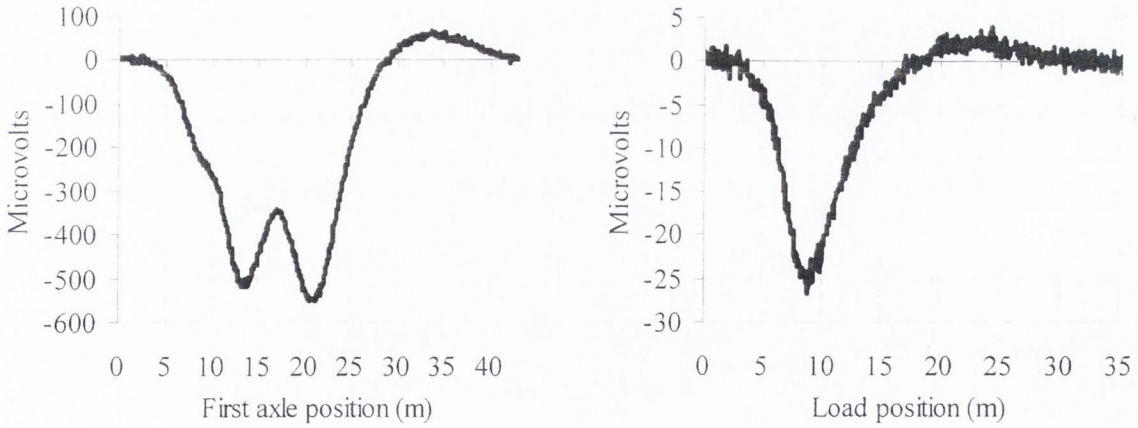

(a) Measured record (b) Experimental Influence line

Figure 8.27 – Calibration of 6-axle truck at 80 km/h

The accuracy classes in full repeatability conditions for runs of the six-axle truck at 80 km/h are given in Table 8.14. There is a significant improvement in all accuracy classes derived from the lower deviation in each of the single runs.

Table 8.14 – Accuracy classification (Luleå) (r1) (6-axle truck at 80 km/h)

(**n**: Total number of vehicles; **m**: mean; **s**: Standard deviation; π_0: level of confidence; δ: tolerance of the retained accuracy class; δ_{min}: minimum width of the confidence interval for π_0; π: Level of confidence of the interval $[-\delta,\delta]$)

	Relative error statistics				Accuracy calculation				
Criterion	**n**	**m (%)**	**s (%)**	**π_0 (%)**	**Class**	**δ (%)**	**δ_{min} (%)**	**π (%)**	**Class Retained**
Single axle	5	2.61	0.91	84.8	**A(5)**	8	4.8	99.5	**D+(20)**
Axle of group	25	-0.10	9.52	97.6	**D+(20)**	30	26.9	98.9	
Group of axles	10	-0.40	1.62	95.0	**A(5)**	7.14	4.9	99.5	
Gross Weight	5	0.02	1.51	84.8	**A(5)**	5	4.5	89.4	

In Table 8.15, the runs of the three-axle and six-axle trucks at 80 km/h are included in the analysis (Limited reproducibility conditions) and the overall accuracy improves from D+(20) to C(15).

Table 8.15 – Accuracy classification (Luleå) (3 and 6-axle trucks at 80 km/h) (R1)

(**n**: Total number of vehicles; **m**: mean; **s**: Standard deviation; π_0: level of confidence; δ: tolerance of the retained accuracy class; δ_{min}: minimum width of the confidence interval for π_0; π: Level of confidence of the interval $[-\delta,\delta]$)

	Relative error statistics				Accuracy calculation				
Criterion	**n**	**m (%)**	**s (%)**	**π_0 (%)**	**Class**	**δ (%)**	**δ_{min} (%)**	**π (%)**	**Class Retained**
Single axle	10	4.48	3.13	85.0	**B+(7)**	11	10.2	89.2	**C(15)**
Axle of group	35	-0.51	11.16	93.0	**C(15)**	25	24.7	93.3	
Group of axles	15	-0.70	2.85	89.1	**A(5)**	7.14	6.6	92.3	
Gross Weight	10	0.04	2.13	85.0	**A(5)**	5	4.9	86.3	

Figure 8.28 illustrates the errors in predicted axle weights using two influence lines (at 50 and 80 km/h). At 50 km/h, errors are bigger due to a higher deviation in the strain response.

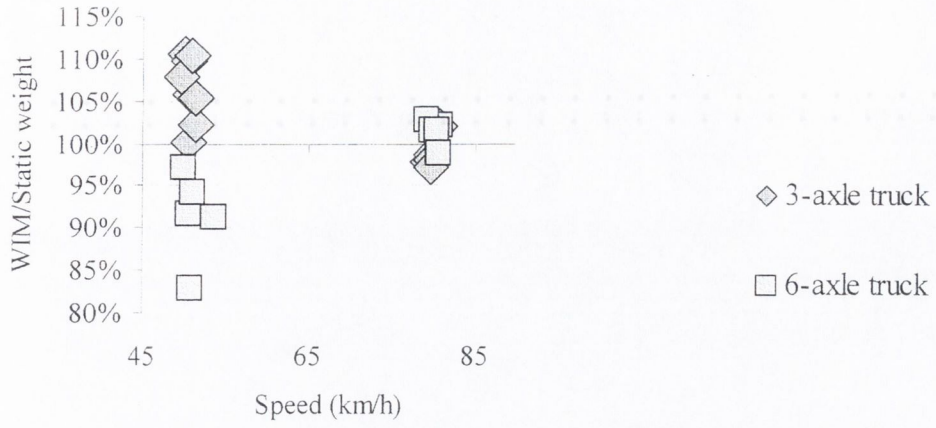

(a) Gross weight

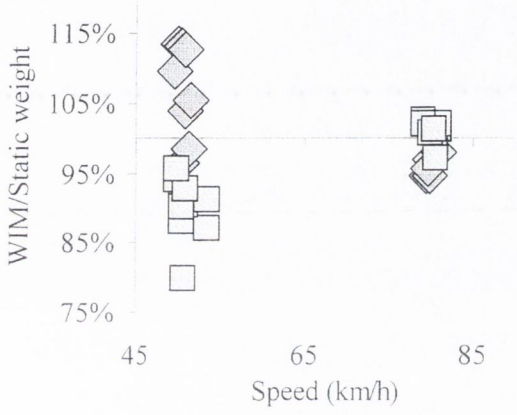

(b) Axle group

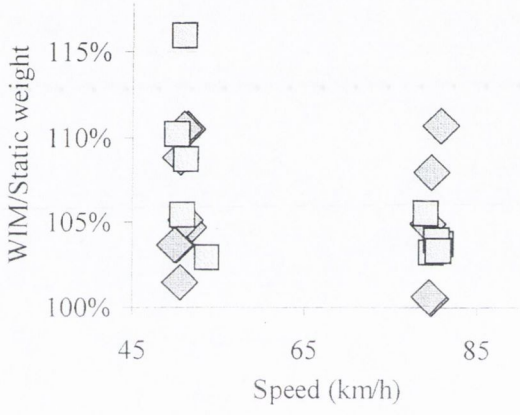

(c) Single axle

Figure 8.28 – Errors in weights by using a theoretical beam model

8.4 BELLEVILLE, TWO SPAN (50 m EACH) CONTINUOUS BRIDGE

The Belleville site is located on the southbound carriageway of the A31 Motorway between Metz and Nancy in North Eastern France. Data was obtained in June 1998 as part of the Continental Motorway Test. The location of the Belleville B-WIM site is marked in Figure 8.29.

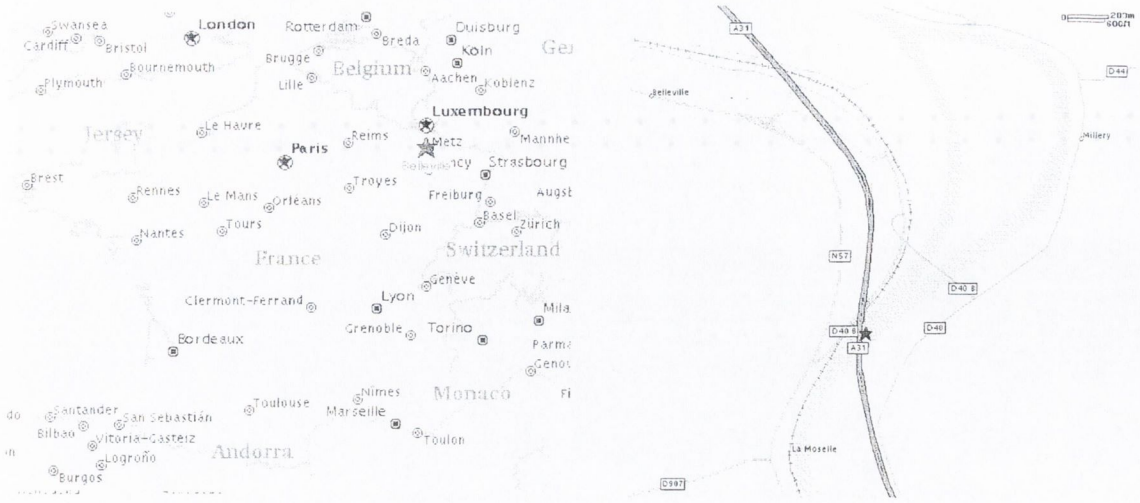

(a) General location (b) Detailed map

Figure 8.29 – Bridge Location (Belleville)

The bridge is a two span composite box girder, consisting of a steel box with a concrete deck (Figure 8.30). The spans are 54.89 and 51.69 m long. There are two lanes of traffic crossing this bridge in the same direction. The speed limit on this section of the road is 130 km/h for cars and 90 km/h for heavy vehicles.

Figure 8.30 – Side View of Belleville Bridge

8.4.1 Installation

The installation of axle detectors, data acquisition equipment and strain gauges is described below.

Axle Detectors

Low-grade piezoelectric axle detectors were permanently embedded into the pavement to record the occurrences of axles in both lanes of traffic. These sensors, together with associated hardware, result in a 20 ms voltage output pulse being transmitted when an axle strikes a sensor. The sensors are located 10.25 m prior to the bridge (Figure 8.31(a)). The installation of these sensors required road closure in dry weather conditions. The coaxial cables from the piezos were connected to the SCXI through an interface as described in Section 4.3.1. There were a lot of difficulties with the signals from the piezo sensors, and some axles were still passing undetected at the time of the test.

In the same experiment, Lutzenberger and Baumgärtner (2000) from the Technische Universität München (TUM) demonstrated how axle and lane identification can be possible from measuring the longitudinal bending of the concrete slab. Records from two locations spaced longitudinally by a fixed amount allow for calculation of speed and axle spacings (Section 4.3.2). They also discuss the influence of road roughness (measured by LCPC) on the bridge and truck response.

Data acquisition equipment

The SCXI data acquisition equipment was placed within the box section of the bridge for safe dry storage (Figure 8.31(b)). The equipment was located at midspan to keep the length of the strain gauge cables and the distance to the piezolectric sensors relatively short. Electricity is available within the bridge. Strain gauges are connected to the SCXI through a four core high quality shielded cable.

(a) Piezos

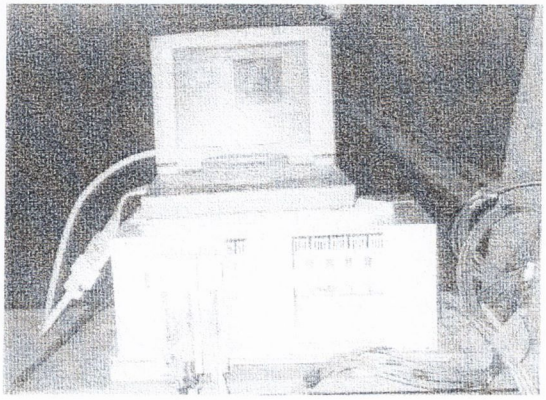

(b) Data Acquisition Equipment

Figure 8.31 – Data Collection Devices (Belleville)

Strain gauges

Strain gauges (120Ω and 2.13 gauge factor) were attached at a number of longitudinal locations along the bridge to test a multiple-sensor BWIM system. Each span is divided into eight sections separated by diaphragm walls as shown in Figure 8.32. Five longitudinal positions were chosen for strain gauge installation. These positions are midspan and three quarter span of the north span, over the central support, and one quarter and midspan of the south span (Figure 8.32).

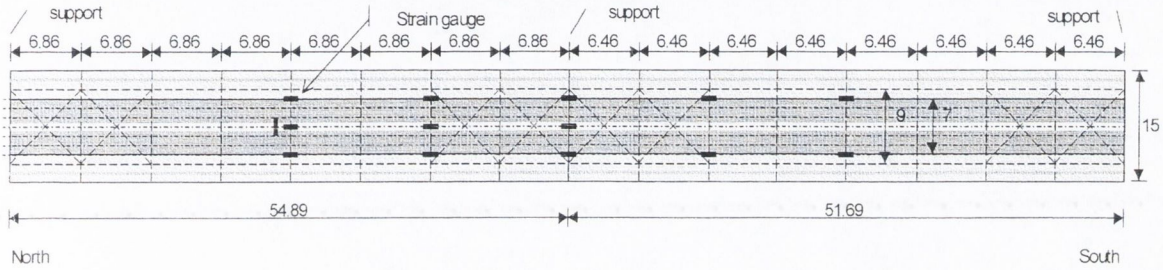

Figure 8.32 – Layout of Belleville Bridge

Seven stiffeners in the longitudinal direction are attached to the soffit plate of the steel box. Additional stiffeners are located in the areas of the bridge close to the central support. The longitudinal bending of two or three vertical stiffeners is measured at each instrumented section as illustrated in Figure 8.33.

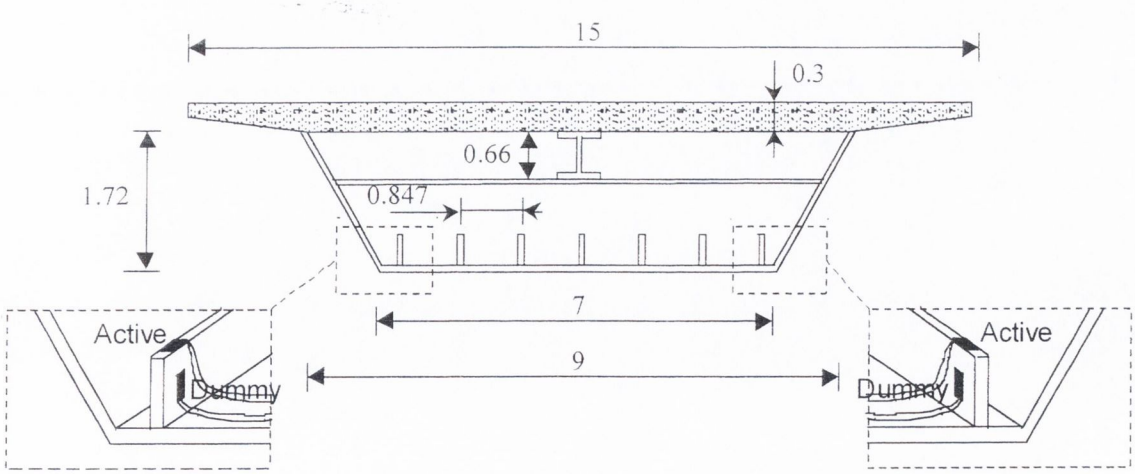

Figure 8.33 – Cross Section and Strain Gauge Location

The protective paint coating of the stiffeners is removed to glue the gauges directly to the bare steel. Each pair of gauges is arranged in a half bridge configuration with one active and one dummy gauge (Section 4.2.1). Originally, strain gauges were installed by the Centre d'Etudes Techniques de l'Equipment de l'est (CETÉ de L'EST) at the two outer stiffeners at 4 longitudinal locations (total of 8 sensor locations). Due to the lack of resolution (Kealy 1997), the author placed more gauges at the central stiffener in three of the four instrumented sections and two sensors in a new section at the middle of the second span. The position of all 13 locations is given in Table 8.16.

Table 8.16 - Distances of strain gauges from support (Belleville)

Sensor location no.	Stiffener No.	Longitudinal position (m)	Sensor location no.	Stiffener No.	Longitudinal position (m)
1	1	27.39	7	1	54.94
2	4	27.39	8	4	54.94
3	7	27.39	9	7	54.94
4	1	41.12	10	1	67.76
5	4	41.12	11	7	67.76
6	7	41.12	12	1	80.69
			13	7	80.69

Unfortunately, as a result of isolation problems and electrical interference, the data obtained at the tests was not usable. The strain measurements carried out by the TUM team at the middle of the north span are used for the accuracy analysis that follows.

8.4.2 Testing

The dynamic properties of the bridge were derived from measured strains and accelerations by Lutzenberger and Baumgärtner (1999). They used this data to design a finite element model of the bridge in correspondence with the real frequencies. Kessler (1997) refined this model and the modes of vibration are represented in Figure 8.34.

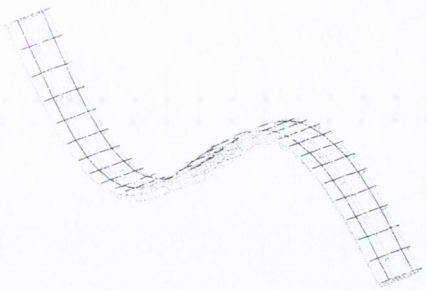

(a) 1st Mode (1.33 Hz)

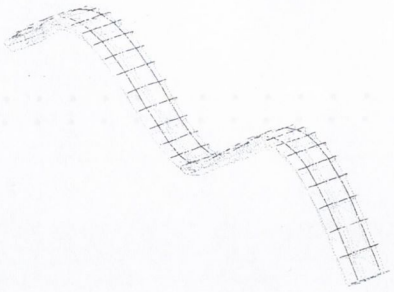

(b) 2nd Mode (2.00 Hz)

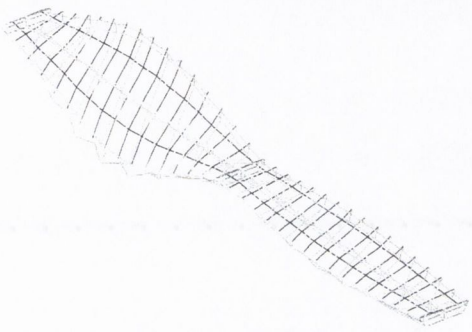

(c) 3rd Mode (4.50 Hz)

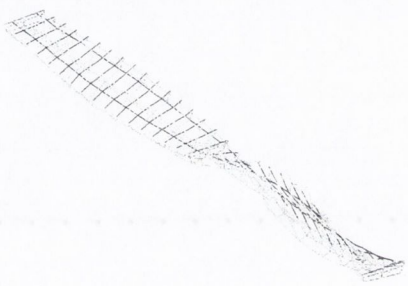

(d) 4th Model (4.58 Hz)

Figure 8.34 - Modes of Vibration of Belleville Bridge

An instrumented vehicle was used during the test. VTH (Finland) provided the data on the dynamic wheel loads applied by the truck. The vehicle is a three axle rigid lorry with axle spacings of 4.20 m and 1.20 m (Figure 8.35(a)). Static axle weights are 58.74, 86.19 and 72.17 kN for the first, second and third axles respectively. A theoretical model of this vehicle has been presented in Section 6.4. All axles are equipped with traditional steel springs. The tandem has dual tyres and all tyres have a diameter of 1.05 m.

Dynamic wheel loads are measured through strain gauges and accelerometers installed on the axles as shown in Figure 8.35(b). Strain gauges measure bending moment of the axle while accelerometers measure the inertial force component. The wheel load applied to the pavement is derived from the bending moment measured by the strain gauges plus the mass outboard of the strain gauges multiplied by the vertical acceleration given by the accelerometers.

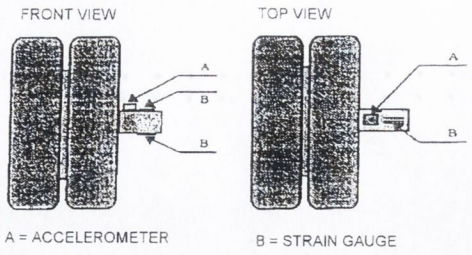

(a) VTH truck

(b) The locations of the sensors on the axle of vehicle

Figure 8.35 – Instrumented vehicle (after Huhtala et al. 1998)

Dynamic wheel load measurements are related to the road section under study using an electric eye to detect reflective tapes glued across the road lane every 10 m. There are a total of 13 strips with the first strip placed 10 m before the bridge joint (just 0.25 m after the second piezo to synchronise recordings of the B-WIM system and truck). The sampling rate is 1000 Hz. A total of six crossings took place at about 80 km/h.

Figure 8.36 shows the wheel forces applied by each axle for one of the runs. There are high dynamic forces prior to the bridge (from 1 to 10 m in Figure 8.36) and at the joint (located at 10 m) due to the unevenness of the road profile. These forces will cause strong bridge vibrations. The wheels of the rear tandem have a dynamic amplification of about 100% at the joint (Figures 8.36(b) and (c)). The forces at the end of the bridge are not as important as the road is relatively smooth along the bridge, except at about 90 m. This is due to a portable WIM system mounted on the road surface that caused wheels to jump and dynamic forces to increase by a maximum of 80% in the right wheel of the third axle (Figure 8.36(c)). There are also small differences between the left and right wheels of an axle caused by the difference in irregularities of each path.

The spectra of dynamic wheel forces are represented in Figure 8.37. There are dominant frequencies of 2.3 Hz for the front axle (body bounce) and 2.3 Hz and 9 Hz (axle vibrations) for the rear tandem.

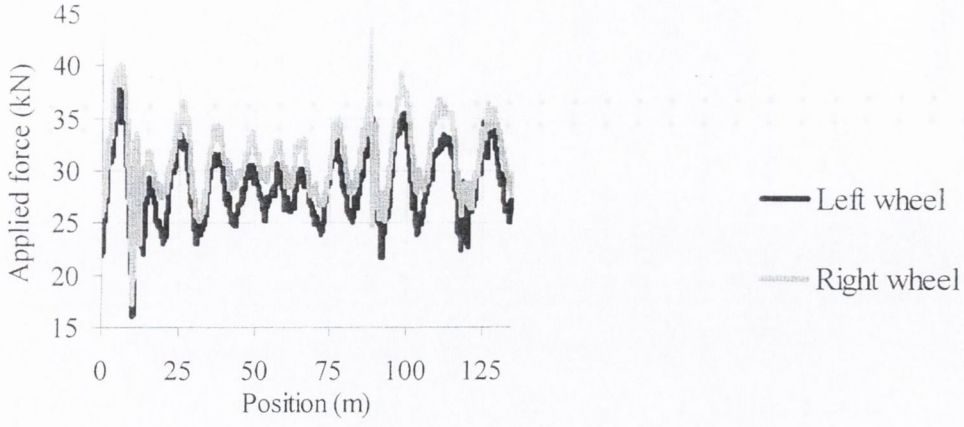

(a) First axle

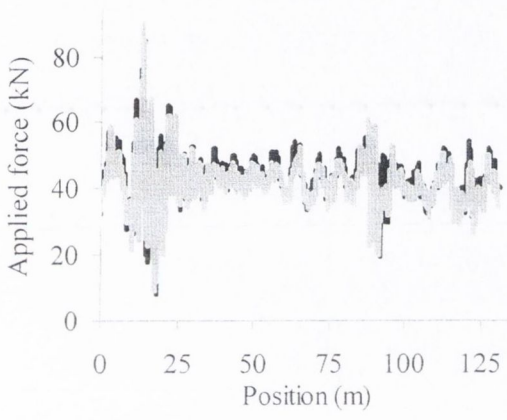

(b) Second axle

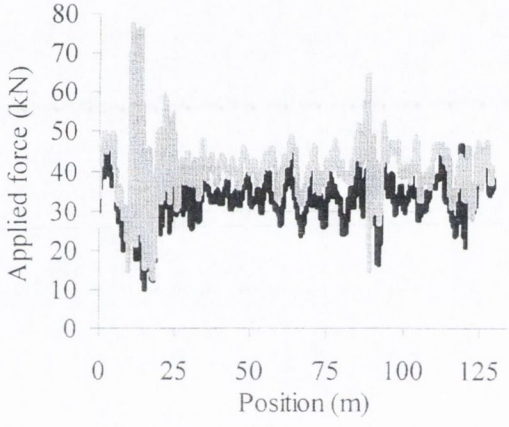

(c) Third axle

Figure 8.36 – Dynamic wheel forces

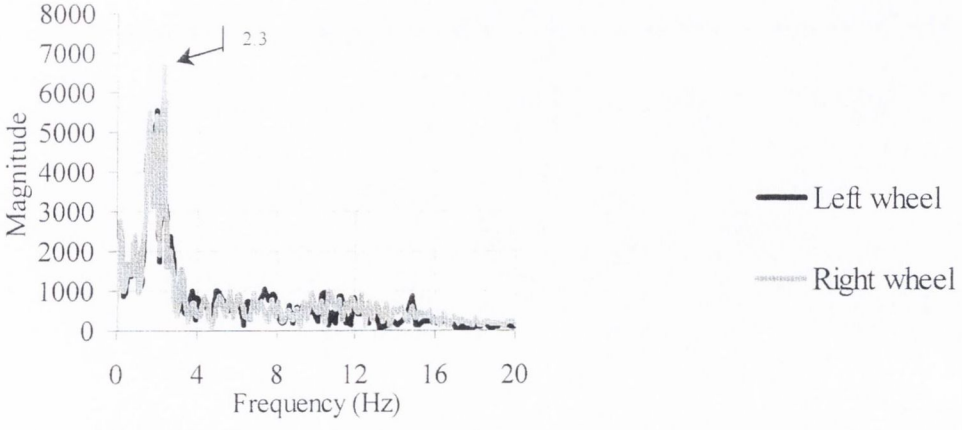

(a) First axle

Figure 8.37 (continued on following page)

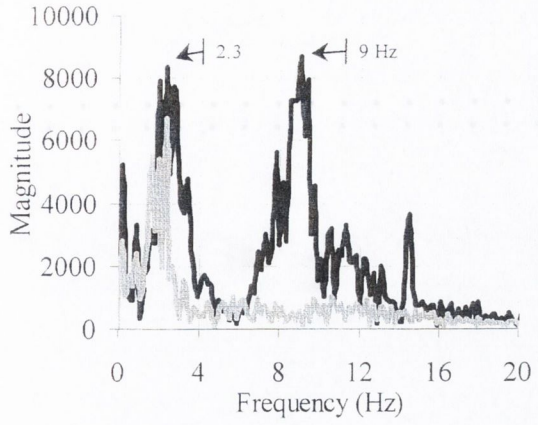

(b) Second axle

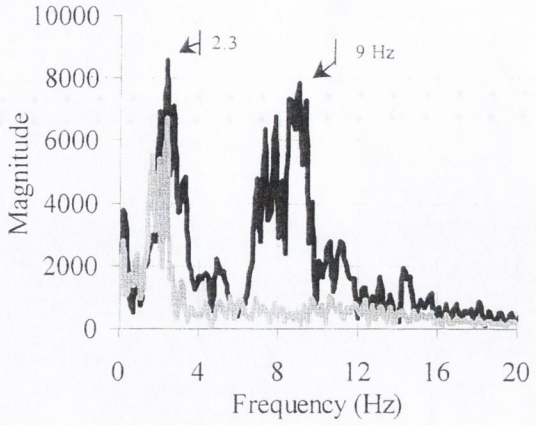

(c) Third axle

Figure 8.37 – Spectra of Dynamic wheel forces

The B-WIM system was calibrated following the experimental procedure described in previous sections. The measured record and its spectra are given in Figure 8.38.

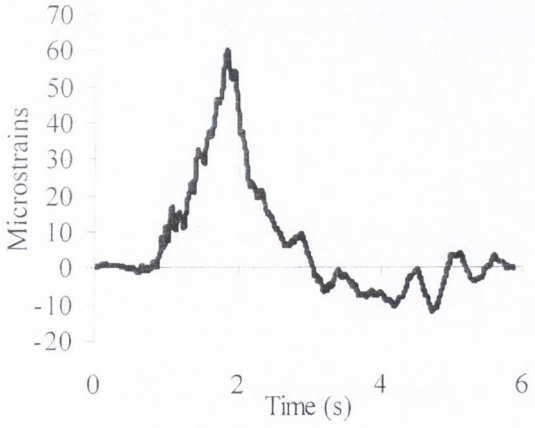

(a) Time Domain

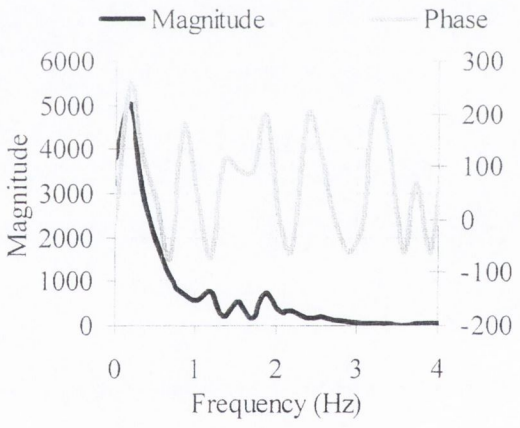

(b) Frequency Domain

Figure 8.38 – Measurements of 3-axle truck at 82.74 km/h (Belleville)

The results of calibration are shown in Figure 8.39.

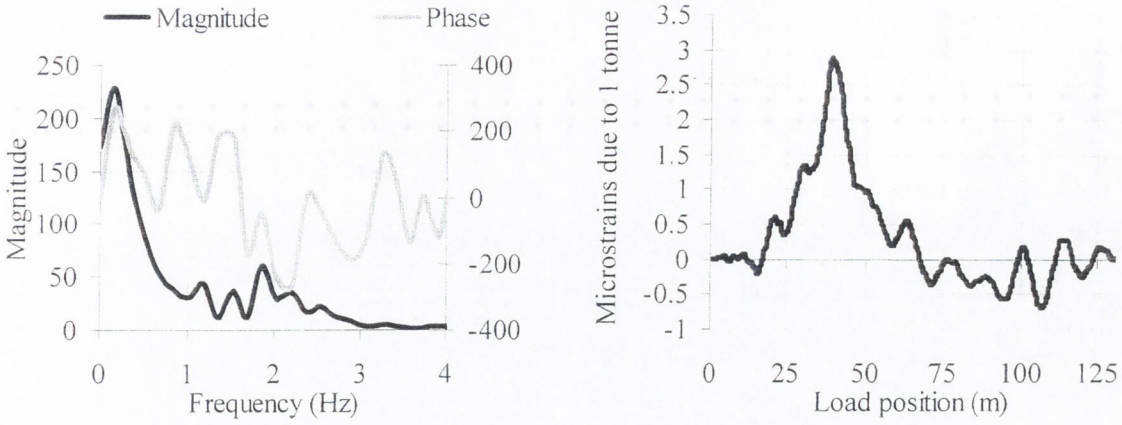

(a) Frequency domain (b) Time domain

Figure 8.39 – Bridge response due to a unit load travelling at 82.74 km/h (Belleville)

The six runs of the VTT truck are analysed in full repeatability conditions (r1) in Table 8.17 by a dynamic algorithm developed by the author. The total unit response due to a load at 82.74 km/h is used directly for all runs. Unlike an influence line, this unit response will be different for other speeds. The algorithm uses the measurements of the longitudinal bending of the steel girder and steel box at midspan. A class B(10) is achieved for gross weight, but the vehicles acts as a whole and individual axle weights can not be predicted.

Table 8.17 – Accuracy classification by dynamic algorithm (r1) (Belleville)

(**n**: Total number of vehicles; **m**: mean; **s**: Standard deviation; π_0: level of confidence; δ: tolerance of the retained accuracy class; δ_{min}: minimum width of the confidence interval for π_0; π: Level of confidence of the interval $[-\delta,\delta]$)

	Relative error statistics				Accuracy calculation				
Criterion	**n**	**m** (%)	**s** (%)	π_0 (%)	**Class**	δ (%)	δ_{min} (%)	π (%)	**Class Retained**
Single axle	6	127.9	49.94	89.6	**E(250)**	300	252.8	96.9	**E(250)**
Group of axles	6	-47.3	22.14	89.6	**E(100)**	110	102.8	93.1	
Gross Weight	6	0.06	2.70	89.6	**B(10)**	10	8.2	95.4	

It was thought that the response of transverse bending might be more sensitive to individual axles. The total response due to a unit moving load is calculated for the transverse bending of the concrete slab. Figures 8.40(a) and (b) show the measured record for the fifth run of the calibration truck and the corresponding spectra.

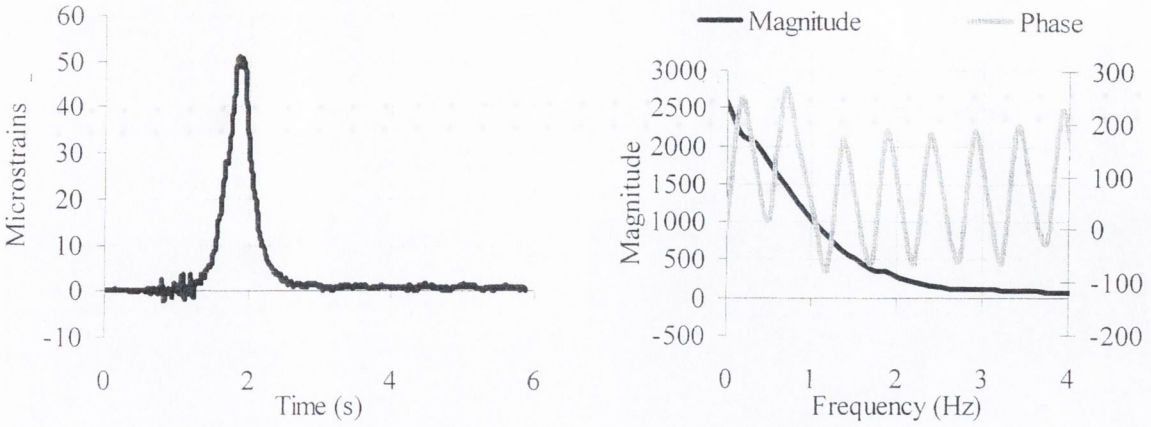

(a) Time Domain (b) Frequency Domain

Figure 8.40 – Transverse bending at midspan due to truck at 82.74 km/h (Belleville)

The corresponding dynamic unit response in frequency and time domains is given in Figures 8.41(a) and (b) respectively.

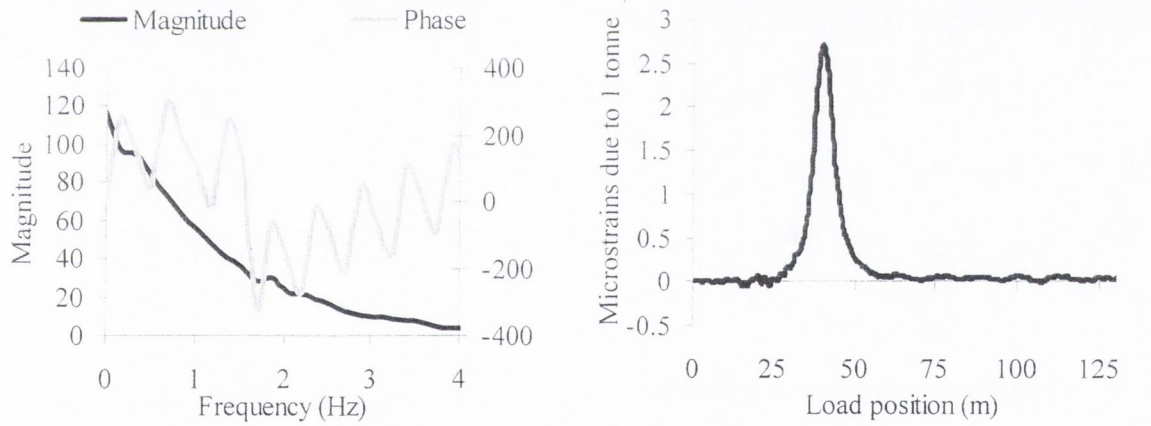

(a) Frequency domain (b) Time domain

Figure 8.41 – Transverse bending due to a unit load travelling at 82.74 km/h (Belleville)

Table 8.18 gives the accuracy classes achieved by a dynamic algorithm based on this transverse bending of the concrete slab. Accuracy in GVW decreases when considering transverse bending instead of longitudinal bending. Transverse bending is a very localised effect that can be isolated from other vehicles in the bridge (the shape of the unit response is narrower), but it is very sensitive to transverse position of the truck on the bridge. In a one-dimensional B-WIM algorithm, transverse location can not be managed and the result in GVW is very poor.

Table 8.18 – Accuracy classification by dynamic algorithm (transverse) (r1) (Belleville)

(**n**: Total number of vehicles; **m**: mean; **s**: Standard deviation; π_0: level of confidence; δ: tolerance of the retained accuracy class; δ_{min}: minimum width of the confidence interval for π_0; π: Level of confidence of the interval $[-\delta,\delta]$)

	Relative error statistics				Accuracy calculation				
Criterion	**n**	**m** (%)	**s** (%)	π_0 (%)	**Class**	δ (%)	δ_{min} (%)	π (%)	**Class Retained**
Single axle	6	100.2	33.30	89.6	**E(180)**	216	183.4	97.0	**E(180)**
Group of axles	6	-35.64	16.91	89.6	**E(75)**	82.5	78.0	92.6	
Gross Weight	6	1.11	11.70	89.6	**E(40)**	40	35.6	93.5	

Figure 8.42 illustrates longitudinal and transverse bending for the six runs of the calibration truck. It can be seen how deviation in strain is higher for transverse bending, probably due to variations in lateral position (Strain peak is around 60 με for longitudinal bending in any run, but varies from 45 to 65 με for transverse bending). Transverse bending appears to be more adequate for weighing individual axles, but this requires a two-dimensional algorithm and more strain sensors to take into count the transverse position of the truck.

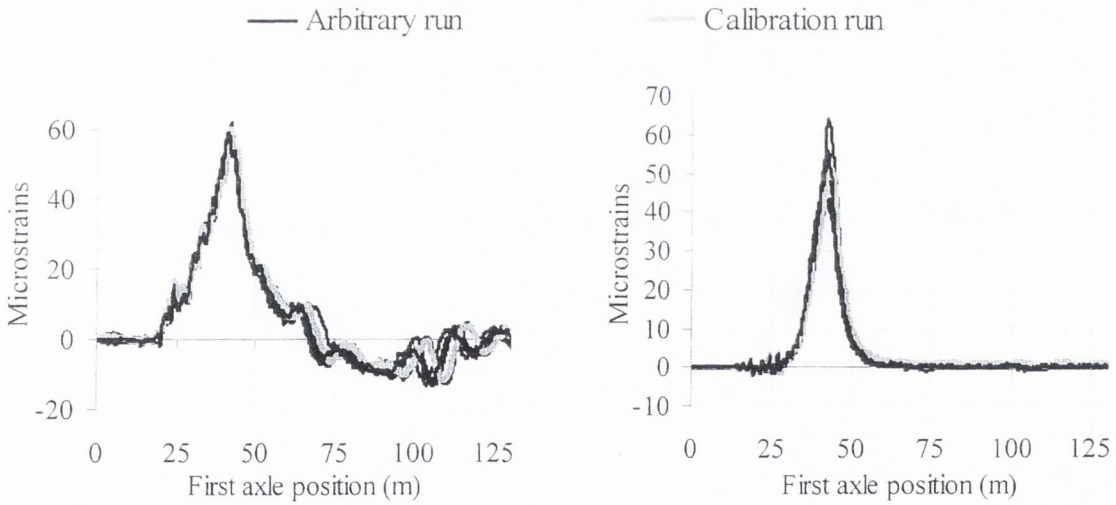

(a) Longitudinal bending (b) Transverse bending

Figure 8.42 – Measured records at midspan due to three-axle truck (Belleville)

8.5 SLOVENIA, MEDIUM SPAN (32 m) SIMPLY SUPPORTED BRIDGE

The fourth site is located in Slovenia. The bridge is a 32 m long simply supported beam and slab. There are five beams along the underside of the bridge and the bridge has two lanes with traffic running in opposing directions. The instrumentation consisted of six longitudinal sections spaced every 4 m (see Figure 8.43). Two strain sensors were placed at each section, on the 2nd and 4th beam of the bridge. Data was recorded at 512 Hz.

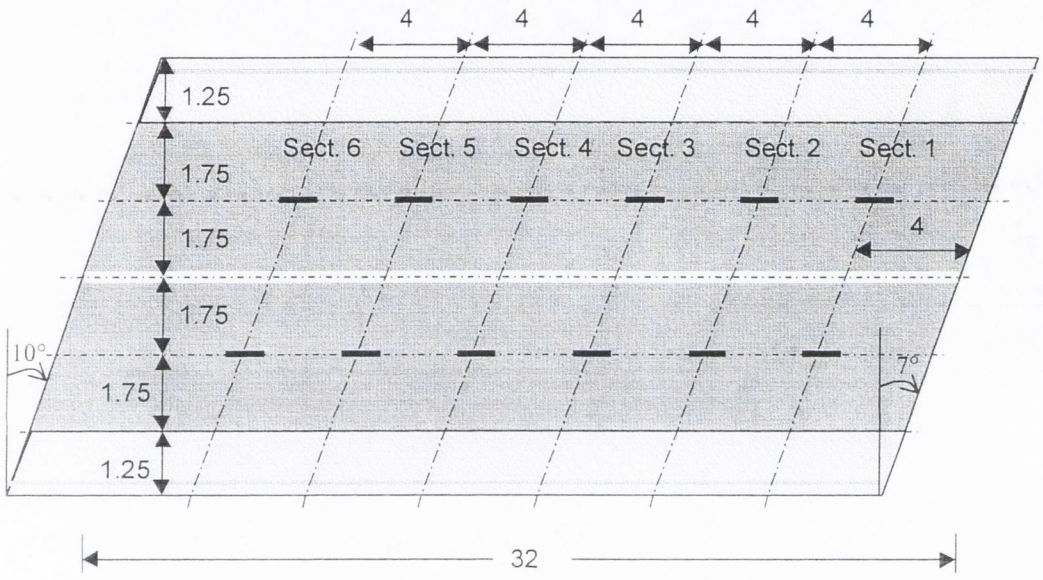

Figure 8.43 – Layout of Slovenian bridge

The dynamic multiple sensor algorithm (Section 7.5.2) is tested for each lane and direction of traffic flow separately. The signal from two sensors at the same section is added together for calculation purposes. This results in six equations (one per longitudinal section) at each instant.

8.5.1 Testing of the northbound carriageway

A two-axle truck with axle spacing of 4.35 m and static weights, 33.93 kN and 126.5 kN in the front and rear axles respectively, is driven over the bridge in the north-south direction at 59.85 km/h. Figure 8.44 shows the record in free vibration corresponding to two sensors at midspan. From this figure, a damped frequency of 3.54 Hz and 5% damping result. The

natural frequency is 3.54 Hz. These parameters have been obtained following the guidelines given in Section 5.2.1.

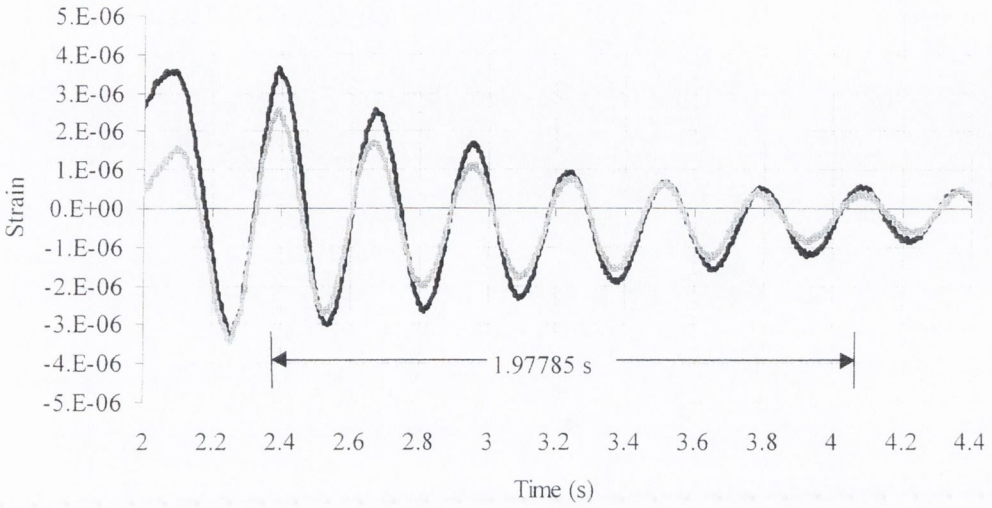

Figure 8.44 – Record in Free vibration (Slovenia)

The system is calibrated by obtaining the spectrum defined by Equations 8.1 and 8.2, and then by calculating the inverse Fourier transform. Measurement on site and dynamic response due to a unit moving load are represented in Figure 8.45 for longitudinal sections 1, 2 and 3 (Figure 8.43), and in Figure 8.46 for sections 4, 5 and 6. The origin of these curves is related to the instant the first axle hits the second axle detector, placed 3.15 m before the bridge joint. By using this reference at a safe distance from the influence of the bridge joint, there is no need to know at what exact position the applied load causes the bridge to start bending. In this way, the uncertainty on the real boundary conditions and the very small strains generally induced near the supports is avoided.

An additional advantage of this calibration method is that it allows for sensors of different sensitivity to be installed without any disturbance to the final results. Thus, a theoretical model of a simply supported bridge would be expected to generate bigger strains at midspan, but this calibration method is based on 'sensors', not structural models representing assumed bridge behaviour.

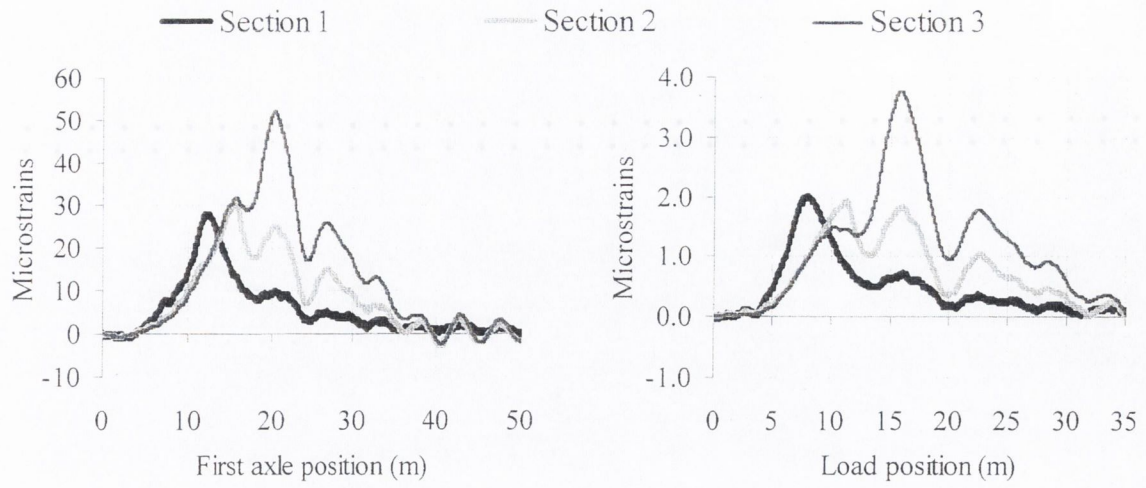

(a) Measurements due to two-axle truck

(b) Total (static + dynamic) bridge response due to a moving unit load

Figure 8.45 – Calibration of sections at 4, 8 and 12 m in northbound lane (Slovenia)

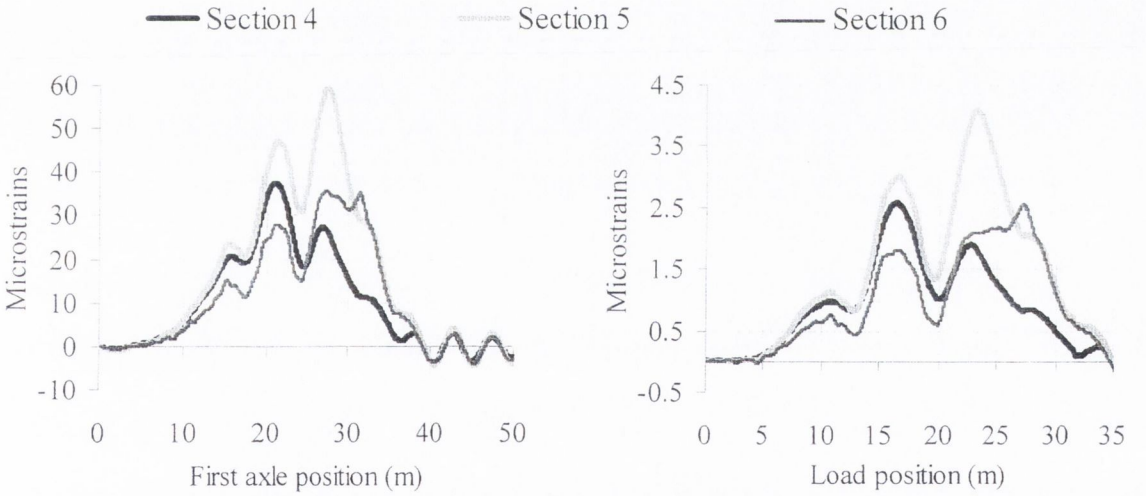

(a) Measurements due to two-axle truck

(b) Total (static + dynamic) bridge response due to a moving unit load

Figure 8.46 – Calibration of sections at 16, 20 and 24 m in northbound lane (Slovenia)

The influence lines obtained in Figures 8.45 and 8.46 are valid only for that speed if a dynamic multi-sensor algorithm is to be used. For other speeds that are not available from calibration; it will be necessary to interpolate from available responses calibrated at similar speeds or otherwise, to derive them from dynamic models. If an influence line is required, dynamics can be removed from this experimental calibration in one of several ways:

(a) Filtering of the total response due to a single load: The risk of suppressing the static component has been reduced as the signal due to one single axle is to be filtered (there are no axle groups). Filtering can be safe if the first natural frequency of the bridge is high enough.

(b) If the first natural frequency of the bridge is relatively low or the real influence line is likely to be very sharp, filtering could smooth out peaks containing part of the static response. In this case, dynamics could be removed through specific models of the bridge behaviour (i.e. Equation 5.31). Hints to obtain the parameters involved in these models are given in Section 9.2.

(c) Another possibility to obtain the influence line is to use the calibration run corresponding to the lowest speed. The bridge response will be closer to the static as the vehicle speed approaches zero (Section 5.3).

The curves obtained in Figures 8.45(b) and 8.46(b) can be used to calculate axle force on a continuous basis as explained in Section 7.5.2 for the multiple-sensor algorithm. The results are shown in Figure 8.47.

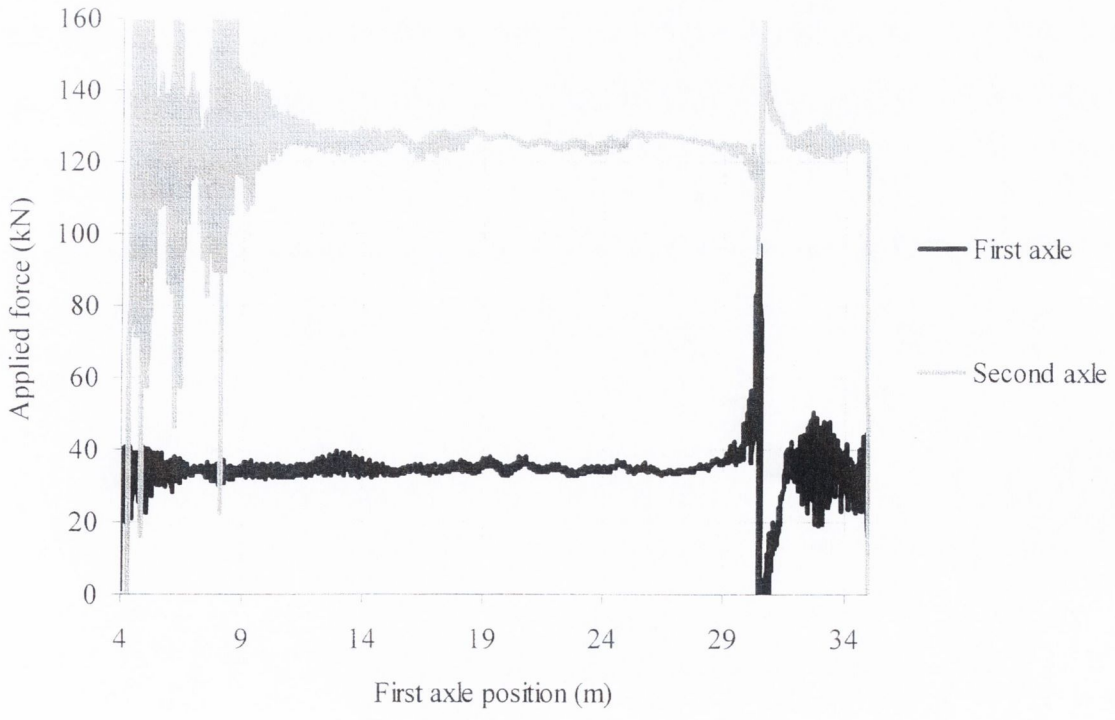

Figure 8.47 – Calculated load history in northbound carriageway (Slovenia)

The origin of the x-axis is related to the location of the second axle detector, 3.15 m before the bridge. Hence, instantaneous calculation of the second axle is only feasible after about 7.5 m, though strains are too small at this stage to validate results. According to this figure, a very good approximation of the static value (34 and 126.5 kN) can be obtained along most of the bridge (except when an axle enters or leaves the bridge due to rounding errors).

8.5.2 Testing of the southbound carriageway

A three axle truck with 3.22 and 1.37 m axle spacings, and 61.19 and 178.66 kN in the front axle and rear tandem respectively, was driven in the south-north direction at 57.56 km/h in the adjacent lane to the one tested in Section 8.5.1. The measurements for each section are shown in Figures 8.48(a) and 8.49(a). The bridge response due to a unit load travelling at 57.56 km/h for this carriageway and direction of flow is represented in Figures 8.48(b) and 8.49(b). The origin of the curves ($x = 0$) is related to the instant the first axle of the vehicle hits the second axle detector, placed 2.55 m before the bridge joint at the south end. Only the total weight of the tandem was available, so it was assumed for the calibration that the total weight of the tandem was evenly distributed between the two individual axles.

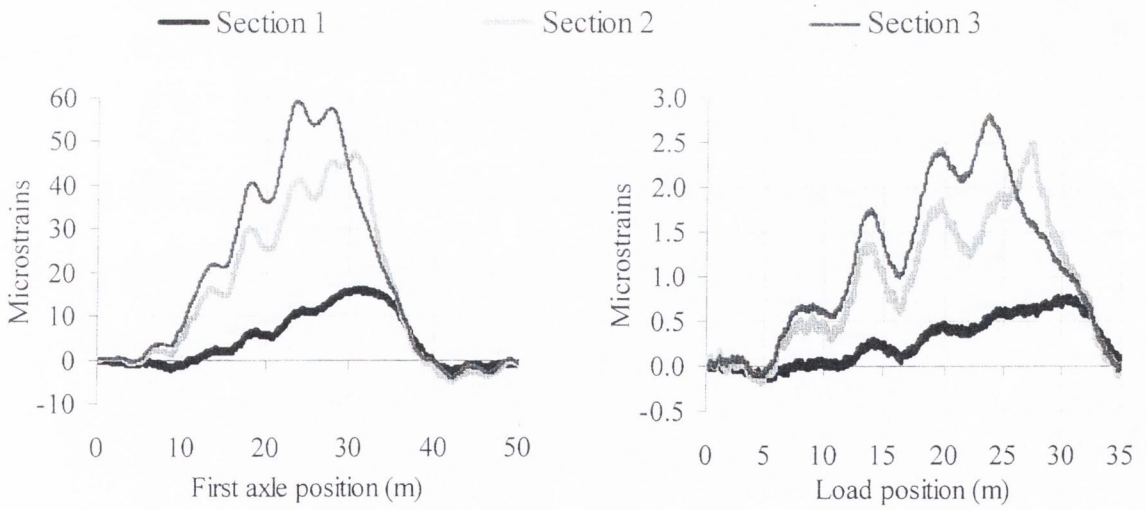

(a) Measurements due to three-axle truck

(b) Total (static + dynamic) bridge response due to a moving unit load

Figure 8.48 – Calibration of sections at 4, 8 and 12 m in southbound lane (Slovenia)

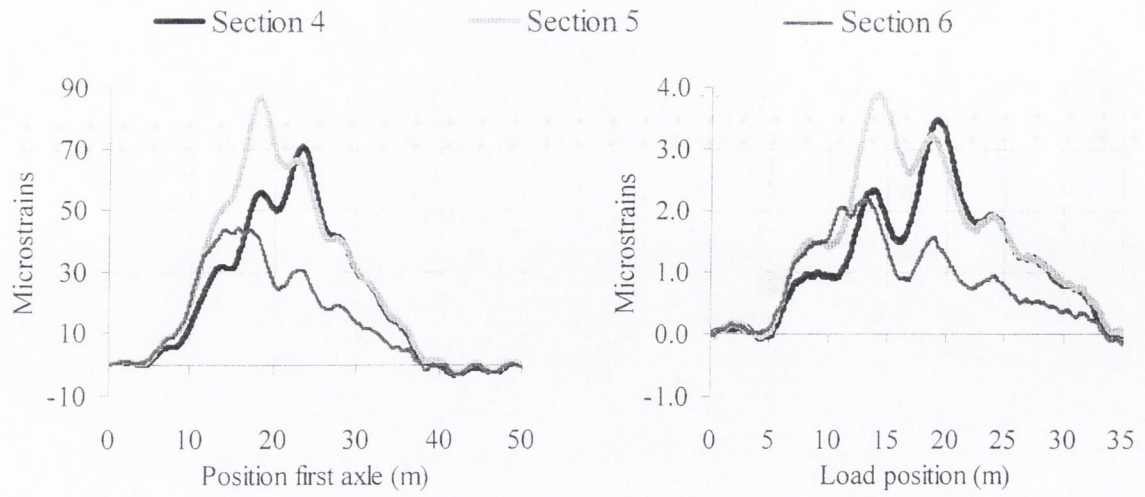

(a) Measurements due to three-axle truck

(b) Total (static + dynamic) bridge response due to a moving unit load

Figure 8.49 – Calibration of sections at 16, 20 and 24 m in southbound lane (Slovenia)

Finally, the load history is represented in Figure 8.50 (real static weights: 61.2 in the front axle and 178.7 kN in the rear tandem). Although calibration has taken place assuming equal load for second and third axles, the second axle appears to be heavier than the third axle from the bridge response and the solution given by the multiple-sensor system.

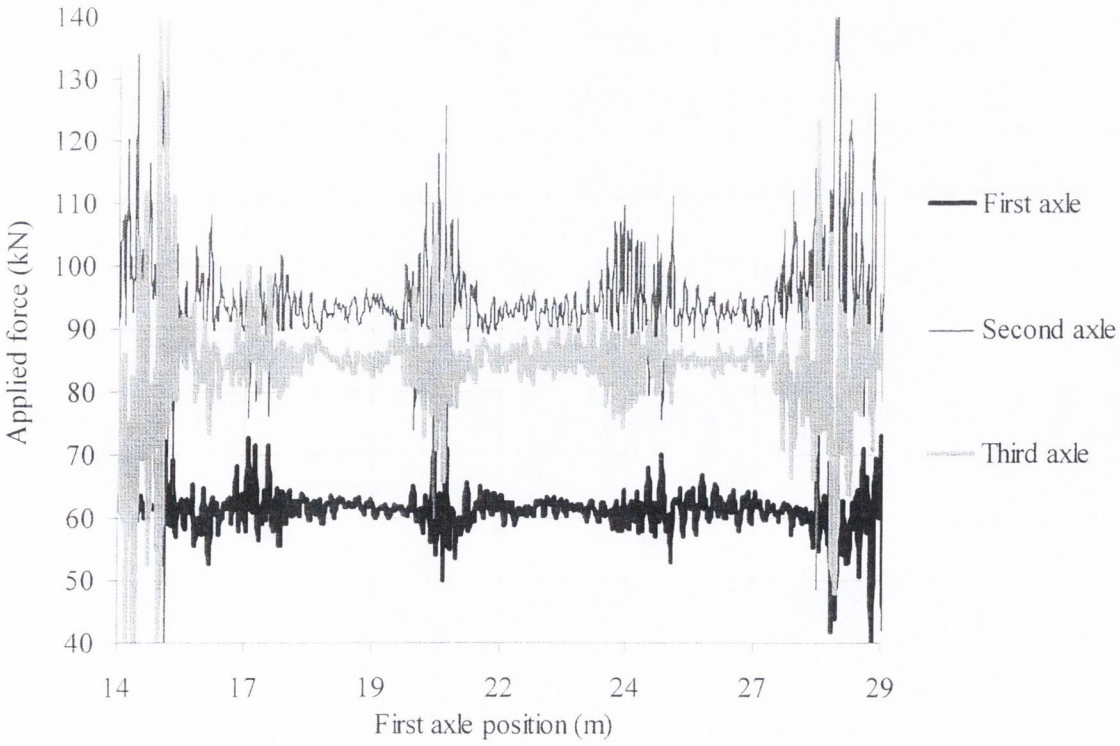

Figure 8.50 – Load history in southbound carriageway (Slovenia)

After first attempts by Kealy (1997), a load history has been reproduced from measurements in a B-WIM site successfully. The algorithm proves to be very accurate in the estimation of the static value from the average of the load history (Figures 8.47 and 8.50). Small errors of 2.6% and –0.57% have been obtained for the two-axle calibration truck in the front and rear axle weight respectively. The errors in the estimation of weights of the three-axle calibration truck have been 0.33% in the front axle and –0.09% in the rear tandem. A multiple-sensor B-WIM system can be a very accurate method of weighing trucks for some particular sites, but further investigation on the ideal number of sensors and their location, and experimental testing based on a wider range of vehicles and speeds are necessary.

8.6 CONCLUSIONS

Four bridges have been instrumented for B-WIM purposes and calibrated under different environmental conditions. An accuracy analysis of the calibration runs has been given according to the COST323 European specification (Appendix B). A new experimental procedure based on the frequency domain has been used to calibrate a B-WIM system by the first time. Apart from the traditional static algorithm, other two new algorithms, DB-WIM and MS-BWIM, have also been analysed with measurements from the field. Though the sample of trucks used to calibrate the system has been very small, first results on accuracy are promising. Further testing with a bigger population size is required in the near future.

The use of a 4 Hz hardware filter in Delgany and Luleå has been a significant source of inaccuracy. In spite of the filtering effect, the use of an experimental influence line based on a spectral calibration over a traditional calibration based on a theoretical beam model improved overall accuracy from E(55) to C(15) in Delgany (one calibration truck travelling with the same load at different speeds). Group of axles criterion also improved from D(25) to A(5). If only the runs at 70 km/h instead of all runs were considered, A(5) overall accuracy could be achieved. In Luleå, overall accuracy D+(20) was obtained using two trucks and different levels of speed. Overall accuracy A(5) could be obtained if using the same truck travelling several times at the same speed while overall accuracy B+(7) would result if using runs of two different trucks travelling at about the same speed. This

difference in accuracy depends on the speed and truck configuration and it is mainly a consequence of the filter. In Belleville, gross vehicle weight is predicted with DB-WIM in an accuracy class B(10), but results in group of axles or single axles are extremely poor. In Slovenia, MS-BWIM is used to depict the axle load history, which average value is very close to the real static weight.

9

NUMERICAL TESTING OF ALGORITHM

9.1 INTRODUCTION

This chapter investigates the performance of a number of B-WIM algorithms (Chapter 7) with data from numerical (Chapter 5) and finite element simulations (Chapter 6). The interaction between bridge, trucks and road roughness involves many parameters which are difficult to identify and allow for when determining the static axle weights. As a result, the accuracy of B-WIM systems varies greatly. The B-WIM algorithms being tested are: traditional static (Section 3.3) with a new spectral calibration; dynamic B-WIM (Section 7.3) (both based on the instrumentation of one longitudinal section) and a static multiple-sensor approach based on many longitudinal locations (Section 7.5.2). Other algorithms have not been object of further consideration due to disadvantages given in Chapter 7. In this study, trucks and bridges are modelled through numerical and finite element approaches as described in Chapters 5 and 6 respectively.

Accuracy classes are determined according to the COST323 European Specification on WIM (Appendix B). Accuracy class for single axles or axles of a group are obtained strictly from the estimated weights provided by each algorithm. Then, individual axle weights are added together to obtain the weight of an axle group or the gross weight. Results for an axle in a group are generally very poor due to the difficulty of separating the individual contributions of each axle. For this reason the COST323 specification allows them to be omitted when classifying a B-WIM system. Accuracy for axles in a group may be improved by distributing the weight predicted for the whole group equally between axles, but it has been preferred to maintain the original axle values for evaluation purposes. Sections 9.2 and 9.3 will show how some algorithms can predict axles in a group accurately without any further manipulation. A calibration factor relates bending moment and change in voltage/strain and theoretically it should be independent of speed. Hence, a common calibration factor has been used for all speeds.

The first part of the chapter uses the numerical simulations provided by an independent source to assess B-WIM accuracy. Green (Queen's University, Kingston, Canada) calculates the strain output at five different locations of a one-dimensional bridge model. A two-axle vehicle is used for calibration. Once the system is calibrated, four-axle vehicles running with different loads, speeds and suspension types are weighed as their movement over the bridge is simulated. Two types of scenario are analysed: smooth and rough road profile. Guidance is provided for the estimation of the parameters governing the bridge behaviour. In the second part, different bridge finite element models are subjected to a common pattern of trucks to check their potential as B-WIM sites. The bridge characteristics appear to be a dominant factor for the accuracy of B-WIM systems. The influence of the sensor location on accuracy is also discussed.

9.2 TESTING WITH GREEN'S ONE DIMENSIONAL DYNAMIC INTERACTION MODEL

Green's one dimensional model has been described in Section 5.6. The bridge is 30 m long. Green calculates strain every 0.01 s (100 Hz) at 5, 10, 15, 20 and 25 m from the bridge support. The B-WIM system is calibrated by the author with a two-axle fully laden linear sprung vehicle (four degrees of freedom). Then, the author tests the system with a four-axle vehicle and two different suspension systems (air and steel leaf). The mechanical characteristics of this truck and the bridge model were not known to the author prior to the analysis. The static and dynamic (DB-WIM) algorithms are based on longitudinal bending at midspan, and the static multiple-sensor algorithm (MS-BWIM) on bending at five points equally spaced along the bridge. The calibration takes place in full repeatability conditions (r1) as defined in the COST323 specification (Appendix B): A two-axle vehicle passing at different speeds, one load and one lateral position on the road. Then, the system is tested in limited reproducibility conditions (R1): two 4-axle vehicles passing over the bridge at different speeds with different loads. Results are given for two different road profiles.

9.2.1 Calibration

The shape of the theoretical influence line is known from beam theory and the static algorithm only requires a calibration factor to adjust the magnitude of the strains to the theoretical model. If the exact influence line for bending moment is used, the calibration

factor is the product of the modulus of elasticity and the section modulus (Section 3.5.1 and Chapter 8 suggest an approach for obtaining the real shape of the influence line from an experimental record). For this analysis, the constant is obtained by dividing the real static gross vehicle weight by the predicted weight of the calibration truck. The calibration of DB-WIM requires additional dynamic parameters (natural frequency, damping) obtained from the record in free vibration. A linear sprung two axle vehicle with 4 m axle spacing, 32.42 kN static weight in the front axle and 59.94 kN in the rear axle is used for calibration.

Smooth Road Profile

At one particular location, bending moment is proportional to strain through the elasticity and section modulus (*ES*) as shown in Equation 3.1. Bending moment depends on the shape of the influence line, bridge length, static axle weights, axle spacings and position of the calibration vehicle. The results of the static calibration are shown in Figure 9.1.

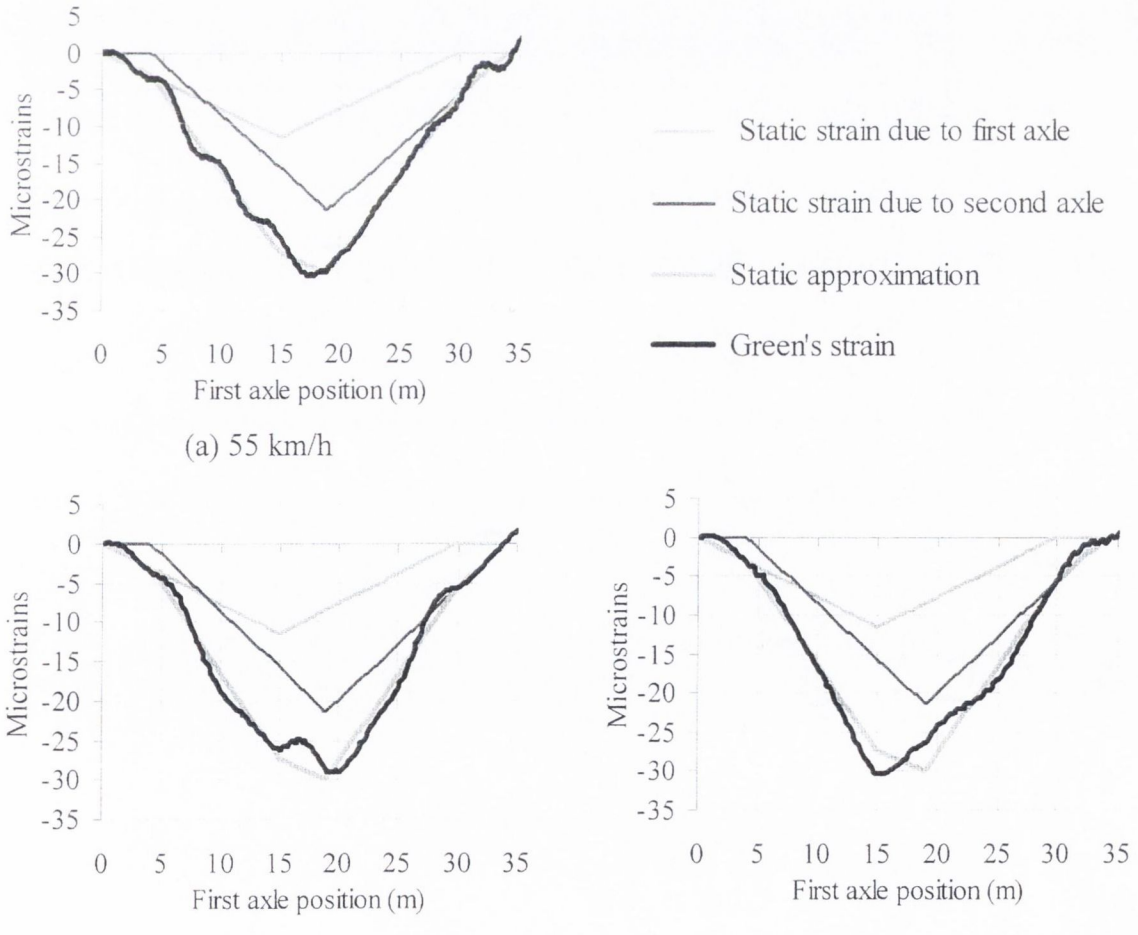

(a) 55 km/h

(b) 70 km/h

(c) 85 km/h

Figure 9.1 – Calibration of a static B-WIM algorithm (smooth profile)

The calibration factor changes for each speed very slightly (2.1056×10^{10} at 55 km/h, 2.1020×10^{10} at 70 km/h and 2.0812×10^{10} at 85 km/h). An average value of 2.0963×10^{10} is adopted.

Other sensor locations used for MS-BWIM are calibrated in the same way. The axle forces predicted by MS-BWIM are compared to the simulated applied forces in Figures 9.2(a) and (b). There is not a clear correspondence between predicted and simulated instantaneous wheel forces, but the average value is very similar in both cases. Dynamic wheel forces are strongly excited by a bump located at about 5 m from the bridge end. Values tend towards infinity at both ends of the instantaneous calculation (very small value of the determinant – Section 7.5.2) and they are not taken into account in the determination of the static weight.

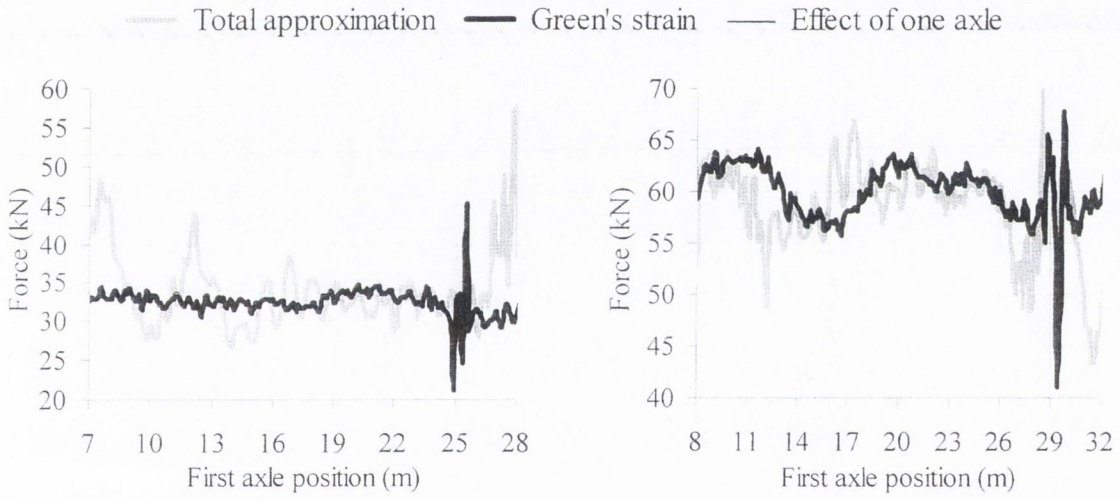

(a) Front axle (b) Rear axle

Figure 9.2 – History of axle forces for vehicle at 55 km/h (smooth profile)

Figure 9.3(a) shows the records in free vibration and Figure 9.3(b) the corresponding spectra for the three runs of the two-axle calibration vehicle. From these Figures, 0.97% damping and 3.33 Hz first natural frequency are obtained (The procedure for their determination is explained in Section 5.2.1).

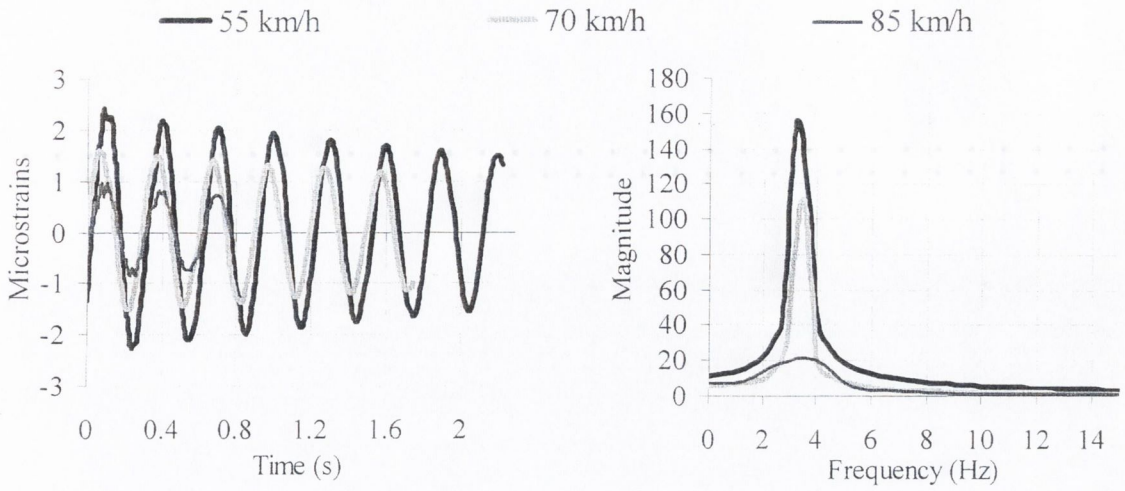

(a) Time Domain (b) Frequency Domain

Figure 9.3 – Record in free vibration (smooth profile)

The mass per unit length of the bridge is related to the first natural frequency through stiffness (EI) and bridge length (Equation 5.3). Section modulus, S, is related to second moment of area, I, by the distance from the deck soffit to the neutral axis, y. An initial estimate of ES is taken from the static algorithm. The static calibration at the lowest speed gives $ES=2.10564 \times 10^{10}$ (Figure 9.1(a)). A better estimate of the section modulus is expected at lower speeds as a higher number of dynamic oscillations will take place around the static response. Ideally, the best estimate of the section modulus would take place by positioning the vehicle statically on the bridge, but this is not always feasible. Tests have been carried out in the past to check the use of a stationary vehicle for calibration (Dempsey 1997). A calibration factor obtained from a strain record due to a vehicle travelling at a typical traffic speed gave better results, but this study used static equations instead of dynamic equations allowing for bridge vibration and damping (as proposed in Section 7.3).

The distance y from the measurement point to the neutral axis can be calculated by minimising an objective function given by the sum of squared differences between measured and theoretical strains. The procedure is represented in Figure 9.4.

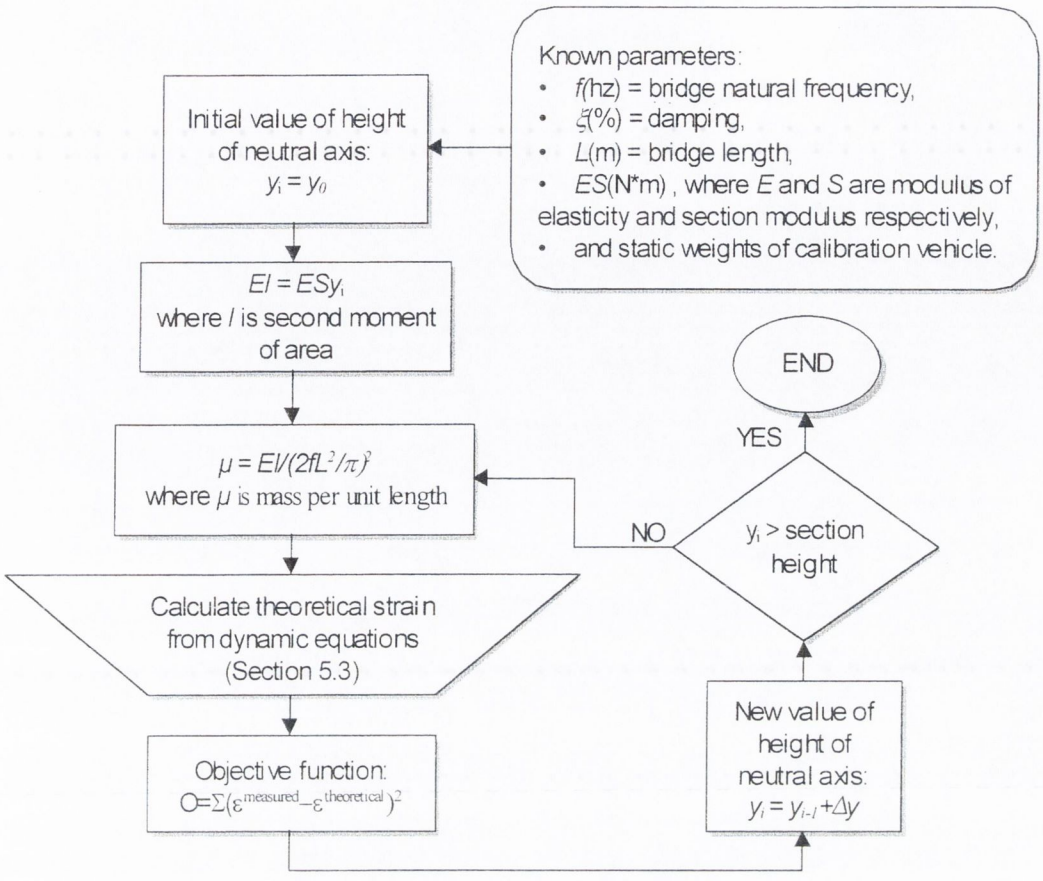

Figure 9.4 – Optimisation process for calculation of mechanical parameters

The values of the objective function for different y and speeds are given in Figures 9.5(a) and (b). From these curves, $y=2$ m. In practise (behaviour differing from beam theory), parameters other than y, i.e. mass per unit length μ, might also need to be optimised.

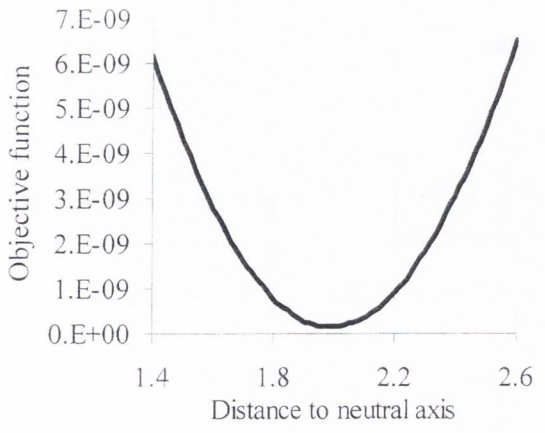

(a) Objective function at 55 km/h

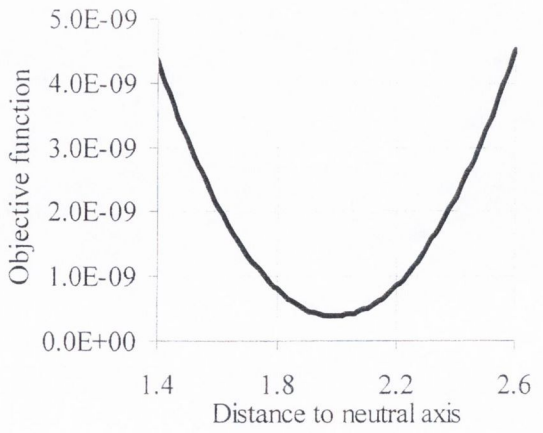

(b) Objective function at 85 km/h

Figure 9.5 – Determination of distance to the neutral axis (smooth profile)

Once the mechanical characteristics of the bridge are known, dynamic equations can be formulated for each speed (Section 5.3). The quality of the approximation of DB-WIM to the simulated response is shown in Figure 9.6.

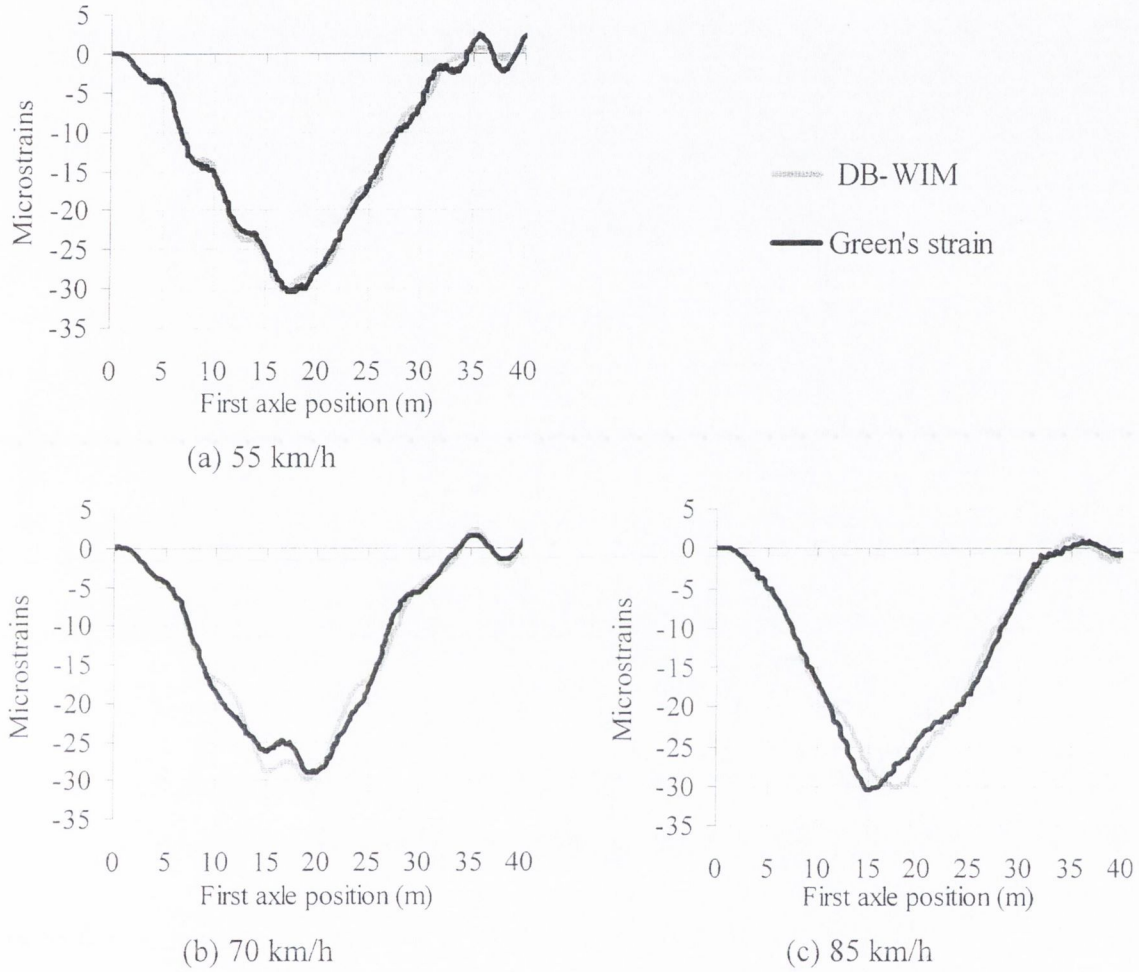

(a) 55 km/h

(b) 70 km/h

(c) 85 km/h

Figure 9.6 – Dynamic approximation (smooth profile)

Figure 9.7 illustrates the results in static weights for the calibration vehicle. The front axle is the lightest and the percentage error tends to be higher than in the rear axle as shown in Figures 9.7(b) and (c). DB-WIM and MS-BWIM are the most accurate algorithms for predicting gross weight and individual axle weights respectively. The traditional static B-WIM is also very accurate for gross vehicle weight. MS-BWIM is slightly worse for predicting gross vehicle weight, but the improvement in individual axle weights is very significant.

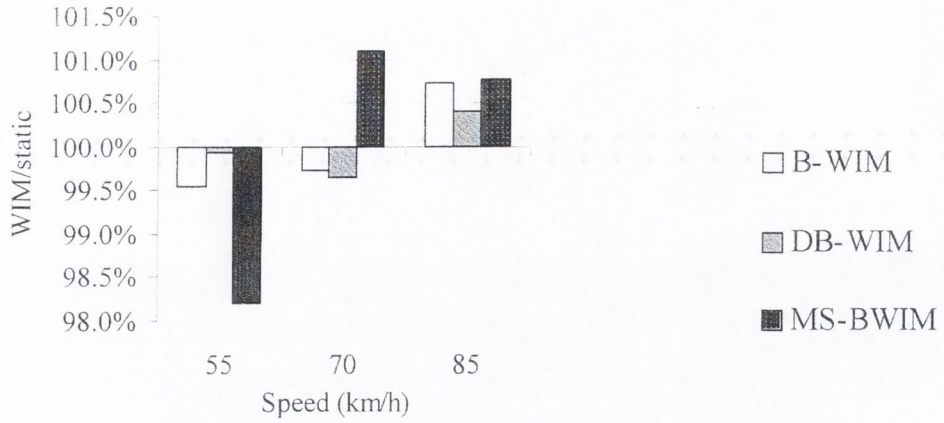

(a) Gross Weight

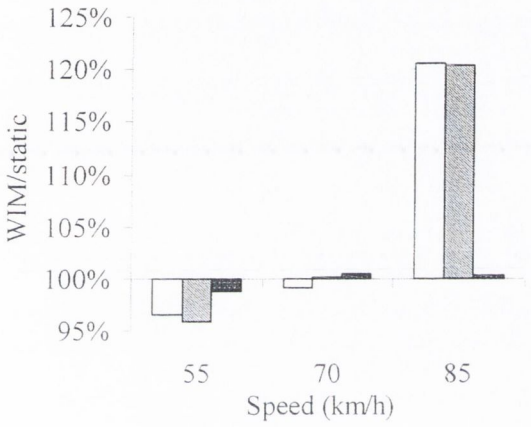

(b) Front axle

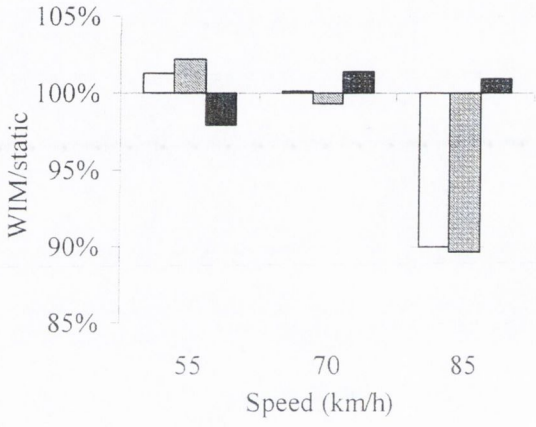

(c) Rear axle

Figure 9.7 – WIM/static weight versus speed (smooth profile)

Rough Road Profile

The calibration of the static algorithm is shown in Figure 9.8. The scale factor between real and predicted gross weight is 2.1197×10^{10} at 55 km/h, 2.1202×10^{10} at 70 km/h and 2.0839×10^{10} at 85 km/h. An average value of 2.0928×10^{10} is adopted as the calibration factor.

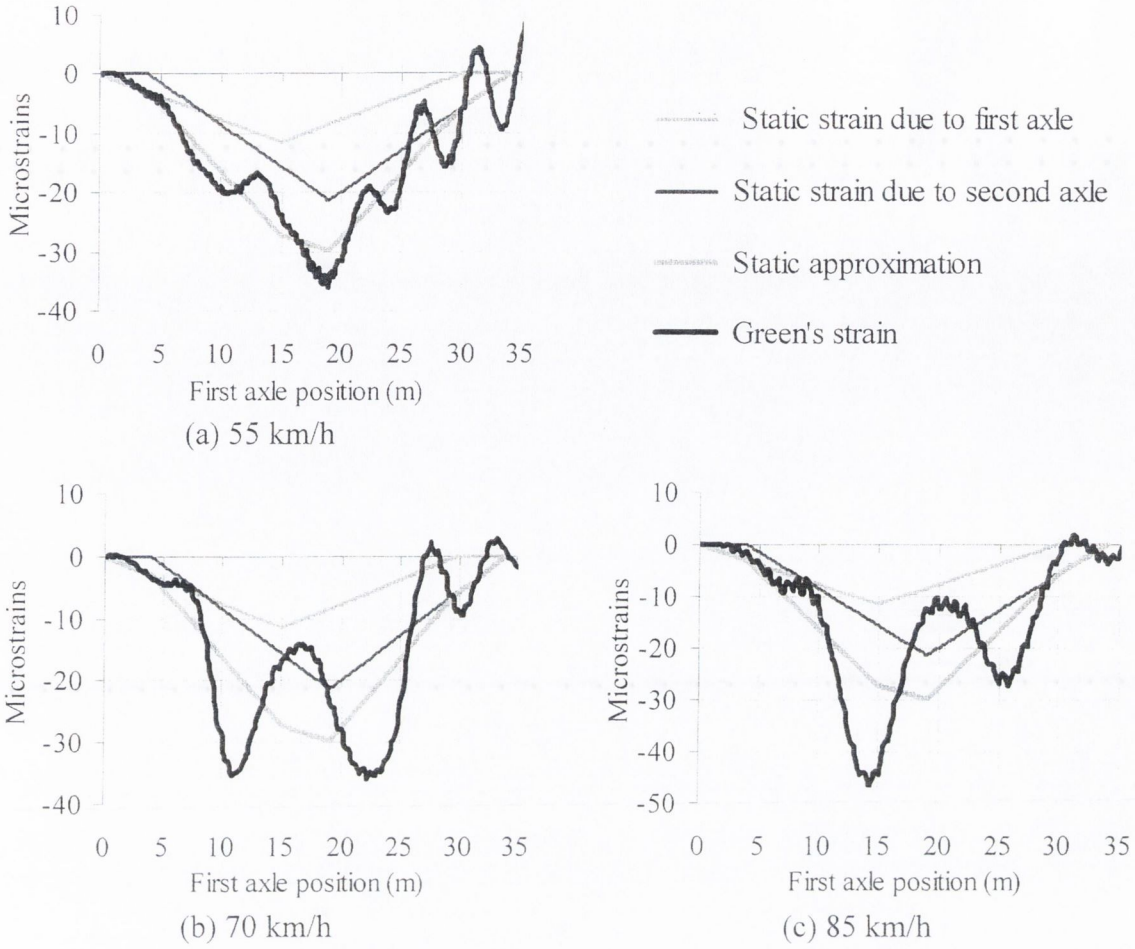

(a) 55 km/h

(b) 70 km/h

(c) 85 km/h

Figure 9.8 – Calibration of a static B-WIM algorithm (rough profile)

In the case of MS-BWIM, the prediction of instantaneous axle forces is not feasible throughout the bridge length. Figure 9.9 shows the results at 55 km/h.

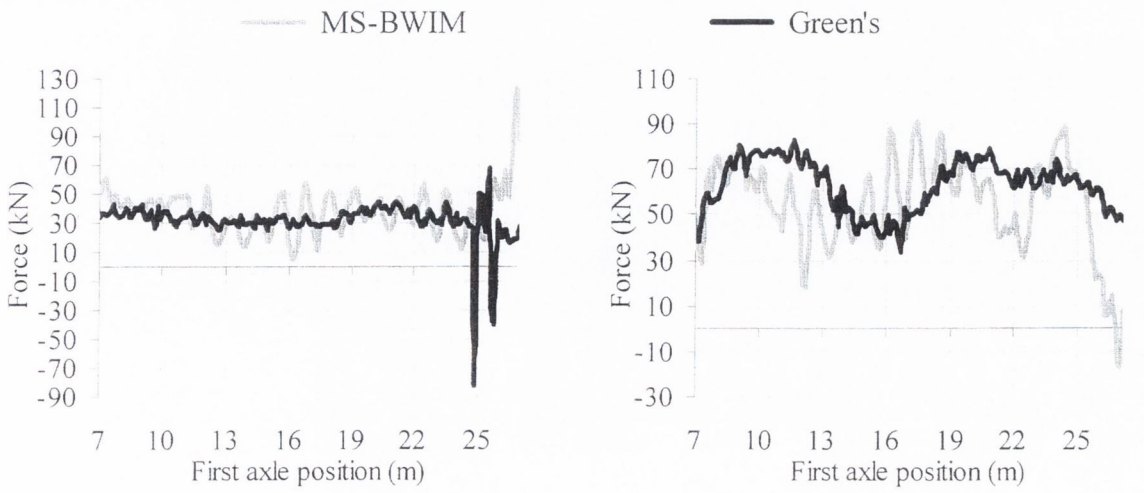

(a) Front axle

(b) Rear axle

Figure 9.9 - History of axle forces for vehicle at 55 km/h (rough profile)

As in the smooth road profile, the forces increase enormously at about 5 m from the bridge end and the instantaneous solution from here to the end of the record is ignored. There is a large increase in oscillations over the smooth case.

Figure 9.10 shows the variation of axle forces at 70 km/h. In Figure 9.10(b), the predicted answer for the rear axle exhibits a low frequency similar to that of the applied force.

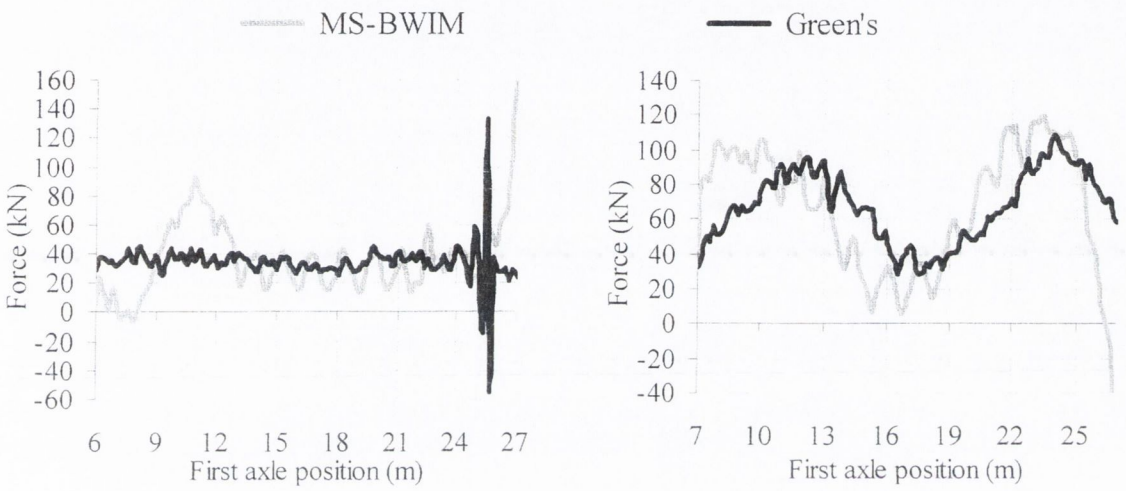

(a) Front axle (b) Rear axle

Figure 9.10 - History of axle forces for vehicle at 70 km/h (rough profile)

The prediction of the static answer proves more difficult at higher speeds, especially in the case of a rough profile. Figure 9.11 shows the calculation at 85 km/h. The estimate of the front axle is overweighed. MS-BWIM is not able to distinguish which is the force applied by each axle due to the strong dynamics and the limitation in the number of sensors. So, Figures 9.11(a) and (b) show how the prediction of the front axle follows a pattern similar to the simulated rear axle.

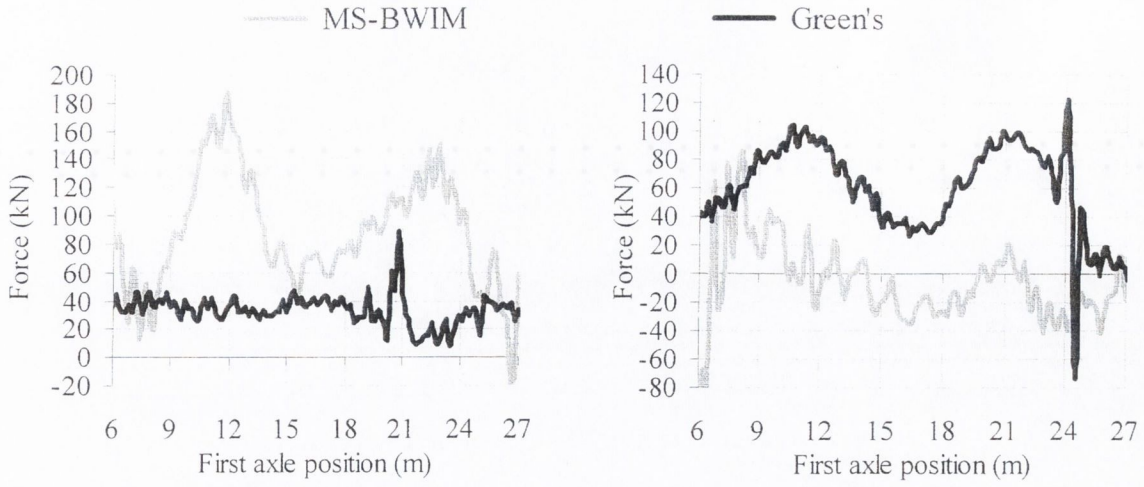

(a) Front axle (b) Rear axle

Figure 9.11 - History of axle forces for vehicle at 85 km/h (rough profile)

For the dynamic algorithm, section modulus is obtained from the run at 55 km/h (2.1197×10^{10}). The same dynamic characteristics as before are found for the bridge with rough road irregularities. From Figure 9.12(a): 3.33 Hz first natural frequency and 0.99% damping are obtained. Figure 9.12(b) represents the value of the objective function at 55 km/h, and the minimum takes place at a distance to the neutral axis of 2 m.

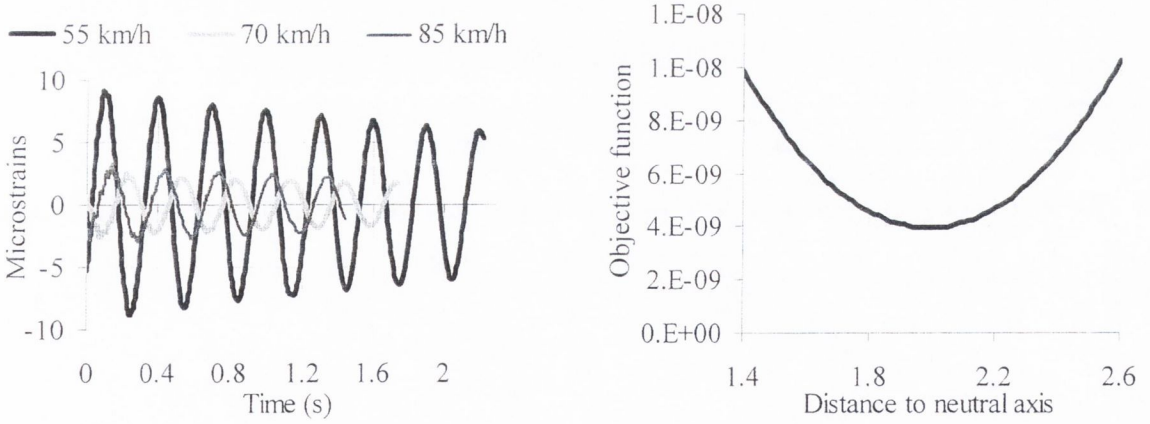

(a) Strain record in Free vibration (b) Distance to the neutral axis

Figure 9.12 – Determination of dynamic characteristics (rough profile)

The matching between the prediction by DB-WIM and the simulated response is shown for different speeds in Figure 9.13.

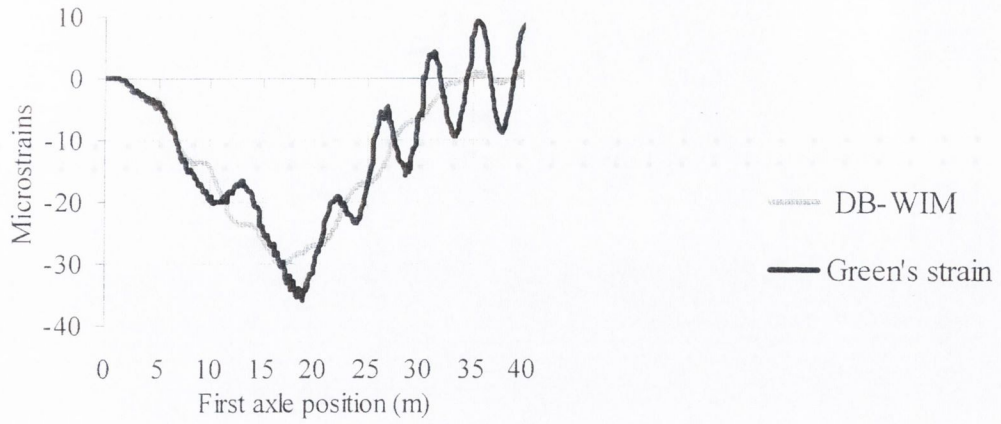

(a) 55 km/h

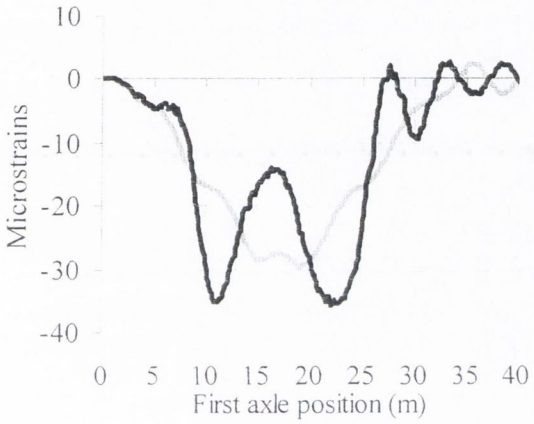

(b) 70 km/h

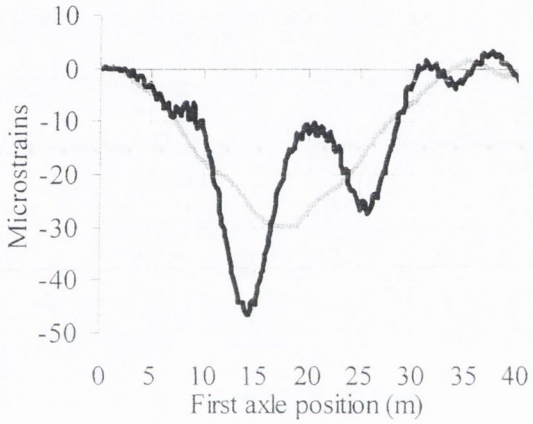

(c) 85 km/h

Figure 9.13 – Dynamic approximation (rough profile)

The errors in individual axle weights for the test vehicle are given in Figure 9.14. Calibration results are much poorer than in the case of a smooth profile (Figure 9.7). Results in individual axle weights at 85 km/h are very inaccurate, but static B-WIM and DB-WIM can predict gross weight within a small threshold.

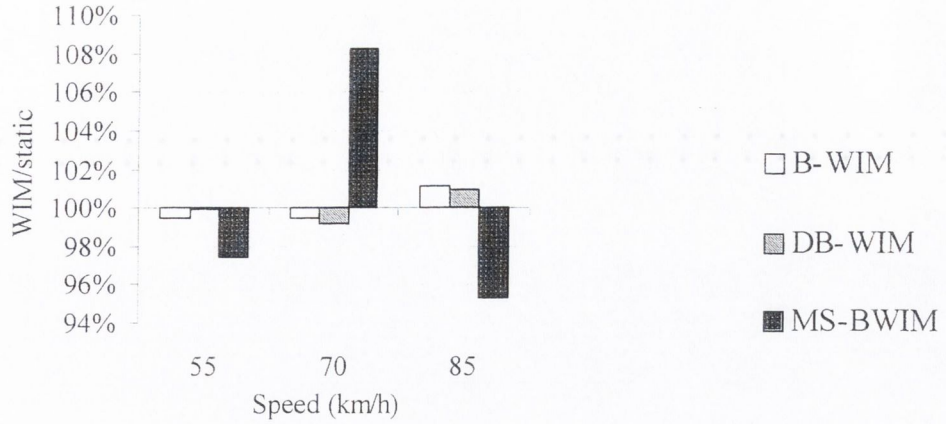

(a) Gross Weight

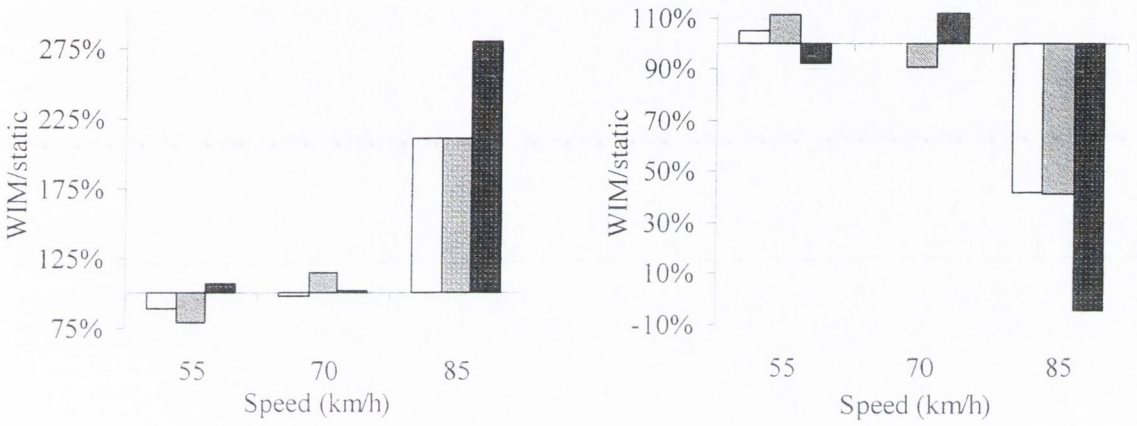

(a) Front axle (b) Rear axle

Figure 9.14 – WIM/static weight versus speed (rough profile)

9.2.2 Check of Accuracy

A four-axle vehicle (axle spacings 3.49, 6.76 and 2 m) is chosen for assessment of the initial calibration. The static weights of this vehicle were unknown to the author prior to the calculations. Two types of suspensions are investigated: air and steel leaf sprung. These two vehicles are driven at three different speeds (55, 70 and 85 km/h) and three loading conditions (unloaded, half and fully laden).

Smooth Road Profile

Figures 9.15 and 9.16 show the approximation by the static B-WIM and DB-WIM algorithms respectively, to the response caused by a fully laden 4-axle truck at 70 km/h.

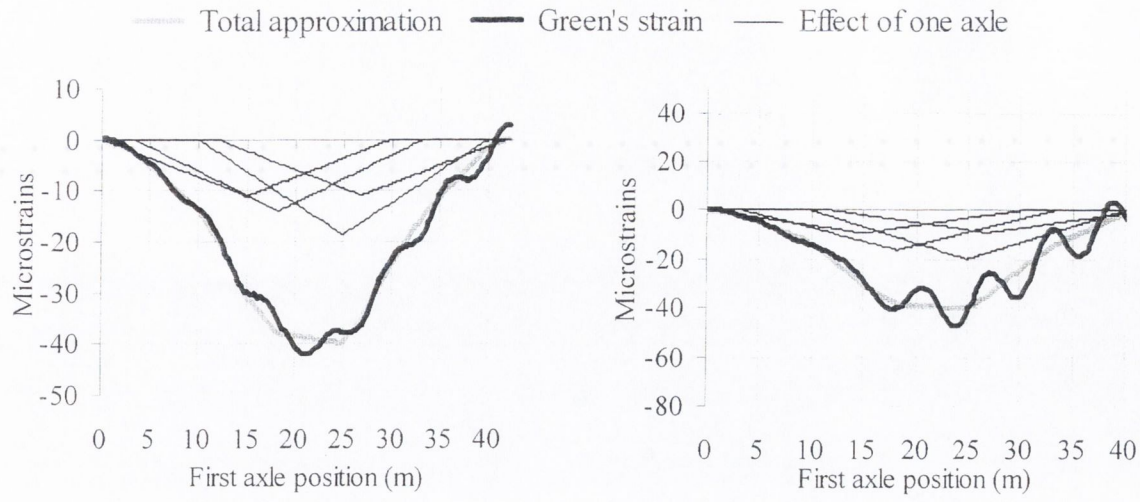

(a) Approximation for air suspension (b) Approximation for steel suspension

Figure 9.15 – Influence of suspension on static B-WIM (smooth profile)

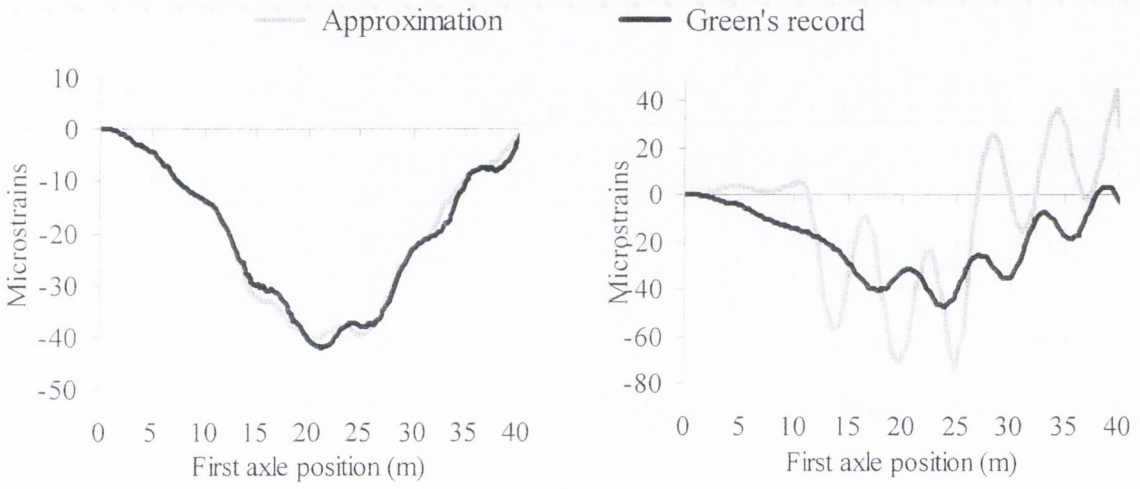

(a) Approximation for air suspension (b) Approximation for steel suspension

Figure 9.16 – Influence of suspension on DB-WIM (smooth profile)

The results illustrated in Figure 9.15 are based on the concept of an influence line, while Figure 9.16 is based on the dynamic answer due to a moving load. The strain record caused by a steel leaf suspension exhibits a higher deviation from the fitted response (by B-WIM or DB-WIM) than air suspension. Hence, predictions of individual axle weights are expected to be more accurate for air suspensions.

Figure 9.17 shows the simulated load history and the prediction by MS-BWIM for the case of a fully loaded 4-axle truck with air suspension travelling at 70 km/h. Figures 9.17(c)

and (d) show that the third and fourth axles allow for an instantaneous solution only when the first axle is located between 17 and 25 m from the bridge start.

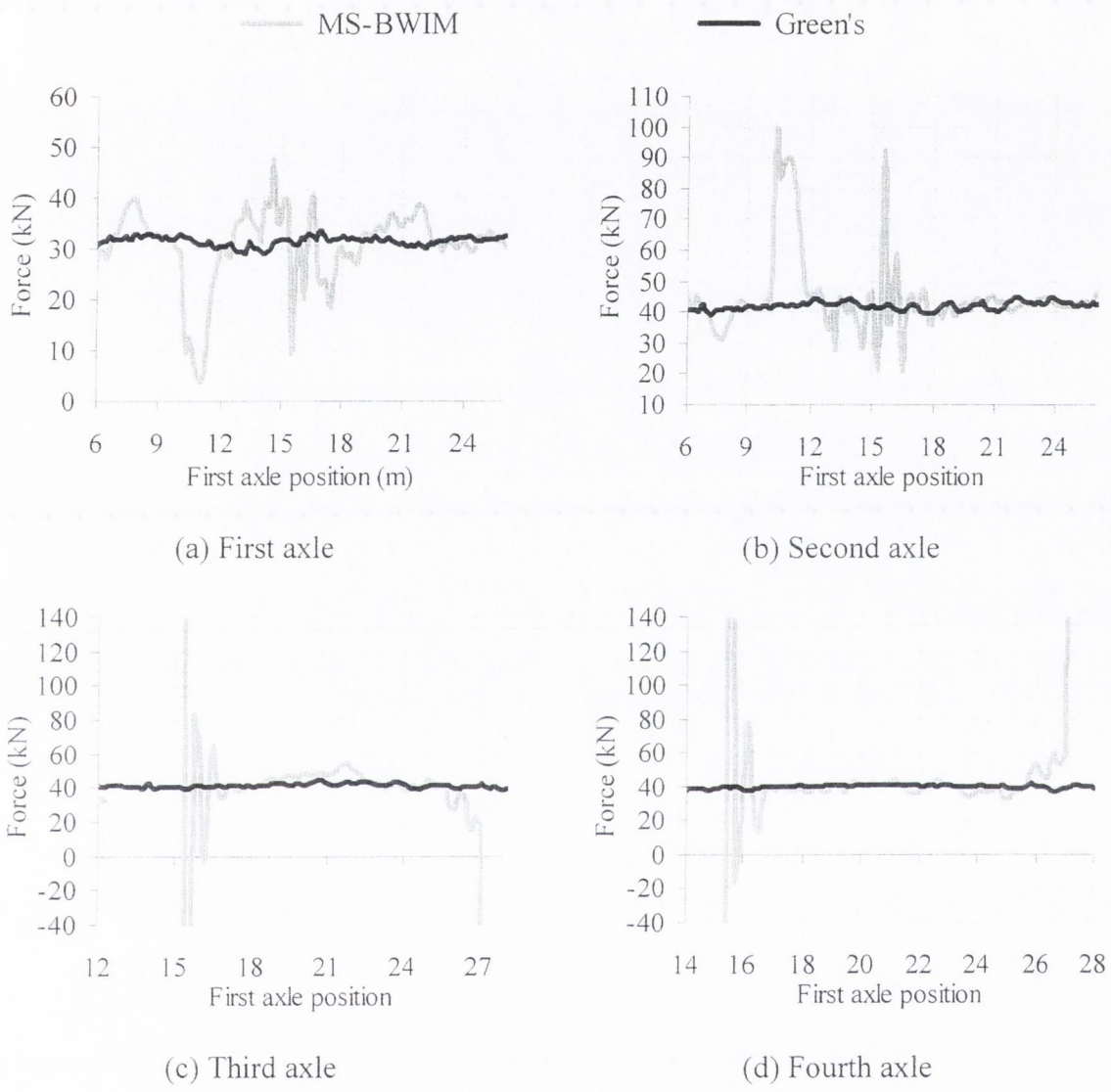

Figure 9.17 – Instantaneous calculation for leaf-sprung 4-axle truck (smooth profile)

Figure 9.18 shows the results of MS-BWIM when using the same truck and speed, but steel suspension. From Figures 9.17(c), 9.17(d), 9.18(c) and 9.18(d), the prediction of the third and fourth axles can be seen to be more difficult for the leaf sprung than the air sprung vehicle.

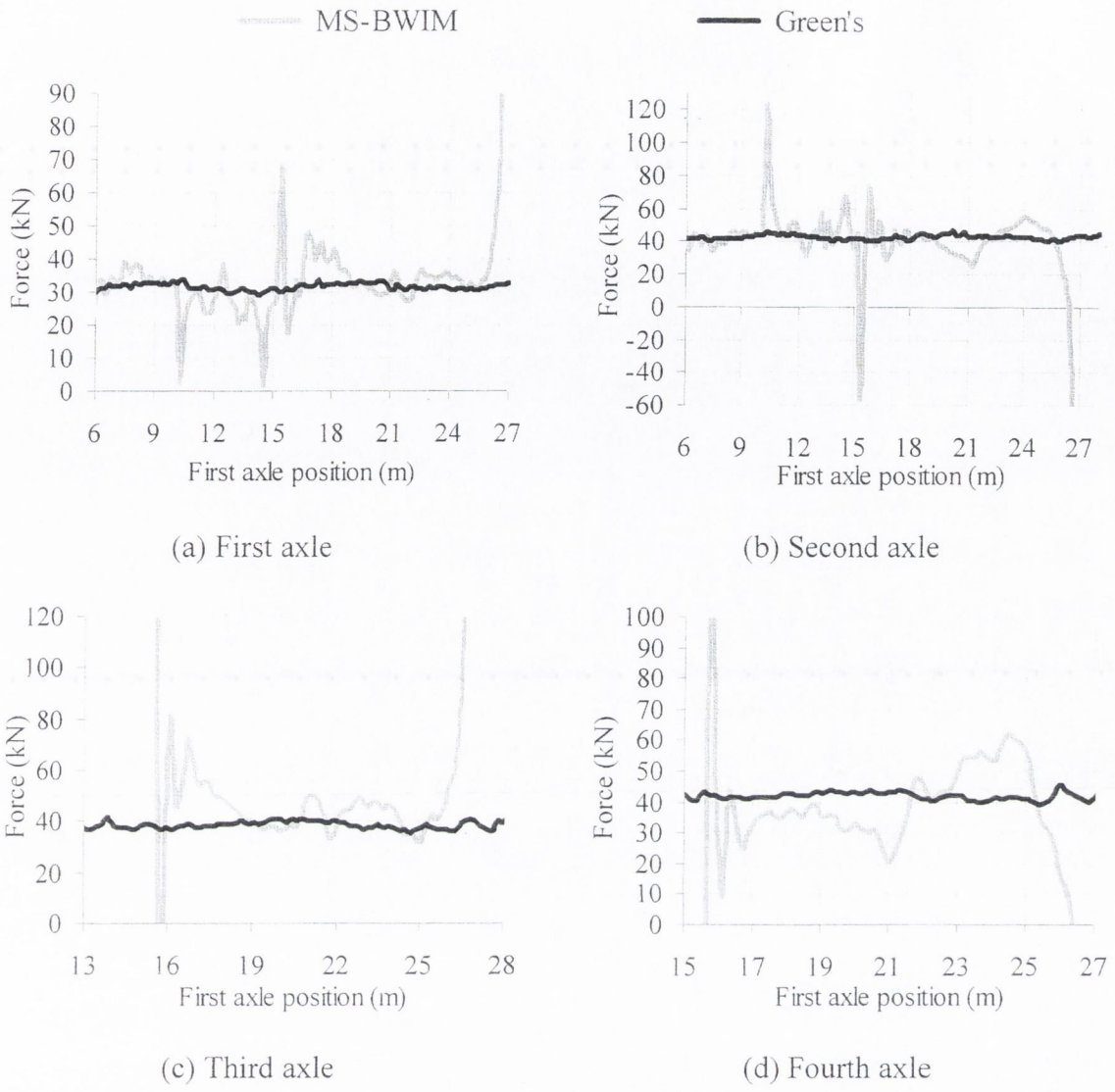

Figure 9.18 – Instantaneous calculation for steel sprung 4-axle truck (smooth profile)

Tables 9.1, 9.2 and 9.3 give accuracy classes for each criterion and algorithm. MS-BWIM is very accurate for all single criteria, even axles of a group in class B(10). The static B-WIM algorithm can predict gross weight accurately (A(5)), but fails to predict single axles (E(45)). DB-WIM is not as accurate as the static B-WIM or MS-BWIM.

Table 9.1 – Accuracy classification for static B-WIM algorithm (beam model) (R1)

(**n**: Total number of vehicles; **m**: mean; **s**: Standard deviation; π_0: level of confidence; δ: tolerance of the retained accuracy class; δ_{min}: minimum width of the confidence interval for π_0; π: Level of confidence of the interval $[-\delta,\delta]$)

	Relative error statistics				Accuracy calculation				
Criterion	**n**	**m (%)**	**s (%)**	π_0 (%)	**Class**	δ (%)	δ_{min} (%)	π (%)	**Class Retained**
Single axle	36	-0.31	21.36	93.1	**E(45)**	54	47.3	96.5	**E(45)**
Group of axles	18	-2.34	7.71	90.3	**C(15)**	18	17.9	90.5	
Gross Weight	18	-0.79	0.93	90.3	**A(5)**	5	2.5	100.	

Table 9.2 – Accuracy classification for DB-WIM algorithm (beam model) (R1)

(**n**: Total number of vehicles; **m**: mean; **s**: Standard deviation; π_0: level of confidence; δ: tolerance of the retained accuracy class; δ_{min}: minimum width of the confidence interval for π_0; π: Level of confidence of the interval $[-\delta,\delta]$)

	Relative error statistics				Accuracy calculation				
Criterion	**n**	**m (%)**	**s (%)**	π_0 (%)	**Class**	δ (%)	δ_{min} (%)	π (%)	**Class Retained**
Single axle	36	5.27	30.57	93.1	**E(65)**	78	68.4	96.4	**E(65)**
Group of axles	18	-7.80	11.88	90.3	**E(30)**	33	30.3	93.4	
Gross Weight	18	0.27	2.63	90.3	**B+(7)**	7	5.9	95.5	

Table 9.3 – Accuracy classification for static MS-BWIM algorithm (beam model) (R1)

(**n**: Total number of vehicles; **m**: mean; **s**: Standard deviation; π_0: level of confidence; δ: tolerance of the retained accuracy class; δ_{min}: minimum width of the confidence interval for π_0; π: Level of confidence of the interval $[-\delta,\delta]$)

	Relative error statistics				Accuracy calculation				
Criterion	**n**	**m (%)**	**s (%)**	π_0 (%)	**Class**	δ (%)	δ_{min} (%)	π (%)	**Class Retained**
Single axle	36	-0.89	3.74	93.1	**B+(7)**	11	8.5	98.3	**B(10)**
Axle of group	36	-0.32	8.31	93.1	**B(10)**	20	18.4	95.4	
Group of axles	18	-0.07	2.70	90.3	**A(5)**	7.14	6.1	95.3	
Gross Weight	18	-0.56	1.46	90.3	**A(5)**	5	3.4	98.8	

If only the runs of the air suspension truck are taken into account, accuracy classes in the new *extended repeatability* conditions (r2) get worse for all algorithms except the dynamic B-WIM as shown in Tables 9.4, 9.5 and 9.6 (While the COST323 specification aims to

allow for differences in test conditions, extended repeatability proves in this case to be a more rigorous test for the algorithms. In any event, as it is more representative, the results for extended repeatability conditions are more relevant than for full repeatability).

Table 9.4 – Accuracy classification for static B-WIM algorithm (beam, air susp.) (r2)

(**n**: Total number of vehicles; **m**: mean; **s**: Standard deviation; π_0: level of confidence; δ: tolerance of the retained accuracy class; δ_{min}: minimum width of the confidence interval for π_0; π: Level of confidence of the interval $[-\delta,\delta]$)

	Relative error statistics				Accuracy calculation				
Criterion	**n**	**m** (%)	**s** (%)	π_0 (%)	**Class**	δ (%)	δ_{min} (%)	π (%)	**Class Retained**
Single axle	18	-0.71	20.17	93.7	**E(50)**	60	50.3	97.6	**E(50)**
Group of axles	9	-1.40	8.44	88.8	**D+(20)**	23	21.7	91.1	
Gross Weight	9	-0.76	0.54	88.8	**A(5)**	5	1.9	100.	

Table 9.5 – Accuracy classification for DB-WIM (beam, air suspension) (r2)

(**n**: Total number of vehicles; **m**: mean; **s**: Standard deviation; π_0: level of confidence; δ: tolerance of the retained accuracy class; δ_{min}: minimum width of the confidence interval for π_0; π: Level of confidence of the interval $[-\delta,\delta]$)

	Relative error statistics				Accuracy calculation				
Criterion	**n**	**m** (%)	**s** (%)	π_0 (%)	**Class**	δ (%)	δ_{min} (%)	π (%)	**Class Retained**
Single axle	18	2.47	24.22	93.7	**E(60)**	72	60.5	97.5	**E(60)**
Group of axles	9	-6.11	10.86	88.8	**E(30)**	33	30.0	92.6	
Gross Weight	9	-0.65	0.67	88.8	**A(5)**	5	2.1	100.	

Table 9.6 – Accuracy classification for static MS-BWIM (beam, air suspension) (r2)

(**n**: Total number of vehicles; **m**: mean; **s**: Standard deviation; π_0: level of confidence; δ: tolerance of the retained accuracy class; δ_{min}: minimum width of the confidence interval for π_0; π: Level of confidence of the interval $[-\delta,\delta]$)

	Relative error statistics				Accuracy calculation				
Criterion	**n**	**m** (%)	**s** (%)	π_0 (%)	**Class**	δ (%)	δ_{min} (%)	π (%)	**Class Retained**
Single axle	18	-1.81	2.56	93.7	**A(5)**	8	7.3	96.2	**C(15)**
Axle of group	18	0.40	8.64	93.7	**C(15)**	25	21.5	97.2	
Group of axles	9	0.71	2.91	88.8	**B+(7)**	10	7.6	96.9	
Gross Weight	9	-0.69	1.60	88.8	**A(5)**	5	4.3	94.3	

All results are represented in Figure 9.19. In comparison with the calibration, the bias on the single axle loads have been multiplied by factors of 0.75, 4.2 and 89 in the static, dynamic and multiple-sensor algorithms respectively, while the standard deviations have increased by more than 100%.

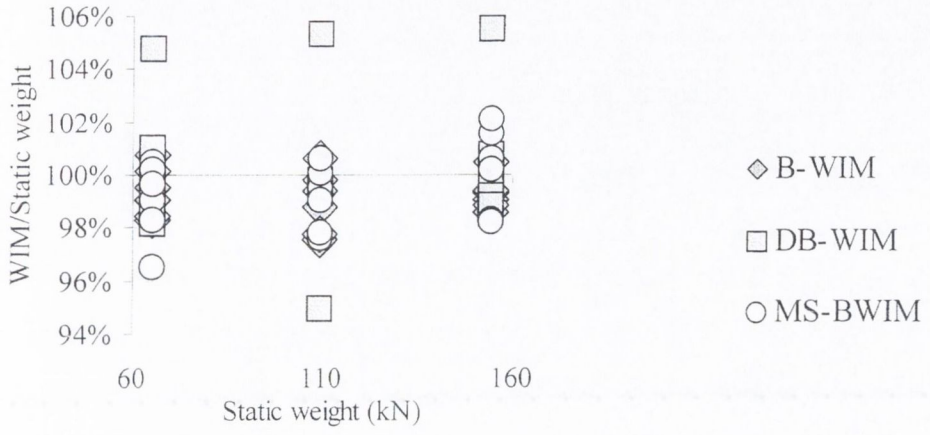

(a) Gross vehicle weight

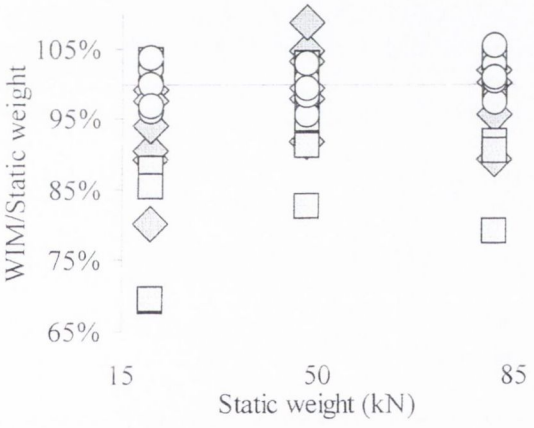

(b) Axle group

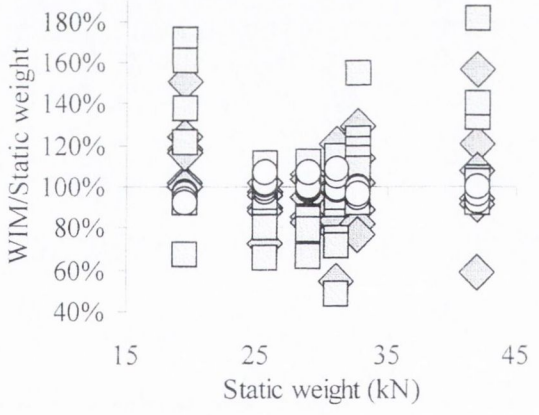

(c) Individual axle weights

Figure 9.19 – WIM/Static versus real static weights

Rough Road Profile

Results for a rough road profile are very poor and only gross weight give sensible levels of accuracy. The poor accuracy of a B-WIM algorithm on a rough profile can be explained by Figures 9.20 and 9.21. Figure 9.20 represents the approximation by the static algorithm to the total strain generated by a fully laden truck at 70 km/h. The total response is far from this static response due to the high dynamic oscillations.

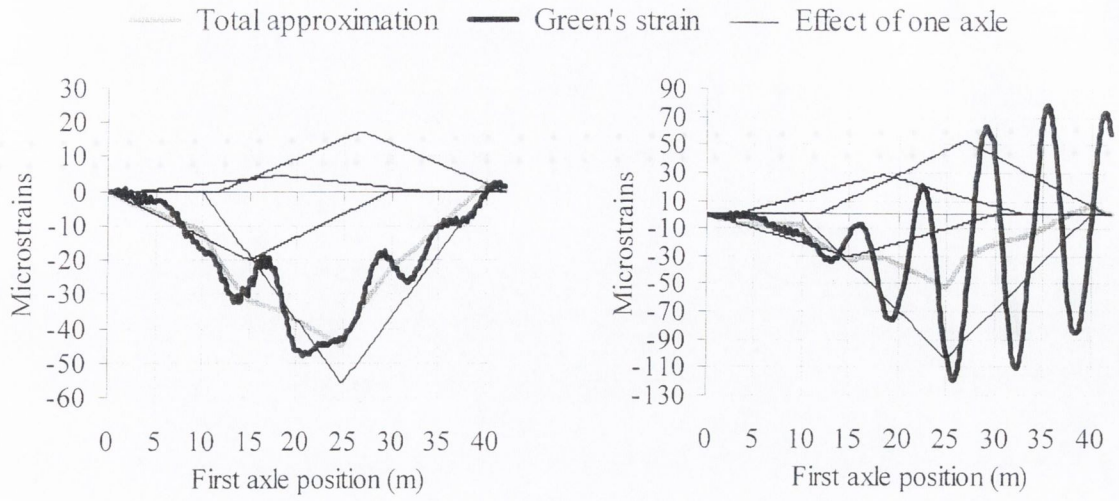

(a) Approximation for air suspension (b) Approximation for steel suspension

Figure 9.20 – Influence of suspension type on static B-WIM (rough profile)

Likewise Figure 9.21 represents the adjustment by DB-WIM. Both static and dynamic algorithms are very inaccurate and their approximations can lead to negative values for individual axle weights: For instance, the second and fourth axles in Figures 9.20(a) and (b) (thin line representing bending moment diagram due to a single axle is over the x-axis). the fourth axle from calculations by DB-WIM in Figure 9.21(a), and the first and fourth axles in Figure 9.21(b). As in the case of a smooth profile, steel leaf suspensions give worse results than air suspensions.

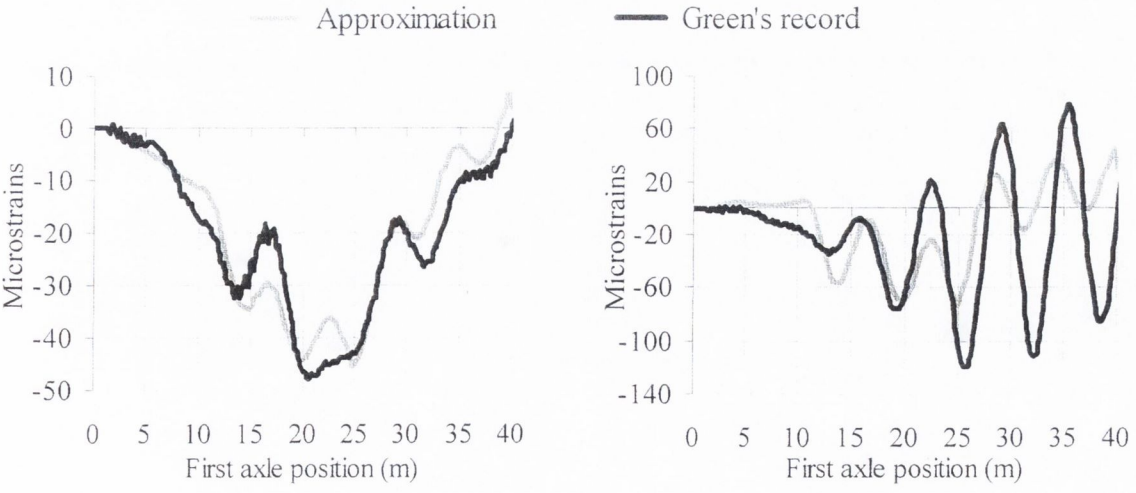

(a) Approximation for air suspension (b) Approximation for steel suspension

Figure 9.21 – Influence of suspension type on DB-WIM (rough profile)

If the road is in a poor condition, algorithms based on linearity and superposition do not appear to offer a valid solution. MS-BWIM is also extremely inaccurate as it minimises the instantaneous solution by using influence lines at many locations. Figure 9.22 shows the results for the same run as Figures 9.20(a) and 9.21(a). The static value can be estimated from instantaneous values when the first axle is located between 18 and 25 m from the bridge start. However, the third axle and fourth axles are strongly overweighed and underweighed respectively (Figures 9.22(c) and (d)).

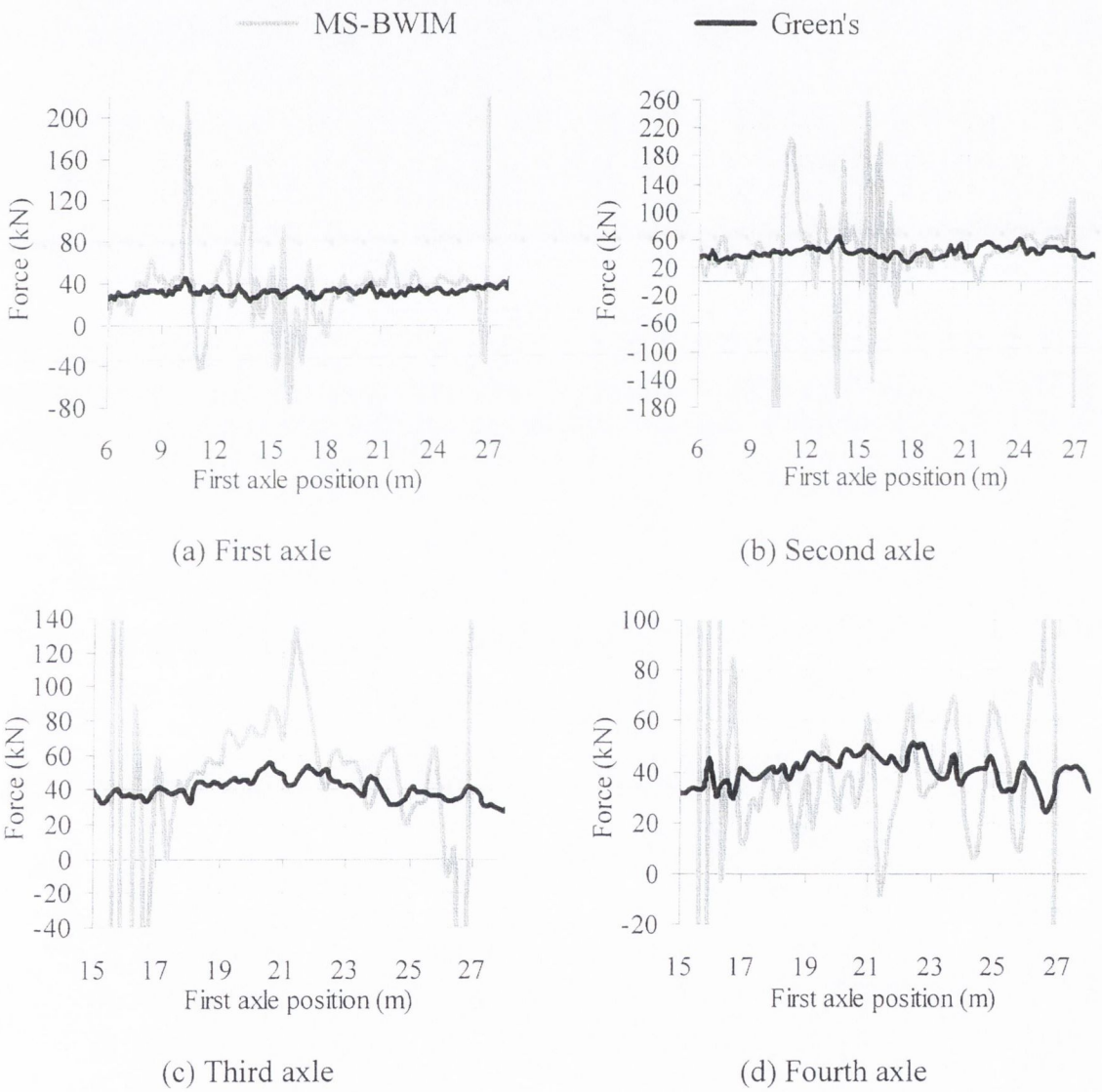

Figure 9.22 – Instantaneous calculation for a 4-axle truck (rough profile)

According to Tables 9.7, 9.8 and 9.9, gross weight is the only criterion which gives reasonable levels of accuracy. The static B-WIM gives the best result – C(15) for gross weight (Table 9.7). The other two algorithms are very inaccurate. However, if the test took

place in extended repeatability conditions (r2) taking into account only the runs of the air suspension truck, the accuracy class for gross weight would be raised to A(5), C(15) and C(15) for the static B-WIM, DB-WIM and MS-WIM algorithms respectively.

Table 9.7 – Accuracy classification for static B-WIM algorithm (beam model) (R1)

(**n**: Total number of vehicles; **m**: mean; **s**: Standard deviation; π_0: level of confidence; δ: tolerance of the retained accuracy class; δ_{min}: minimum width of the confidence interval for π_0; π: Level of confidence of the interval $[-\delta,\delta]$)

	Relative error statistics				Accuracy calculation				
Criterion	**n**	**m (%)**	**s (%)**	π_0 (%)	**Class**	δ (%)	δ_{min} (%)	π (%)	**Class Retained**
Single axle	36	-9.46	135.4	93.1	**E(300)**	360	300.4	97.3	**E(300)**
Group of axles	18	15.60	42.52	90.3	**E(100)**	110	100.1	93.6	
Gross Weight	18	0.95	5.71	90.3	**C(15)**	15	13.0	94.9	

Table 9.8 – Accuracy classification for DB-WIM algorithm (beam model) (R1)

(**n**: Total number of vehicles; **m**: mean; **s**: Standard deviation; π_0: level of confidence; δ: tolerance of the retained accuracy class; δ_{min}: minimum width of the confidence interval for π_0; π: Level of confidence of the interval $[-\delta,\delta]$)

	Relative error statistics				Accuracy calculation				
Criterion	**n**	**m (%)**	**s (%)**	π_0 (%)	**Class**	δ (%)	δ_{min} (%)	π (%)	**Class Retained**
Single axle	36	11.44	178.7	93.1	**E(395)**	474	396.0	97.3	**E(395)**
Group of axles	18	-15.59	55.86	90.3	**E(130)**	143	129.1	93.8	
Gross Weight	18	3.53	21.93	90.3	**E(50)**	50	49.8	90.4	

Table 9.9 – Accuracy classification for static MS-BWIM algorithm (beam model) (R1)

(**n**: Total number of vehicles; **m**: mean; **s**: Standard deviation; π_0: level of confidence; δ: tolerance of the retained accuracy class; δ_{min}: minimum width of the confidence interval for π_0; π: Level of confidence of the interval $[-\delta,\delta]$)

	Relative error statistics				Accuracy calculation				
Criterion	**n**	**m (%)**	**s (%)**	π_0 (%)	**Class**	δ (%)	δ_{min} (%)	π (%)	**Class Retained**
Single axle	36	-4.03	14.90	93.1	**E(30)**	36	33.9	94.8	**E(30)**
Group of axles	18	-4.89	21.42	90.3	**E(50)**	55	49.1	94.1	
Gross Weight	18	-4.07	12.13	90.3	**E(30)**	30	28.3	92.4	

Figure 9.23 illustrates the estimation of every identity in the sample.

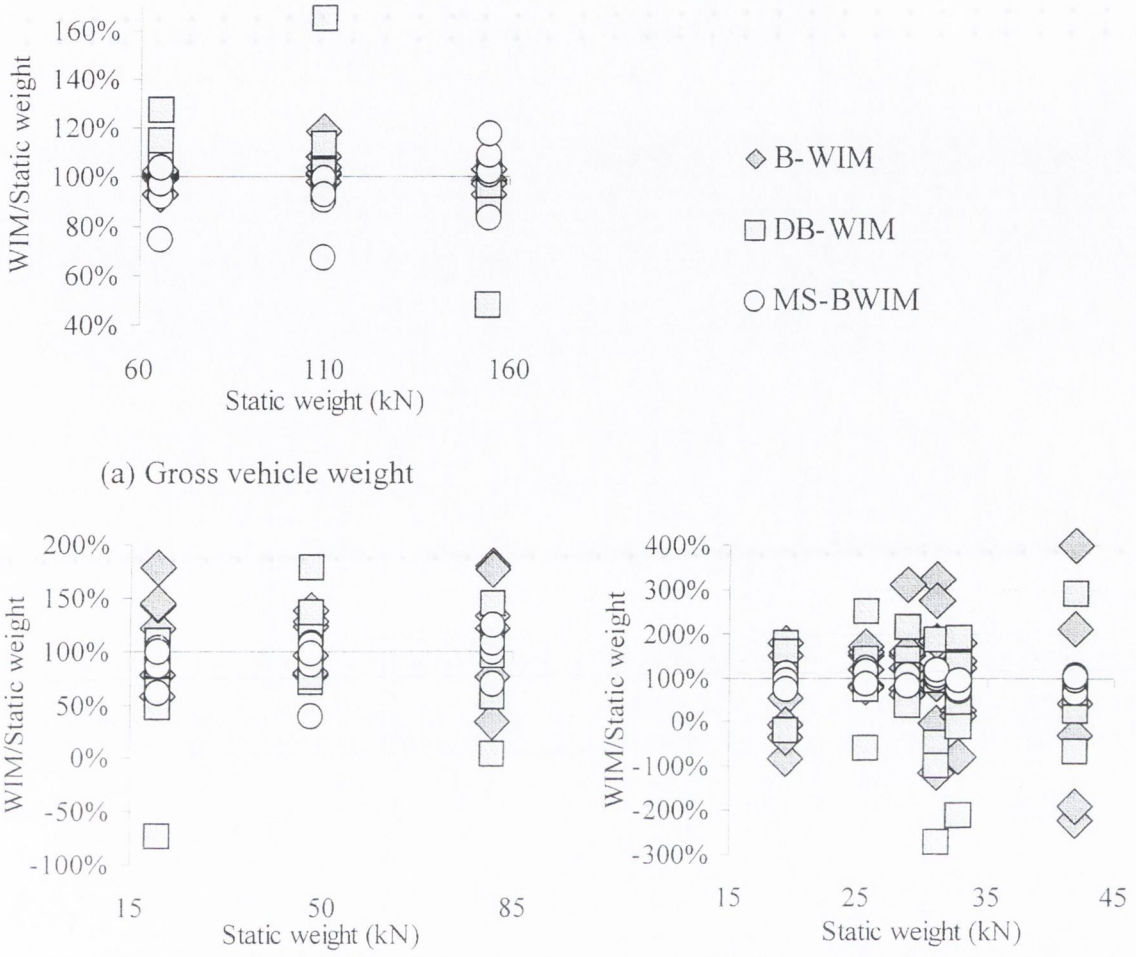

(a) Gross vehicle weight

(b) Axle group

(c) Individual axle weights

Figure 9.23 – WIM/Static versus real static weights

9.3 TESTING WITH FINITE ELEMENT MODELS

Different types of bridge are used as the scenario for analysing the accuracy of each algorithm. The objective is analysing the influence of bridge dynamics on B-WIM accuracy for different B-WIM algorithms. It is hoped to achieve an improvement over the traditional static algorithm with the use of new locations and/or algorithms. Two and three-axle trucks with front axle and rear single axle or tandem are used in the tests. Individual axles of group spaced at 1.2 m. The redistribution of load between closely spaced axles is important, and the calculation of their individual weights is usually problematic. Truck

models are described in Section 6.4. The simulations take place under Limited Reproducibility conditions (R1).

The set of two vehicles are crossed over the bridge with three loading conditions at three different speed levels: 55, 70 and 85 km/h. The road surface roughness is generated from power spectral density functions based on the International Standards Organisation specifications for 'good' conditions. The characteristics of the simulations are given in Chapter 6.

The algorithms, based on strain from one longitudinal section, use sensors located at midspan unless otherwise specified. The positions of the sensors for the MS-BWIM approach are defined for each bridge. Strain is output every 0.004 s (250 Hz). The shape of the influence lines has been obtained from the models.

9.3.1 Isotropic Single Span Slab

Details of this 16 m bridge (First natural frequency 4.51 Hz) are given in Section 6.5.1. The traditional static B-WIM algorithm is tested with a different number of transverse locations at midspan: (a) 2 sensors at midspan (one in each lane at 2.5 m from the centreline) and (b) 8 sensors at midspan (spaced one metre apart along both lanes). The response of these sensors is added together before applying the algorithm. This sum is expected to compensate for torsional bending. Global accuracy remains C(15) regardless of the number of sensors at midspan (Tables 9.10 and 9.11).

Table 9.10 – Accuracy classification for static B-WIM (2 sensors) (Isotropic slab) (R1)

(**n**: Total number of vehicles; **m**: mean; **s**: Standard deviation; π_0: level of confidence; δ: tolerance of the retained accuracy class; δ_{min}: minimum width of the confidence interval for π_0; π: Level of confidence of the interval $[-\delta,\delta]$)

	Relative error statistics				Accuracy calculation				
Criterion	**n**	**m** (%)	**s** (%)	π_0 (%)	**Class**	δ (%)	δ_{min} (%)	π (%)	**Class Retained**
Single axle	27	2.17	6.97	92.1	**C(15)**	20	16.1	97.5	**C(15)**
Group of axles	9	-2.20	2.73	83.4	**B+(7)**	10	7.3	96.2	
Gross Weight	18	0.01	0.95	90.3	**A(5)**	5	2.2	100.	

The results with a higher number of sensors are not more accurate (Table 9.11). In practice, B-WIM uses more than two sensors along one longitudinal section to overcome the limitations of the measurement devices (minimum detectable change in voltage, noise interference, etc.).

Table 9.11 – Accuracy classification for static B-WIM (8 sensors) (Isotropic slab) (R1)

(**n**: Total number of vehicles; **m**: mean; **s**: Standard deviation; π_0: level of confidence; δ: tolerance of the retained accuracy class; δ_{min}: minimum width of the confidence interval for π_0; π: Level of confidence of the interval $[-\delta,\delta]$)

	Relative error statistics				Accuracy calculation				
Criterion	**n**	**m** (%)	**s** (%)	π_0 (%)	**Class**	δ (%)	δ_{min} (%)	π (%)	**Class Retained**
Single axle	27	2.16	6.97	92.1	**C(15)**	20	16.1	97.5	**C(15)**
Group of axles	9	-2.22	2.74	83.4	**B+(7)**	10	7.3	96.1	
Gross Weight	18	0.01	0.98	90.3	**A(5)**	5	2.2	100.	

Table 9.12 shows results for the dynamic algorithm based on one longitudinal section. Overall accuracy decreases to D+(20). There is a slight improvement in accuracy for gross weight, but the use of the dynamic algorithm is not justifiable for this particular bridge.

Table 9.12 – Accuracy classification for DB-WIM algorithm (Isotropic slab) (R1)

(**n**: Total number of vehicles; **m**: mean; **s**: Standard deviation; π_0: level of confidence; δ: tolerance of the retained accuracy class; δ_{min}: minimum width of the confidence interval for π_0; π: Level of confidence of the interval $[-\delta,\delta]$)

	Relative error statistics				Accuracy calculation				
Criterion	**n**	**m** (%)	**s** (%)	π_0 (%)	**Class**	δ (%)	δ_{min} (%)	π (%)	**Class Retained**
Single axle	27	3.50	8.97	92.1	**D+(20)**	25	21.1	96.7	**D+(20)**
Group of axles	9	-3.61	3.80	83.4	**B(10)**	13	10.6	93.3	
Gross Weight	18	0.00	0.80	90.3	**A(5)**	5	1.8	100.	

The B-WIM static algorithm is more accurate because it generates a hypothetical static response closer to the static strain than the DB-WIM curve is to the total strain. The approximation by DB-WIM of the runs for the heaviest three-axle truck at 55 and 85 km/h is shown in Figures 9.24(a) and (b) respectively. Bridge vibrations in the tail of the strain record are not properly matched at highest speeds. The source of this inaccuracy is the non-

linear nature of the dynamic problem. DB-WIM is unaware of the initial conditions of displacement, velocity and acceleration of the bridge, which induces a deviation in the matching, particularly significant when the first axle leaves the bridge.

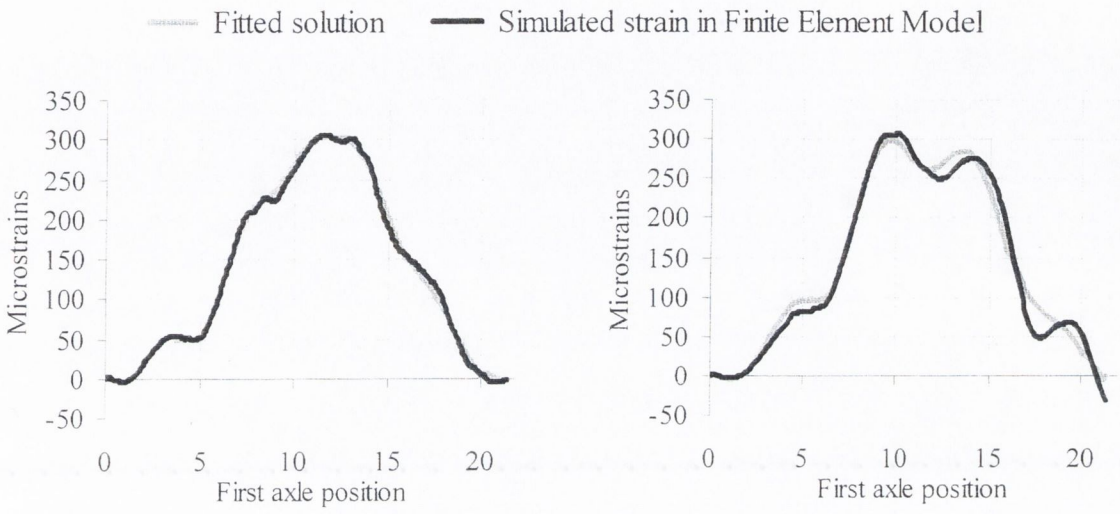

(a) Three-axle truck at 55 km/h (b) Three-axle truck at 85 km/h

Figure 9.24 – Approximation by the static and dynamic Algorithms

If the DB-WIM is applied purely to the strain record before the first axle leaves the bridge, accuracy should improve. Results are shown in Table 9.13. Overall accuracy increases to C(15), but the static approach still offers a slightly better solution.

Table 9.13 – Accuracy classification for DB-WIM (shorter record) (Isotropic slab) (R1)

(**n**: Total number of vehicles; **m**: mean; **s**: Standard deviation; π_0: level of confidence; δ: tolerance of the retained accuracy class; δ_{min}: minimum width of the confidence interval for π_0; π: Level of confidence of the interval $[-\delta,\delta]$)

	Relative error statistics				Accuracy calculation				
Criterion	**n**	**m** (%)	**s** (%)	π_0 (%)	**Class**	δ (%)	δ_{min} (%)	π (%)	**Class Retained**
Single axle	27	2.99	8.33	92.1	**C(15)**	20	19.4	93.1	**C(15)**
Group of axles	9	-2.96	2.43	83.4	**B+(7)**	10	7.4	96.6	
Gross Weight	18	0.02	1.39	90.3	**A(5)**	5	3.1	99.4	

Hence, it can be concluded that DB-WIM is not valid in situations where the bridge has been previously excited (i.e. initial state of vibration due to the passing of a preceding truck). Accordingly, DB-WIM should not be applied to very short span bridges.

The MS-BWIM system was tested with strain at three longitudinal sections (4, 8 and 12 m) and two transverse positions per section (under the slow and fast lane at 2.5 m from the centreline). Six static equations can be formulated at each instant (one per sensor), but the algorithm is not able to predict an instantaneous solution at all times. There are instants where numerical errors appear and they should be removed from the calculations. The determinant has very small values when there is a change in the number of axles on the bridge. Thus, for the 2-axle truck with 5 m axle spacing, the instantaneous solution will tend towards infinity at 5 m and 16 m (the contribution of an axle entering or leaving the bridge to the overall strain is negligible). As the number of axles increases, the length of the bridge where the instantaneous calculation is feasible decreases as does the accuracy. Accuracy classes for this choice of sensors are given in Table 9.14. Compared to the algorithms based on one longitudinal location, there is an improvement from C(15) to A(5). Therefore, if the criterion for an axle of group is considered, overall accuracy D+(20) is achieved (accuracy by algorithms based on one longitudinal location for axle of a group is very poor). However, as the COST323 specification does not require axles of groups for B-WIM systems, the system is strictly of class A(5).

Table 9.14 – Accuracy classification for static MS-BWIM (3 longit. sections) (slab) (R1)

(**n**: Total number of vehicles; **m**: mean; **s**: Standard deviation; π_0: level of confidence; δ: tolerance of the retained accuracy class; δ_{min}: minimum width of the confidence interval for π_0; π: Level of confidence of the interval $[-\delta,\delta]$)

	Relative error statistics				Accuracy calculation				
Criterion	**n**	**m (%)**	**S (%)**	π_0 (%)	**Class**	δ (%)	δ_{min} (%)	π (%)	**Class Retained**
Single axle	27	-1.15	2.73	92.1	**A(5)**	8	6.5	97.5	**D+(20)**
Axle of group	18	-1.07	12.34	90.3	**D+(20)**	30	27.9	92.9	
Group of axles	9	1.01	1.52	83.4	**A(5)**	7.14	3.9	99.3	
Gross Weight	18	0.01	0.83	90.3	**A(5)**	5	1.9	100.	

The number and location of the sensors have a strong influence on the duration for which the instantaneous solution is possible. Next, the MS-BWIM system is tested with sensors located every 2 m all along the bridge. Two transverse sensors under the slow and fast lanes are considered for each longitudinal section (Their results are added together). This results in 7 static equations solved by a least squares fitting technique as described in Section 7.5.2. The instantaneous solution is feasible for longer and the final average value

should be closer to the static weight. This time, the overall accuracy is B+(7), or A(5) excluding the axle of group criterion (Table 9.15). This MS-BWIM system offers a very significant improvement over all previous approaches. The increase in the number of instrumented sections from 3 to 7 has raised accuracy for axles of group from D+(20) to B+(7).

Table 9.15 – Accuracy classification for static MS-BWIM (7 longit. sections) (slab) (R1)

(**n**: Total number of vehicles; **m**: mean; **s**: Standard deviation; π_0: level of confidence; δ: tolerance of the retained accuracy class; δ_{min}: minimum width of the confidence interval for π_0; π: Level of confidence of the interval $[-\delta,\delta]$)

	Relative error statistics				Accuracy calculation				
Criterion	**n**	**m (%)**	**S (%)**	π_0 (%)	**Class**	δ (%)	δ_{min} (%)	π (%)	**Class Retained**
Single axle	27	-0.45	1.39	92.1	**A(5)**	8	3.2	100.	**B+(7)**
Axle of group	18	0.88	4.42	90.3	**B+(7)**	14	10.1	98.2	
Group of axles	9	0.57	0.54	83.4	**A(5)**	7.14	1.6	100.	
Gross Weight	18	0.00	0.64	90.3	**A(5)**	5	1.5	100.	

Figure 9.25 shows the results achieved by the different algorithms.

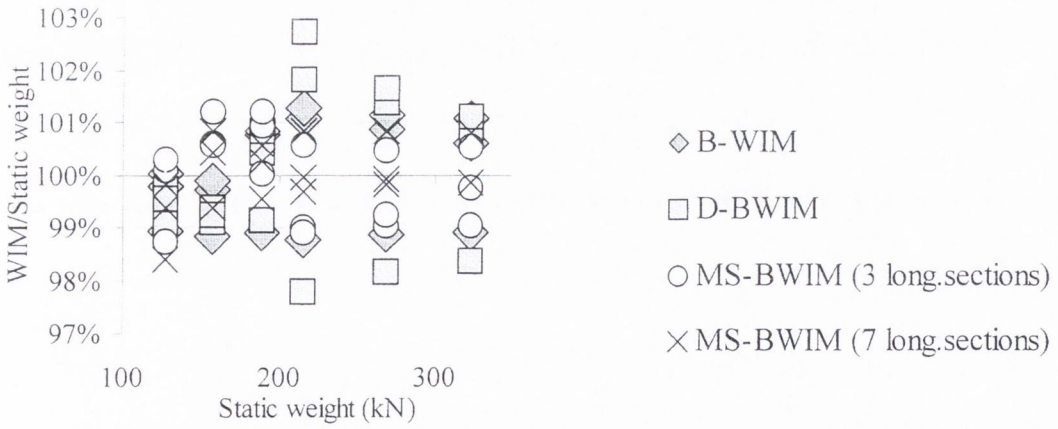

(a) Gross vehicle weight

Figure 9.25 (continued on following page)

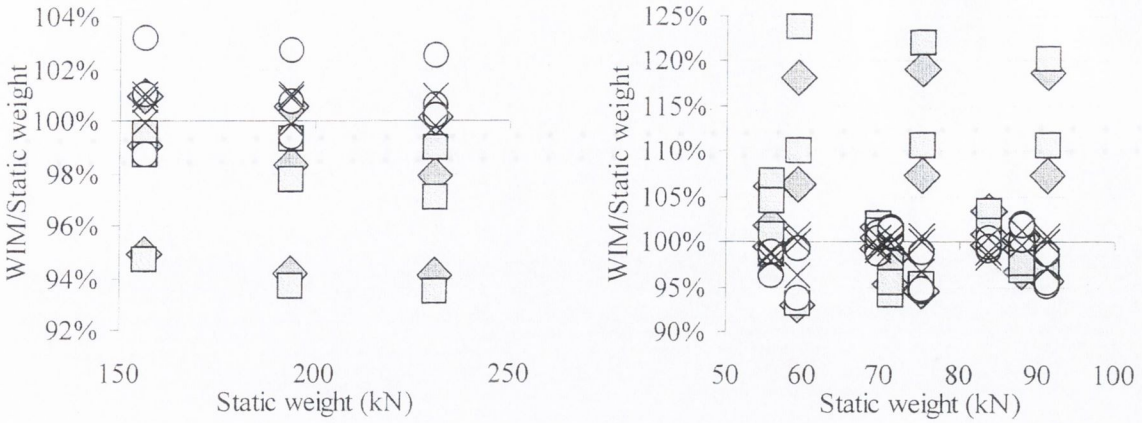

(b) Axle group (c) Individual axle weights

Figure 9.25 – WIM/Static versus real static weights (Isotropic slab)

The previous results for MS-BWIM were obtained by averaging the instantaneous values for each axle. However, the potential of an instantaneous calculation can be further exploited. If the dynamic oscillation of the predicted load is considered, accuracy could be expected to improve (i.e., avoiding deviations that depend on the time the truck is on the bridge). The dominant frequency of higher amplitude can be obtained through the spectra of the varying axle load amplitude (generally corresponding to the first natural frequency of the bridge, but it could be another frequency resulting from the bridge-truck interaction). Then, the static value can be obtained through the average of an exact number of periods. The same process can be used to remove remaining frequency components. If the lower frequency components can not be detected by the spectra (i.e. readings that do not complete a period), the parameters of the harmonic oscillation (amplitude, frequency and phase) can be adjusted to the available data. Figure 9.26(a) represents the original history of axle forces obtained by MS-BWIM. Figures 9.26(b) and 9.26(c) show the removal of frequency components in successive steps. Averaging the values in Figure 9.26(c) results in 52.9 and 68.5 kN, slightly smaller than the real static axle weights of 55.7 and 71.2 kN respectively. The final static value can be derived from Figure 9.26(c) by applying trigonometry to the remaining low frequency component. This technique can be of great interest in bridges where the number of dynamic oscillations is not high enough.

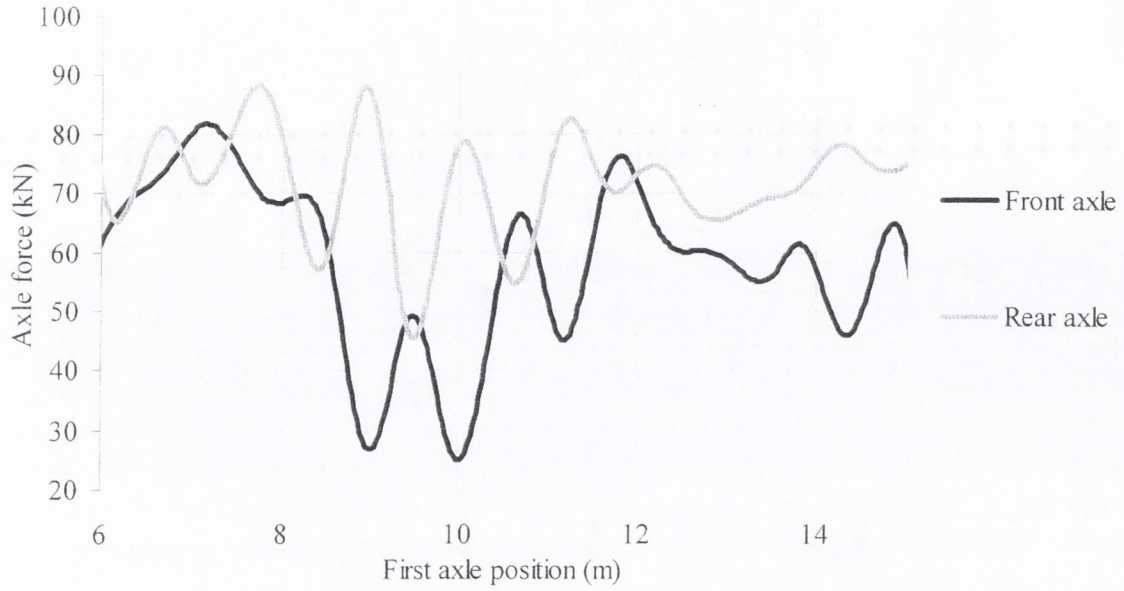

(a) Initial Prediction of Instantaneous axle forces

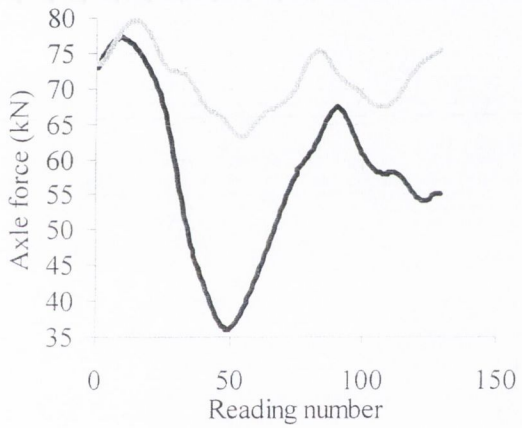

(b) Removal of 13.16 Hz frequency

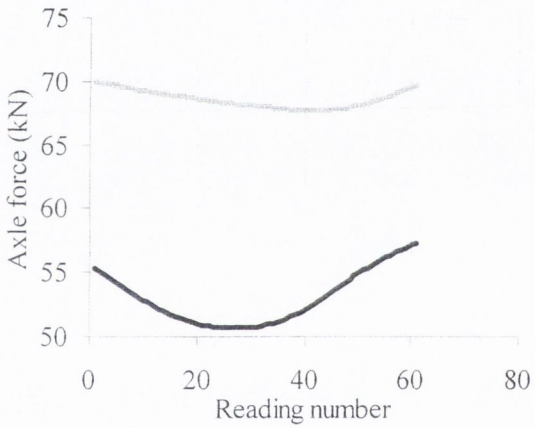

(c) Removal of 3.62 Hz frequency

Figure 9.26 – Estimation of static value (fully laden two-axle truck at 55 km/h)

Effect of truck lateral location

All previous runs were located in the same lateral path (inner wheels at 1 m from the bridge centreline). In this section, new runs with small variations in the lateral position on the road are included in the accuracy analysis. The inner wheels of the truck are in the slow lane at 0, 1 and 2 m from the bridge centreline (Figure 6.40). The prediction in weights by the static algorithm is shown in Figure 9.27.

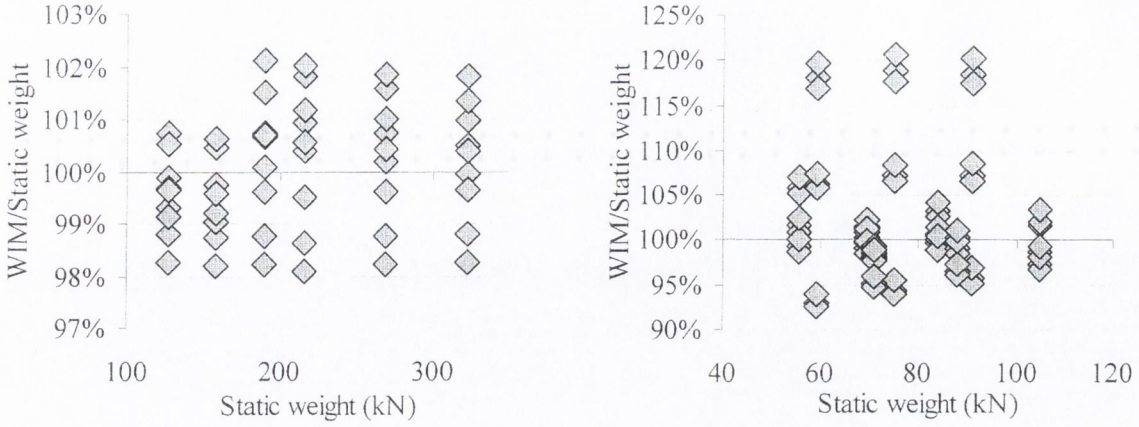

(a) Gross vehicle weight (b) Individual axle weights

Figure 9.27 – WIM/Static versus real static weights

The static algorithm maintains the same accuracy classes as Table 9.10 (one lateral position) for each individual criterion (Table 9.16). Accuracy of individual axle weight results are more robust (higher confidence interval) as a result of a bigger sample.

Table 9.16 – Accuracy classification for static B-WIM (2 sensors) (Isotropic slab) (R1)

(**n**: Total number of vehicles; **m**: mean; **s**: Standard deviation; π_0: level of confidence; δ: tolerance of the retained accuracy class; δ_{min}: minimum width of the confidence interval for π_0; π: Level of confidence of the interval $[-\delta,\delta]$)

	Relative error statistics				Accuracy calculation				
Criterion	**n**	**m** (%)	**s** (%)	π_0 (%)	**Class**	δ (%)	δ_{min} (%)	π (%)	**Class Retained**
Single axle	81	2.21	6.93	94.6	C(15)	20	15.77	98.7	**C(15)**
Group of axles	27	-2.26	2.67	92.1	B+(7)	10	7.25	99.0	
Gross Weight	54	0.01	1.12	94.0	A(5)	5	2.46	99.9	

In this case, the transverse location of the truck does not affect accuracy. However, a two-dimensional algorithm as proposed in Section 7.6 can improve results in bridges sensitive to the transverse location. This algorithm is based on a database of influence lines for each truck transverse location. The correct influence line can be chosen at each instant by minimising errors between measured and theoretical strains (instead of using a common influence line as with one-dimensional models).

9.3.2 Two-Span Isotropic Slab

Details of this 37-m bridge (First natural frequency 4.18 Hz) are given in Section 6.5.2. The static B-WIM system uses strain at the middle of the first span (at two points symmetric about the centreline and spaced 5 m transversely). Table 9.17 shows how a global accuracy of D+(20) is achieved. Compared to the single span studied in the previous section, the algorithm is less accurate in this longer bridge due to the difficulty of weighing single axles and the higher dynamics at the midspan section. Accuracy in GVW and axle groups remains at A(5) and B+(7) respectively.

The same sensors are used to test the dynamic B-WIM algorithm. Results are shown in Table 9.18. Accuracy in single axles improves from D+(20) to B(10). However, if the criterion of axle of group is considered, the overall accuracy decreases down to E(60).

Table 9.17 – Accuracy classification for static B-WIM (midspan) (Two-span slab) (R1)

(**n**: Total number of vehicles; **m**: mean; **s**: Standard deviation; π_0: level of confidence; δ: tolerance of the retained accuracy class; δ_{min}: minimum width of the confidence interval for π_0; π: Level of confidence of the interval $[-\delta,\delta]$)

	Relative error statistics				Accuracy calculation				
Criterion	**n**	**m** (%)	**s** (%)	π_0 (%)	**Class**	δ (%)	δ_{min} (%)	π (%)	**Class Retained**
Single axle	27	1.71	9.67	92.1	**D+(20)**	25	21.8	96.0	**D+(20)**
Group of axles	9	-1.56	3.91	83.4	**B+(7)**	10	9.4	86.9	
Gross Weight	18	0.02	1.39	90.3	**A(5)**	5	3.1	99.4	

Table 9.18 – Accuracy classification for DB-WIM algorithm (Two-span slab) (R1)

(**n**: Total number of vehicles; **m**: mean; **s**: Standard deviation; π_0: level of confidence; δ: tolerance of the retained accuracy class; δ_{min}: minimum width of the confidence interval for π_0; π: Level of confidence of the interval $[-\delta,\delta]$)

	Relative error statistics				Accuracy calculation				
Criterion	**n**	**m** (%)	**s** (%)	π_0 (%)	**Class**	δ (%)	δ_{min} (%)	π (%)	**Class Retained**
Single axle	27	1.97	5.85	92.1	**B(10)**	15	13.6	95.1	**E(60)**
Axle of group	18	1.82	29.13	90.3	**E(60)**	77	65.7	95.3	
Group of axles	9	-1.88	2.15	83.4	**A(5)**	7.14	5.9	92.9	
Gross Weight	18	0.00	0.63	90.3	**A(5)**	5	1.4	100.	

The central support is expected to suffer less dynamic vibrations, and a static B-WIM system based on this location is also tested. Table 9.19 shows an improvement in single axle weights from B(10) to A(5), and in axle of a group from E(60) to B(+7). The system is extraordinarily accurate, even for individual axles in a group. Global accuracy is B+(7). The most accurate class, A(5), is reached if the criterion of axle of group is ignored.

Table 9.19 – Accuracy classification for static B-WIM (central support) (Two-span slab)

(**n**: Total number of vehicles; **m**: mean; **s**: Standard deviation; π_0: level of confidence; δ: tolerance of the retained accuracy class; δ_{min}: minimum width of the confidence interval for π_0; π: Level of confidence of the interval $[-\delta,\delta]$)

	Relative error statistics				Accuracy calculation				
Criterion	**n**	**m (%)**	**s (%)**	**π_0 (%)**	**Class**	**δ (%)**	**δ_{min} (%)**	**π (%)**	**Class Retained**
Single axle	27	-0.25	2.45	92.1	**A(5)**	8	5.5	99.2	**B+(7)**
Axle of group	18	-0.18	5.54	90.3	**B+(7)**	14	12.5	94.1	
Group of axles	9	0.45	0.58	83.4	**A(5)**	7.14	1.5	100.	
Gross Weight	18	0.00	0.56	90.3	**A(5)**	5	1.3	100.	

The MS-BWIM system use strains at 5.9, 9.5, 11.9, 17.9, 23.9, 27.5 and 29.9 m from the bridge start in two transverse positions (under the slow and fast lanes at 2.5 m from the centreline). A global accuracy of B(10) is obtained in Table 9.20. The best option appears to be the static algorithm purely based on the instrumentation of the central support section. The consideration of other less accurate longitudinal locations in an instantaneous calculation results in a lower accuracy class.

Table 9.20 – Accuracy classification for static MS-BWIM (Two-span isotropic slab) (R1)

(**n**: Total number of vehicles; **m**: mean; **s**: Standard deviation; π_0: level of confidence; δ: tolerance of the retained accuracy class; δ_{min}: minimum width of the confidence interval for π_0; π: Level of confidence of the interval $[-\delta,\delta]$)

	Relative error statistics				Accuracy calculation				
Criterion	**n**	**m (%)**	**s (%)**	**π_0 (%)**	**Class**	**δ (%)**	**δ_{min} (%)**	**π (%)**	**Class Retained**
Single axle	27	1.16	3.00	92.1	**A(5)**	8	7.1	95.8	**B(10)**
Axle of group	18	-1.22	7.17	90.3	**B(10)**	20	16.3	96.3	
Group of axles	9	-1.43	1.31	83.4	**A(5)**	7.14	3.8	99.6	
Gross Weight	18	0.01	1.18	90.3	**A(5)**	5	2.7	99.8	

Finally, Figure 9.28 shows the performance of each algorithm in the estimation of gross vehicle weight, axle group and single axle.

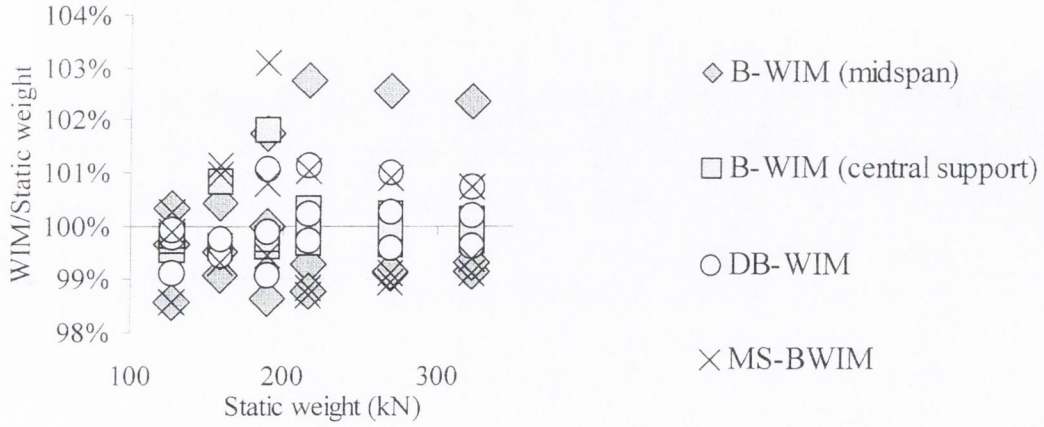

(a) Gross vehicle weight

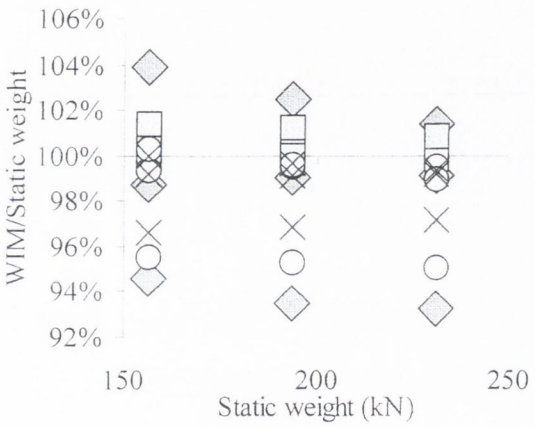

(b) Axle group

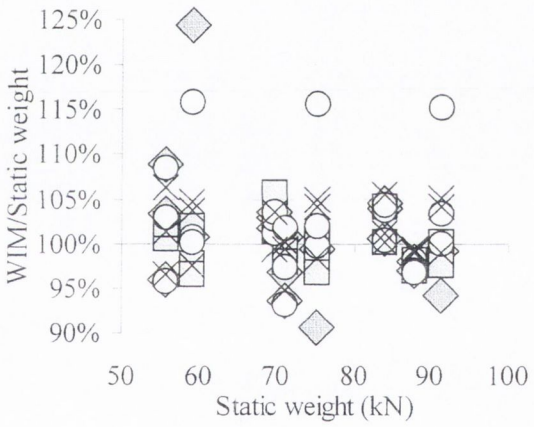

(c) Individual axle weights

Figure 9.28 – WIM/Static versus real static weights (Two-span isotropic slab)

9.3.3 Slab with Edge Cantilever

Details of this 20 m bridge (First natural frequency 4.80 Hz) are given in Section 6.5.3. The results of the static algorithm are based on strains by two sensors located at the midspan section. This bridge is stiffer than the single span isotropic slab in Section 9.3.1. This bridge has also a longer span with a higher first natural frequency. Bridge dynamics are expected to be smaller and the average of the varying axle forces closer to the static value. Accuracy should improve with respect to the global accuracy C(15) obtained in the single span isotropic slab. Consistently, Table 9.21 shows an accuracy of B(10) when ignoring the criterion of axle of group. This last criterion has a very poor accuracy E(70).

Table 9.21 – Accuracy classification for static B-WIM (Slab with edge cantilever) (R1)

(**n**: Total number of vehicles; **m**: mean; **s**: Standard deviation; π_0: level of confidence; δ: tolerance of the retained accuracy class; δ_{min}: minimum width of the confidence interval for π_0; π: Level of confidence of the interval $[-\delta,\delta]$)

	Relative error statistics				Accuracy calculation				
Criterion	**n**	**m** (%)	**s** (%)	π_0 (%)	**Class**	δ (%)	δ_{min} (%)	π (%)	**Class Retained**
Single axle	27	0.73	5.64	92.1	**B(10)**	15	12.6	96.7	**E(70)**
Axle of group	18	1.80	33.54	90.3	**E(70)**	89	75.6	95.4	
Group of axles	9	-0.53	2.25	83.4	**A(5)**	7.14	5.2	95.4	
Gross Weight	18	0.01	0.80	90.3	**A(5)**	5	1.8	100.	

Table 9.22 gives accuracy classes when applying a dynamic B-WIM to the same sensors. The dynamic approach is less accurate and unsuitable for this type of bridge behaviour.

Table 9.22 – Accuracy classification for DB-WIM (Slab with edge cantilever) (R1)

(**n**: Total number of vehicles; **m**: mean; **s**: Standard deviation; π_0: level of confidence; δ: tolerance of the retained accuracy class; δ_{min}: minimum width of the confidence interval for π_0; π: Level of confidence of the interval $[-\delta,\delta]$)

	Relative error statistics				Accuracy calculation				
Criterion	**n**	**m** (%)	**s** (%)	π_0 (%)	**Class**	δ (%)	δ_{min} (%)	π (%)	**Class Retained**
Single axle	27	1.54	6.88	92.1	**C(15)**	20	15.6	97.9	**E(90)**
Axle of group	18	2.21	42.26	90.3	**E(90)**	113	95.3	95.6	
Group of axles	9	-1.38	2.81	83.4	**A(5)**	7.14	6.9	85.5	
Gross Weight	18	0.00	0.72	90.3	**A(5)**	5	1.6	100.	

MS-BWIM uses strain in six different points at 4.5, 9.5 and 14.5 m from the bridge start in two transverse positions (under the slow and fast lane at 2.5 m from the centreline). MS-BWIM offers the most accurate overall class A(5) (Table 9.23).

Figure 9.29(c) illustrates how MS-BWIM is the best solution for individual axles. However, B-WIM is lightly more reliable when estimating axle group or gross weight (Figures 9.29(a) and (b)).

Table 9.23 – Accuracy classification for static MS-BWIM (Slab with edge cantilever) (R1)

(**n**: Total number of vehicles; **m**: mean; **s**: Standard deviation; π_0: level of confidence; δ: tolerance of the retained accuracy class; δ_{min}: minimum width of the confidence interval for π_0; π: Level of confidence of the interval $[-\delta,\delta]$)

	Relative error statistics				Accuracy calculation				
Criterion	**n**	**m (%)**	**s (%)**	π_o **(%)**	**Class**	δ **(%)**	δ_{min} **(%)**	π **(%)**	**Class Retained**
Single axle	27	0.76	3.40	92.1	**A(5)**	8	7.7	93.4	**A(5)**
Axle of group	18	-0.50	3.42	90.3	**A(5)**	10	7.8	97.2	
Group of axles	9	-0.53	1.81	83.4	**A(5)**	7.14	4.3	98.5	
Gross Weight	18	0.03	1.92	90.3	**A(5)**	5	4.3	95.0	

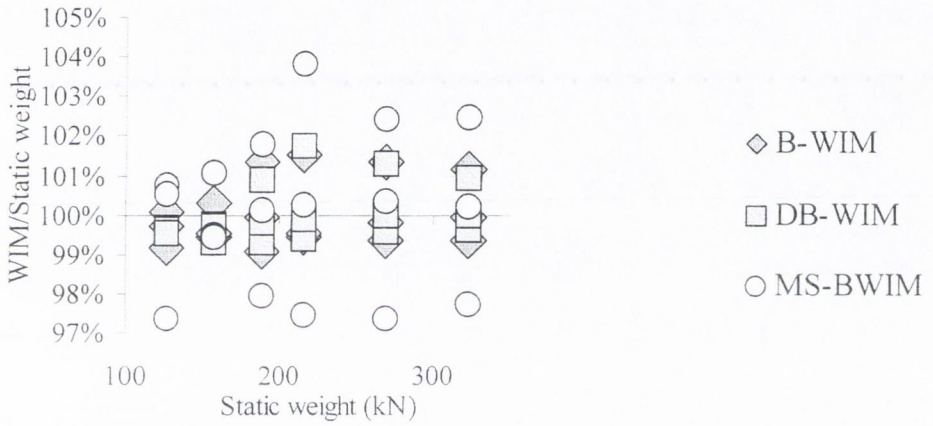

(a) Gross vehicle weight

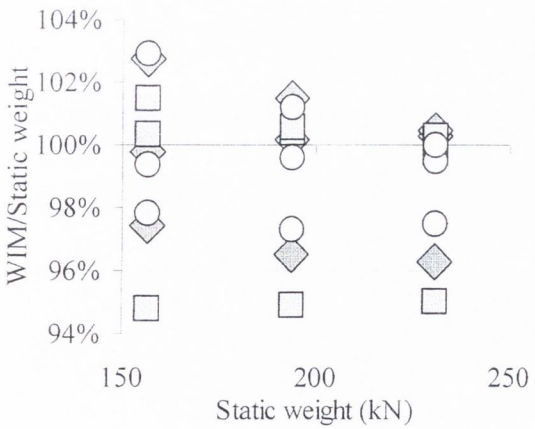

(b) Axle group

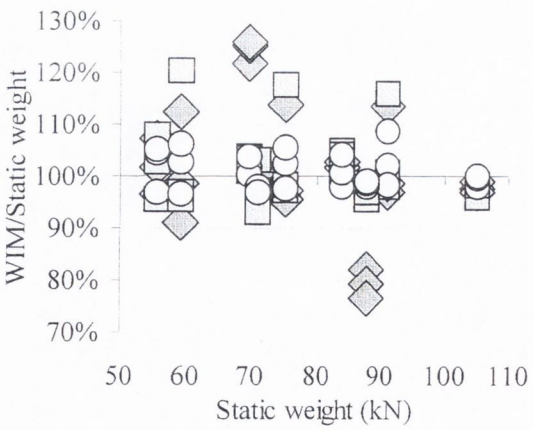

(c) Individual axle weights

Figure 9.29 – WIM/Static versus real static weights (Slab with edge cantilever)

9.3.4 Voided Slab Deck

Details of this 25 m bridge (First natural frequency 3.80 Hz) are given in Section 6.5.4. The static B-WIM algorithm uses two sensors at midspan (one sensor in each lane at 2.5 m from centreline). This bridge is longer and more flexible than the previous slab with edge cantilever. Thus, poorer results are expected, particularly for single axle weights. Table 9.24 shows how the overall accuracy class comes down to D(25).

Table 9.24 – Accuracy classification for static B-WIM algorithm (Voided Slab) (R1)

(**n**: Total number of vehicles; **m**: mean; **s**: Standard deviation; π_0: level of confidence; δ: tolerance of the retained accuracy class; δ_{min}: minimum width of the confidence interval for π_0; π: Level of confidence of the interval $[-\delta,\delta]$)

	Relative error statistics				Accuracy calculation				
Criterion	**n**	**m (%)**	**s (%)**	**π_0 (%)**	**Class**	**δ (%)**	**δ_{min} (%)**	**π (%)**	**Class Retained**
Single axle	27	-3.47	12.00	92.1	**D(25)**	30	27.6	94.7	**D(25)**
Group of axles	9	3.96	6.56	83.4	**C(15)**	18	16.5	88.0	
Gross Weight	18	0.00	0.48	90.3	**A(5)**	5	1.1	100.	

The dynamic algorithm is tested with the same sensors and accuracy improves from D(25) to C(15) (Table 9.25).

Table 9.25 – Accuracy classification for dynamic B-WIM algorithm (Voided Slab) (R1)

(**n**: Total number of vehicles; **m**: mean; **s**: Standard deviation; π_0: level of confidence; δ: tolerance of the retained accuracy class; δ_{min}: minimum width of the confidence interval for π_0; π: Level of confidence of the interval $[-\delta,\delta]$)

	Relative error statistics				Accuracy calculation				
Criterion	**n**	**m (%)**	**s (%)**	**π_0 (%)**	**Class**	**δ (%)**	**δ_{min} (%)**	**π (%)**	**Class Retained**
Single axle	27	2.74	8.38	92.1	**C(15)**	20	19.4	93.2	**C(15)**
Group of axles	9	-2.75	3.83	83.4	**B+(7)**	10	10.0	83.6	
Gross Weight	18	0.00	0.72	90.3	**A(5)**	5	1.6	100.	

The MS-BWIM system use strain in six different points at 6.5, 12.5 and 18.5 m from the bridge start in two transverse positions (under the slow and fast lane at 2.5 m from the centreline). As shown in Table 9.26, MS-BWIM is more inaccurate for gross weight and

axle group than algorithms based on one longitudinal section. The cause is the reduced number and inappropriate location of sensors that only allow for an instantaneous solution for a short period of time (along one meter for the tandem at highest speed). Compared to the previous slab with edge cantilever, this is a longer bridge that requires more sensors to cover most of the vehicle path effectively. Therefore, static equations are not a good reference for the behaviour of this bridge as accuracy in Table 9.24 reveals.

Table 9.26 – Accuracy classification for static MS-BWIM algorithm (Voided Slab) (R1)

(**n**: Total number of vehicles; **m**: mean; **s**: Standard deviation; π_0: level of confidence; δ: tolerance of the retained accuracy class; δ_{min}: minimum width of the confidence interval for π_0; π: Level of confidence of the interval $[-\delta,\delta]$)

	Relative error statistics				Accuracy calculation				
Criterion	**n**	**m** (%)	**s** (%)	π_0 (%)	**Class**	δ (%)	δ_{min} (%)	π (%)	**Class Retained**
Single axle	27	-2.65	6.71	92.1	C(15)	20	15.8	97.8	**D+(20)**
Group of axles	9	4.99	7.03	83.4	D+(20)	23	18.2	93.9	
Gross Weight	18	0.27	5.58	90.3	C(15)	15	12.6	95.7	

Figure 9.30 illustrates the accuracy for different approaches. Percentage errors in individual axle weights generally increase for higher speeds and lower weights (Figure 9.30(c)).

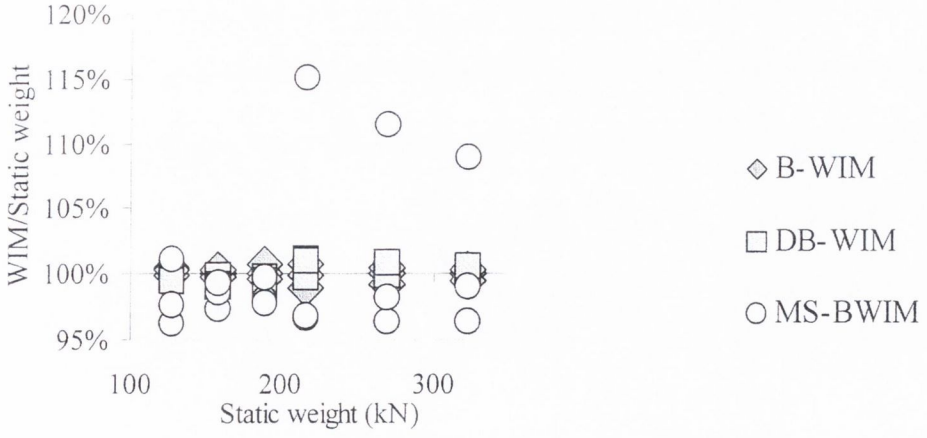

(a) Gross vehicle weight

Figure 30 (continued on following page)

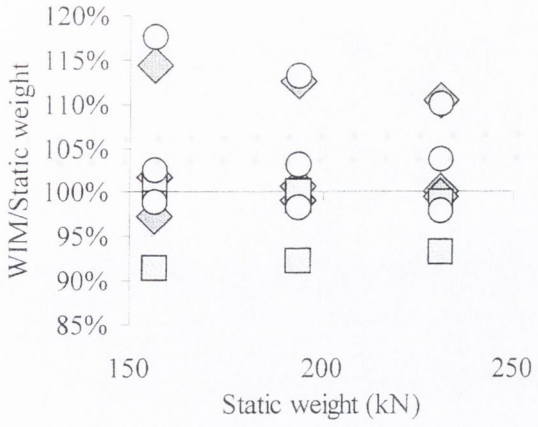

(b) Axle group

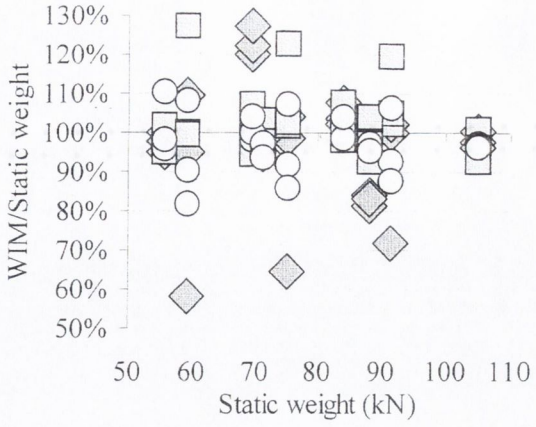

(c) Individual axle weights

Figure 9.30 – WIM/Static versus real static weights (Voided slab deck)

9.3.5 Beam and Slab

Details of this 20 m bridge (first natural frequency 6.13 Hz) are given in Section 6.5.5. This bridge has the same length, less stiffness (higher static strain) and higher first natural frequency than the slab with edge cantilever. At the midspan section, transverse bending of the slab is more significant than longitudinal bending. In preceding sections, the magnitude of this transverse bending was too small to be considered. Unlike longitudinal bending, the influence line for transverse bending has opposite curvature under the slow and fast lanes. The algorithms based on one longitudinal location use two sensors at the midspan section. Three different possibilities are studied:

(a) use of the beam longitudinal strain (sum of two sensors 3 m apart, located symmetrically about the centreline) (accuracy analysis in Table 9.27),

(b) use of the slab longitudinal bending (sum of two sensors 4 m apart, located symmetrically about the centreline) (Table 9.28), and

(c) use of the slab transverse bending (difference of two sensors 4 m apart, located symmetrically about the centreline) (Table 9.29).

If the axle of a group criterion is included in the analysis, a best overall result of B+(7) is obtained with installation (c), compared to D(25) and E(30) for options (a) and (b) respectively. If axle of group is ignored in the analysis, overall accuracy raises to A(5) when using transverse strain and B+(7) for longitudinal bending. Hence, though B-WIM

systems have always used longitudinal bending for weighing purposes, the measurement of transverse bending must require further attention for particular sites.

Table 9.27 – Accuracy classification for static B-WIM (beam) (Beam&Slab bridge) (R1)

(**n**: Total number of vehicles; **m**: mean; **s**: Standard deviation; π_0: level of confidence; δ: tolerance of the retained accuracy class; δ_{min}: minimum width of the confidence interval for π_0; π: Level of confidence of the interval $[-\delta,\delta]$)

	Relative error statistics				Accuracy calculation				
Criterion	**n**	**m (%)**	**s (%)**	π_0 (%)	**Class**	δ (%)	δ_{min} (%)	π (%)	**Class Retained**
Single axle	27	-1.13	3.96	92.1	**B+(7)**	11	9.1	96.9	**D(25)**
Axle of group	18	-0.96	14.89	90.3	**D(25)**	35	33.6	91.8	
Group of axles	9	1.39	1.64	83.4	**A(5)**	7.14	4.4	98.6	
Gross Weight	18	0.00	0.50	90.3	**A(5)**	5	1.1	100.	

Table 9.28 – Accuracy classification for static B-WIM (slab longitud. strain) (B&S) (R1)

(**n**: Total number of vehicles; **m**: mean; **s**: Standard deviation; π_0: level of confidence; δ: tolerance of the retained accuracy class; δ_{min}: minimum width of the confidence interval for π_0; π: Level of confidence of the interval $[-\delta,\delta]$)

	Relative error statistics				Accuracy calculation				
Criterion	**n**	**m (%)**	**s (%)**	π_0 (%)	**Class**	δ (%)	δ_{min} (%)	π (%)	**Class Retained**
Single axle	27	-0.57	4.29	92.1	**B+(7)**	11	9.6	95.8	**E(30)**
Axle of group	18	-0.37	15.87	90.3	**E(30)**	41	35.7	94.8	
Group of axles	9	0.85	1.61	83.4	**A(5)**	7.14	4.0	99.2	
Gross Weight	18	0.00	0.46	90.3	**A(5)**	5	1.0	100.	

Table 9.29 – Accuracy classification for static B-WIM (slab transvers. strain) (B&S) (R1)

(**n**: Total number of vehicles; **m**: mean; **s**: Standard deviation; π_0: level of confidence; δ: tolerance of the retained accuracy class; δ_{min}: minimum width of confidence interval for π_0; π: Level of confidence of $[-\delta,\delta]$)

	Relative error statistics				Accuracy calculation				
Criterion	**n**	**m (%)**	**s (%)**	π_0 (%)	**Class**	δ (%)	δ_{min} (%)	π (%)	**Class Retained**
Single axle	27	0.50	2.07	92.1	**A(5)**	8	4.7	99.8	**B+(7)**
Axle of group	18	-0.09	5.39	90.3	**B+(7)**	14	12.1	94.9	
Group of axles	9	-0.45	0.52	83.4	**A(5)**	7.14	1.4	100.	
Gross Weight	18	0.00	0.30	90.3	**A(5)**	5	0.7	100.	

The dynamic algorithm is applied to the longitudinal bending of two beams at midspan. Results, given in Table 9.30, are more accurate than the static algorithm based on longitudinal bending, but not as accurate as the algorithm based on transverse bending.

Table 9.30 – Accuracy classification for DB-WIM (Beam and Slab bridge) (R1)

(**n**: Total number of vehicles; **m**: mean; **s**: Standard deviation; π_0: level of confidence; δ: tolerance of the retained accuracy class; δ_{min}: minimum width of the confidence interval for π_0; π: Level of confidence of the interval $[-\delta,\delta]$)

	Relative error statistics				Accuracy calculation				
Criterion	**n**	**m (%)**	**s (%)**	π_0 (%)	**Class**	δ (%)	δ_{min} (%)	π (%)	**Class Retained**
Single axle	55	0.79	8.95	91.6	C(15)	20	18.3	91.6	**C(15)**
Group of axles	27	0.17	8.22	89.1	C(15)	18	16.9	89.1	
Gross Weight	28	0.55	5.55	89.3	C(15)	15	11.5	89.3	

The MS-BWIM system measures longitudinal bending on the bottom slab deck of three different sections at 4.5, 9.5 and 14.5 m from the bridge start (in two transverse locations under the slow lane and fast lane at 2.0 m from the centreline). A system of six equations can be formulated at each instant: one relating transverse bending and another relating longitudinal bending for each one of the three instrumented sections (The longitudinal strain at each sensor in a section can be added together while the transverse bending is subtracted). However this arrangement fails to predict an instantaneous solution when there are three axles on the bridge. A new arrangement based purely on longitudinal bending of six sensors offers a solution for a small portion of the bridge. The results for this last arrangement are shown in Table 9.31. An overall accuracy B(10) is better than other algorithms based on longitudinal bending at one single location, but worse than the algorithm based on transverse bending at midspan.

Figure 9.31 shows the percentage of predicted weight over the static weight for different algorithms and criteria.

Table 9.31 – Accuracy classification for static MS-BWIM (Beam and Slab bridge) (R1)

(**n**: Total number of vehicles; **m**: mean; **s**: Standard deviation; π_0: level of confidence; δ: tolerance of the retained accuracy class; δ_{min}: minimum width of the confidence interval for π_0; π: Level of confidence of the interval $[-\delta,\delta]$)

	Relative error statistics				Accuracy calculation				
Criterion	**n**	**m (%)**	**s (%)**	**π_0 (%)**	**Class**	**δ (%)**	**δ_{min} (%)**	**π (%)**	**Class Retained**
Single axle	27	0.33	2.08	92.1	**A(5)**	8	4.7	99.8	**B(10)**
Axle of group	18	-0.71	6.43	90.3	**B(10)**	20	14.5	98.1	
Group of axles	9	-0.38	1.32	83.4	**A(5)**	7.14	3.1	99.8	
Gross Weight	18	0.02	1.33	90.3	**A(5)**	5	3.0	99.5	

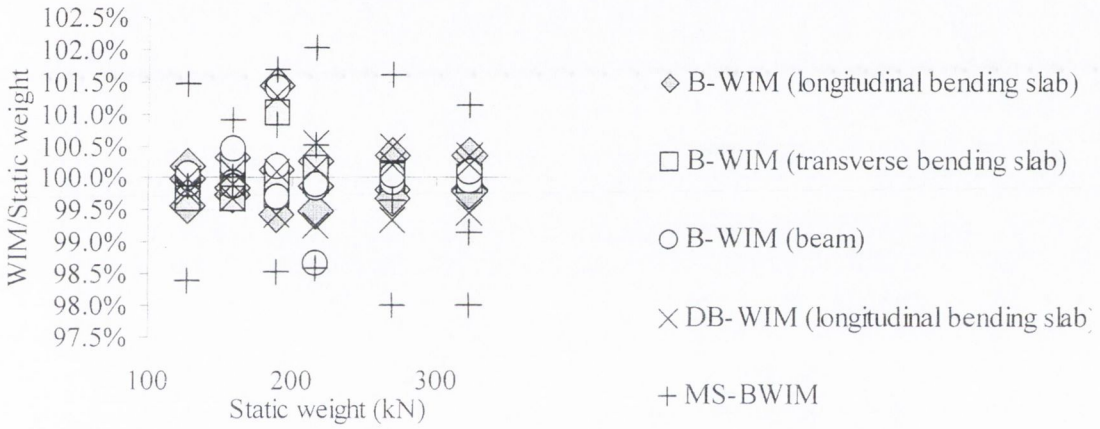

(a) Gross vehicle weight

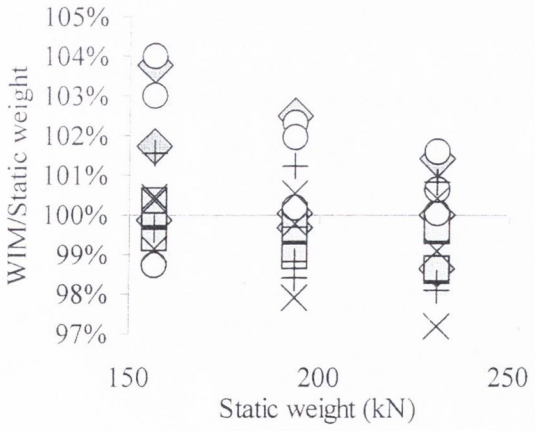

(b) Axle group

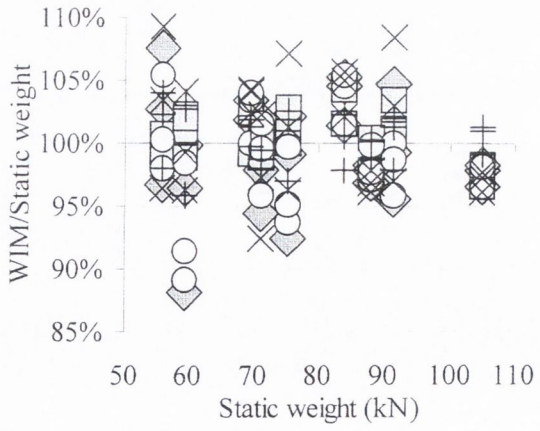

(c) Individual axle weights

Figure 9.31 – WIM/Static versus real static weights (Beam and slab)

9.3.6 Skew

Details of this 15 m bridge (first natural frequency 7.41 Hz) are given in Section 6.5.6. Dynamics are less significant than for the straight slab of the same length described in Section 9.3.1. However, a 45° skew can have a very negative influence on final results (Sections 3.2.2 and 3.7.2). Two sensors at 7.5 m from the bridge start and spaced 4 m symmetrically about the centreline are used as input for the static B-WIM algorithm. Table 9.32 shows how a global accuracy of E(50) is obtained (compared to C(15) in the straight slab). Accuracy classes A(5) and B+(7) are achieved for gross weight and group of axles criteria respectively.

Table 9.32 – Accuracy classification for static B-WIM algorithm (Skew bridge) (R1)

(**n**: Total number of vehicles; **m**: mean; **s**: Standard deviation; π_0: level of confidence; δ: tolerance of the retained accuracy class; δ_{min}: minimum width of the confidence interval for π_0; π: Level of confidence of the interval $[-\delta,\delta]$)

	Relative error statistics				Accuracy calculation				
Criterion	**n**	**m** (%)	**s** (%)	π_0 (%)	**Class**	δ (%)	δ_{min} (%)	π (%)	**Class Retained**
Single axle	27	-6.97	21.89	92.1	**E(50)**	60	50.6	96.7	**E(50)**
Group of axles	9	6.58	0.92	83.4	**B+(7)**	10	8.2	99.1	
Gross Weight	18	0.02	1.40	90.3	**A(5)**	5	3.2	99.3	

A dynamic algorithm based on the same sensors also gives poor results for single axle weights (Table 9.33).

Table 9.33 – Accuracy classification for dynamic B-WIM algorithm (Skew bridge) (R1)

(**n**: Total number of vehicles; **m**: mean; **s**: Standard deviation; π_0: level of confidence; δ: tolerance of the retained accuracy class; δ_{min}: minimum width of the confidence interval for π_0; π: Level of confidence of the interval $[-\delta,\delta]$)

	Relative error statistics				Accuracy calculation				
Criterion	**n**	**m** (%)	**s** (%)	π_0 (%)	**Class**	δ (%)	δ_{min} (%)	π (%)	**Class Retained**
Single axle	27	-9.07	19.20	92.1	**E(45)**	54	46.1	96.5	**E(45)**
Group of axles	9	9.36	1.84	83.4	**B(10)**	13	12.7	86.8	
Gross Weight	18	0.02	1.34	90.3	**A(5)**	5	3.0	99.5	

Strain is obtained in six different points at 3.5, 7.5 and 11.5 m from the bridge start in two transverse positions (under the slow and fast lane at 2.0 m from the centreline) are used for testing the MS-BWIM algorithm. These locations allow an instantaneous solution for the two-axle truck, but they fail to predict axles while there are three axles on the bridge and no accuracy classification can be provided. The limitations of the MS-BWIM are due to the characteristics of the influence lines for this choice of sensors. An instantaneous solution might be possible by using a higher number of sensors placed along the vehicle path (Section 7.5.2).

Though accuracy for individual axle weights is poor for the skewed bridge, there can be a reasonable prediction of gross weight as shown in Figure 9.32.

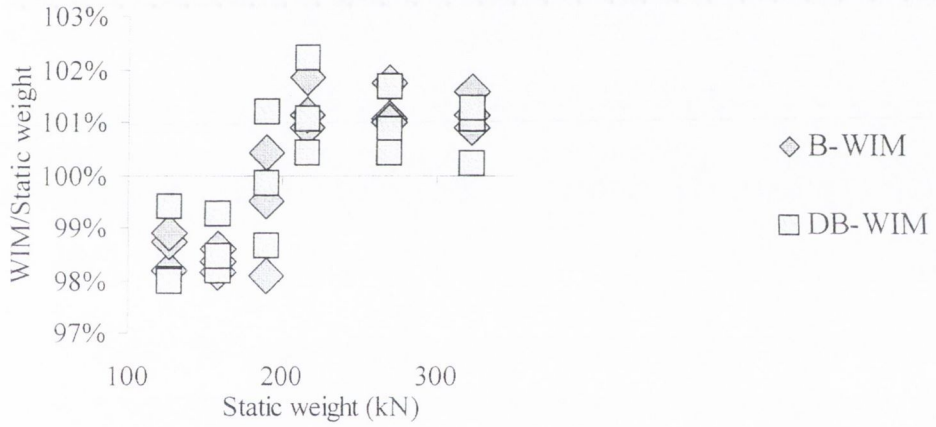

(a) Gross vehicle weight

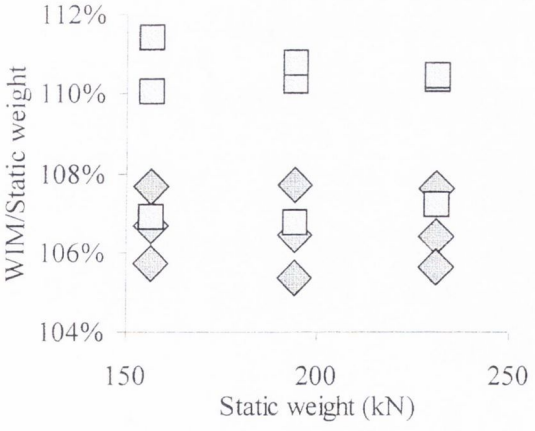

(b) Axle group

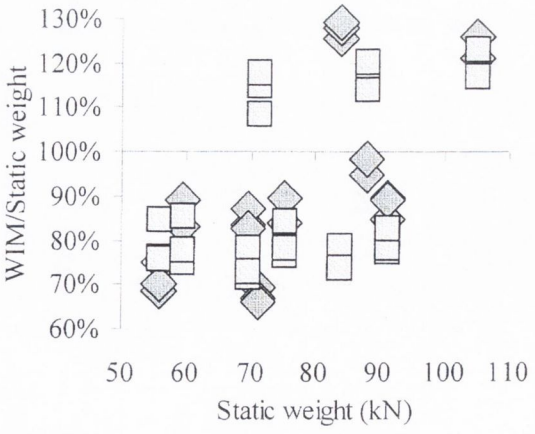

(c) Individual axle weights

Figure 9.32 – WIM/Static versus static weights (Skew bridge)

9.3.7 Cellular

Details of this two span 62 m bridge (first natural frequency 2.95 Hz) are given in Section 6.5.7. Compared to the previous types of bridge, this is the longest and accuracy is expected to decrease (as mentioned in Section 3.2.2). It also has the lowest first natural frequency. The B-WIM algorithm based on one longitudinal location is tested initially with two sensors measuring longitudinal bending, and secondly with two sensors measuring transverse bending (all located under the bottom plate at midspan). The results of longitudinal bending at the sensors are added, but the transverse bending of both sensors is subtracted as their influence lines have opposite signs.

The use of transverse bending improves accuracy in individual axle weights from E(95) to E(30) (Tables 9.34 and 9.35). Transverse bending is not too influenced by other traffic far from the sensor location and it can be an alternative in long span bridges. GVW is determined more accurately by measuring longitudinal bending (smaller δ_{min}). A combination of transverse and longitudinal bending appears to be the best solution for this type of bridge behaviour.

Table 9.34 – Accuracy classification for static B-WIM (longitud. bending) (Cellular) (R1)
(**n**: Total number of vehicles; **m**: mean; **s**: Standard deviation; π_0: level of confidence; δ: tolerance of the retained accuracy class; δ_{min}: minimum width of the confidence interval for π_0; π: Level of confidence of the interval $[-\delta,\delta]$)

	Relative error statistics				Accuracy calculation				
Criterion	**n**	**m** (%)	**s** (%)	π_0 (%)	**Class**	δ (%)	δ_{min} (%)	π (%)	**Class Retained**
Single axle	27	-0.92	8.39	92.1	**C(15)**	20	18.8	94.1	**E(95)**
Axle of group	18	-2.15	45.41	90.3	**E(95)**	119	102.3	95.1	
Group of axles	9	0.97	4.12	83.4	**B+(7)**	10	9.6	85.7	
Gross Weight	18	0.00	0.49	90.3	**A(5)**	5	1.1	100.	

Table 9.35 – Accuracy classification for static B-WIM (transver. bending) (Cellular) (R1)

(**n**: Total number of vehicles; **m**: mean; **s**: Standard deviation; π_0: level of confidence; δ: tolerance of the retained accuracy class; δ_{min}: minimum width of the confidence interval for π_0; π: Level of confidence of the interval $[-\delta,\delta]$)

	Relative error statistics				Accuracy calculation				
Criterion	**n**	**m** (%)	**s** (%)	π_0 (%)	**Class**	δ (%)	δ_{min} (%)	π (%)	**Class Retained**
Single axle	27	0.42	4.02	92.1	**B+(7)**	11	9.0	97.1	**E(30)**
Axle of group	18	-0.26	17.15	90.3	**E(30)**	41	38.6	92.5	
Group of axles	9	-0.30	1.70	83.4	**A(5)**	7.14	3.9	99.1	
Gross Weight	18	0.01	0.90	90.3	**A(5)**	5	2.0	100.	

As in Section 9.3.2, the static B-WIM algorithm is tested with longitudinal bending at the central support. Results are given in Table 9.36. Overall accuracy is again better than at midspan (D+(20) compared to E(30)). Single axles are also one class better, but the Gross Weight is more accurately predicted by the longitudinal bending at midspan.

Table 9.36 – Accuracy classification for static B-WIM (central support) (Cellular) (R1)

(**n**: Total number of vehicles; **m**: mean; **s**: Standard deviation; π_0: level of confidence; δ: tolerance of the retained accuracy class; δ_{min}: minimum width of the confidence interval for π_0; π: Level of confidence of the interval $[-\delta,\delta]$)

	Relative error statistics				Accuracy calculation				
Criterion	**n**	**m** (%)	**s** (%)	π_0 (%)	**Class**	δ (%)	δ_{min} (%)	π (%)	**Class Retained**
Single axle	27	-0.41	2.21	92.1	**A(5)**	8	5.0	99.6	**D+(20)**
Axle of group	18	-1.05	12.87	90.3	**D+(20)**	30	29.0	91.5	
Group of axles	9	0.51	1.12	83.4	**A(5)**	7.14	2.7	99.9	
Gross Weight	18	0.00	0.10	90.3	**A(5)**	5	2.0	100.	

The dynamic algorithm is tested with the longitudinal bending of two sensors placed at midspan. Accuracy classes in Table 9.37 are better than the static algorithm based on the same longitudinal strain (Table 9.34), but they are less accurate than transverse strain (Table 9.35) or the location at central support (Table 9.36).

Table 9.37 – Accuracy classification for DB-WIM algorithm (Cellular bridge) (R1)

(**n**: Total number of vehicles; **m**: mean; **s**: Standard deviation; π_0: level of confidence; δ: tolerance of the retained accuracy class; δ_{min}: minimum width of the confidence interval for π_0; π: Level of confidence of the interval $[-\delta,\delta]$)

	Relative error statistics				Accuracy calculation				
Criterion	**n**	**m (%)**	**s (%)**	π_0 (%)	**Class**	δ (%)	δ_{min} (%)	π (%)	**Class Retained**
Single axle	27	0.73	4.43	92.1	**B+(7)**	11	10.0	94.9	**E(35)**
Axle of group	18	-0.27	19.21	90.3	**E(35)**	47	43.3	93.2	
Group of axles	9	-0.56	1.22	83.4	**A(5)**	7.14	3.0	99.9	
Gross Weight	18	0.00	0.50	90.3	**A(5)**	5	1.1	100.	

The MS-BWIM system measures longitudinal bending at twelve different points on the bottom slab deck (7.5, 15.5, 23.5, 31.5, 39.5 and 47.5 m from the bridge start in two transverse positions under the slow and fast lane at 2.5 m from the centreline. The results of these two transverse positions are added together at each section). The instantaneous calculation has a solution for only a very small portion of the bridge due to the long distance between sensors, which leads to the poor accuracy shown in Table 9.38.

Table 9.38 – Accuracy classification for static MS-BWIM algorithm (Cellular bridge) (R1)

(**n**: Total number of vehicles; **m**: mean; **s**: Standard deviation; π_0: level of confidence; δ: tolerance of the retained accuracy class; δ_{min}: minimum width of the confidence interval for π_0; π: Level of confidence of the interval $[-\delta,\delta]$)

	Relative error statistics				Accuracy calculation				
Criterion	**n**	**m (%)**	**s (%)**	π_0 (%)	**Class**	δ (%)	δ_{min} (%)	π (%)	**Class Retained**
Single axle	27	-0.32	6.87	92.1	**C(15)**	20	15.3	98.2	**D(25)**
Group of axles	9	3.38	11.06	83.4	**D(25)**	28	26.0	87.2	
Gross Weight	18	0.32	6.15	90.3	**C(15)**	15	13.9	93.1	

The inaccuracy of MS-BWIM is mainly caused by the failure to predict axle group weight in two runs of the unloaded three-axle vehicle, as shown in Figure 9.33.

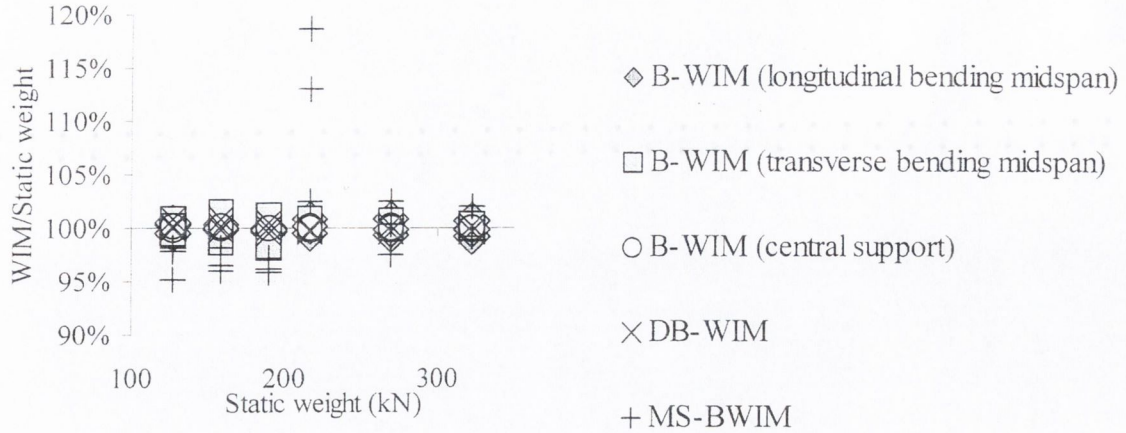

(a) Gross vehicle weight

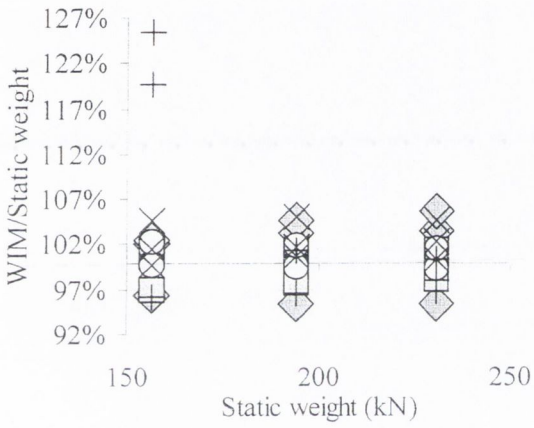

(b) Axle group

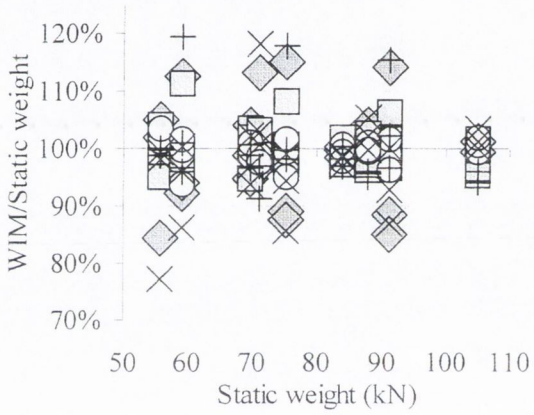

(c) Individual axle weights

Figure 9.33 – WIM/Static versus real static weights (Two-span cellular bridge)

9.4 SUMMARY

This chapter has analysed the performance of three B-WIM algorithms on different bridges. The algorithms are:

- Static B-WIM algorithm based on one longitudinal location, as defined in Section 3.3,
- Dynamic B-WIM algorithm (DB-WIM) based on one longitudinal location, as defined in Section 7.3,
- Static multiple-sensor BWIM (MS-BWIM) algorithm as defined in Section 7.5.2.

Other algorithms such as the spectral approach in Section 7.2 or the dynamic MS-BWIM algorithm in Section 7.5 have not been considered. It was found that the first algorithm did not give good results when having more than two axles on a bridge (Section 7.2.5).

Compared to the dynamic MS-BWIM algorithm, the static version of the multiple sensor system was preferred because the static B-WIM algorithm has generally been more accurate than DB-WIM and it involves fewer parameters (both one-sensor and multiple-sensor algorithms are based on the same equations).

First, a beam model was analysed. The system was calibrated with a two-axle linear sprung vehicle and tested with a four-axle non-linear sprung vehicle (11 degrees of freedom). Air and steel suspensions on both smooth and rough pavements were considered. In smooth road conditions, MS-BWIM achieved the most accurate overall class B+(7) (corresponding to the criterion of individual axle weights). The traditional static B-WIM had the same accuracy class, A(5), for gross vehicle weight as MS-BWIM, but it failed to predict individual axle weights accurately (E(45)). The 30 m span length makes it difficult to identify individual axles from strain at only one location, and MS-BWIM derives a more accurate value from the load history. DB-WIM was the most inaccurate system regardless of the criterion adopted. The performance of DB-WIM improves when considering air suspensions, but it can not cover for different dynamic behaviours. DB-WIM approximates the total strain with a particular dynamic model (i.e., based on moving constant loads). If this approximation is not good, then an averaging of all dynamics, as carried out in the static algorithm, gives better results.

The poorest results were obtained with steel suspensions on rough profiles. The truck forces in the steel-sprung vehicle are excited more strongly than in the air-sprung model (heavily damped). Bridge strains also oscillate with higher amplitudes when crossed by the steel suspension truck. This is probably due to the proximity of the frequencies of the truck and the bridge, which results in huge errors in any B-WIM algorithm. In these conditions, the estimation of individual axle weights is very inaccurate, but the traditional static B-WIM algorithm can still provide reasonable values for gross vehicle weight (C(15)). The explanation is twofold:

- Averaging the effect of dynamics caused by the traditional static algorithm (more accurate than the dynamic modelling of the total strain as attempted by the DB-WIM algorithm),
- Sensor location at midspan (MS-BWIM considers other sensor locations which are not as accurate and this results in higher errors).

Results for the beam model are summarised in Table 9.39 under limited reproducibility conditions.

Table 9.39 - Accuracy results for Green's simulations

Road profile	Criterion	One longitudinal location algorithms		Static Multiple-Sensor
		Static	Dynamic	
Smooth	Single axle	E(45)	E(65)	B+((7)
	Group of axles	C(15)	E(30)	A(5)
	Gross weight	A(5)	B+(7)	A(5)
	Overall	E(45)	E(65)	B+(7)
Rough	Single axle	E(300)	E(395)	E(30)
	Group of axles	E(100)	E(130)	E(50)
	Gross weight	C(15)	E(50)	E(30)

The performance of B-WIM on a 16 m long isotropic slab has been considered. All three algorithms have achieved class A(5) for gross vehicle weight. The traditional static algorithm based on the midspan location has reached an overall class of C(15). When increasing the number of sensors at midspan from 2 to 8, the system has remained in the same class for each criterion. DB-WIM has also reached class C(15) overall. MS-BWIM has provided an overall accuracy class of A(5). MS-BWIM calculates individual axles more accurately than any other algorithm. When the lateral truck position was changed, there was no loss in accuracy.

In a two-span isotropic slab (total length 37 m), it was found that the best location for weighing is at the central support. The static B-WIM algorithm achieves an overall accuracy of A(5) at the central support location, while only D+(20) is reached at midspan. MS-BWIM also provides A(5) accuracy overall. DB-WIM is in class B(10) overall using strain at midspan, better than D+(20) using the static algorithm at the same location. This is a case where the approximation of the total strain by a dynamic model results in better accuracy than approximating the static response. DB-WIM might be preferred if the central support is not accessible. However, only a reduced number of truck configurations were tested: four-axle articulated vehicle in the beam model and two- and three-axle rigid vehicle in the finite element models. The testing of more trucks will allow a more realistic accuracy threshold for the site under study to be determined.

A slab with edge cantilever (20 m long) has resulted in class A(5) for gross vehicle weight or axle group for any of the B-WIM algorithms under study. A(5), B(10) and C(15) were obtained for individual axle weights using MS-BWIM, static B-WIM and DB-WIM respectively. The dynamic oscillations of this bridge were small, and the static version of the algorithm (based on one or multiple sensors) gave better results than trying to model those oscillations by DB-WIM.

A voided slab deck (25 m) bridge has also been tested. The first natural frequency is relatively low (3.80 Hz) and dynamic oscillations have higher amplitudes than in the preceding slab with edge cantilever. In this case, DB-WIM achieves an overall accuracy class C(15), better than D(25) using the static algorithm or D+(20) using MS-BWIM. MS-BWIM achieves poorer results for gross weight (C(15)) than the other two algorithms (A(5)). For the combination of sensors chosen in this bridge, the instantaneous calculation by MS-BWIM is only feasible for a very small portion of the bridge (for a small part of the strain record) and the estimation of gross weight is poor. The algorithms based purely on one longitudinal location obtain the gross vehicle weight more accurately as they use all strain readings along the bridge. Therefore, DB-WIM appears to approximate the total strain very accurately, though the algorithm should be tested with other truck configurations.

A beam and slab (20 m long) bridge has been tested. When applying the static B-WIM algorithm to the response of this bridge, it has been found that transverse bending can provide a more accurate estimation of weights than longitudinal bending (overall accuracy class A(5) for transverse bending compared to B+(7) for longitudinal bending at midspan). MS-BWIM is in class A(5). DB-WIM can only achieve C(15).

Results for a 45° skew bridge (15 m long) were poor, except for gross vehicle weight and group of axles. The sensors chosen for the MS-BWIM did not allow for an instantaneous calculation. Further study on the ideal number and location of multiple sensors is required.

Finally, a two-span cellular bridge (62 m long) was tested. As in the other two-span continuous bridge, best results are obtained when using the static B-WIM algorithm at the central support (overall accuracy class A(5)). If using strain at midspan, the static algorithm based on transverse bending achieves B+(7), compared to C(15) if based on

longitudinal bending. DB-WIM reaches B+(7) when applied to longitudinal bending at midspan. The span is too long for the reduced number of sensors chosen for the MS-BWIM system, and an instantaneous calculation can only take place for a short period of time. Hence, MS-BWIM falls in overall accuracy class D(25).

Table 9.40 summarises accuracy results for different algorithms based on longitudinal strain and finite element simulations under limited reproducibility conditions.

Table 9.40 - Accuracy results for finite element models

Bridge type	**Criterion**	**One longitudinal algorithms based on location at midspan**		**Static Multiple-Sensor**
		Static	**Dynamic**	
Isotropic slab	Single axle	C(15)	C(15)	A(5)
	Group of axles	B+(7)	B+(7)	A(5)
	Gross weight	A(5)	A(5)	A(5)
	Overall	C(15)	C(15)	A(5)
Two span isotropic slab	Single axle	D+(20)	B(10)	A(5)
	Group of axles	B+(7)	A(5)	A(5)
	Gross weight	A(5)	A(5)	A(5)
	Overall	D+(20)	B(10)	A(5)
Slab with edge cantilever	Single axle	B(10)	C(15)	A(5)
	Group of axles	A(5)	A(5)	A(5)
	Gross weight	A(5)	A(5)	A(5)
	Overall	B(10)	C(15)	A(5)
Voided slab deck	Single axle	D(25)	C(15)	C(15)
	Group of axles	C(15)	B+(7)	D+(20)
	Gross weight	A(5)	A(5)	C(15)
	Overall	D(25)	C(15)	D+(20)
Beam and slab	Single axle	B+(7)	C(15)	A(5)
	Group of axles	A(5)	C(15)	A(5)
	Gross weight	A(5)	C(15)	A(5)
	Overall	B+(7)	C(15)	A(5)
Skew	Single axle	E(50)	E(45)	-
	Group of axles	B+(7)	B(10)	-
	Gross weight	A(5)	A(5)	-
	Overall	E(50)	E(45)	-
Two span Cellular	Single axle	C(15)	B+(7)	C(15)
	Group of axles	B+(7)	A(5)	D(25)
	Gross weight	A(5)	A(5)	C(15)
	Overall	C(15)	B+(7)	D(25)

The static algorithm can produce different accuracy classes depending on the strain type and location. Table 9.41 gives accuracy results for strains other than longitudinal bending at midspan.

Table 9.41 - Accuracy results for static algorithm based on one longitudinal location and different type of strains

Bridge type	**Strain**	**Single axle**	**Group of axles**	**Gross weight**	**Overall**
Two span isotropic slab	Longitudinal bending at midspan	D+(20)	B+(7)	A(5)	D+(20)
	Longitud.bending at central support	A(5)	A(5)	A(5)	A(5)
Beam and slab	Longitudinal bending of beam	B+(7)	A(5)	A(5)	B+(7)
	Longitudinal bending of slab	B+(7)	A(5)	A(5)	B+(7)
	Transverse bending of slab	A(5)	A(5)	A(5)	A(5)
Two span Cellular	Longitudinal bending at midspan	C(15)	B+(7)	A(5)	C(15)
	Transverse bending at midspan	B+(7)	A(5)	A(5)	B+(7)
	Longitud. bending at central support	A(5)	A(5)	A(5)	A(5)

10

CONCLUSIONS

10.1 INTRODUCTION

The purpose of this research has been to increase the accuracy of B-WIM systems by improving the algorithm used for weight calculation. Considerable progress has been made in data acquisition hardware and software. This advance in data acquisition technology has allowed the measurement of voltage from axle detectors and a lot of strain sensors with good resolution and high scanning rates. Software has been developed to process this voltage information into vehicle classification and weights on a continuous basis.

Strain is the result of all axle forces that are on the bridge. On the one hand, this record can make it difficult to distinguish the contribution of each axle at each instant. On the other hand, a long continuous record of the whole truck weight is available. Hence, B-WIM systems will generally tend to be more accurate for calculating gross weights than axle weights. Inaccurate assumed characteristics for influence lines, bridge and vehicle dynamics, etc., have been shown to be sources of error for the traditional static B-WIM algorithm. An accurate separation of dynamic and static components is difficult to establish even at relatively high frequencies. The frequencies at which statics and dynamics are mixed together will depend on the vehicle speed, axle configuration, bridge length, stiffness and natural frequency. New B-WIM algorithms have been developed to overcome limitations derived from the bridge-vehicle interaction.

The accuracy of any pavement WIM system is influenced by two factors: vehicle dynamics and the pavement. The WIM system should be such that the road type would be the main limiting factor (COST323 1997). However, as individual pavement WIM sensors can only measure the wheel load for a very short period of time, the dynamic characteristics of the truck can only be estimated from its scant information. Attempts are made by multiple-sensor pavement WIM systems (MS-WIM) to incorporate truck dynamics in their algorithms through the use of many sensors and instantaneous readings. A similar

approach has been adopted here for B-WIM. If, instead of using only one longitudinal location, a multiple-sensor B-WIM system is employed, the history of axle loads along the bridge can be described. Compared to pavement MS-WIM systems, a B-WIM system allows for a continuous measurement of the applied wheel forces, but the part of the measurements due to bridge damping and inertial forces or due to truck forces needs to be quantified. Additionally, the use of several sensors can have different B-WIM applications:

- Determination of axles, spacings and speed in a FAD (**F**ree of **A**xle **D**etector) system.
- Improvement in accuracy over traditional algorithms based on one sensor location.
- Better knowledge of bridge structural behaviour and truck dynamics.

B-WIM algorithms that take into account the dynamic as well as the static response of a bridge to a passing truck have also been introduced. Some features of these algorithms are the calculation of a theoretical total response instead of purely the static one, the consideration of more strain sensors and the application of best fitting techniques in the frequency domain.

10.2 RESULTS

The accuracy of different B-WIM algorithms has been analysed with data from trials in the field. Unless otherwise specified, the axle of a group criterion is not considered when giving overall accuracy as this is not required for B-WIM systems in the COST323 specification. Due to the limitations in the number of trucks and bridges used in the experiments, numerical and finite element techniques have been developed to simulate B-WIM data and further evaluate the performance of these algorithms.

A vehicle modelled as a linear discrete mass-spring-damper system moving on a beam has revealed the influence of the calibration truck parameters on B-WIM accuracy. A general finite element formulation for the solution of the bridge-vehicle dynamic interaction problem has also been presented. It is based on a Lagrange multiplier technique. Simulation results were in agreement with other numerical methods. This formulation is applicable to any vehicle and bridge finite element model, and it considers the bridge pavement as a random surface irregularity. There is no limitation concerning the complexity (number of degrees of freedom) of the bridge structure and vehicle model to be

analysed. These theoretical models have made possible the study of alternative arrangements of strain sensors.

10.2.1 Experimental Results

A novel calibration procedure for determining the curve to be taken as reference in a static/dynamic algorithm has been introduced. This method is based on the spectrum of the measured signal and it has been used to calibrate B-WIM data from experiments in Ireland, Sweden, France and Slovenia. It is proven to be more accurate than other calibration methods based on theoretical models. Therefore, it has the advantage of adjusting boundary conditions, structural response and sensor sensitivity more directly than other experimental adjustments based on the time domain. All records/influence lines can be related to a period of time from the instant that the first axle of the vehicle hits an axle detector prior to the bridge to some instant where there is certainty of the vehicle having left the bridge. There is no need to know the exact point when the bridge starts to bend.

In Delgany, testing took place in two periods: May and July 1997. The bridge is 30° skew, 16 m long and simply supported. Overall accuracy of C(15) and E(40) are obtained with the new calibration method in May and July respectively. The criterion of gross weight remains in A(5) in May and decreases to B+(7) in July. The change in accuracy from May to July is attributed to the installation and/or sensitivity of the sensors, as a few sensors had to be replaced after the first test. For the same tests, overall accuracy decreases to E(55) in May and E(60) in July if using a theoretical beam model. Furthermore, overall accuracy by the experimental approach increases to A(5) in May if full repeatability conditions are considered. This accuracy is only C(15) when using a wide range of speeds due to the influence of a 4 Hz hardware filter.

In Luleå (June 1997), an overall accuracy of D+(20) is obtained if using one influence line and limited reproducibility conditions. However, A(5) is obtained if using full repeatability conditions at speeds of about 80 km/h and a 6-axle truck configuration. If the runs of a 3-axle truck at about 80 km/h are also taken into account, overall accuracy decreases from A(5) to B+(7). As in Delgany, the consideration of more truck configurations and speeds introduces an error due to the 4 Hz hardware low-pass filter applied in these experiments. Filtering removed not only dynamics, but also part of the static bridge response. The

smoothing action of the filter depends on the truck configuration, vehicle speed and the shape of the influence line, and its use in signal processing should be restricted as much as possible (i.e. to post-processing, where original data can be recoverable).

A dynamic algorithm based on one longitudinal location has been tested in a long span bridge in Belleville. The bridge is a continuous two-span bridge of about 50 m per span. The section is made of a concrete slab and steel box. Longitudinal bending was measured at midspan of the first span and an accuracy class B(10) was obtained for gross weight in full repeatability conditions. Individual axle weights could not be estimated accurately as the vehicle acts as a whole concentrated load on such a long bridge. However, transverse bending of the concrete slab is more important and localised for this bridge than longitudinal bending of the steel box (more similar to a beam response), and its application in B-WIM systems could lead to more accurate results. A two-dimensional algorithm that allows for transverse position of the truck appears to be necessary if transverse bending is to be used for weight calculations in the near future.

The multiple-sensor B-WIM algorithm has been analysed with data from a bridge in Slovenia. Each section has been calibrated separately and a load history has been reproduced for each axle along most of the bridge length. Only those instants when an axle enters or leaves the bridge do not qualify for an instantaneous calculation due to rounding errors. The record offers an instantaneous solution with small oscillations around an average value very close to the real static axle weight. These oscillations and inaccuracy increase with a higher number of axles on the bridge. The presence of more axles requires more instrumented sections on the bridge to maintain an acceptable level of accuracy. Hence, the MS-BWIM system is not recommended in medium to long span bridges.

10.2.2 Theoretical Results

When the criterion of axle of group is not considered, the criterion of single axle is generally the one determining the overall accuracy. The results for this criterion in the finite element simulations are summarised in Table 10.1. The multiple-sensor algorithm is the most accurate, except for the central support location in two-span bridges, where a static algorithm based on one sensor location can be slightly more accurate. This is due to the absence of significant dynamics at this location. The dynamic algorithm cannot

compete with the static algorithm, except for the longitudinal bending at midspan of a two-span isotropic slab and voided slab deck. Though the multiple-sensor algorithm appears to be more accurate in most of the cases, it also requires a more expensive installation. It is clearly necessary to determine if the levels of accuracy required by the user can be achieved with a simpler solution.

Table 10.1 - Accuracy results for single axle criterion

Bridge type	**Len. (m)**	**Freq. (Hz)**	**One longitudinal location algorithms**		**Static Multiple-Sensor**
			Static	**Dynamic**	
Beam model	30	3.33	E(45)	E(65)	B+(7)
Isotropic Slab	16	4.51	C(15)	C(15)	A(5)
Two span isotropic slab	37	4.18	D+(20) midspan A(5) central support	B(10)	A(5)
Slab edge cantilever	20	4.80	B(10)	C(15)	A(5)
Voided slab deck	25	3.80	D(25)	C(15)	C(15)
Beam and slab	20	6.13	B+(7) beam B+(7) longit. slab A(5) transv. slab	C(15)	A(5)
Skew	15	7.41	E(50)	E(45)	-
Two span Cellular	62	2.95	C(15) longit. midpan B+(7) trans. midspan A(5) central support	C(15)	C(15)

In addition to simulations generated by the author, Green has provided data to test the accuracy achieved by each algorithm. Static weights were withheld from the author until after submission of the calculated WIM results. The bridge is idealised as a 30 m long simply supported beam. The dynamic properties of the bridge are derived from strains caused by a two-axle linear sprung vehicle used for calibration. Then, four-axle truck models (nonlinear suspension elements), validated experimentally, are used to test accuracy. Two different types of road profile and suspension were used. Results are summarised in Table 10.2.

Table 10.2 – Accuracy classification for Green's simulations

Road profile	**Criterion**	**One longitudinal location algorithms**		**Static multiple-sensor**
		Static	**Dynamic**	
Smooth	Single axle	E(45)	E(65)	B+(7)
Smooth	Axle group	C(15)	E(30)	A(5)
Smooth	Gross weight	A(5)	B+(7)	A(5)
Rough	Gross weight	C(15)	E(50)	E(30)

In smooth road conditions, the multiple-sensor algorithm is the most accurate with B+(7) overall accuracy, and A(5) for the gross weight criterion. Accuracy by the static algorithm based on one longitudinal position is also A(5) for gross weight. The dynamic algorithm is not able to match the total strain as accurately as the static and it only reaches B+(7) for gross weight. It has been seen that B-WIM accuracy decreases for steel suspensions as bridge dynamic response is more important. In rough road conditions, the static algorithm achieves C(15) for gross weight, while the results for all other criterions and/or algorithms fall in class E.

10.3 DISCUSSION

Speed and axle spacings have been found to be significant sources of inaccuracy in the past. These parameters are the result of a direct measurement in the field. The improvement in axle detection hardware and the application of optimisation techniques to allow for errors in axle spacings and speed have reduced their influence on final accuracy noticeably. However, even though both parameters were totally accurate, this thesis has revealed that other parameters can produce very important errors. These are parameters related to the dynamic excitation of the bridge. The level of this excitation will depend on the truck mechanical characteristics and the conditions of the road prior to and on the bridge. Rough road profiles result in very poor results for any existing B-WIM algorithm. In this situation, only the traditional static B-WIM algorithm can provide reasonable results for gross weight. It is felt by the author that when bridge dynamics are highly excited, the fitting technique carried out by the traditional algorithm is more accurate than trying to model the total strains. Additionally, a truck with the same axle weights could result in a very different bridge response depending on their mechanical parameters. So, steel suspensions are estimated less accurately than air suspensions, as they are not as heavily damped. It has also been seen that the traditional static B-WIM algorithm generally achieves reasonable results in gross vehicle weight regardless of the accuracy in individual axle weights. It looks as if similar levels of gross vehicle weight develop similar levels of total strain energy, and Moses' approach identified this energy.

The implementation of a static B-WIM algorithm is easier than a dynamic B-WIM algorithm. DB-WIM can only be justified in bridges with a smooth road profile, low natural frequencies and a high bridge dynamic component. For example:

- If the bridge is too short, the strain response does not exhibit a sufficient number of dynamic oscillations to compensate each other. In this case, the DB-WIM algorithm based on one longitudinal location can offer a better solution. However, it is necessary to check that the dynamic bridge model approximates the measured strain well. A number of truck configurations representative of the traffic should be employed to ensure that the assumptions of the model are correct.
- DB-WIM might give a more accurate result when the total response is strongly influenced by speed. The maximum bridge response occurs for some pseudo-frequencies of the vehicle. An increase in the bridge response can also take place when the wheels vibrate in phase resulting in a higher total dynamic component. This phenomenon is more important at some speeds and a simple dynamic model can allow for this variation in the strain response better than a static approach.

In bridges with high natural frequency and low dynamics, a static B-WIM algorithm should be used. If a high level of accuracy is required, a static multiple-sensor B-WIM algorithm (MS-BWIM) can improve accuracy in individual axle weights over a single-sensor algorithm very significantly. However, there is still a need to analyse the number and location of sensors that guarantee a better instantaneous solution. If the bridge has a long span, MS-BWIM might require an excessive number of sensors and other possibilities such as the measurement of transverse bending should be considered.

There are cases where the static B-WIM algorithm is more accurate than MS-BWIM, i.e., in the central support location of a two-span bridge. It is obvious that, if the response of a bridge were purely static, the traditional B-WIM algorithm would be totally accurate. As the response of the bridge differs from the static, the traditional B-WIM algorithm loses accuracy. In the case of bending at the central support, the dynamic excitation at this point is very small compared to the static component and the traditional B-WIM algorithm is still very accurate. As the multiple-sensor algorithm considers new locations, which are not as close to the static answer, the final accuracy might not be as good as using only measurements at the central support.

Regardless of the algorithm, accuracy of Bridge WIM systems is expected to improve in bridges with a minimum dynamic response, this is, with a natural frequency out of the truck frequency range and/or with smooth surface profiles. Bridges generally vary in natural frequency from 1 Hz to 15 Hz. Short span bridges are more likely to match the axle hop frequency while longer bridges might couple with the vehicle body frequency (1.5 to 4.5 Hz). In any case, there is often a dynamic amplification that will decrease the accuracy of a Bridge WIM system. In the author's opinion, an improvement of the actual levels of accuracy can be achieved by feeding a database with strain recorded for different truck configurations. Then, each truck type could be calibrated in a different way according to the vehicle classification and characteristics of the bridge response. Axle spacings and speed are a reference for the first classification of the vehicle. A second classification of the vehicle can be established from the amplitude of the dynamic oscillations, resulting from the bridge-truck interaction. A detailed study of these curves will reveal if the separation of the static/dynamic truck components can be done more accurately.

10.4 SUGGESTIONS FOR FUTURE RESEARCH

In order to examine the influence of dynamics on B-WIM systems, the author developed a bridge-truck dynamic interaction model. There are a lot of aspects of this model that can be further improved for testing of B-WIM systems. For example: the modelling of the tyres, assumed to remain in contact with the bridge surface and the approach at all times, the vehicle suspension, represented by a simple linear spring in parallel with a viscous damping element, or the spectral description of the road profile, defined uni-dimensionally. Field tests are also necessary for experimental validation. The COST323 specification on WIM (Appendix B) indicates some characteristics of the road profile as an indication of the accuracy that might be achievable in a WIM site. However, this classification is not enough for B-WIM, as it does not allow for the presence of a large road irregularity prior to or on the bridge (i.e., the joint), and neither does it consider the influence of the bridge structural behaviour. Accurate simulations of a truck crossing over a bridge will allow researchers to predict what accuracy a Bridge WIM system might achieve depending on the bridge type and road conditions before installing a system in the field.

The weight of a steer axle is usually less than the static weight for a moving vehicle as a result of drag and friction effects. This reduction must be quantified and it should be taken into account during calibration. Higher calibration methods treating vehicles according to their type, weight and type of axle will further improve B-WIM accuracy. More progress is also expected in the area of Free of Axle Detector systems, a very promising technology that does not require any sensor on the road.

All B-WIM research to date has concentrated on a single truck event. However, bridges with high traffic density or long span structures are likely to be traversed by more than one vehicle simultaneously. The performance of B-WIM systems when weighing simultaneous traffic events needs to be tested in the near future. An algorithm purely based on one longitudinal location would have a lot of difficulty to determine which value corresponds to each vehicle (e.g., two axles of different vehicles entering the bridge simultaneously at the same speed). Thus, the problem of multiple presence of vehicles should be tackled with a two-dimensional MS-BWIM algorithm. If there are two lanes involved in the problem, this algorithm needs to allow for two different influence lines contributing to the total strain: one due to a unit axle running over one lane and another due to a unit axle running over the other lane. The theoretical basis for this algorithm has been established. A dynamic model of more than one truck on a bridge can be used as a tool for preliminary studies.

The B-WIM algorithm can be further improved by the consideration of axle loads as random stochastic processes. The randomness of the applied axle load is a result of the random variability of the initial conditions at the instant the axle arrives on the bridge, the random motions of the vehicle due to the random roadway unevenness, etc. Based on theoretical simulations or experiments (i.e., by using an instrumented truck), a correlation between the statistics of the moving load and the measured strains could be established. The spectral density of the generalised strain might be expressed as a function of the spectral density of the generalised force. The statistical characteristics of measured strain can be calculated directly, and work on the solution of the inverse problem (statistical characteristics of input loads) might result in a significant improvement in accuracy for B-WIM systems. The use of pattern recognition techniques and artificial neural networks can also be incorporated into B-WIM calculations. All of these areas of research could lead to

the identification of truck mechanical characteristics (apart from static weights) through a B-WIM system.

A

WEIGH IN MOTION TERMS

Basic definitions of terms specially relevant to WIM and its applications are provided. This terminology of WIM is part of the work on prestandardisation developed within the framework of the COST action 323 (1996). The evaluation of WIM system performance is related to the following criteria:

- The site (road, bridge)
- Characteristics of the traffic
- The measured parameters from the WIM station
- Metrological and statistical elements
- Specific characteristics of the vehicles
- The test method used for qualification, calibration,
- The data processing method
- The required performance and applications

The glossary of terms presented in this Appendix is divided in five parts: Bridge Engineering, Metrology, Traffic and Road, Vehicle and Weighing. A more detailed document is available in different languages in the Internet[8] (Siffert and Žnidari□ 1998).

A.1 BRIDGE

Abutment: End support structure for bridge deck.

Beam: Structural member designed to carry loads between or beyond points of support, usually narrow in relation to its length and horizontal or nearly so.

Bearing: Component designed to transfer the load from a structural member onto a fixed support while allowing relative displacement.

Bridge: Civil engineering works that affords passage to pedestrians, animals, vehicles, waterways and services above obstacles or between two points at a height above the ground.

Column: Structural member of slender form, usually vertical, that transmits to its base the forces, primarily in compression, that are applied to it.

Culvert (box): Covered channel or large pipe that forms a watercourse below ground level, usually under a road or railway.

Expansion joint: Joint that permits relative movement caused by expansion and contraction of a structure.

Girder: Large fabricated metal beam that comprises top and bottom members and either solid or open web or webs.

Orthotropic deck bridge: Bridge in which the deck consists of a stiffened steel plate.

Pier: Column in which the breadth in one direction is in excess of four times the breadth in the other direction.

Slab: Thick, flat or shaped component usually larger than 300 mm square, used to form a covering.

Stiffener: Assemblage of metal plates used to increase the stiffness of an (orthotropic) deck.

A.2 METROLOGY

Accuracy: The closeness of agreement between a test result and the accepted reference value. Accuracy = Trueness + Precision

Accuracy class: class of measuring instruments that meet certain metrological requirements that are intended to keep errors within specified limits.

Accuracy of measurement: Closeness of the agreement between the result of a measurement and a true value accepted as a reference value.

Arithmetic mean; average: The sum of the values of a sample divided by the number of values. First moment of a (sample) distribution.

Bias: The difference between the expectation of the test results and an accepted reference value.

Calibration: Adjustment to a reference level of any measurement device.

Calibration (correction) factor: numerical factor by which the uncorrected result of a measurement is multiplied to compensate for systematic error.

Coefficient of regression: A coefficient of a variable in the equation of a regression curve or a regression surface.

Coefficient of variation: ratio of the standard deviation to the mean of a data sample.

Confidence interval Confidence interval: interval which contains the true value of a parameter represented by a random variable, with a given probability

Confidence level: probability that an interval contains the true value of a parameter represented by a random variable.

Deviation: value minus its reference value.

Doubtful values: Observations in a sample, far separated in value from the remainder with a weak probability of appearance.

Drift: slow change of the result of measurement with time.

Durability test: A test to verify that the equipment under test is capable of maintaining its performance characteristics over a period of use.

Error of result: The test result minus the accepted reference value (of the characteristic). Difference between a measured value and the true value or the accepted reference (relative and absolute errors).

Increment: The value of the smallest change in value that can be indicated or recorded by digital device in normal operation.

Influence quantity: Quantity other than that measured which affects the result of the measurement.

Initial zero-setting mechanism: Automatic means provided to set the indication to zero at the time the instrument is switched on and before it is ready for use.

Measurand: particular quantity subject to measurement.

Measurement: set of operations having the object of determining a value on a quantity

Measuring chain: series of elements of a measuring instrument or system that constitutes the path of the measurement signal from the input to the output.

Measurement procedure: set of operations, specifically described, used in the performance of particular measurements according to a given method.

Outliers: value(s) in a series of homogeneous data which has(ve) a much lower probability of occurrence than expected according to the sample size and distribution; an outlier is suspected of being an erroneous measurement, and may be eliminated under certain conditions.

Performance test: A test to check that the equipment under test is capable of performing its intended functions; if it is made just after the initial installation or after an important repair, it becomes an acceptance test.

Precision: The closeness between independent test results obtained under specified repeatability conditions.

Random error: A component of the error which, in the course of a number of test results for the same characteristic, varies in an unpredictable way.

Range: The whole interval extent on which a parameter measurement is valid with a given system. The difference between the largest and the smallest measurement value.

Raw result: result of a measurement before correction for systematic errors.

Relative error: error of measurement divided by a true value of the measurand.

Repeatability (of results): closeness of the agreement between the results of successive measurements of the same variable carried out under the same conditions of measurement (called repeatability conditions): same procedure, same observer, same instrument in same conditions, same location, repetition over a short period of time...), homogeneous with respect to the environmental conditions.

Reproducibility (of results): closeness of the agreement between the results of measurements of the same measurand (variable)carried out by similar instruments under changed conditions of measurement (called reproducibility conditions): several observers, measuring instrument, locations, times etc

Resolution: The smallest value of a parameter that can be distinguished by a measurement device in the measurement range.

Sensitivity: change in the response of a measuring instrument divided by the corresponding change in the stimulus.

Specification: A requirement usually dealing with the design, construction, or marking of a weighing or measuring device. Specifications are directed primarily to the manufacturers of devices.

Standard: material measure, measuring instrument, reference material or measuring system intended to define, realise, conserve or reproduce a unit or one or more values of a quantity to serve as a reference. A technical specification approved by a recognised body for repeated or continuous application with which compliance is not compulsory.

Standard deviation: The positive square root of the variance. It is the quantity characterising the scattering of a sample of data (dispersion of the results).

Systematic error: A component of the error which, in the course of a number of test results for the same characteristic, remains constant or varies in a predictable way.

Tolerance: Width of a confidence level in which an error remains with a specified or required confidence level. The defined limit of allowable departure from the true value of a quantity measured or estimated by a system. Permissible variation of the specified value of a quantity.

Trueness: The closeness between the arithmetic mean value obtained from a large series of test results and an accepted reference value.

Trueness: Ability of a measuring instrument to give results free from systematic error.

User requirement: A requirement dealing with the selection, installation, use, or maintenance of a weighing or measuring device. User requirements are directed primarily to the users of devices.

Variance: Centred second moment of a (sample) distribution, which characterises the scattering of this distribution. A measure of dispersion, which is the sum of the squared deviations of observations from their average divided by one less than the number of observations.

A.3 ROAD AND TRAFFIC

Aggressivity: Capacity of heavy vehicles to cause damage to the pavement.

Capacity: The maximum rate of flow which vehicles can traverse a point or uniform section of a lane or roadway during a given time period under prevailing roadway, traffic, and control conditions.

Climbing line: An extra traffic lane provided on long uphill gradients to allow slower-moving vehicles to be removed from the main uphill traffic stream.

Control system: The hardware and software used to monitor and control traffic

Count: The number of vehicles (or pedestrians) that have passed a point.

Density: The ratio of the summation of the lengths of the vehicles on a given length of carriageway or lane.

Design capacity: The maximum rate of flow for specified operating conditions.

Design speed: A design criterion used for providing a consistent and co-ordinated alignment.

Divided road: A highway with separated roadways for traffic in opposite directions.

Dual carriageway: A highway with at least two lanes for the exclusive use of traffic in each direction.

Future design year: The future year for which roads are designed.

Gradient: Rate of change of elevation in the longitudinal direction of a roadway

Level of service: A measure of the operating conditions which occur on a given lane or roadway when it is accommodating a specific traffic volume.

Median: The portion of a divided highway separating the lanes for traffic in opposite directions.

Motorway: High-speed road, usually divided with grade-separated intersections.

Paved outer shoulder: The portion of the roadway contiguous with the traffic lanes for accommodation of stopped vehicles and for emergency use.

Pavement: Running surface of traffic lanes.

Standard axle: reference axle with a unit Aggressivity (damage power value equal to 1.)

Traffic: Vehicles and pedestrians using the road system

Traffic capacity: The maximum flow of vehicles that can proceed through a certain point during a given period of time.

Traffic engineering: The design and application of techniques for traffic management

Traffic flow (or traffic volume): Number of vehicles passing a specified point in a specified period of time.

Traffic lane: The portion of the carriageway for the movement of a single line of vehicles.

Traffic management: all kind of measures to care of traffic.

Undivided road: A highway consisting of one roadway, with one or more traffic lanes, carrying traffic in opposite directions.

Vehicle counter: Device for vehicle counting. Automatic traffic flow counter that stores data during specified time.

Vehicle counting: Action which consists of determining automatically or manually the number of vehicles passing a specified point during a specified time.

Verge: An unpaved level strip contiguous with the outer shoulder.

A.4 VEHICLE

Axle: an axle consists of two or more wheel assemblies lying approximately on a common axis oriented transversely to the nominal direction of motion of the vehicle.

Axle group-Group of axles: Set of axles in the same lorry, tractor, trailer or semi-trailer, spaced less than 2m each from the next one.

Axle of a group: Axle of a vehicle that belongs to a group of axles.

Elementary axle: axle from a vehicle An elementary axle can belong to a tandem or tridem axle.

Passenger Car Unit (PCU): Used to express in comparable fashion volumes of traffic of dissimilar make-up.

Silhouette: Category of vehicle defined by different parameters concerning the vehicle such as axle number and spacing..

Single axle: axle separated by 2 metres or more from the nearest axle of the same vehicle.

Tandem axle: group of two non isolated axles. Group of two axles, spaced less than 2m each from the next one.

Tridem axle: group of three non isolated axles. Group of three axles, spaced less than 2m each from the next one.

Twin wheel: group of two wheels fixed under a half axle.

Wheel assembly: half axle with one or more tyres.

A.5 WEIGHING

Axle group load: Sum of loads of an axle group.

Axle-load scale: A scale installed in a fixed location, having a load-receiving element specially adapted to determine the combined load of all wheels or a single axle or on a tandem axle of a vehicle.

Bar sensor: sensor in form of a bar containing piezoelectric or piezo-quartz sensor. A bar is generally installed in a groove in the pavement and is smaller than a tyre imprint length. Therefore, if used as a weighing sensor, the signal must be integrated during the time where the tyre applies a pressure on it.

Bridge WIM (system): WIM using an instrumented bridge (measuring strains) as a large scale. The response measured in some of the bridge elements are used to determine throughout software the gross weights and sometimes the axle loads of vehicles crossing the bridge.

Capacitive mat or strip: a mat or strip sensor which measures an applied force by the variation in capacitance (dielectric coefficient) of isolated plates.

Detector: device or substance that indicates the presence of a phenomenon without necessarily providing a value for an associated quantity. The detector organise the information providing from sensors.

Distance between axles or axle spacing: distance measured centre to centre between axles.

Distance between vehicles: distance separating two vehicles moving in the same direction. Distance between the rear bumper of the first vehicle and the front bumper of the second vehicle. Unit: meters

Dynamic load = Impact force: Force applied to the pavement by a wheel/axle while the vehicle is travelling at speed; by extension, sum of the forces applied by all the axles of a vehicle (may be measured at the same time or at the same place).

Fibre optic sensor: strip sensor incorporating an optic fibre; the fibre bending resulting from an applied force (by a wheel or an axle) modifies the light propagation conditions; the applied force may be derived from this modification.

Force: Product of mass and acceleration due to gravity.

Gap: The interval of time or distance between the rear of a vehicle and the front of a vehicle immediately following it.

Gross vehicle mass: mass of vehicle and its content. (kilograms or tons)

Gross vehicle weight: Static gross weight = mass of a whole vehicle multiplied by the acceleration due to gravity. Dynamic (or in motion-) gross weight: Sum of the forces applied by all the axles of a vehicle (may be measured at the same time or at the same place).

Headway: The interval of time or distance between the front of a vehicle and the front of a vehicle immediately following it.

High Speed WIM (HS-WIM): Weigh in motion under usual traffic speed conditions.

Impact factor: ratio of the force applied to the pavement by a wheel/axle while the vehicle is travelling at speed to the static wheel/axle load; by extension, gross impact factor = sum of the forces applied by all the axles of a vehicle (may be measured at the same time or at the same place) divided by the static gross weight.

Influence line: Graph of response such as strain or moment versus location of an applied unit point force.

Influence surface: Two dimensional graph of response such as strain or moment versus location of an applied unit point force.

Load: Force that acts on a structure or a member. Unit: Newton

Load cell: A device, which can be electrical, hydraulic... that produces a signal proportional to the load applied to it.

Low speed WIM: Weigh in motion in such particular conditions, as to minimise the effects of accelerations, (difference between static and dynamic load). That is obtained by using a specific weigh-area outside of the usual traffic lanes, an horizontal pavement with good evenness and vehicles moving at uniform and low speed (1 to 25km/h).

Magnetic (or inductive) loop: Electric cable buried in the pavement or bonded on the pavement surface and used for vehicle detection and counting. A metallic mass passing the loop changes the magnetic field, that causes a signal(frequency) send through the cable.

Mass: Constant ratio between applied forces and corresponding accelerations. The mass unit is the kilogram.

Mean speed: It is the covered distance divided by the time of course.

Monitoring: Permanent checking of the integrity of a system.

Occupancy (or detection) rate: The proportion of time during which a detector detects.

Piezo-electric cable: coaxial cable containing a piezoelectric substance, which converts a strain or pressure applied into an electrical signal which may be related to the applied strain or pressure.

Piezo-electric sensor: strip sensor built in with a piezoelectric cable. Types of piezoelectric sensors are:-piezoceramic: sensors containing a piezo-electric substance in form of ceramic powder.-piezopolymers sensors: multilayer coaxial cable or strip containing piezo-polymer substance.

Piezoquartz sensor: strip, bar or plate with incorporated piezoelectric quartz.

Piezo-resistive sensor: sensor which measures an applied force through a variation in its electrical resistance.

Pneumatic axle detector: Axle detector made from road hose or hoses.

Pneumatic converter: Device for the conversion of an high-pressure pulse of air into an electronic pulse.

Presence time: Presence time: the time during which a vehicle is continuously present within the detection zone.

Response time: The period of time between activation of the detector and the arrival of the signal in a traffic information system (or into digital memory)

Road hose/tube: Rubber tube which responds to the passing of a wheel or axle by the emission of a high-pressure pulse of air.

Sensor: element of a measuring instrument or measuring chain that is directly affected by the parameter to be measured.

Static load: Force applied to a structure which is static and not generated movements. Force due to the gravity exerted from a body or a part of them(vehicle, axle..). Example: For a wheel or an axle: force applied on the pavement by the wheel or by all the wheels from an axle when the vehicle is not moving.

Static weighing: measuring of mass or load of a static object; by extension, measuring of a vertical force of a no moving body (wheel, axle from a vehicle).

Strain amplifier (mechanical): (mechanical) Device which responds to the application of a strain with the generation of a larger strain.

Strain gauge: Device for measuring small displacements from which strains can be calculated.

Strip sensor: sensor in form of a strip containing piezoelectric or piezo-quartz material. It bar is generally installed in a groove in the pavement or bonded on the pavement surface. If used as a weighing sensor, the signal must be integrated during the time where the tyre applies a pressure on it.

Tape switch: Axle detector made from two strips of metal which make an electrical contact in response to an applied impact force.

Tyre load: Force applied by a tyre to the pavement (in Newtons).

Vehicle on-board weighing system: A weighing system designed as an integral part of or attached to the frame, chassis, lifting mechanism, or bed of a vehicle, trailer etc.

Vehicle speed or velocity: Measured distance divided by a time unit. Unit: meter/second or km/hour.

Vehicle weighing: To measure weight or mass of vehicles considered as a unique body. Estimation of the weight by addition of the results of weighing all the wheels or axles from a vehicle.

Weigh: to measure mass or weight.

Weigh bridge: large scale which measures the complete vehicle weight statically at once (approved for legal weighing and generally used as a reference).

Weigh zone: Zone in which a vehicle must be located when it is weighed.

Weighing instrument: Measuring instrument that serves to determine the mass of a load by using the action of gravity.

Weighing of wheels or axles: To measure the force applied by a wheel or an axle on the pavement.

Weighing plate: Plate fitted with sensors (example: a bending plate fitted with strain gauges). According its size, the device is adapted for weighing a wheel, a half axle, an axle or an axle group.

Weigh in motion: The process of estimating the mass or weight of a moving vehicle. To measure the impact forces or dynamic load produced by a moving system (wheels, axles of a vehicle)

Weight: Force equivalent to the product of mass and acceleration due to gravity. Unit: Newton

Wheelbase: distance measured centre to centre from the front axle to the rear axle.

Wheel load: the sum of the tyre loads on all tyres included in the wheel assembly which comprises a half axle).

Wheel-load weighers: Compact, self-contained, portable weighing elements specially adapted to determining the wheel loads or axle loads of vehicles on highways for the enforcement.

WIM system: Consists of sensors and supporting instruments. It detects the presence of a moving vehicle and evaluates tyre loads, axle loads, total weight and other information such as speed, axle spacing and silhouettes

B

STATISTICAL ISSUES (COST 323 SPECIFICATION)

There are numerous applications for WIM systems each requiring a particular configuration and level of accuracy of measurement. To be able to evaluate and compare the performance of these systems, it is necessary to define criteria for evaluation or for acceptance. Jacob and O'Brien (1997, 1998) describe the philosophy behind the European WIM specification, prepared by the COST323 management committee. This specification gives an indication of what accuracy might be achievable from sites with particular characteristics, and what accuracy might be acceptable for various needs (COST 323 1997). Calibration and testing procedure for WIM systems are considered. Accuracy classes are defined on the basis of the width of the confidence interval within the measured results lie. The specification defines seven accuracy classes, A(5), B+(7), B(10), C(15), D+(20), D(25) and E. For each class, confidence interval widths are specified for gross weights, weights of axles, axle groups, speed, inter-axle distance and axle/vehicle count. The required level of confidence is a function of the test conditions and the number of test runs.

The WIM system accuracy classification is based on comparisons of measured results against reference values which, it is anticipated, would generally be determined by statically weighing trucks. To comply with a given accuracy class, the calculated probability that individual results (i.e. static load W_s) are within the confidence interval $[W_s(1-\delta),W_s(1+\delta)]$, or that individual relative errors are within the confidence interval $[-\delta,+\delta]$, must exceed a specified minimum, π_0. The confidence interval width, δ, is a function of the accuracy class and the specified values are given in Table B.1 for each identity.

Table B.1 – Tolerances of the Accuracy Classes (Confidence Interval Width for Relative Errors)

Type of measurement	Domain of use	Confidence interval width δ(%) for Each Accuracy Class					
		A(5)	B+(7)	B(10)	C(15)	D(25)	E
Gross weight	Greater than 35 kN	5	7	10	15	25	>25
Group of axles	Greater than 20 kN	7	10	13	18	28	>28
Single axle	Greater than 20 kN	8	11	15	20	30	>30
Axle of a group	Greater than 20 kN	10	15	20	25	35	>35
Speed	Greater than 30 km/h	2	3	4	6	10	>10
Inter-axle distance		2	3	4	6	10	>10
Axle/vehicle count		1	1	1	3	5	>5

Three main types of application are identified for road authorities, decision makers and WIM users (COST323 1997):

- Statistics: Economical and technical studies of freight transport, general traffic evaluation on roads and bridges, collecting statistical data, etc.. δ in the range of 15 to 30% (class C(15), or D(25)).
- Infrastructure and preselection: Detailed analysis of traffic, design and maintenance of roads and bridges, accurate classification of vehicles, preselection for enforcement, etc.. δ in the range of 10 to 20% (class B(10), or C(15)).
- Enforcement or legal weight limits: Enforcement, commercial and industrial applications. δ: 5 to 10% (class A(5), or B+(7)).

B.1 CALIBRATION

Pre-weighed trucks are preferred for calibration of WIM systems. The specification defines four levels of repeatability/reproducibility test conditions as follows:

- Full Repeatability Conditions (r1): One vehicle passes several times at the same speed, load and lateral position.
- Extended Repeatability Conditions (r2): One vehicle passes several times at different speeds, different loads and with small variations in lateral position (in accordance with typical traffic).

- Limited Reproducibility Conditions (R1): A small set of vehicles (typically 2 to 10), representative in weight and silhouette of typical traffic, is used. Each vehicle passes several times, at different combinations of speed and load and with small variations in lateral position.
- Full Reproducibility Conditions (R2): A large sample of vehicles (some tens to a few hundred), taken from the traffic flow and representative of it, is used for calibration.

Calibration under full repeatability conditions is not recommended unless the customer approves. The vehicle should be typical of the traffic being weighed and should be driven in fully loaded, half-loaded and eventually unloaded conditions, and at speed levels representative of the site. Calibration under limited reproducibility (or extended reproducibility) conditions is recommended. The set of calibration vehicles and loading cases should be representative of the traffic pattern. In an initial verification, in which the same sample is used for calibration and for accuracy analysis, to be accepted in an accuracy class defined by δ, the specification requires that the confidence interval becomes $[-k.\delta, +k.\delta]$ for the relative errors at a level of confidence greater than π_0. If the calibration is made using repeated runs of pre-weighed trucks, k is taken equal to be 0.8. This value of k gives the best agreement between the accuracy results for a system from the initial verification check and the in-service check.

B.2 ACCURACY CLASSIFICATION FOR IN-SERVICE WIM SYSTEMS

Repeated runs of pre-weighed test vehicles, and/or the use of single runs of pre- or post-weighed vehicles from the traffic flow can be used to assess the accuracy of an operational WIM system. When the in-service accuracy of a system must be verified, the test may be carried out during various time periods and environmental repeatability or reproducibility conditions are defined:

- Environmental Repeatability (I): The test time period is limited to a few hours such that the temperature, climatic and environmental conditions do not vary significantly during the measurements.
- Limited Environmental Reproducibility (II): The test time period extends over at least 24 hours period, or preferably over a few days within the same week or month, such

that the temperature, climatic and environmental conditions vary during the measurements, but no seasonal effect has to be considered.

- Full Environmental Reproducibility (III): The test time period extends over a whole year or more, or at least over several days spread all over a year, such that the temperature, climatic and environmental conditions vary during the measurements and all the site seasonal conditions are encountered.

The specification does not allow recalibration of the system with the sample of data collected for the in-service test, and therefore the eventual bias must not be removed. It is recommended to perform the check in conditions (R1) or (R2). It may be done in conditions (r2) but with at least 3 loading conditions uniformly distributed within the range of axle/gross weights to be weighed, and 10 runs per loading case. It is not recommended to perform the check in conditions (r1), unless special agreement of the user. After such an in-service verification, and if a large bias is found which leads to a lower accuracy class than expected, a recalibration may be carried out.

The minimum probability, π_0, is a function of the sample size n and the test conditions (repeatability or reproducibility (r1) to (R2), environmental variability (I) to (III)). The minimum values π_0 of the required level of confidence for the centered confidence intervals specified in Table B.1 are given in Tables B.2 to B.4. For sample size not mentioned in these Tables, the figures may be interpolated.

Table B.2 – Minimum levels of confidence π_0, of the centred confidence intervals (in %) case of a test under 'Environmental Repeatability' (I)

Sample size (n) **Test conditions**	**10**	**20**	**30**	**60**	**120**	**∞**
Full repeatability	*95*	*97.2*	*97.9*	*98.4*	*98.7*	*99.2*
Extended repeatability	*90*	*94.1*	*95.3*	*96.4*	*97.1*	*98.2*
Limited reproducibility	*85*	*90.8*	*92.5*	*94.2*	*95.2*	*97.0*
Full reproducibility	*80*	*87.4*	*89.6*	*91.8*	*93.1*	*95.4*

Table B.3 – Minimum levels of confidence π_0, of the centred confidence intervals (in %) case of a test under 'Limited Environmental Reproducibility' (II)

Sample size (n) Test conditions	10	20	30	60	120	∞
Full repeatability	*93.3*	*96.2*	*97.0*	*97.8*	*98.2*	*98.9*
Extended repeatability	*87.5*	*92.5*	*93.9*	*95.3*	*96.1*	*97.5*
Limited reproducibility	*81.9*	*88.7*	*90.7*	*92.7*	*93.9*	*96.0*
Full reproducibility	*76.6*	*84.9*	*87.4*	*90.0*	*91.5*	*94.3*

Table B.4 – Minimum levels of confidence π_0, of the centred confidence intervals (in %) case of a test under 'Full Environmental Reproducibility' (III)

Sample size (n) Test conditions	10	20	30	60	120	∞
Full repeatability	*91.4*	*95.0*	*96.0*	*97.0*	*97.6*	*98.5*
Extended repeatability	*84.7*	*90.7*	*92.4*	*94.1*	*95.1*	*96.8*
Limited reproducibility	*78.6*	*86.4*	*88.7*	*91.1*	*92.5*	*95.0*
Full reproducibility	*73.0*	*82.3*	*85.1*	*88.1*	*89.8*	*93.1*

B.3 PROCEDURE FOR THE ASSESSMENT OF ACCURACY OF A WIM SYSTEM

The relative errors with respect to the static weights and loads (or any other accepted reference values) are calculated, for each measurement of gross weight, single axle load, etc., as follows:

$$x_i = \frac{Wd_i - Ws_i}{Ws_i} \qquad \text{(B.1)}$$

where Wd_i and Ws_i are the in-motion measured value and the reference (static) value respectively on the same unit. Then, the sample statistics to be calculated and used to classify the system are the mean m, the standard deviation s and the number of values, n of all the measured values (x_1, x_2, ..,x_n) for each identity.

The confidence level π may be either estimated by a theoretical method using the sample statistics of the test, or, in some cases, by a sample proportion. An individual value is considered of a relative error, taken randomly from a Normally distributed sample of size n, with a sample mean m and standard deviation s. A lower bound π, on the probability for

that individual value to be in the centered confidence interval $[-\delta,+\delta]$, is given at the confidence interval $(1-\alpha)$ by:

$$\pi = \Phi(u_1) - \Phi(u_2) \tag{B.2}$$

where

$$u_1 = \frac{(\delta - m)}{s} - \frac{t_{v,1-\alpha/2}}{\sqrt{n}} \tag{B.3}$$

$$u_2 = \frac{(-\delta - m)}{s} + \frac{t_{v,1-\alpha/2}}{\sqrt{n}} \tag{B.4}$$

and Φ is the cumulative distribution function of a Student variable, and $t_{v,1-\alpha/2}$ is a Student variable with $v=n-1$ degrees of freedom. The parameter α is taken to equal 0.05. Then the estimated level of confidence π, for each sample (and criterion) is calculated using Equation B.2. For the case of an initial verification (same data used for calibration and checking), δ is replaced by $k.\delta$ in Equation B.2.

The accuracy level of the WIM system is assessed using one of two methods:

- For each sub-population (sample) corresponding to a criterion from Table B.1, and for the proposed (required) accuracy class defined by δ, the acceptance test is:
  a) If $\pi \geq \pi_0$, the system is accepted in that class;
  b) If $\pi < \pi_0$, the system can not be accepted in the proposed accuracy class, and the acceptance test is repeated with a lower accuracy class (a greater δ). π should be recalculated using Equation B.2.
- An alternative way is to calculate, using Equation B.2, the (lowest) value of δ which provides: $\pi = \pi_0$, and then to check that δ is less than value specified in Table B.1 for the proposed accuracy class and criterion. This approach allows a system to be classified in any accuracy class defined by an arbitrary δ-value (the best one). It is mainly recommended for detailed research and testing studies.

Table B.5 shows the result of an accuracy classification for given sample statistics. It can be seen that the WIM system fulfils the requirements of class B+(7), and, for the single axle, group of axles and gross weight criterions, class A(5). The δ_{min} value refers to the lowest δ value that gives a theoretical π value equal to the required π_0 value. Accordingly, gross weight is the most accurate criterion in this classification.

Table B.5 – Accuracy classification

(**n**: Total number of vehicles; **m**: mean; **s**: Standard deviation; π_0: level of confidence; δ: tolerance of the retained accuracy class; δ_{min}: minimum width of the confidence interval for π_0; π: Level of confidence of the interval $[-\delta,\delta]$)

	Relative error statistics				Accuracy calculation				
Criterion	**n**	**m** (%)	**s** (%)	π_0 (%)	**Class**	δ (%)	δ_{min} (%)	π (%)	**Class Retained**
Single axle	27	0.50	2.07	92.1	**A(5)**	8	4.7	99.8	**B+(7)**
Axle of group	18	-0.09	5.39	90.3	**B+(7)**	14	12.1	94.9	
Group of axles	9	-0.45	0.52	83.4	**A(5)**	7.14	1.4	100.	
Gross Weight	18	0.00	0.30	90.3	**A(5)**	5	0.7	100.	

B.4 CHOICE OF WIM SITE

The site characteristics can have a significant influence on the performance of WIM systems. A rough road surface induces high dynamic forces leading to inaccurate results. Deflection, rutting and pavement cracking can cause sensor failure. So, WIM sites are divided in three classes according to rutting, deflection and evenness (Table B.6). Table B.7 indicates the accuracy class that is likely to be achievable at a site of a given class.

The accuracy of a bridge WIM system also depends highly on the selection of the weighing site, particularly on the type of the superstructure and the evenness of the approach.

Table B.6 – Classification and Criteria of WIM sites

			WIM Site Class		
			I Excellent	II Good	III Acceptable
Rutting (3 m – beam)		Rut depth max. (mm)	≤ 4	≤ 7	≤ 10
Deflection (quasi-static) (130 kN – axle)	Semi-rigid pavements	mean deflection (10^{-2} mm)	≤ 15	≤ 20	≤ 30
		left/right difference (10^{-2} mm)	± 3	± 5	± 10
	All bitumen pavements	mean deflection (10^{-2} mm)	≤ 20	≤ 35	≤ 50
		left/right difference (10^{-2} mm)	± 4	± 8	± 12
	Flexible pavements	mean deflection (10^{-2} mm)	≤ 30	≤ 50	≤ 75
		left/right difference (10^{-2} mm)	± 7	± 10	± 15
Deflection (dynamic) (50 kN – load)	Semi-rigid pavements	deflection (10^{-2} mm)	≤ 10	≤ 15	≤ 20
		left/right difference (10^{-2} mm)	± 2	± 4	± 7
	All bitumen pavements	mean deflection (10^{-2} mm)	≤ 15	≤ 25	≤ 35
		left/right difference (10^{-2} mm)	± 3	± 6	± 9
	Flexible pavements	mean deflection (10^{-2} mm)	≤ 20	≤ 35	≤ 55
		left/right difference (10^{-2} mm)	± 5	± 7	± 10
Evenness	IRI index APL[1]	Index (m/km)	0 – 1.3	1.3 – 2.6	2.6 – 4
		Rating (SW,MW,LW)[1]	9 - 10	7 - 8	5 - 6

[1] *The APL is a car-towed device used to measure longitudinal profile in the short (SW), medium (MW) and long wavelengths (LW) respectively.*

Table B.7 – WIM Accuracy Class Likely to be Achievable in given WIM Site Class

Accuracy Class	WIM Site Class		
	I (Excellent)	II (Good)	III (Acceptable)
Class A(5)	Sufficient	Insufficient	Insufficient
Class B+(7)	Sufficient	May be sufficient	Insufficient
Class B(10)	Sufficient	Sufficient	Insufficient
Class C(15)	More than sufficient	Sufficient	Sufficient
Class D+(20)	More than sufficient	More than sufficient	Sufficient
Class D(25)	More than sufficient	More than sufficient	Sufficient

C

DATA ACQUISITION HARDWARE

This Appendix describes the PC-based instrumentation used by the Irish team for acquiring data in the different experiments described in Chapter 8. This instrumentation is based on the SCXI product line from National Instruments[13]. The SCXI system is used as a front-end signal conditioning system cabled to a PCMCIA DAQ card as depicted in Figure C.1, and it includes: analog input signal-conditioning modules, chassis, terminal blocks and cabling assemblies. Analog signals from the modules are multiplexed back to the DAQ card, which acts as a system controller and digitizes the conditioned signals directly into PC memory.

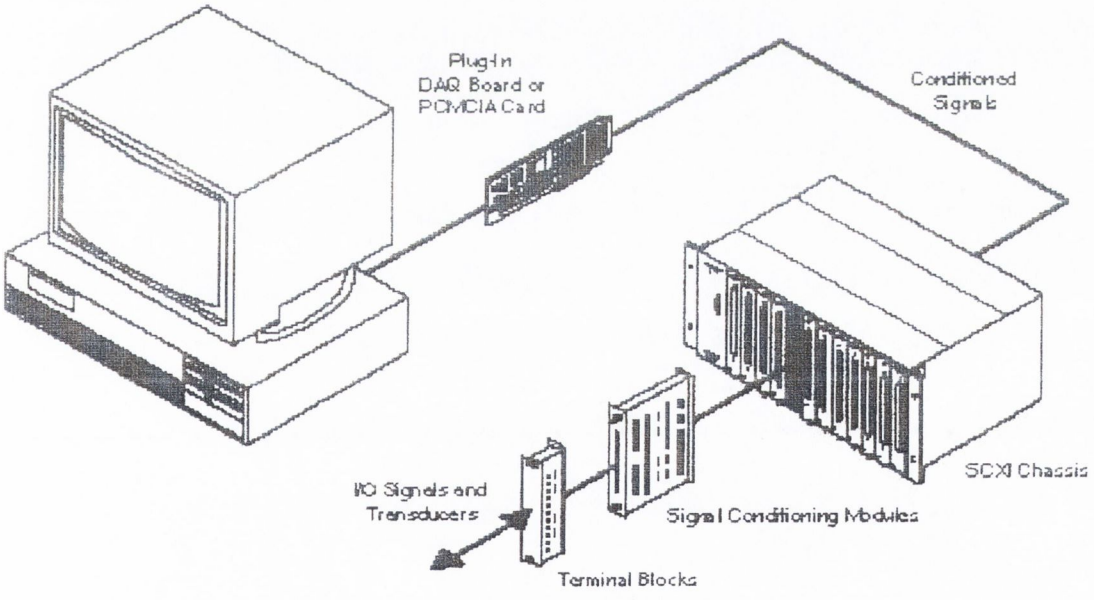

Figure C.1 – SCXI Signal Conditioning Front-End System for Plug-In DAQ Boards[13]

Personal Computer

The personal computer incorporates a PCMCIA port for data acquisition (Figure C.2(a)). The data transfer capabilities of the computer can drastically limit the maximum speed of data acquisition. DAQ cards and computers capable of making DMA (**D**irect **M**emory **A**ccess) transfers are recommended. DMA uses dedicated hardware to transfer data

directly into the system memory, and the processor is released for the accomplishment of other tasks.

The size of the hard drive limits the amount of data that can be acquired. Apart from the memory size, high-speed and unfragmented drives are recommended when large amounts must be recorded.

Chassis

The SCXI chassis circuitry acts as a conduit for signal routing, transferring data, programming modules and passing time signals. The model SCXI-1001 used in the experiments is represented in Figure C.2(b). This is a 12-slot chassis, that can be chained up to other eight chassis with a single DAQ device and is ideal for high-channel count systems (National Instruments 1996). Signals can be scanned from several modules in several chassis at rates up to 333 kS/s. The cable assembly that will connect the PCMCIA card to the SCXI chassis must be selected according to the card type.

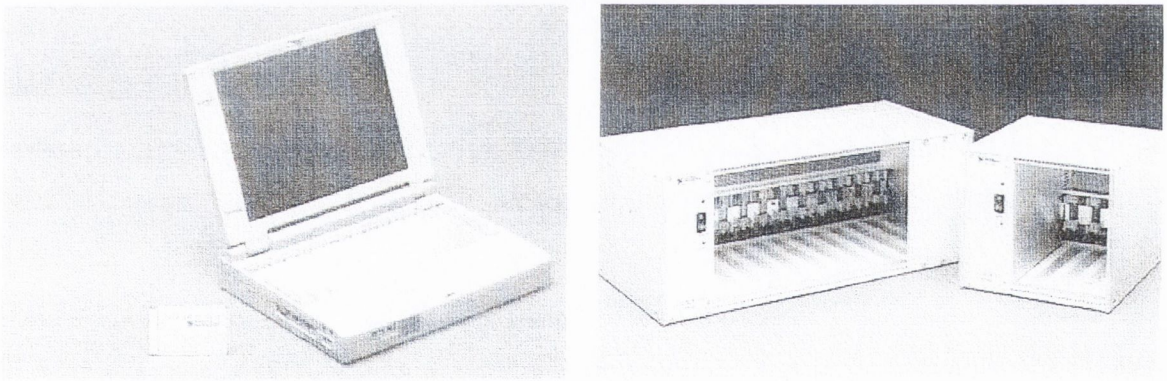

(a) Data Acquisition Card and Labtop (b) Chassis SCXI-1001

Figure C.2 – Data acquisition components[13]

Signal Conditioning

The mission of the modules handling signal conditioning include:

- Amplifying the low strain signals to increase the resolution and reduce noise. Gain is applied to the low-level signals within the SCXI chassis located close to the transducers, sending only high-level signals to the PC, minimising the effects of noise on the readings.

- Isolating strain signals and computer to protect the computer from high-voltage transients and strain readings from differences in ground potentials.
- Multiplexing, this is, a single measuring device samples one channel, switches to the next channel, samples it, switches to the next channel, and so on. Because the same analog-to-digital converter (ADC) is sampling many channels instead of one, the effective sampling rate of each individual channel is inversely proportional to the number of channels sampled.
- Filtering unwanted signals (i.e. noise) before being digitised by the DAQ card.
- Generating external voltage required by strain or road sensors.

The SCXI-1121 (Figure C.3(a)) is a 4-channel isolation amplifier module with transducer excitation sources (3.333 / 10 V). The SCXI-1121 includes a gain amplifier (1 to 2000) and lowpass noise filter (4 Hz / 10 kHz) with complete channel to channel electrical isolation (250 Vrms). Gain and filtering are independently configurable on each channel via jumpers. The maximum sampling rate is 333 kS/s, though it will depend on the DAQ card and cable assembly. The module also includes half-bridge completion circuitry consisting of two 4.5 kΩ resistors. This circuitry is enabled when using strain gauges in a quarter or half Bridge configuration and disabled when taking measurements from a full Bridge or road sensor.

The channel in the SCXI-1121 is configured for gain 2000 and 3.333 V voltage excitation (e_o) if recording a signal from strain gauges of the type described in Section 4.2. Channels receiving a signal from pneumatic converters are configured for gain 1 and 3.333 V (Section 4.3.1). The gain and voltage are chosen to provide a current that allows the acquisition of strain or rubber tube measurements successfully. When piezos were employed, as their interface requires a higher excitation voltage than the one provided by the SCXI module, an extra 15 V external source was applied.

The SCXI-1321 terminal block (Figure C.3(b)) connects signals from strain transducers or road sensors to the module block. It consists of screw terminals in a fully shielded enclosure with strain-relief clamps that hold signal wires securely in place. In combination with the SCXI-1121 module, this terminal block adds manual offset nulling and programmable shunt calibration for each channel. If the bridge is balanced, e_i*(unstrained)*

in Equations 4.2, 4.4 and 4.5 becomes zero. When a quarter bridge is necessary, an extra resistor must be placed between the positive input channel and the negative excitation output.

Field Wiring

The integrity of the acquired data depends upon the entire analog signal path. Interference noise can be minimised by proper cabling and shielding. The Irish team uses a 4-core signal cable. Each core consists of a 7/0·2 mm-tinned copper-stranded conductor, insulated with PVC.

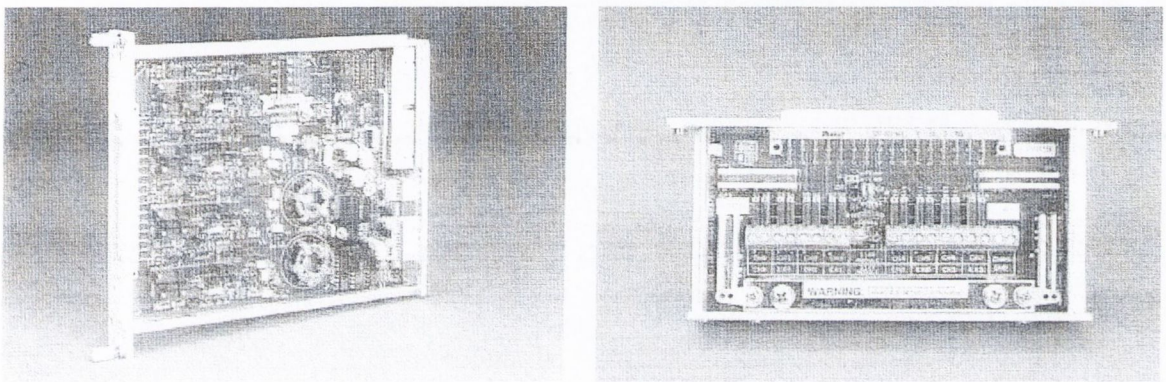

(a) Module block SCXI-1121 (b) Terminal block SCXI-1321

Figure C.3 – Electronic components[13]

Sampling Rate, Resolution, Range and Gain

According to Nyquist's Theorem, an analog signal containing components up to some maximum frequency f_l Hz may be completely represented by regularly spaced samples, provided the sampling rate is at least $2f_l$ samples per second. This corresponds to two samples per period of the highest frequency present and it is a minimum sampling rate which avoids aliasing. In practise, a higher sampling rate is chosen to leave a margin between adjacent spectral repetitions. Generally, the highest frequency component with a significant contribution to the bridge response would be well below the frequency of main power supply (50/60 Hz), a source of unwanted noise. However, a minimum scanning frequency of 200 Hz is recommended for an accurate synchronisation between strain readings and axle detectors or for FAD purposes (Section 4.3.2).

Two different types of resolution have been used: a 12 bit card (model DAQCard-AI-16E-4[13]) and a 16 bit DAQ card (model DAQCard-AI-16XE-50[13]). The 16-bit converter divides the analog range into 2^{16} divisions. The disadvantage of this better resolution card is the inferior sampling rate (20 KS/s for multiple-channel sampling), but it is more than sufficient for WIM purposes. The range, resolution and gain available on a DAQ board determine the smallest detectable change in voltage. If the resolution were 12 bits, range 3.333 V and gain 2000, the theoretical resolution of one bit would be:

$$\frac{3.333}{2000 * 2^{12}} = 40.86 \mu V \qquad \text{(C.1)}$$

In the same conditions of range and gain, a 16-bit card can measure a minimum voltage 16 times smaller than the one given in Equation C.1. Section 3.7.4 describes how B-WIM achieved an accuracy class B(10) in the final experiment in Luleå, thanks among other factors to the use of a 16-bit card instead of the previous 12-bit card.

C.2 INSTALLATION

The computer containing the DAQ card must be disconnected from the SCXI chassis and the SCXI chassis turned off. After having made any necessary changes and having verified the jumper settings (National Instruments 1994), the SCXI-1121 modules are inserted into the board guides of the chassis. Its front mounting panel is screwed to the SCXI chassis. The next step is connecting the SCXI-1121 to the terminal block SCXI-1321 by:

- Connecting the SCXI-1121 front connector to its mating connector on the terminal block.
- Making sure that the SCXI-1121 top and bottom thumbscrews do not obstruct the rear panel of the terminal block.
- Tightening the top and bottom screws on the back of the terminal block to hold it securely in place.

Finally, the installation is checked, the SCXI chassis is turned on, and the computer is turned on and reconnected to the chassis.

Connection between Signal and Terminal block

In order to connect the terminal block to the signal wires, the following steps are carried out:

- The grounding screw of the top cover of the terminal block SCXI-1321 is removed.
- The top cover of the shield is snapped out by placing a screwdriver in the groove at the bottom of the terminal block.
- Then, the signal wires are slid one at a time, through the front panel strain-relief opening.
- The wires are connected to the screw terminals as explained further on.
- The larger strain-relief screws are tightened.
- The top cover back is snapped in place.
- The grounding screw is reinserted to ensure proper shielding.

Signal wires are fixed in the input channel of the terminal block in different ways depending on the signal source. Figure C.4 shows the diagram of the SCXI-1321 terminal block[13].

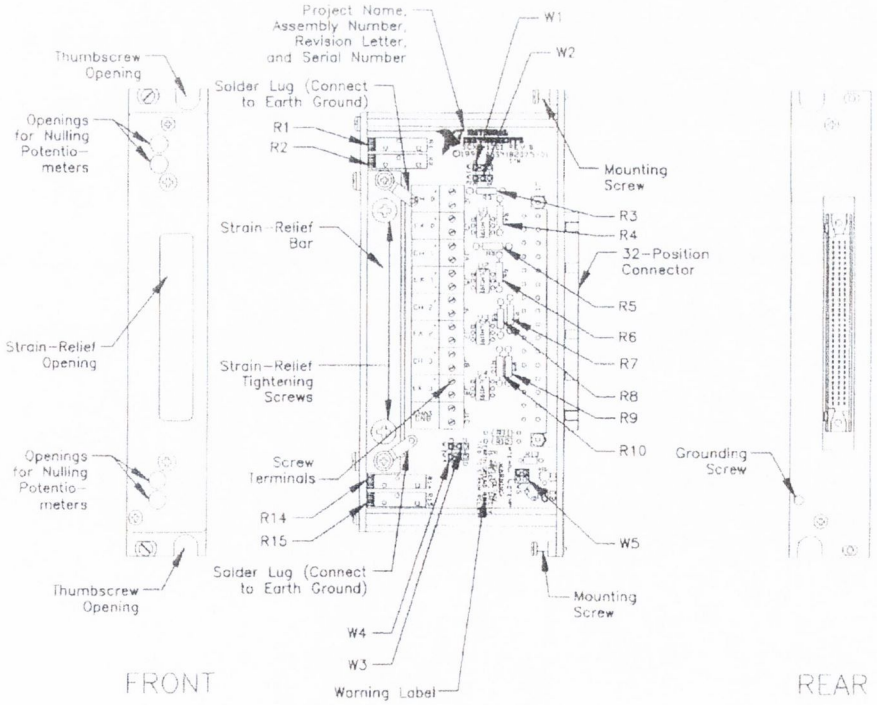

Figure C.4 – SCXI Parts Locator Diagram (after National Instruments 1993)

Figure C.5 shows the configuration of one channel in the terminal block for two types of axle detector: rubber tubes and piezos respectively. The signal from rubber tubes and piezos come from different interfaces described in Section 4.3.1. In the case of Figure C.5(b), the Traffic 2000 interface opens the circuit while there are no vehicles on the sensors. CH+ is wired to the supply via a 10 kΩ resistor so the input reads the supply voltage.

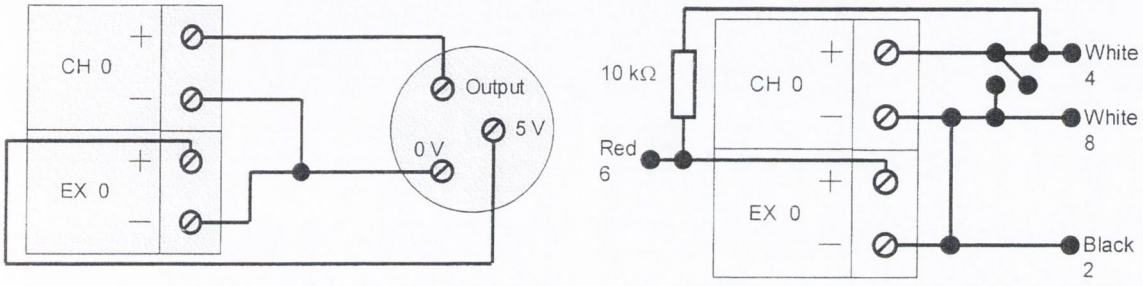

(a) Rubber Tubes (pressure sensor) (b) Piezos

Figure C.5 – Signal wiring in the case of axle detectors

Figure C.6 illustrates the connections that take place when using strain gauges in different Wheatstone Bridge arrangements. In Figure C.6(a), the meaning of the resistors depends on the configuration that is chosen. Resistors will be active and dummy or in tension and compression, if using a quarter or half Wheatstone bridge respectively.

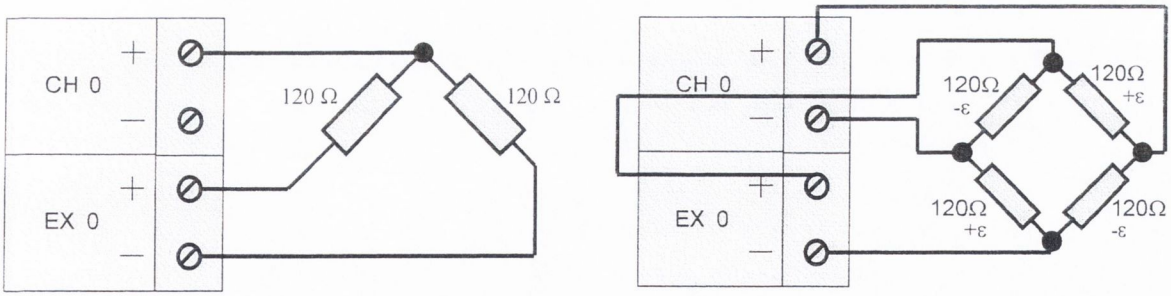

(a) Quarter/Half Bridge (b) Full Bridge

Figure C.6 – Signal wiring in the case of strain gauges

D

BRIDGE WEIGH IN MOTION PROGRAM

The main menu of the B-WIM program displays the following options:

A. Data acquisition
B. Voltage signal
C. Strain & time storage
D. Calibration
E. Calculation of Weights
F. Files
Q. Quit

Option A – Data Acquisition

The following options are presented when option A is selected in the main menu:

A.1) Configure NI-DAQ
A.2) Record Data in Labview Binary format
A.3) Record Data in Text format viewing the signal
A.4) Convert Labview Binary file into Text
A.5) Convert Text into Binary C format
A.6) Compress/Decompress/Delete/See file
A.7) Backup or restore from tape
A.8) Main Menu

The PCMCIA DAQ card includes NI-DAQ driver software[13] for controlling the SCXI system outlined in Appendix C. Option A.1 is a shortcut to this software whose main window is illustrated in Figure D.1(a). The user specifies the DAQ card, cabling assembly, chassis type and the module type to be used in each slot. Figure D.1(b) shows the configuration of a chassis slot for a SCXI-1121 module. Each terminal block, channel gain and filter are initialised. This

specification of the hardware component settings is necessary prior to running any DAQ program.

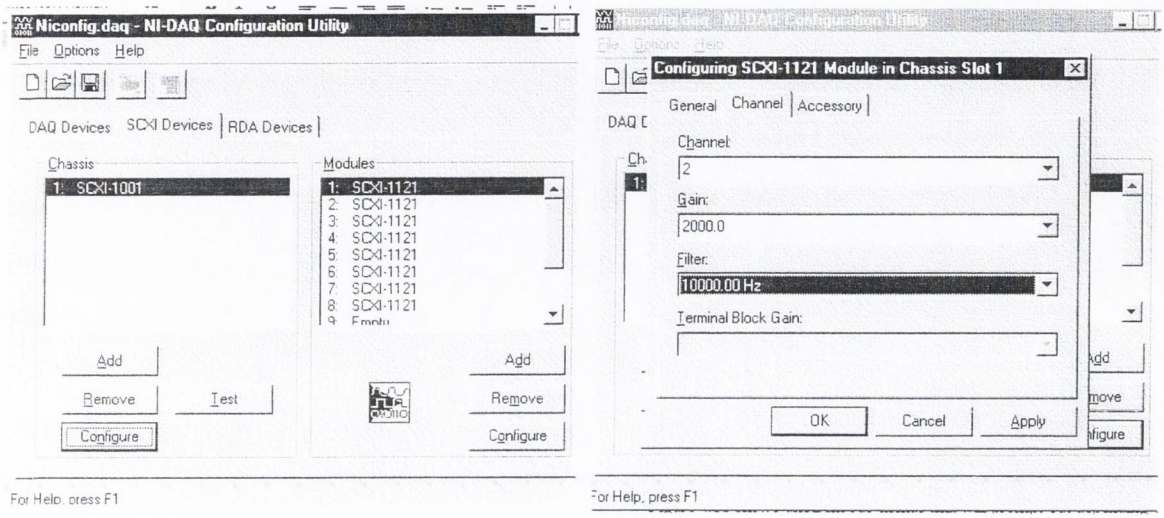

(a) SCXI Configuration (b) SCXI-1121 Module Configuration

Figure D.1 – NI-DAQ Configuration Utility

Options A.2, A.3 and A.4 provide access to the Labview programs for the DAQ, developed by Kealy (1997) and were referred to at the start of this section.

Option A.4 converts the recorded binary Labview file into text (Figure D.2(a)). As part of the heading in the binary file, information on the starting time, date, scanning frequency and number of channels is output in addition to the corresponding voltage for each channel.

Once the text file is obtained, it will be re-converted into Binary C (Option A.5). The rest of the B-WIM program is written in C as it processes calculations faster than Labview. Binary files are preferred as they take less memory and they do not require a slow sequential search as in the case for a text file. The previous conversion into text was effected because of the difficulty of passing from Labview binary format (written in 12-bit unsigned word) to C (8 and 16-bit) directly. Apart from voltages, the heading of each Binary C file will store data on the starting time and date, and additional information on:

- The site: Location, route and road condition, direction of traffic flow and number of lanes.

- The bridge: Typology, section characteristics, number of spans and longitudinal and transverse dimensions.
- Scanning frequency and filter type.
- The correspondence between channel number, and sensor type (specifying which are axle detectors and which are strain transducers), and exact location of each sensor relative to the first support of the bridge.

Before starting the conversion into Binary C, the program displays the installation layout and allows for the modification of erroneous data through the interface shown in Figure D.2(b).

Options A.6 and A.7 provide access to commercial software for restoring/backing up files to a tape, and compressing, decompressing or deleting them from the hard drive to solve storage problems. After zipping, a binary file can be reduced from its original size by a factor of forty.

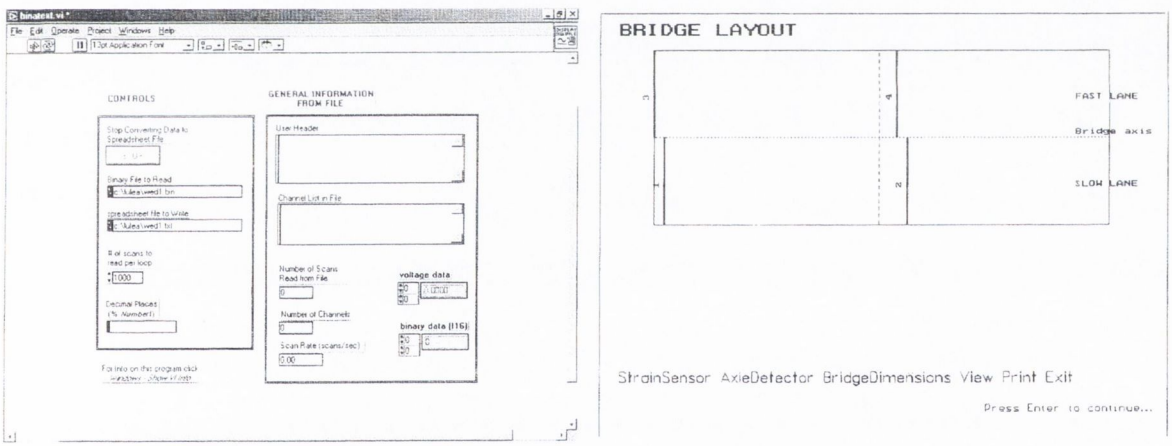

(a) Conversion Binary Labview into text (b) Sensor layout

Figure D.2 – Conversion from Binary Labview into Binary C

Option B – Voltage Signal

The sub-menus that will appear when checking the voltage signal are:

B.1) Date, Time and Location characteristics

B.2) Convert text file into Turbo C binary format

B.3) Convert binary file into text

B.4) Analyse voltage signal from axle detectors

B.5) Analyse voltage signal from strain gauges

B.6) Main menu

Option B.1 displays the characteristics of the site for an existing Binary-C file. Option B.2 is identical to A.5. Option B.3 converts an existing Binary C file into text format. This option also allows the conversion of the whole Binary C file or the specification of the starting and ending scan of the segment to be converted.

Option B.4 allows numerical or graphical axle identification. The graphical display of the signal from the road sensors is shown in Figure D.3. This program shows the passing of each axle as a vertical discontinuous line with the scan number corresponding to the axle hit on the screen. The upper part of the screen shows the measured voltage and the lower part the first derivative with time. The different parameters for axle detection (p,r) can be adjusted on the screen to ensure that every axle is identified. Other control parameters such as maximum number of axles or maximum feasible number of scans between tubes allow for other anomalies to be detected. These values can vary for different sites depending on the installation and hardware settings.

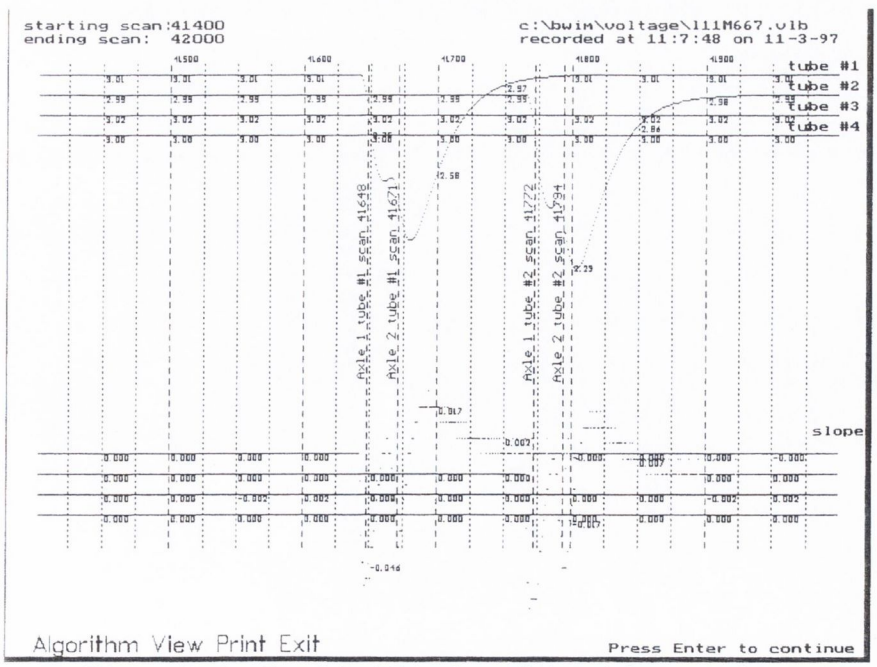

Figure D.3 - Graphical Display of signal from road sensors

Option B.5 visualises the output of each strain transducer. A starting scan number is given for options B.4 and B.5 to search the traffic file. The number of scans to be viewed and the scale can be adjusted in every window.

Option C – Strain and Time Storage

Once the parameters for axle detection have been properly adjusted in Option B, Option C will proceed to store only the scan numbers corresponding to axle hits and strain due to the passing of a vehicle on the bridge. Those intervals of time where there is no traffic on the bridge will not be saved. The objective of this simplification is reducing storage and it speeds up the calculation of weights in a later process. After running this option, the screen shows statistics for each lane on the total number of vehicles of each class and the number of errors due to a missed or extra axle in a tube. If errors are excessive, it will be necessary to re-adjust the axle detection parameters.

Another option in Menu C extracts all information on times from a given vehicle number to another vehicle number. Once the vehicle which is the object of study has been detected in the time file, the corresponding strain record can also be extracted in text.

Option D – Calibration

The calibration menu is as follows:

D.1) Enter Truck characteristics
D.2) Enter Bridge characteristics
D.3) Enter Strain characteristics
D.4) Obtain Calibration parameters from time file
D.5) Obtain Calibration factor
D.6) View calibration adjustment graphically
D.7) Main menu

Option D.1 enquires about the number of axles, axle spacings and static weights of the calibration truck. Option D.2 enquires about the span length, distance from the tube to the bridge support and distance from the bridge support to the location of the strain transducers.

Option D.3 enquires about the name of the strain file containing the record of the calibration truck, the starting scan of the record (instant in which the first axle hits the first tube), duration in scans, scanning frequency and average velocity.

If Option D.4 is chosen, all the characteristics requested in D.2 and D.3 will be read from the heading of the Binary C file. In this case, number of axles, axle spacings and static weights of the last test vehicle are shown on the screen. If they are not correct, the user can modify them. The search can be initialised to a certain starting scan. Then, the program will start to look for a vehicle with similar characteristics. The user stops the search once the correct vehicle has been identified.

Option D.5 determines the calibration factor based on Section 3.3 and Option D.6 displays the quality of the adjustment as shown in Figure D.4.

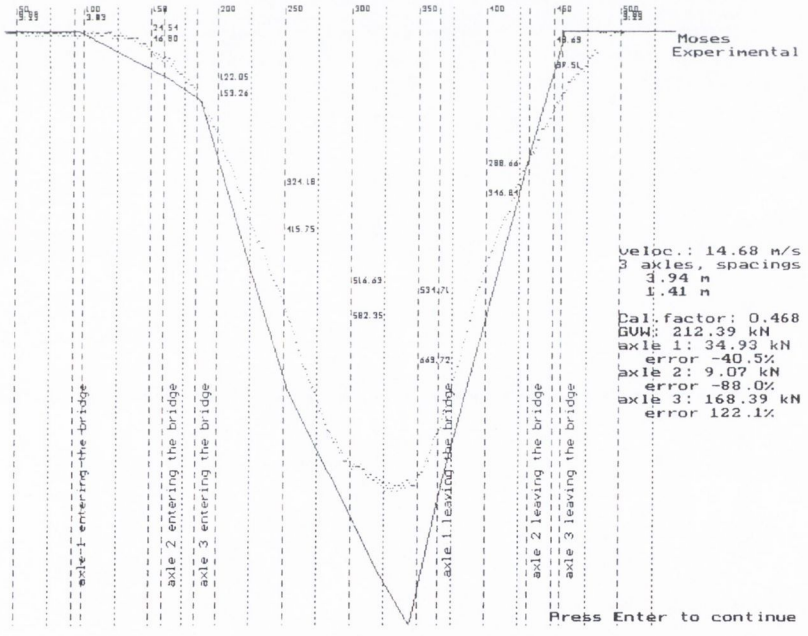

Figure D.4 - Calibration

Option E – Calculation of Weights

Finally, the menu for calculating weights provides the following options:

E.1) Calculate Weights for a particular traffic event

E.2) Calculate Weights for a whole file

E.3) Change calibration factor, recalculating weights

E.4) See weight file

E.5) Main Menu

As the vehicles and times have already been classified in Option C, Option E.1 allows the selecting of a particular vehicle number and obtaining the corresponding weights. Option E.2 will calculate weights for a whole traffic file. Option E.3 allows the changing of the calibration factor and recalculating the whole traffic file. Option E.4 displays the output file on screen. The row of each output file contains information on an individual vehicle. Each column represents a specific characteristic of a traffic event. Table D.1 shows a small portion of this output file for a given voltage input.

Table D.1 - WIM Data Output

DD	MM	YY	HH	mm	ss	hh	event	L	HEAD	GAP	SPD	Length	AX	WBTOT	W1-2	W2-3	W3-4	GVW(kN)	AW(kN)-1	AW(
12	7	97	2	27	41	30	9	0	3549	3532	25.37	4.54	2	2.54	2.54	0	0	7.72	1.3	
12	7	97	2	28	16	79	10	0	17141	17124	25.09	4.46	2	2.46	2.46	0	0	11.19	2.49	
12	7	97	2	31	8	20	11	0	19915	19898	25.54	4.5	2	2.5	2.5	0	0	9.98	1.41	
12	7	97	2	34	27	36	13	0	175	157	24.18	4.42	2	2.42	2.42	0	0	7.83	1.35	
12	7	97	2	34	29	11	14	0	27154	27137	26.61	4.61	2	2.61	2.61	0	0	10.8	2.61	
12	7	97	2	36	13	43	6	1	36377	36360	27.57	4.7	2	2.7	2.7	0	0	12.43	1.02	
12	7	97	2	39	0	65	15	0	1194	1179	27.91	4.29	2	2.29	2.29	0	0	9.18	3.36	
12	7	97	2	39	12	60	16	0	7533	7517	27.18	4.39	2	2.39	2.39	0	0	7.4	2.08	
12	7	97	2	40	27	93	17	0	18874	18855	23.68	4.65	2	2.65	2.65	0	0	12.23	2.47	
12	7	97	2	42	17	20	7	1	7945	7933	38.8	4.79	2	2.79	2.79	0	0	11.28	1.64	
12	7	97	2	43	36	65	8	1	31811	31765	25.18	11.67	4	9.67	3.12	5.14	1.41	109	6.25	
12	7	97	2	43	36	67	18	0	9244	9200	29.34	13.03	4	11.03	3.52	5.87	1.64	120.82	24.09	
12	7	97	2	45	9	11	19	0	7827	7814	35.56	4.63	2	2.63	2.63	0	0	5.03	1.46	
12	7	97	2	46	27	39	20	0	354	339	28.47	4.45	2	2.45	2.45	0	0	8.19	2.4	

The meaning of the columns in Table D.1 are as follows:

- *DD*: Day, *MM*: Month, *YY*: Year, indicating the date that this traffic event took place.
- *HH*: Hour, *mm*: Minute, *ss*: Second, *hh*: Hundredths of a Second, indicating the arrival time of the vehicle onto the bridge.
- *Event*: Number of vehicle arriving into that lane for that file.
- *L*: Identification number for the lane where the vehicle is travelling (0: Slow; 1: Fast).
- *HEAD*: Time (hundredths of a second) between the first axle of two consecutive vehicles.

- *GAP*: Time (hundredths of a second) between the rear and the front of two consecutive vehicles.
- *SPD*: Speed in m/s.
- *Length*: Vehicle length calculated as total wheelbase plus 2 m.
- *AX*: Number of axles.
- *WBTOT*: Total wheelbase calculated as spacing between first and last axle.
- *W1-2*: Spacing between 1st and 2nd axle in m, *W2-3*: Spacing between 2nd and 3rd axle in m, and so on.
- *GVW(kN)*: Gross Vehicle Weight in kN.
- *AW(kN)-1*: Weight of 1st axle in kN, *AW(kN)-2*: Weight of 2nd axle in kN, and so on.

The source code and executable files of the program are included in the CD-ROM (Appendix H). Further details on the files, structures and data types of the program are given in a word document in the disc.

E

RUNGE-KUTTA METHOD

The solution of a first order differential equation by the method of Runge-Kutta is presented. Then, the method of Runge-Kutta is applied to a second order differential equation. The latter is solved by transforming the second order differential equation into two first order equations.

E.1 FIRST ORDER DIFFERENTIAL EQUATION

Equation E.1 represents a first order differential equation.

$$\frac{dz}{dt} = g(t,z) \tag{E.1}$$

$z(t)$ can be expressed in terms of the Taylor series in the neighborhood of z_i. Given a time increment $h = \Delta t$, if the first derivative is replaced by an average slope and the higher order derivatives are ignored, when a value z_i is known, the next increment z_{i+1} is given as shown in Equation E.2:

$$z_{i+1} = z_i + \left(\frac{dz}{dt}\right)_{iav} h \tag{E.2}$$

If Runge-Kutta method is used, the average slope in the interval h is made of four estimates of the increment as shown in Equation E.3:

$$z_{i+1} = z_i + \frac{h}{6}(Y_1 + 2Y_2 + 2Y_3 + Y_4) \tag{E.3}$$

where

$$Y_1 = hg(t_i, z_i) \tag{E.4}$$

$$Y_2 = hg(t_i + \frac{h}{2}, z_i + \frac{Y_1}{2}) \tag{E.5}$$

$$Y_3 = hg(t_i + \frac{h}{2}, z_i + \frac{Y_2}{2}) \tag{E.6}$$

$$Y_4 = hg(t_i + h, z_i + Y_3) \tag{E.7}$$

E.2 SECOND ORDER DIFFERENTIAL EQUATION

For example, the differential equation for a single degree of freedom system has the form given by Equation E.1:

$$m\frac{d^2z(t)}{dt^2} + c\frac{dz(t)}{dt} + kz(t) = f(t) \tag{E.8}$$

where m, c and k are constants, and $z(t)$ and $f(t)$ are functions depending on variable t.

By re-arranging Equation E.1, it is obtained:

$$\frac{d^2z(t)}{dt^2} = \frac{1}{m}\left[f(t) - kz(t) - c\frac{dz(t)}{dt} \right] \tag{E.9}$$

By re-writting $y(t) = \frac{dz(t)}{dt}$,

$$\frac{d^2z(t)}{dt^2} = \frac{1}{m}\left[f(t) - kz(t) - cy(t)\right] \tag{E.10}$$

and if re-naming $F(z,y,t)=\frac{d^2z}{dt^2}$:

$$F(z,y,t)=\frac{1}{m}\left[f(t)-kz(t)-cy(t)\right] \tag{E.11}$$

So, Equation E.8 has been reduced to the following two first order equations:

$$y(t)=\frac{dz(t)}{dt} \tag{E.12}$$

$$\frac{dy(t)}{dt}=F(z,y,t) \tag{E.13}$$

If Runge-Kutta method is used, the average slope in the interval h is made of four terms and four values (t, z, y and F) as shown in the following recurrence formulae:

$$z_{i+1}=z_i+\frac{h}{6}(Y_1+2Y_2+2Y_3+Y_4) \tag{E.14}$$

$$y_{i+1}=y_i+\frac{h}{6}(F_1+2F_2+2F_3+F_4) \tag{E.15}$$

The values in Equations E.14 and E.15 are obtained as shown in Table E.1.

Table E.1 – Runge-Kutta terms

t	z	$y = \frac{dz}{dt}$	$F = \frac{dy}{dt} = \frac{d^2z}{dt^2}$
$T_1 = t_i$	$Z_1 = z_i$	$Y_1 = y_i$	$F_1 = f(T_1, Z_1, Y_1)$
$T_2 = t_i + \frac{h}{2}$	$Z_2 = z_i + Y_1 \frac{h}{2}$	$Y_2 = y_i + F_1 \frac{h}{2}$	$F_2 = f(T_2, Z_2, Y_2)$
$T_3 = t_i + \frac{h}{2}$	$Z_3 = z_i + Y_2 \frac{h}{2}$	$Y_3 = y_i + F_2 \frac{h}{2}$	$F_3 = f(T_3, Z_3, Y_3)$
$T_4 = t_i + h$	$Z_4 = z_i + Y_3 h$	$Y_4 = y_i + F_3 h$	$F_4 = f(T_4, Z_4, Y_4)$

Displacement (z), velocity $\left(\frac{dz}{dt}\right)$ and acceleration $\left(\frac{d^2z}{dt^2}\right)$ of the system can be calculated for each iteration i. The initial values are $z_{t=t_0}$ and $\left(\frac{dz}{dt}\right)_{t=t_0}$ However, in the case of a truck crossing a bridge, there is not force applied at $t = 0$ and the initial conditions are zero. Then, the computation can be started by assuming the acceleration varies linearly from $\left(\frac{d^2z}{dt^2}\right)_{t=t_0} = 0$ to $\left(\frac{d^2z}{dt^2}\right)_{t=t_1}$ during the first time interval.

F

BRIDGE-TRUCK DYNAMIC INTERACTION USING MSC/NASTRAN

Models for Static, Modal, Transient Response (Direct and Modal), Frequency Response (Direct and Modal), Random Response, Non-linear static and Non-linear Transient can be written, read or the standard printed output file can be read for postprocessing. The File Export Analysis Model command allows to write a model into a file that can be read by NASTRAN (*nast682.exe*). This file contains three required sections : Executive Control, Case Control, and Bulk Data. Caseco and Bulk sections are input through text files with a field format defined in Quick Reference Guide (MSC/NASTRAN for Windows 1998). This Appendix gives examples of these two files to be written in the bridge-truck interaction model.

F.1 GENERATION OF MSC/NASTRAN INTERACTION MODEL

The dialog boxes that are displayed when chosing the File Export command are described first.

- *Analysis Format* (Figure F.1(a)). Choose analysis type *3.Transient Dynamic/ Time History* and *MSc/NASTRAN* model. Press *OK*.
- *Write model to NASTRAN* (Figure F.1(b)). Write name of file, i.e. *test.dat*. Press *Write*.
- *NASTRAN Analysis Control* (Figure F.2(a)). Make sure the correct analysis type (Transient dynamic), load set and constraint set are selected. Press *Advanced.*
- *NASTRAN Dynamic Analysis. Direct Solution* Type. Press *OK.*
- *NASTRAN Executive and Solution Control* (Figure F.2(b)). Press *OK.*

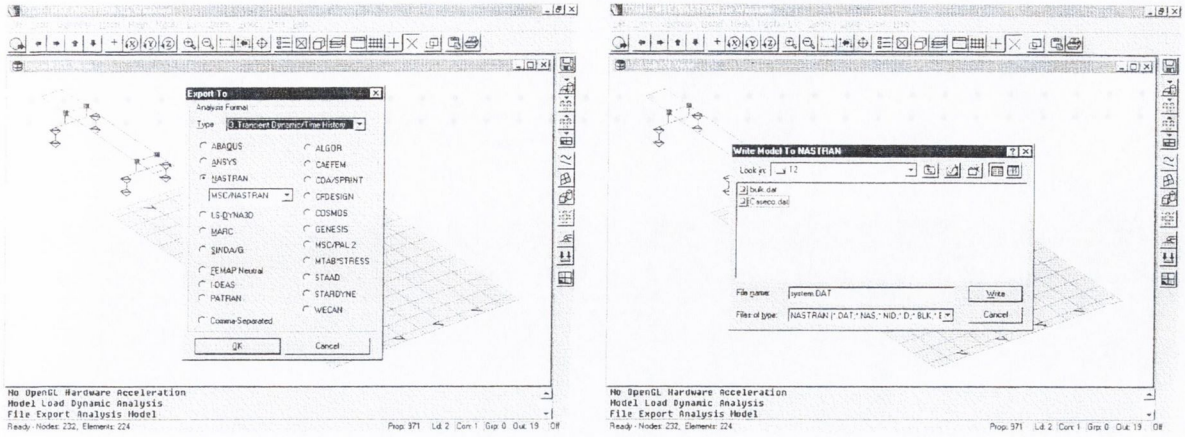

(a) Analysis Format (b) Write Model to

Figure F.1 – Export to a File

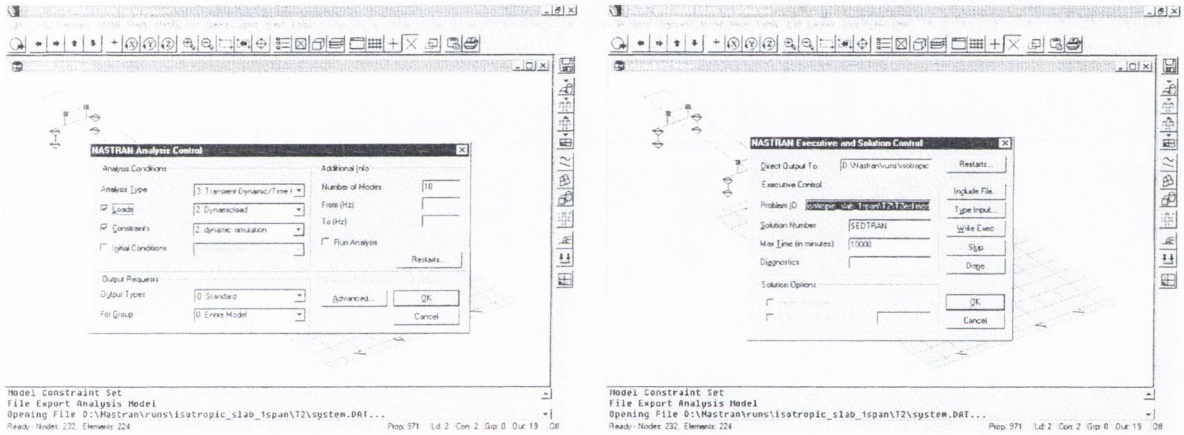

(a) Analysis Control (b) Executive and Solution Control

Figure F.2 – Analysis, Executive and Solution Control

- *NASTRAN Caseco Control*. There are two parts: Output and Analysis Case Request. In the first part, *0. Print Only* must be selected and all other ticks in boxes relating to output requests must be removed (Figure F.3(a)). In the second part, choose *Include File*, and select *caseco.dat* file (Figure F.3(b)). Press *Open*. Press *OK*.

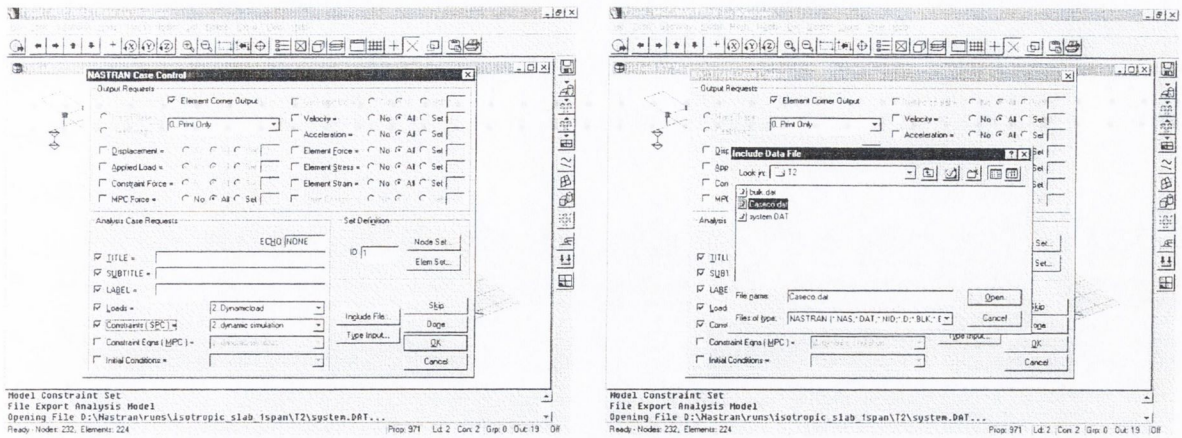

(a) Output Request (b) Analysis Case Request

Figure F.3 – Caseco Section

- *NASTRAN Bulk Data Section* (Figure F.4(a)). Select *Include File*, select the adequate *bulk.dat* for this interaction (Figure F.4(b)), press *Open*, press *OK. Exit and Save*.

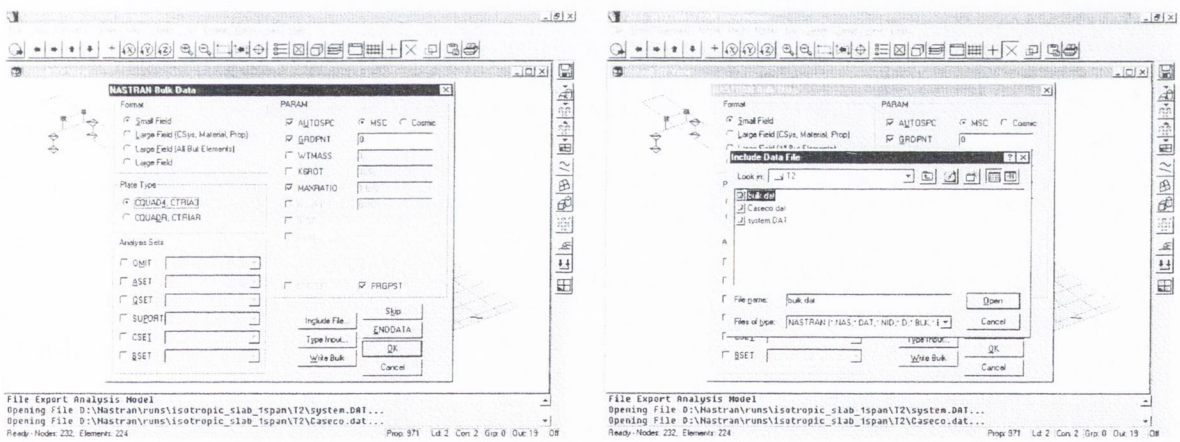

(a) Bulk options (b) Include File

Figure F.4 – Bulk Data Section

F.2 CASE CONTROL

After the Executive Control is finished, a dialog box appears in case of a structural analysis, which is divided into three readily understable areas : (1) Set definition, (2) Analysis Case Requests, and (3) Output Requests.

Usually ouput for all nodes/elements are required. If the output is to be limited, A NASTRAN SET must be defined to select the corresponding node or element IDs. The NASTRAN output must always be read into the original MSC/N4W model. MSC/N4W will read many types of NASTRAN output, including :

- DISPLACEMENT – Displacements/Eigenvectors
- VELOCITY – Velocities
- ACCELERATION – Accelerations
- MPCFORCES – Multipoint Constraint Forces
- SPCFORCES – Constraint Forces
- OLOAD – Applied Loads
- FORCE – Element Forces
- STRESS – Element Stresses (Linear and Nonlinear)
- STRAIN – Element Strains (Linear and Nonlinear)
- ESE – Element Strain Energy ,....

In addition, MSC/N4W will also read Complex Output, in both Magnitude/Phase or Real/Imaginary format, for most of the above structural types. An example of Case Control input file is given in Table F.1.

Table F.1 – *Caseco.dat* file

```
$ Input Specification
NONLINEAR=2
K2GG=STIF
PARAM,COUPMASS,1
$ SET- Definition of points and elements where output is required
SET 1 = 300000,301000,185
SET 2 = 19,20,59,60,99,100,139,140,179,180,219,220,259
$ Output Specification
DISPLACEMENT(SORT1) = 1
VELOCITY(SORT1) = 1
ACCELERATION(SORT1) = 1
FORCE(SORT1) = 1
STRESS(SORT1) = 2
STRAIN(SORT1) = 2
```

F.3 BULK DATA ENTRY

The Bulk data file contains the interaction forces between bridge and truck models. These forces are based on a Lagrange multiplier technique described in Section 6.2. Bulk files are generated for some given characteristics of the models through code developed by the author. An example of input and the corresponding bulk file for a single-vehicle event planar model is listed next.

Table F.2 shows the input file for the generation of the *bulk.dat* for a planar single vehicle. The format of this file is printed automatically through enquiries on the computer screen (Section 6.3).

Table F.2 – Input file for planar single vehicle model

```
Analysis_type:(1)1-D_or_(3)3-D
1
Total_Number_vehicles
1
Number_axles
2
Axle_Spacing_from_first_axle:
0
5
Axle_loads[Nw]:
10000
20000
Number_speed_points
2
Time_speed_relationship(sec-m/s)
0
20
20
20
Total_Number_Nodes_in_Path:
5
Nodes_Id_coordinates_path
10
0
11
1
12
2
13
3
14
4
```

Table F.2 (continuation)

```
Approach_Length(m):
10
Road_Profile_Type:1)Theoretical,2)Measured,3)Flat
3
Geometric_mean_spatial_Frequency[a]
0
Minimum_frequency(Hz):
1
Maximum_frequency(Hz):
20
Number_frequencies:
100
```

The preceding input file produces the *bulk.dat* file listed in Table F.3.

Table F.3 – Bulk file for spatial model of two-vehicle event in Table F.2.

$.....	$.....	$.....	$.....	$.....	$.....	$.....	$.....	$.....	$.....
SPOINT	400000								
SPOINT	402000								
$.....	$.....	$.....	$.....	$.....	$.....	$.....	$.....	$.....	$.....
SPOINT	500000								
SPOINT	502000								
$.....	$.....	$.....	$.....	$.....	$.....	$.....	$.....	$.....	$.....
SPOINT	100001	THRU	100005						
=	*2000	=	*2000						
SPOINT	200001	THRU	200005						
=	*2000	=	*2000						
$.....	$.....	$.....	$.....	$.....	$.....	$.....	$.....	$.....	$.....
DMIG	STIF	0	6	1	1				
$.....	$.....	$.....	$.....	$.....	$.....	$.....	$.....	$.....	$.....
DMIG	STIF	100001			100001		1		
=	=	*1	=	=	*1	=	=		
3									
DMIG	STIF	102001			102001		1		
=	=	*1	=	=	*1	=	=		
3									
DMIG	STIF	200001			200001		1		
=	=	*1	=	=	*1	=	=		
3									
DMIG	STIF	202001			202001		1		
=	=	*1	=	=	*1	=	=		
3									
$.....	$.....	$.....	$.....	$.....	$.....	$.....	$.....	$.....	$.....
DMIG	STIF	400000			400000		0		
DMIG	STIF	402000			402000		0		
DMIG	STIF	500000			500000		1		

Table F.3 (continuation)

DMIG	STIF	502000			502000		1		
DMIG	STIF	300000	3		400000		1		
DMIG	STIF	302000	3		402000		1		
$.....	$.....	$.....	$.....	$.....	$.....	$.....	$.....	$.....	$.....
DAREA	100001	100001		1					
TLOAD2	100001	100001		0	0.5	0.55	0	0	
	0	0							
DAREA	110001	100001		-1199.99					
TLOAD2	110001	110001		0	0.5	0.55	0	0	
	0	2							
DAREA	120001	100001		15999.98					
TLOAD2	120001	120001		0	0.5	0.55	0	0	
	0	3							
DAREA	102001	102001		1					
TLOAD2	102001	102001		0	0.75	0.8	0	0	
	0	0							
DAREA	112001	102001		-1199.99					
TLOAD2	112001	112001		0	0.75	0.8	0	0	
	0	2							
DAREA	122001	102001		15999.98					
TLOAD2	122001	122001		0	0.75	0.8	0	0	
	0	3							
DAREA	100002	100002		1					
TLOAD2	100002	100002		0	0.55	0.6	0	0	
	0	0							
DAREA	110002	100002		-1199.99					
TLOAD2	110002	110002		0	0.55	0.6	0	0	
	0	2							
DAREA	120002	100002		15999.98					
TLOAD2	120002	120002		0	0.55	0.6	0	0	
	0	3							
DAREA	130002	100002		1199.999					
TLOAD2	130002	130002		0	0.5	0.55	0	0	
	0	2							
DAREA	140002	100002		-15999.9					
TLOAD2	140002	140002		0	0.5	0.55	0	0	
	0	3							
DAREA	102002	102002		1					
TLOAD2	102002	102002		0	0.8	0.85	0	0	
	0	0							
DAREA	112002	102002		-1199.99					
TLOAD2	112002	112002		0	0.8	0.85	0	0	
	0	2							
DAREA	122002	102002		15999.98					
TLOAD2	122002	122002		0	0.8	0.85	0	0	
	0	3							
DAREA	132002	102002		1199.999					

Table F.3 (continuation)

TLOAD2	132002	132002		0	0.75	0.8	0	0	
	0	2							
DAREA	142002	102002		-15999.9					
TLOAD2	142002	142002		0	0.75	0.8	0	0	
	0	3							
DAREA	100003	100003		1					
TLOAD2	100003	100003		0	0.6	0.65	0	0	
	0	0							
DAREA	110003	100003		-1200					
TLOAD2	110003	110003		0	0.6	0.65	0	0	
	0	2							
DAREA	120003	100003		16000.04					
TLOAD2	120003	120003		0	0.6	0.65	0	0	
	0	3							
DAREA	130003	100003		1199.999					
TLOAD2	130003	130003		0	0.55	0.6	0	0	
	0	2							
DAREA	140003	100003		-15999.9					
TLOAD2	140003	140003		0	0.55	0.6	0	0	
	0	3							
DAREA	102003	102003		1					
TLOAD2	102003	102003		0	0.85	0.9	0	0	
	0	0							
DAREA	112003	102003		-1200					
TLOAD2	112003	112003		0	0.85	0.9	0	0	
	0	2							
DAREA	122003	102003		16000.04					
TLOAD2	122003	122003		0	0.85	0.9	0	0	
	0	3							
DAREA	132003	102003		1199.999					
TLOAD2	132003	132003		0	0.8	0.85	0	0	
	0	2							
DAREA	142003	102003		-15999.9					
TLOAD2	142003	142003		0	0.8	0.85	0	0	
	0	3							
DAREA	100004	100004		1					
TLOAD2	100004	100004		0	0.65	0.7	0	0	
	0	0							
DAREA	110004	100004		-1199.99					
TLOAD2	110004	110004		0	0.65	0.7	0	0	
	0	2							
DAREA	120004	100004		15999.98					
TLOAD2	120004	120004		0	0.65	0.7	0	0	
	0	3							
DAREA	130004	100004		1200.002					
TLOAD2	130004	130004		0	0.6	0.65	0	0	
	0	2							

Table F.3 (continuation)

DAREA	140004	100004		-16000					
TLOAD2	140004	140004		0	0.6	0.65	0	0	
	0	3							
DAREA	102004	102004		1					
TLOAD2	102004	102004		0	0.9	0.95	0	0	
	0	0							
DAREA	112004	102004		-1199.99					
TLOAD2	112004	112004		0	0.9	0.95	0	0	
	0	2							
DAREA	122004	102004		15999.98					
TLOAD2	122004	122004		0	0.9	0.95	0	0	
	0	3							
DAREA	132004	102004		1200.002					
TLOAD2	132004	132004		0	0.85	0.9	0	0	
	0	2							
DAREA	142004	102004		-16000					
TLOAD2	142004	142004		0	0.85	0.9	0	0	
	0	3							
DAREA	130005	100005		1199.999					
TLOAD2	130005	130005		0	0.65	0.7	0	0	
	0	2							
DAREA	140005	100005		-15999.9					
TLOAD2	140005	140005		0	0.65	0.7	0	0	
	0	3							
DAREA	132005	102005		1199.999					
TLOAD2	132005	132005		0	0.9	0.95	0	0	
	0	2							
DAREA	142005	102005		-15999.9					
TLOAD2	142005	142005		0	0.9	0.95	0	0	
	0	3							
$.....	$.....	$.....	$.....	$.....	$.....	$.....	$.....	$.....	$.....
DAREA	200001	200001		-9.99999					
TLOAD2	200001	200001		0	0.5	0.55	0	0	
	0	1							
DAREA	210001	200001		199.9999					
TLOAD2	210001	210001		0	0.5	0.55	0	0	
	0	2							
DAREA	202001	202001		-9.99999					
TLOAD2	202001	202001		0	0.75	0.8	0	0	
	0	1							
DAREA	212001	202001		199.9999					
TLOAD2	212001	212001		0	0.75	0.8	0	0	
	0	2							
DAREA	200002	200002		-9.99999					
TLOAD2	200002	200002		0	0.55	0.6	0	0	
	0	1							
DAREA	210002	200002		199.9999					

Table F.3 (continuation)

TLOAD2	210002	210002		0	0.55	0.6	0	0	
	0	2							
DAREA	220002	200002		9.999998					
TLOAD2	220002	220002		0	0.5	0.55	0	0	
	0	1							
DAREA	230002	200002		-199.999					
TLOAD2	230002	230002		0	0.5	0.55	0	0	
	0	2							
DAREA	202002	202002		-9.99999					
TLOAD2	202002	202002		0	0.8	0.85	0	0	
	0	1							
DAREA	212002	202002		199.9999					
TLOAD2	212002	212002		0	0.8	0.85	0	0	
	0	2							
DAREA	222002	202002		9.999998					
TLOAD2	222002	222002		0	0.75	0.8	0	0	
	0	1							
DAREA	232002	202002		-199.999					
TLOAD2	232002	232002		0	0.75	0.8	0	0	
	0	2							
DAREA	200003	200003		-10					
TLOAD2	200003	200003		0	0.6	0.65	0	0	
	0	1							
DAREA	210003	200003		200.0003					
TLOAD2	210003	210003		0	0.6	0.65	0	0	
	0	2							
DAREA	220003	200003		9.999998					
TLOAD2	220003	220003		0	0.55	0.6	0	0	
	0	1							
DAREA	230003	200003		-199.999					
TLOAD2	230003	230003		0	0.55	0.6	0	0	
	0	2							
DAREA	202003	202003		-10					
TLOAD2	202003	202003		0	0.85	0.9	0	0	
	0	1							
DAREA	212003	202003		200.0003					
TLOAD2	212003	212003		0	0.85	0.9	0	0	
	0	2							
DAREA	222003	202003		9.999998					
TLOAD2	222003	222003		0	0.8	0.85	0	0	
	0	1							
DAREA	232003	202003		-199.999					
TLOAD2	232003	232003		0	0.8	0.85	0	0	
	0	2							
DAREA	200004	200004		-9.99999					
TLOAD2	200004	200004		0	0.65	0.7	0	0	
	0	1							

Table F.3 (continuation)

DAREA	210004	200004		199.9999					
TLOAD2	210004	210004		0	0.65	0.7	0	0	
	0	2							
DAREA	220004	200004		10.00001					
TLOAD2	220004	220004		0	0.6	0.65	0	0	
	0	1							
DAREA	230004	200004		-200					
TLOAD2	230004	230004		0	0.6	0.65	0	0	
	0	2							
DAREA	202004	202004		-9.99999					
TLOAD2	202004	202004		0	0.9	0.95	0	0	
	0	1							
DAREA	212004	202004		199.9999					
TLOAD2	212004	212004		0	0.9	0.95	0	0	
	0	2							
DAREA	222004	202004		10.00001					
TLOAD2	222004	222004		0	0.85	0.9	0	0	
	0	1							
DAREA	232004	202004		-200					
TLOAD2	232004	232004		0	0.85	0.9	0	0	
	0	2							
DAREA	200005	200005		9.999998					
TLOAD2	200005	200005		0	0.65	0.7	0	0	
	0	1							
DAREA	210005	200005		-199.999					
TLOAD2	210005	210005		0	0.65	0.7	0	0	
	0	2							
DAREA	202005	202005		9.999998					
TLOAD2	202005	202005		0	0.9	0.95	0	0	
	0	1							
DAREA	212005	202005		-199.999					
TLOAD2	212005	212005		0	0.9	0.95	0	0	
	0	2							
$.....	$.....	$.....	$.....	$.....	$.....	$.....	$.....	$.....	$.....
NOLIN2	2	11	3	-1	100002		400000		
=	=	=	=	=	*2000	=	*2000		
NOLIN2	2	12	3	-1	100003		400000		
=	=	=	=	=	*2000	=	*2000		
NOLIN2	2	13	3	-1	100004		400000		
=	=	=	=	=	*2000	=	*2000		
NOLIN2	2	10	5	-1	200001		400000		
=	=	=	=	=	*2000	=	*2000		
NOLIN2	2	11	5	-1	200002		400000		
=	=	=	=	=	*2000	=	*2000		
NOLIN2	2	12	5	-1	200003		400000		
=	=	=	=	=	*2000	=	*2000		
NOLIN2	2	13	5	-1	200004		400000		

Table F.3 (continuation)

=	=	=	=	=	*2000	=	*2000		
NOLIN2	2	14	5	-1	200005		400000		
=	=	=	=	=	*2000	=	*2000		
$.....	$.....	$.....	$.....	$.....	$.....	$.....	$.....	$.....	$.....
NOLIN2	2	400000		1	100002		11	3	
=	=	*2000	=	=	*2000	=	=	=	
NOLIN2	2	400000		1	100003		12	3	
=	=	*2000	=	=	*2000	=	=	=	
NOLIN2	2	400000		1	100004		13	3	
=	=	*2000	=	=	*2000	=	=	=	
NOLIN2	2	400000		1	200001		10	5	
=	=	*2000	=	=	*2000	=	=	=	
NOLIN2	2	400000		1	200002		11	5	
=	=	*2000	=	=	*2000	=	=	=	
NOLIN2	2	400000		1	200003		12	5	
=	=	*2000	=	=	*2000	=	=	=	
NOLIN2	2	400000		1	200004		13	5	
=	=	*2000	=	=	*2000	=	=	=	
NOLIN2	2	400000		1	200005		14	5	
=	=	*2000	=	=	*2000	=	=	=	
$.....	$.....	$.....	$.....	$.....	$.....	$.....	$.....	$.....	$.....
NOLIN2	2	500000		1	100002		11	3	
=	=	*2000	=	=	*2000	=	=	=	
NOLIN2	2	500000		1	100003		12	3	
=	=	*2000	=	=	*2000	=	=	=	
NOLIN2	2	500000		1	100004		13	3	
=	=	*2000	=	=	*2000	=	=	=	
NOLIN2	2	500000		1	200001		10	5	
=	=	*2000	=	=	*2000	=	=	=	
NOLIN2	2	500000		1	200002		11	5	
=	=	*2000	=	=	*2000	=	=	=	
NOLIN2	2	500000		1	200003		12	5	
=	=	*2000	=	=	*2000	=	=	=	
NOLIN2	2	500000		1	200004		13	5	
=	=	*2000	=	=	*2000	=	=	=	
NOLIN2	2	500000		1	200005		14	5	
=	=	*2000	=	=	*2000	=	=	=	
$.....	$.....	$.....	$.....	$.....	$.....	$.....	$.....	$.....	$.....
DAREA	10	10	3	10000					
TLOAD2	10	10		0	0.5	0.55	0	0	
	0	0							
DAREA	10010	10	3	-199999					
TLOAD2	10010	10010		0	0.5	0.55	0	0	
	0	1							
DAREA	2010	10	3	20000					
TLOAD2	2010	2010		0	0.75	0.8	0	0	
	0	0							

Table F.3 (continuation)

DAREA	12010	10	3	-399999					
TLOAD2	12010	12010		0	0.75	0.8	0	0	
	0	1							
DAREA	11	11	3	199999.9					
TLOAD2	11	11		0	0.5	0.6	0	0	
	0	1							
DAREA	10011	11	3	-399999					
TLOAD2	10011	10011		0	0.55	0.6	0	0	
	0	1							
DAREA	2011	11	3	399999.9					
TLOAD2	2011	2011		0	0.75	0.85	0	0	
	0	1							
DAREA	12011	11	3	-799999					
TLOAD2	12011	12011		0	0.8	0.85	0	0	
	0	1							
DAREA	12	12	3	200000					
TLOAD2	12	12		0	0.55	0.65	0	0	
	0	1							
DAREA	10012	12	3	-400000					
TLOAD2	10012	10012		0	0.6	0.65	0	0	
	0	1							
DAREA	2012	12	3	400000.1					
TLOAD2	2012	2012		0	0.8	0.9	0	0	
	0	1							
DAREA	12012	12	3	-800000					
TLOAD2	12012	12012		0	0.85	0.9	0	0	
	0	1							
DAREA	13	13	3	200000					
TLOAD2	13	13		0	0.6	0.7	0	0	
	0	1							
DAREA	10013	13	3	-399999					
TLOAD2	10013	10013		0	0.65	0.7	0	0	
	0	1							
DAREA	2013	13	3	400000.1					
TLOAD2	2013	2013		0	0.85	0.95	0	0	
	0	1							
DAREA	12013	13	3	-799999					
TLOAD2	12013	12013		0	0.9	0.95	0	0	
	0	1							
DAREA	14	14	3	199999.9					
TLOAD2	14	14		0	0.65	0.7	0	0	
	0	1							
DAREA	2014	14	3	399999.9					
TLOAD2	2014	2014		0	0.9	0.95	0	0	
	0	1							
$.....	$.....	$.....	$.....	$.....	$.....	$.....	$.....	$.....	$.....
DLOAD	999	1	1	100001	1	110001	1	120001	

Table F.3 (continuation)

	1	*102001*	*1*	*112001*	*1*	*122001*	*1*	*100002*	
	1	*110002*	*1*	*120002*	*1*	*130002*	*1*	*140002*	
	1	*102002*	*1*	*112002*	*1*	*122002*	*1*	*132002*	
	1	*142002*	*1*	*100003*	*1*	*110003*	*1*	*120003*	
	1	*130003*	*1*	*140003*	*1*	*102003*	*1*	*112003*	
	1	*122003*	*1*	*132003*	*1*	*142003*	*1*	*100004*	
	1	*110004*	*1*	*120004*	*1*	*130004*	*1*	*140004*	
	1	*102004*	*1*	*112004*	*1*	*122004*	*1*	*132004*	
	1	*142004*	*1*	*130005*	*1*	*140005*	*1*	*132005*	
	1	*142005*	*1*	*200001*	*1*	*210001*	*1*	*202001*	
	1	*212001*	*1*	*200002*	*1*	*210002*	*1*	*220002*	
	1	*230002*	*1*	*202002*	*1*	*212002*	*1*	*222002*	
	1	*232002*	*1*	*200003*	*1*	*210003*	*1*	*220003*	
	1	*230003*	*1*	*202003*	*1*	*212003*	*1*	*222003*	
	1	*232003*	*1*	*200004*	*1*	*210004*	*1*	*220004*	
	1	*230004*	*1*	*202004*	*1*	*212004*	*1*	*222004*	
	1	*232004*	*1*	*200005*	*1*	*210005*	*1*	*202005*	
	1	*212005*	*1*	*10*	*1*	*10010*	*1*	*2010*	
	1	*12010*	*1*	*11*	*1*	*10011*	*1*	*2011*	
	1	*12011*	*1*	*12*	*1*	*10012*	*1*	*2012*	
	1	*12012*	*1*	*13*	*1*	*10013*	*1*	*2013*	
	1	*12013*	*1*	*14*	*1*	*2014*			
$.....*	*$*.....*	*$*.....*	*$*.....*	*$*.....*	*$*.....*	*$*.....*	*$*.....*	*$*.....*	*$*.....*

G

ANALYSIS OF OBJECTIVE FUNCTION

The objective function is illustrated in Figures G.1 to G.6. The following steps are carried out for the generation of these figures:

- Obtain axle weights using static algorithm.
- Obtain axle weights using dynamic algorithm.
- Compare both solutions to known input weights for simulation.
- Plot contours for various parameters in this multi-variable optimisation problem to show how sometimes the solution might be missed.

In Figure G.1, front axle weight and speed are varied. A small change in speed has a strong influence on the value of the objective function (more sharp than Figure 7.13). The objective function for the dynamic approach has greater curvature.

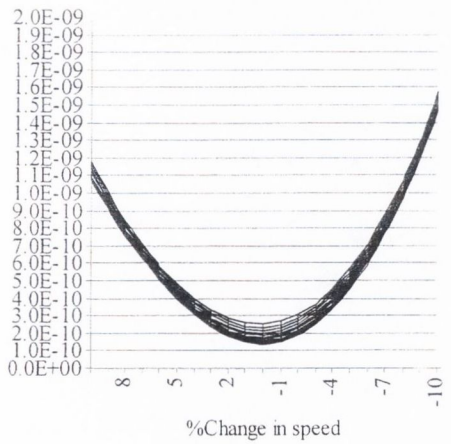

(a) Linear static approach (-10% to 10%)

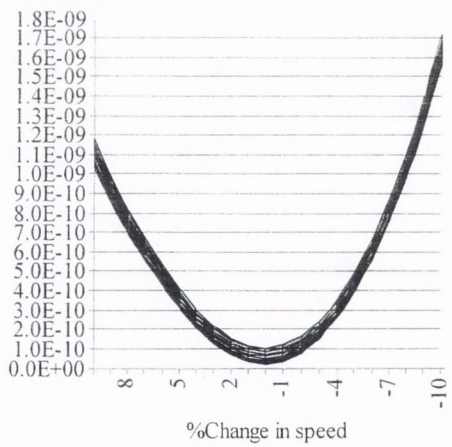

(b) Linear dynamic approach (-10% to 10%)

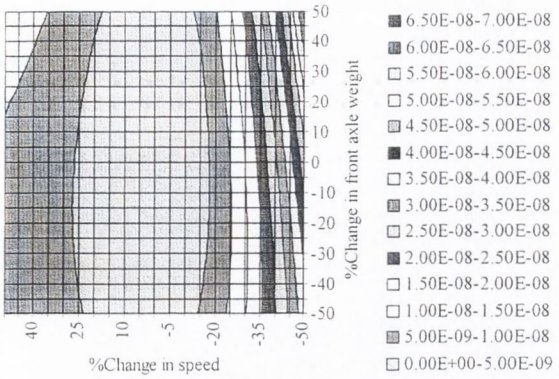

(c) Linear static approach (-50% to 50%)

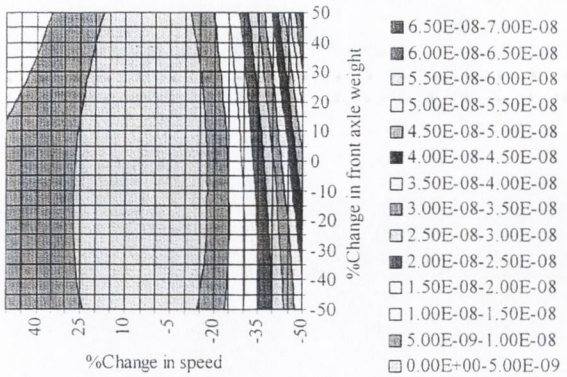

(d) Linear dynamic approach (-50% to 50%)

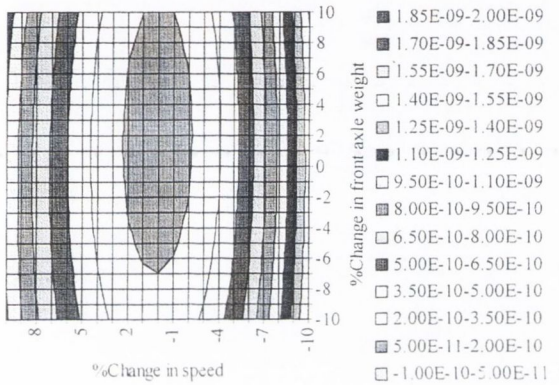

(e) Linear static approach (-10% to 10%)

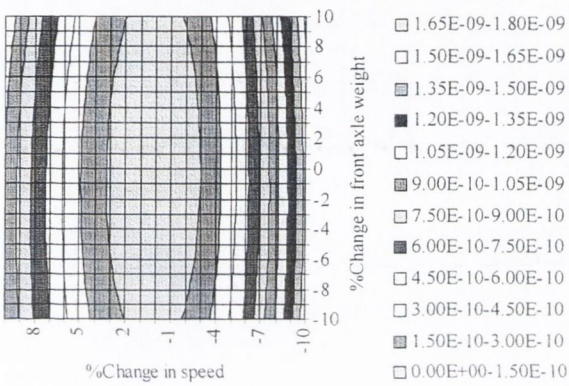

(f) Linear dynamic approach (-10% to 10%)

Figure G.1 - Objective function for variables: Front axle weight and speed

The same conclusions are obtained when rear axle weight and speed are modified (Figure G.2). In this case there is a slight skew in the contours.

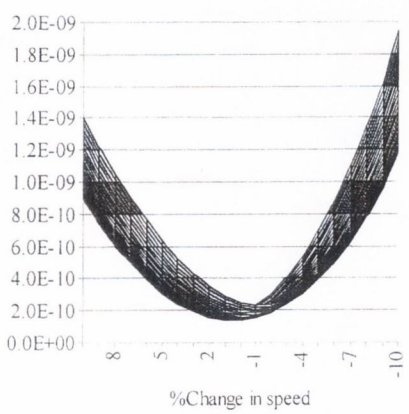

(a) Linear static approach (-10% to 10%)

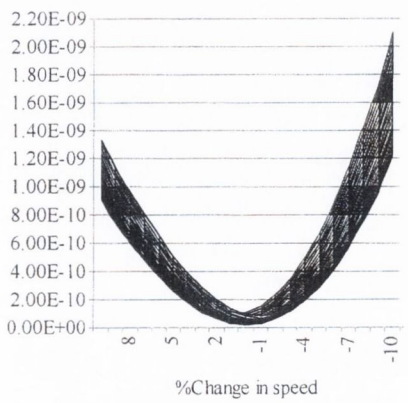

(b) Linear dynamic approach (-10% to 10%)

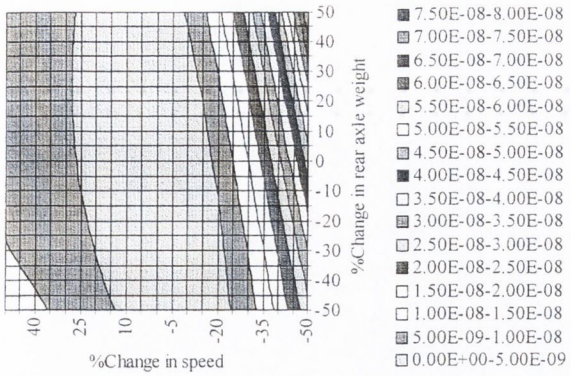

(c) Linear static approach (-50% to 50%)

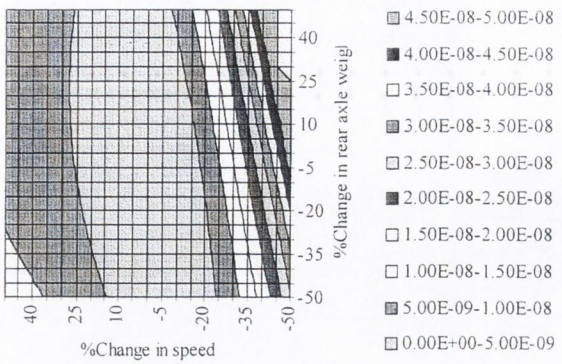

(d) Linear dynamic approach (-50% to 50%)

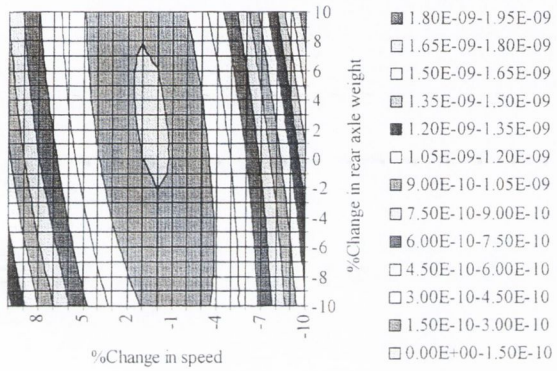

(e) Linear static approach (-10% to 10%)

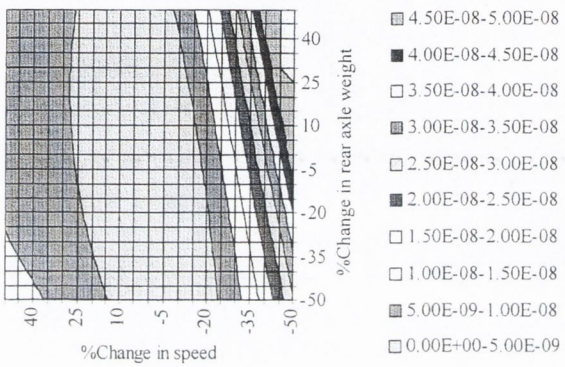

(f) Linear dynamic approach (-10% to 10%)

Figure G.2 - Objective function for variables: Rear axle weight and speed

In Figure G.3, the effect of a change in axle spacing and front axle weight on the objective function is analysed. It can be seen that optimisation does not lead a fully accurate solution in the static case. In Figure G.3(e), the ordinate for a 0% change in axle weight meets the 0% change in axle spacing out of the solution area, and about 2% error would result. The dynamic approach finds the exact solution inside the area where the objective function contours are closer. A good estimation of the initial value of axle spacing will speed up the optimisation process.

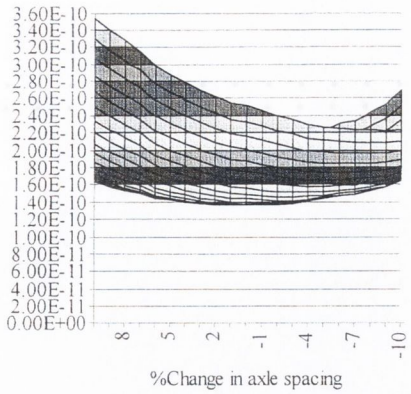

(a) Linear static approach (-10% to 10%)

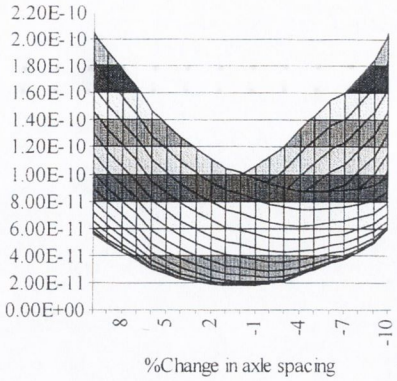

(b) Linear dynamic approach (-10% to 10%)

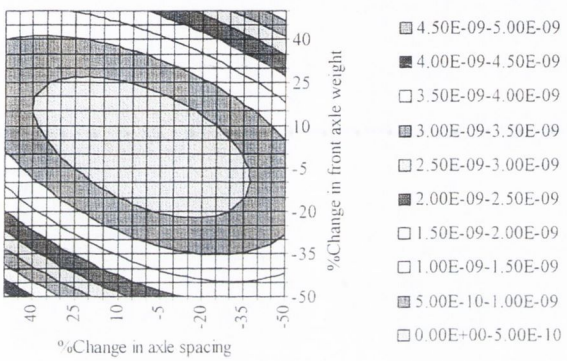

(c) Linear static approach (-50% to 50%)

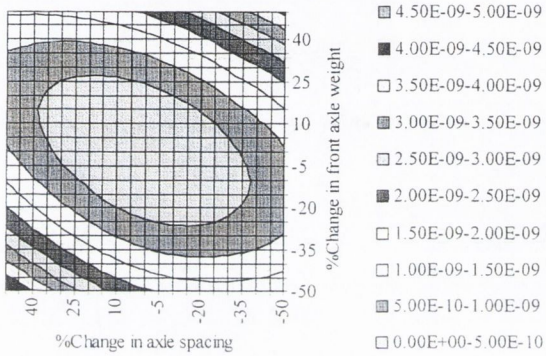

(d) Linear dynamic approach (-50% to 50%)

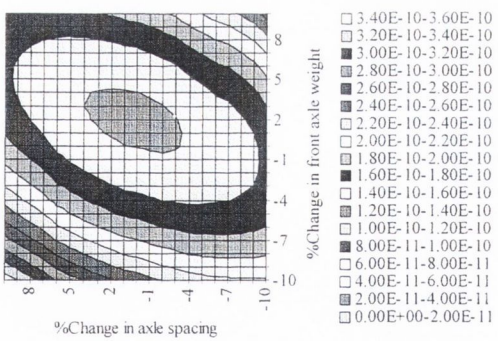

(e) Linear static approach (-10% to 10%)

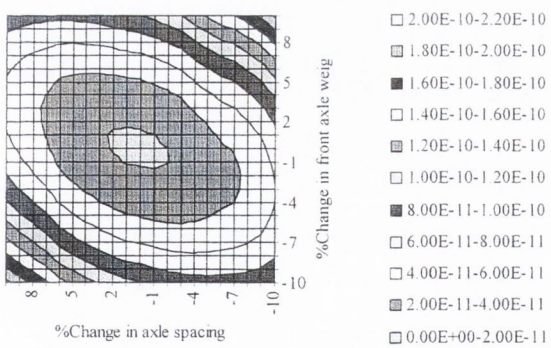

(f) Linear dynamic approach (-10% to 10%)

Figure G.3 - Objective function for variables: Front axle weight and axle spacing

Figure G.4 studies the influence of speed and rear axle weight on the objective function. The same conclusions as before apply.

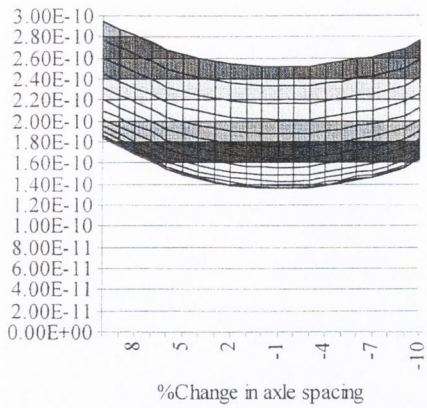

(a) Linear static approach (-10% to 10%)

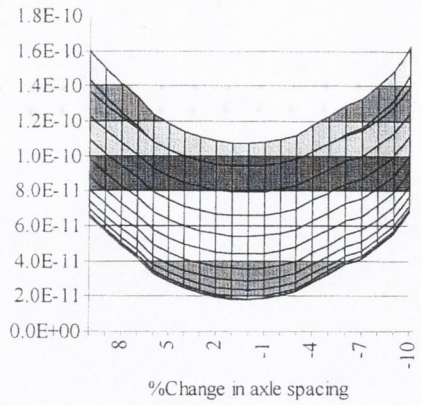

(b) Linear dynamic approach (-10% to 10%)

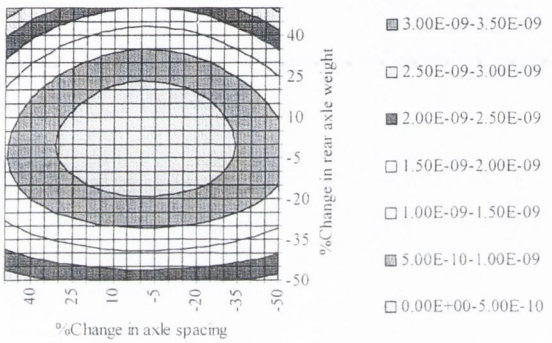

(c) Linear static approach (-50% to 50%)

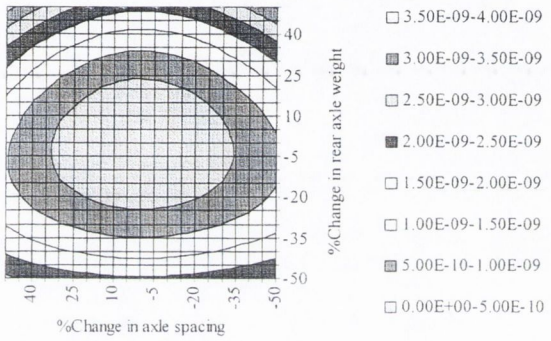

(d) Linear dynamic approach (-50% to 50%)

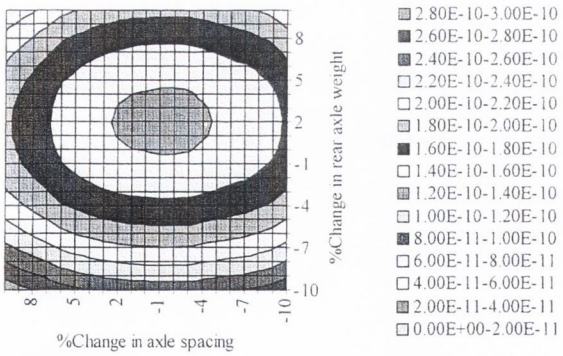

(e) Linear static approach (-10% to 10%)

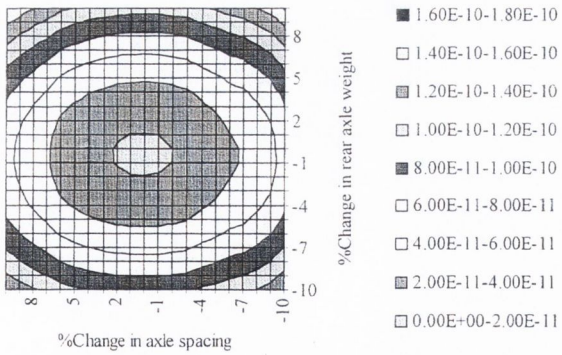

(f) Linear dynamic approach (-10% to 10%)

Figure G.4 - Objective function for variables: Rear axle weight and axle spacing

Finally, Figure G.5 shows the influence of axle spacing and speed. A small error in any of these two variables has a very negative effect on the final accuracy of both algorithms. Speed

and axle spacing appear to be dependent, and there is insufficient to solve for both using optimisation.

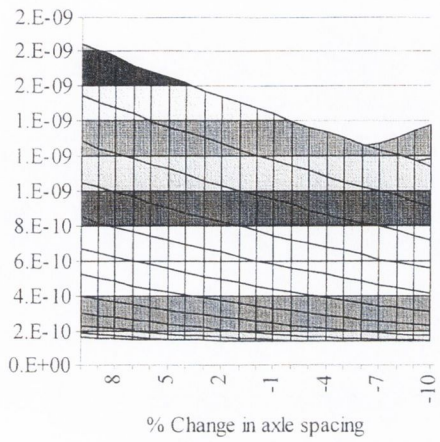

(a) Linear static approach (-10% to 10%)

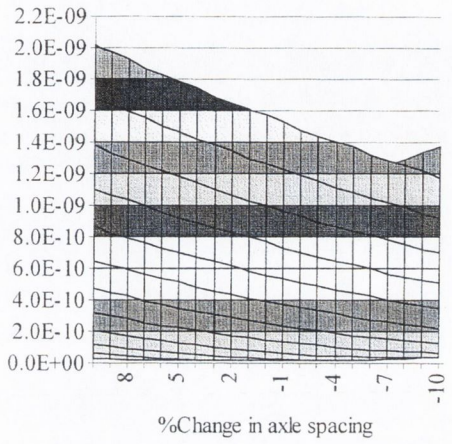

(b) Linear dynamic approach (-10% to 10%)

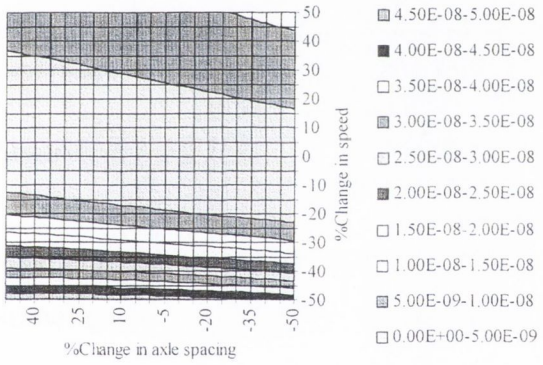

(c) Linear static approach (-50% to 50%)

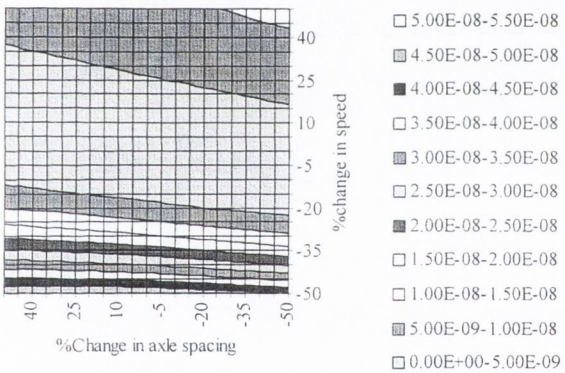

(d) Linear dynamic approach (-50% to 50%)

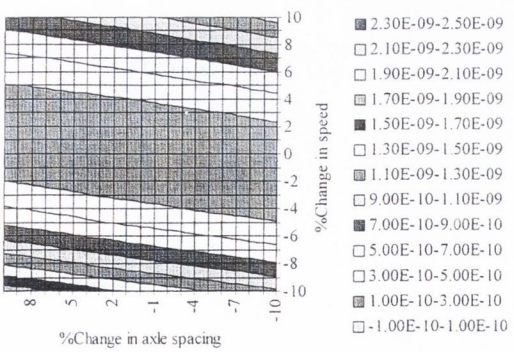

(c) Linear static approach (-10% to 10%)

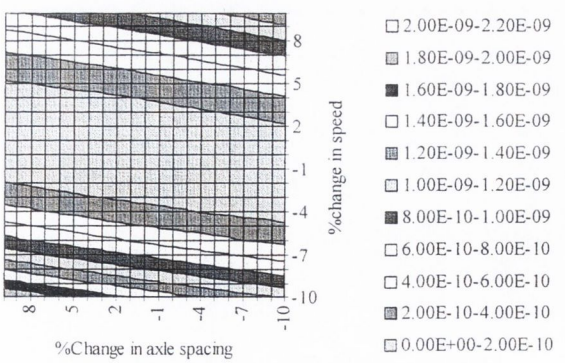

(d) Linear dynamic approach (-10% to 10%)

Figure G.5 - Objective function for variables: Speed and axle spacing

H

CONTENTS OF CD-ROM

The CD-ROM supplied with the thesis contains all the source code developed by the author, plus an electronic version of the thesis. Dynamic models, results from theoretical simulations and measurements on the field are also included. Table H.1 lists the folders contained in the CD-ROM disc. Word documents inside the folders explain in detail their content (i.e., instructions for running the programs).

Table H.1 – List of Folders

Folder name	**Content**	**Chapters**
Thesis	Electronic version of the thesis	1 to 10
Algorithm	Source code for B-WIM algorithms	3, 7
BWIM	Source code for B-WIM system	4
Nastran	Finite element models, results and code for simulations	6
Numerical	Planar models, results and code for numerical simulations	5
Experimental	Measurements from experiments	8

References

- Baumgärtner, W. (1998), 'Bridge-truck interaction: simulation, measurements and load identification', in *5th International Symposium on Heavy Vehicle Weights and Dimensions*, Maroochydore, Australia, March/April.
- Baumgärtner, W. (1999), 'Bridge-Vehicle Interaction using Extended FE Analysis', *Heavy Vehicle Systems, Int. Journal of Vehicle Design*, Vol. **6**, Nos. 1-4, pp.1–12.
- Blab, R., Stanczyk, D. & Caprez, M. (1997), 'European activities on Weigh-In-Motion (WIM) systems on roads', in *Proceedings of the WAVE Mid-Term Seminar*, Published by the Laboratoire Central des Ponts et Chaussées (LCPC), Delft, Holland, pp. 109-118, September.
- Caprez, M. (1998), 'WIM Application to Pavements', in *Pre-proceedings of the 2nd European Conference on Weigh-In-Motion*, eds. E.J. O'Brien & B. Jacob, Lisbon, Portugal, pp. 281-290.
- Cantieni, R. (1983), 'Dynamic Load Tests on Highway Bridges in Switzerland – 60 Years Experience of EMPA' in *EMPA Report No. 211, Swiss Federal Laboratories for Materials Testing and Research*, Dübendorf, Switzerland.
- Caussignac, J-M., Larcher, S. & Rougier, J.C. (1998), 'Weigh-In-Motion using Optical Fibre Technology', in *Pre-proceedings of the 2nd European Conference on Weigh-In-Motion*, eds. E.J. O'Brien & B. Jacob, Lisbon, Portugal, pp. 429-434.
- Caussignac, J-M. & Rougier, J-C. (1999), 'Fibre Optic WIM Sensor and Optoelectronic System – Preliminary Tests', in *Proceedings of the Final Symposium of the project WAVE*, Ed. B. Jacob, Hermes Science Publications, Paris, France, pp. 255-264.
- Cebon, D. (1999), 'Multiple-Sensor WIM Systems', in *Proceedings of the Final Symposium of the project WAVE*, Ed. B. Jacob, Hermes Science Publications, Paris, France, pp. 177-196.

- Chompooming, K. & Yener, M. (1995), 'The Influence of Roadway Surface Irregularities and Vehicle Deceleration on Bridge Dynamics using the Method of Lines', *Journal of Sound and Vibration*, Vol. **183**, No. 4, pp. 567–589.
- Chou, C.P. & Tsai, H.-Y. (1999), 'Study of the Application of High Speed Weigh-In-Motion to Law Enforcement', in *Post-proceedings of the 2nd European Conference on Weigh-In-Motion*, eds. E.J. O'Brien & B. Jacob, Lisbon, Portugal, pp. 27-36.
- Cifuentes, A.O. (1989a), *Using MSC/NASTRAN: Statics and Dynamics*, Springer-Verlag New York Inc.
- Cifuentes, A.O. (1989b), "Dynamic response of a beam excited by a moving mass", *Finite Elements in Analysis and Design 5*, Elsevier Science Publishers B.V., Amsterdam, pp. 237-246.
- Clough, R.W. & Penzien, J. (1975), *Structural Dynamics*, McGraw Hill.
- Collop, A.C., Al-Hakim, B., Thom, N.H. & Lloyd, W.G. (1998), 'The use of WIM Data in Traffic Assessment', in *Pre-proceedings of the 2nd European Conference on Weigh-In-Motion*, eds. E.J. O'Brien & B. Jacob, Lisbon, Portugal, pp. 303-312.
- Craig, R.R.Jr. (1981), *Structural Dynamics*, John Wiley & Sons.
- Crémona, C. & Carracilli, J. (1998), 'Evaluation of Extreme Traffic Load Effects in Cable Stayed and Suspension Bridges', in *Pre-proceedings of the 2nd European Conference on Weigh-In-Motion*, eds. E.J. O'Brien & B. Jacob, Lisbon, Portugal, pp. 243-252.
- COST323 (1996), *Terminology of WIM (Glossary of Terms)*, Draft 1.2, EUCO_COST/323/8/96, ed. B. Jacob, LCPC, Paris, August.
- COST323 (1997), *European Specification on Weigh-In-Motion of Road Vehicles*, Draft 2.2, EUCO_COST/323/6/97, ed. B. Jacob, LCPC, Paris, June.
- Dempsey, A.T. (1997), 'The Accuracy of Bridge Weigh-In-Motion Systems', Ph.D. Thesis, Trinity College Dublin, Ireland.
- Dempsey, A.T., Jacob, B. & Carracilli, J. (1998a), 'Orthotropic Bridge Weigh-In-Motion for Determining Axle and Gross Vehicle Weights', in *Pre-proceedings of the 2nd European Conference on Weigh-In-Motion*, eds. E.J. O'Brien & B. Jacob, Lisbon, Portugal, pp. 435-444.

- Dempsey, A.T., Žnidaric, A. & O'Brien. E.J. (1998b), 'Development of a Dynamic Bridge Weigh-In-Motion Algorithm' in *Proceedings of the 5th International Symposium on Heavy Vehicles Weights and Dimensions*, Maroochydore, Australia.
- Dempsey, A.T. & Brady, S.P. (1999), 'Verification of Assumptions in the Dynamic Multiple Sensor Bridge Weigh-In-Motion Algorithm – The Effect of Superposition of Moving Constant Loads on Simply Supported Beams', *Departmental Report 1999-01, Department of Civil Engineering, University College Dublin*, Dublin.
- Dempsey, A.T., Jacob, B. & Carracilli, J. (1999a), 'Orthotropic Bridge WIM for determining Axle and Gross Vehicle Weights', in *Proceedings of the Final Symposium of the project WAVE*, Ed. B. Jacob, Hermes Science Publications, Paris, France, pp. 227-238.
- Dempsey, A., Žnidaric, A., Brady, S., González, A., O'Brien, E. & Lavric, I. (1999b), 'A Free Axle Detection Bridge Weigh In Motion System', presented in *Fifth Series of Vehicle-Infrastructure Interaction Conferences*, Cracovia, Polland, September.
- Dempsey, A., Keogh, D. & Jacob, B. (2000) 'Orthotropic Steel Bridges: Management Tools for Live Load and Fatigue Assessment', *Bridge Management Four*, Edited by M.J. Ryall, G.A.R. Parker and J.E. Harding, Thomas Telford, University of Surrey, UK, pp. 592-600.
- Dijk, R.V. (1999), 'Enforcement of Regulations concerning Overloading by the Introduction of a WIM-VID Network on the Motorways in the Netherlands', in *Proceedings of the Final Symposium of the project WAVE*, Ed. B. Jacob, Hermes Science Publications, Paris, France, pp. 69-72.
- Dolcemascolo, V. & Jacob, B. (1998), 'Multiple Sensor Weigh-In-Motion: Optimal Design and Experimental Study', in *Pre-proceedings of the 2nd European Conference on Weigh-In-Motion*, eds. E.J. O'Brien & B. Jacob, Lisbon, Portugal, pp. 129-138.
- Dolcemascolo, V., Jacob, B., Boutillier, B. & Reversat-Brulant, L. (1998), 'Accuracy Assessment of a Low Speed Weigh-In-Motion System', in *Pre-proceedings of the 2nd European Conference on Weigh-In-Motion*, eds. E.J. O'Brien & B. Jacob, Lisbon, Portugal, pp. 345-354.

- Dolcemascolo, V. (1999), 'Performance of Multiple-Sensor WIM Systems by Testing', in *Proceedings of the Final Symposium of the project WAVE*, Ed. B. Jacob, Hermes Science Publications, Paris, France, pp. 195-202.
- Dolcemascolo, V. & Jacob, B. (1999), 'Use of Multiple Sensor WIM for Enforcement and Road Pricing', in *Proceedings of the Final Symposium of the project WAVE*, Ed. B. Jacob, Hermes Science Publications, Paris, France, pp. 33-44.
- Dunmill, I.R. (1998), 'The Development of an OIML International Recommendation for Automatic Instruments for Weighing Road Vehicles in Motion', in *Pre-proceedings of the 2nd European Conference on Weigh-In-Motion*, eds. E.J. O'Brien & B. Jacob, Lisbon, Portugal, pp. 185-192.
- Fertis, D.G. (1995), *Mechanical and Structural Vibrations*, John Wiley & Sons, Inc.
- Flanigan, C.C. (1994), 'Accurate Enforced Motion Analysis using MSC/NASTRAN Superelements', in *1994 MSC/NASTRAN World Users Conference,* Orlando, Florida, June 20-24.
- Frýba, L. (1972), *Vibration of Solids and Structures under Moving Loads*, Noordhoff International Publishing, Groningen, The Netherlands.
- Gagarin, N., Flood, I. & Albrecht, P. (1994), 'Computing Truck Attributes with Artificial Neural Networks', *Journal of Computing in Civil Engineering*, ASCE, Vol. **8**, No. 2, April, pp. 179 – 200.
- Gangarao, H.V.S. & Vali, A. (1990), 'Truck-tire Steel Grid Deck Contact Pressure Distribution', *Journal of Structural Engineering*, ASCE (US), Vol. **116**, No. 3, March, pp. 791 – 808.
- George, L.-A. (1999), 'User's Remaining Needs for WIM', in *Proceedings of the Final Symposium of the project WAVE*, Ed. B. Jacob, Hermes Science Publications, Paris, France, pp. 141-146.
- Ghosn, M. & Xu, Q., 'Estimating Bridge Dynamics Using the Weigh-In-Motion Algorithm' in *Transportation Research Record 1200, Department of Civil Engineering, The City College of New York*, New York.
- González, A. (1996), 'Bridge Weigh In Motion for Horizontal Loading', M.Sc. Thesis, Trinity College Dublin, Ireland.

- González, A. & O'Brien, E.J. (1998), 'The Development of a Dynamic Bridge Weigh-In-Motion Algorithm', in *Pre-proceedings of the 2nd European Conference on Weigh-In-Motion*, eds. E.J. O'Brien & B. Jacob, Lisbon, Portugal, pp. 445-453.
- González, A. Brady, S.P. & O'Brien, E.J. (1999), 'A Dynamic Multi-Sensor Bridge Weigh-In-Motion Algorithm', in *Proceedings of the Final Symposium of the project WAVE*, Ed. B. Jacob, Hermes Science Publications, Paris, France, pp. 209-216.
- Green, M. & Cebon, D. (1994), 'Dynamic Response of Highway Bridges to Heavy Vehicle Loads: Theory and Experimental Validation', *Journal of Structural Engineering*, ASCE, Vol. **121**, No. 2, February, pp. 272–282.
- Green, M., Cebon, D. & Cole D.J. (1995), 'Effects of Vehicle Suspension Design on Dynamics of Highway Bridges', *Journal of Structural Engineering*, ASCE, Vol. **121**, No. 2, February, pp. 272–282.
- Hambly, E.C. (1991), *Bridge Deck Behaviour*, 2nd Edition, Chapman & Hall.
- Hallström, B. (1999), 'Durability Implications of Cold Climates on WIM System', in *Proceedings of the Final Symposium of the project WAVE*, Ed. B. Jacob, Hermes Science Publications, Paris, France, pp. 93-100.
- Henau, A.D. (1998), 'Weigh In Motion of Road Vehicles in Belgium', in *Pre-proceedings of the 2nd European Conference on Weigh-In-Motion*, eds. E.J. O'Brien & B. Jacob, Lisbon, Portugal, pp. 419-428.
- Henau, A.D. & Jacob, B. (1998), 'European Test Programme of WIM Systems: Cold Environmental Test and Continental Motorway Test', in *Pre-proceedings of the 2nd European Conference on Weigh-In-Motion*, eds. E.J. O'Brien & B. Jacob, Lisbon, Portugal, pp. 381-388.
- Henny, R. (1997), 'Quality Assurance of WIM Data', in *Proceedings of the WAVE Mid-Term Seminar*, Published by the Laboratoire Central des Ponts et Chaussées (LCPC), Delft, Holland, pp. 37-44, September.
- Henny, R.J. (1999), 'Experimental Use of WIM with Video for Control of Overloading', in *Post-proceedings of the 2nd European Conference on Weigh-In-Motion*, eds. E.J. O'Brien & B. Jacob, Lisbon, Portugal, pp. 37-46.

- Hoose, N. & Kunz, J. (1998), 'Implementation and Tests of a Quartz Crystal Sensor WIM System', in *Pre-proceedings of the 2nd European Conference on Weigh-In-Motion*, eds. E.J. O'Brien & B. Jacob, Lisbon, Portugal, pp. 461-466.
- Huhtala, M., Halonen, P. & Miettinen, V. (1998), 'Cold Environmental Test at Luleå: Calibration of WIM Systems using an Instrumented Vehicle', in *Pre-proceedings of the 2nd European Conference on Weigh-In-Motion*, eds. E.J. O'Brien & B. Jacob, Lisbon, Portugal, pp. 409-418.
- Huhtala, M. (1999), 'Factors affecting Calibration Effectiveness', in *Proceedings of the Final Symposium of the project WAVE*, Ed. B. Jacob, Hermes Science Publications, Paris, France, pp. 297-306.
- Hwang, E.-S. & Nowak, A.S. (1991), 'Simulation of Dynamic Load for Bridges', *Journal of Structural Engineering*, ASCE, Vol. **117**, No. 5, May, pp. 1413–1434.
- Jacob, B. & O'Brien, E.J. (1997), 'European Specification on Weigh-In_Motion of Road Vehicles', in *Proceedings of the WAVE Mid-Term Seminar*, Published by the Laboratoire Central des Ponts et Chaussées (LCPC), Delft, Holland, pp. 19-36, September.
- Jacob, B. (1998a), 'Action COST 323: Weigh-In-Motion of Road Vehicles', in *Pre-proceedings of the 2nd European Conference on Weigh-In-Motion*, eds. E.J. O'Brien & B. Jacob, Lisbon, Portugal, pp. 25-33.
- Jacob, B. (1998b), 'Application of Weigh-In-Motion Data to Fatigue of Road Bridges', in *Pre-proceedings of the 2nd European Conference on Weigh-In-Motion*, eds. E.J. O'Brien & B. Jacob, Lisbon, Portugal, pp. 219-230.
- Jacob, B. & Dolcemascolo, V. (1998), 'Spatial Repeatability of Dynamic Loading on a Pavement', in *Pre-proceedings of the 2nd European Conference on Weigh-In-Motion*, eds. E.J. O'Brien & B. Jacob, Lisbon, Portugal, pp. 291-302.
- Jacob, B. & O'Brien E.J. (1998), 'European Specification on Weigh-In-Motion of Road Vehicles (COST323)', in *Pre-proceedings of the 2nd European Conference on Weigh-In-Motion*, eds. E.J. O'Brien & B. Jacob, Lisbon, Portugal, pp. 171-184.
- Jacob, B. (1999), 'WAVE – European Research Project on WIM', in *Proceedings of the Final Symposium of the project WAVE*, Ed. B. Jacob, Hermes Science Publications, Paris, France, pp. 15-30.

- Jacob, B. & Stanczyk, D. (1999), 'Calibration of Highly Accurate WIM Systems for Legal Applications', in *Proceedings of the Final Symposium of the project WAVE*, Ed. B. Jacob, Hermes Science Publications, Paris, France, pp. 55-68.
- Jacob, B., O'Brien E.J. & Stanczyk, D. (2000), *WAVE Final Report*, Ed. B. Jacob, Hermes Science Publications, Paris, France.
- Jehaes, S. & Hallström, B. (1998), 'Accuracy Analysis of WIM systems for the Cold Environmental Test: Final Results', in *Post-proceedings of the 2nd European Conference on Weigh-In-Motion*, eds. E.J. O'Brien & B. Jacob, Lisbon, Portugal, pp. 63-72.
- Jehaes, S. (1999a), 'European Test Programme of WIM Systems', in *Proceedings of the Final Symposium of the project WAVE*, Ed. B. Jacob, Hermes Science Publications, Paris, France, pp. 81-92.
- Jehaes, S. (1999b), 'Test of WIM Systems in Cold Climates', in *Proceedings of the Final Symposium of the project WAVE*, Ed. B. Jacob, Hermes Science Publications, Paris, France, pp. 285-296.
- Kealy, N.J. (1997), 'The Development of a Multiple Longitudinal Sensor Location Bridge Weigh-In-Motion System', M.Sc. Thesis, Trinity College Dublin, Ireland.
- Kealy, N.J. & O'Brien, E.J. (1998), 'The Development of a Multi-sensor Bridge Weigh-In-Motion System', *5th International Symposium on Heavy Vehicle Weights and Dimensions*, Maroochydore, Australia, March/April, pp. 222-235.
- Kessler, K. (1997), 'Analysis of Measured and Simulation Data with respect to Truck Load Identification', Diploma Work, Technische Universität München Lehrstuhl für Baumechanic.
- Kirkegaard, P.H, Nielsen, S.R.K. & Enevoldsen, I. (1997), 'Heavy vehicles on minor highway bridges – Dynamic modelling of vehicles and bridges', Department of Building Technology and Structural Engineering, Aalborg University, ISSN 1395-7953 R9721, December.
- Lutzenberger, S. & Baumgärtner, W. (1999), 'Interaction of an Instrumented Truck crossing Belleville Bridge', in *Proceedings of the Final Symposium of the project WAVE*, Ed. B. Jacob, Hermes Science Publications, Paris, France, pp. 239-240.
- Lutzenberger, S. & Baumgärtner, W. (2000) 'Evaluation of Measured Bridge Responses due to an Instrumented Truck and Free Traffic', *Bridge Management*

Four, Edited by M.J. Ryall, G.A.R. Parker and J.E. Harding, Thomas Telford, University of Surrey, UK, pp. 72-80.

- Major, A. (1980), *Dynamics in Civil Engineering IV*, Akademiai Kiado, Budapest.
- Marchadour, Y. (1998), 'Weighing of Road Vehicles in France for Enforcement ', in *Pre-proceedings of the 2nd European Conference on Weigh-In-Motion*, eds. E.J. O'Brien & B. Jacob, Lisbon, Portugal, pp. 339-344.
- McNulty, P. (1999), 'Testing of an Irish Bridge Weigh In Motion System', M.Sc. Thesis, University College Dublin, Ireland.
- Michaltsos, G., Sophianopoulos, D. & Kounadis, A.N. (1996), 'The Effect of a Moving Mass and other Parameters on the Dynamic Response of a Simply Supported Beam', *Journal of Sound and Vibration*, ASCE, Vol. **191**, No. 3, pp. 357–362.
- Missen, R. (1998), 'European Legislation on the Maximum Weights and Dimensions of Motor Vehicles', in *Pre-proceedings of the 2nd European Conference on Weigh-In-Motion*, eds. E.J. O'Brien & B. Jacob, Lisbon, Portugal, pp. 3-12.
- Moses, F. (1979), 'Weigh-In-Motion System using Instrumented Bridges', Transportation Engineering Journal, ASCE, **105**, TE3, pp. 233-249.
- MSC/NASTRAN for Windows (1997a), *User's Guide*, The MacNeal-Schwendler Corporation, USA.
- MSC/NASTRAN for Windows (1997b), *Command Reference Guide*, The MacNeal-Schwendler Corporation, USA.
- MSC/NASTRAN for Windows (1997c), *Basic Dynamic Analysis User's Guide Version 69*, The MacNeal-Schwendler Corporation, USA.
- MSC/NASTRAN for Windows (1997d), *Advanced Dynamic Analysis User's Guide Version 70*, The MacNeal-Schwendler Corporation, USA.
- MSC/NASTRAN for Windows (1998), *Quick Reference Guide Version 70.5*, The MacNeal-Schwendler Corporation, USA.
- MSC/NASTRAN for Windows (1999), *Quick Start Guide*, The MacNeal-Schwendler Corporation, USA.
- Narayanan R. & Roberts T.M. (1991), *Structures Subjected to Dynamic Loading, Stability and Strength*, Elsevier Science Publishers LTD.

- Nashif, A.D., Jones, D.I.G. & Henderson, J.P. (1985), *Vibration Damping*, John Wiley & Sons, Inc.
- National Instruments (1993), *SCXI-1321 Offset-Null and Shunt-Calibration Terminal Block Installation Guide*, Part Number 320622-01, National Instruments Corporation, August.
- National Instruments (1994), *SCXI-1121 User Manual*, National Instruments Corporation.
- National Instruments (1996), *SCXI™ Chassis User Manual*, National Instruments Corporation.
- Newton, W.H. (1998), 'Enforcement Applications of Weigh-In-Motion', in *Pre-proceedings of the 2nd European Conference on Weigh-In-Motion*, eds. E.J. O'Brien & B. Jacob, Lisbon, Portugal, pp. 331-338.
- Newton, W. (1999), 'Use and Applications of WIM Data', in *Proceedings of the Final Symposium of the project WAVE*, Ed. B. Jacob, Hermes Science Publications, Paris, France, pp. 123-130.
- O'Brien, E.J., Dempsey, A.T., Žnidaric, A. & Baumgärtner, W. (1997), 'Development of Bridge WIM Systems and Procedures', in *Proceedings of the WAVE Mid-Term Seminar*, Published by the Laboratoire Central des Ponts et Chaussées (LCPC), Delft, Holland, pp. 101-110, September.
- O'Brien, E.J., Bailey, S.F., O'Connor A.J., Enevoldsen, I. & Žnidaric, A. (1998a), 'Bridge Applications of Weigh-In-Motion', in *Pre-proceedings of the 2nd European Conference on Weigh-In-Motion*, eds. E.J. O'Brien & B. Jacob, Lisbon, Portugal, pp. 209-218.
- O'Brien, E., O'Connor, A. & González, A. (1998b), 'Eurocode for traffic loads on bridges (EC1.3) - Calibration for Irish conditions', *Research Report No. 98-001*, Department of Civil, Structural & Environmental Engineering, Trinity College, March.
- O'Brien, E., Dempsey, A., Žnidaric, A. & Baumgärtner, W. (1999a), 'High-Accuracy Bridge-WIM Systems and future Applications', in *Proceedings of the Final Symposium of the project WAVE*, Ed. B. Jacob, Hermes Science Publications, Paris, France, pp. 45-54.

- O'Brien, E., Žnidaric, A. & Dempsey, A.T. (1999b), 'Comparison of Two independently Developed Bridge Weigh-In-Motion Systems', *Heavy Vehicle Systems, Int. J. of Vehicle Design*, Vol. **6**, Nos 1/4, pp. 147-162.
- O'Brien, E. & Keogh, D. (1999), *Bridge Deck Analysis*, E&FN Spon, London.
- O'Connor, A.J., Jacob, B., O'Brien E.J. & Prat, M. (1998), 'Effect of Traffic Loads on Road Bridges – Preliminary Studies for the Re-Assessment of the Traffic Load Model for Eurocode 1, Part 3', in *Pre-proceedings of the 2nd European Conference on Weigh-In-Motion*, eds. E.J. O'Brien & B. Jacob, Lisbon, Portugal, pp. 231-242.
- O'Connor, C. & Chan, T.H.T. (1988a), 'Dynamic Wheel Loads from Bridge Strains', *Journal of Structural Engineering*, ASCE, Vol. **114**, No. 8, August, pp. 1703–1723.
- O'Connor, C. & Chan, T.H.T. (1988b), 'Wheel Loads from Bridge Strains: Laboratory Studies', *Journal of Structural Engineering*, ASCE, Vol. **114**, No. 8, August, pp. 1724–1740.
- O'Connor, J.M. (1994), 'The Development of a Weigh In Motion System in Ireland', M.Sc. Thesis, Trinity College Dublin, Ireland.
- O'Connor, T. (1996), 'Spatial Repeatability of Vehicle Impact Forces on Road Pavements', M.Sc. Thesis, Trinity College Dublin, Ireland.
- O'Connor, T., O'Brien, E.J. & Jacob, B. (1999), 'An Experimental Investigation of Spatial Repeatability', *Heavy Vehicle Systems, Int. J. of Vehicle Design*, Vol. **7**, No 1, pp. 64-82.
- OECD (1997), 'Dynamic Interaction of Heavy Vehicles with Roads and Bridge', Final Report of the Committee, *DIVINE Project*, Ottawa, Canada, June.
- Ojio, T., Yamada, K. & Shinkai, H. (2000) 'BWIM Systems using Truss Bridges', *Bridge Management Four*, Edited by M.J. Ryall, G.A.R. Parker and J.E. Harding, Thomas Telford, University of Surrey, UK, pp. 378-386.
- Peters, R.J. (1984), 'AXWAY – A System to Obtain Vehicle Axle Weights', in *Proceedings 12th ARRB Conference*, **12**(1), pp. 17-29.
- Peters, R.J. (1986), 'An Unmanned and Undetectable Highway Speed Vehicle Weighing System', in *Proceedings 13th ARRB Conference*, **13**(6), pp. 70-83.

- Peters, R.J. (1998), 'Low Cost Calibration Management', in *Pre-proceedings of the 2nd European Conference on Weigh-In-Motion*, eds. E.J. O'Brien & B. Jacob, Lisbon, Portugal, pp. 153-160.
- Rao, S.S. (1984), *Optimization: Theory and Applications*, 2nd Edition, John Wiley & Sons.
- Sainte-Marie, J., Argoul, P., Jacob, B. and Dolcemascolo, V. (1998), 'Multiple Sensor WIM Using Reconstruction Algorithms of the Dynamic Axle Loads', in *Pre-proceedings of the 2nd European Conference on Weigh-In-Motion*, eds. E.J. O'Brien & B. Jacob, Lisbon, Portugal, pp. 109-118.
- Sainte-Marie, J. (1999), 'Multiple Sensors WIM and Vehicle-Pavement Interaction', in *Proceedings of the Final Symposium of the project WAVE*, Ed. B. Jacob, Hermes Science Publications, Paris, France, pp. 169-176.
- Schaeffer, H.G. (1977), *NASTRAN Primer: Static and Normal Modes*, Schaeffer Analysis, College Park, Maryland.
- Scheuter, F. (1998), 'Evaluation of Factors Affecting WIM System Accuracy', in *Pre-proceedings of the 2nd European Conference on Weigh-In-Motion*, eds. E.J. O'Brien & B. Jacob, Lisbon, Portugal, pp. 371-380.
- Siffert, F. & Žnidaric, A. (1998), 'Multilingual Glossary of Weigh In Motion', in *Pre-proceedings of the 2nd European Conference on Weigh-In-Motion*, eds. E.J. O'Brien & B. Jacob, Lisbon, Portugal, pp. 91-96.
- Snyder, R.E. (1992), 'Field Trials of Low-Cost Bridge WIM' in *Publication FHWA-SA-92-014*, Washington DC.
- Stanczyk, D. (1999), 'New Calibration Procedure by Axle Rank', in *Proceedings of the Final Symposium of the project WAVE*, Ed. B. Jacob, Hermes Science Publications, Paris, France, pp. 307-316.
- Stanczyk, D. & Jacob, B. (1999), 'Continental Motorway Test of Weigh-In-Motion Systems: Final Results', in *Post-proceedings of the 2nd European Conference on Weigh-In-Motion*, eds. E.J. O'Brien & B. Jacob, Lisbon, Portugal, pp. 51-62.
- Stergioulas, L.K., Cebon, D. & Macleod, M.D. (1998), 'Enhancing Multiple-Sensor WIM Systems', in *Pre-proceedings of the 2nd European Conference on Weigh-In-Motion*, eds. E.J. O'Brien & B. Jacob, Lisbon, Portugal, pp. 119-128.

- Tierney, O.F., O'Brien, E.J. & Peters, R.J. (1996) 'The Accuracy of Australian and European Culvert Weigh-in-Motion Systems', *National Traffic Data Acquisition Conference (NATDAQ '96)*, Vol. II, ed. G. Knoebel, Alliance for Transportation Research, Albuquerque, New Mexico, pp. 647-656.
- Wong, J.Y. (1993), *Theory of ground vehicles*, John Wiley & Sons.
- Yang, Y.-B. & Lin, B.-H. (1995), 'Vehicle-Bridge Interaction Analysis by Dynamic Condensation Method', *Journal of Structural Engineering*, ASCE, Vol. **121**, No. 11, November, pp. 1636-1643.
- Žnidaric, A. & Baumgärtner, W. (1998), 'Bridge Weigh-In-Motion Systems – An Overview', in *Pre-proceedings of the 2nd European Conference on Weigh-In-Motion*, eds. E.J. O'Brien & B. Jacob, Lisbon, Portugal, pp. 139-152.
- Žnidaric, A., Lavric, I. & Kalin, J. (1998), 'Extension of Bridge WIM systems to Slab Bridges', in *Pre-proceedings of the 2nd European Conference on Weigh-In-Motion*, eds. E.J. O'Brien & B. Jacob, Lisbon, Portugal, pp. 263-272.
- Žnidaric, A., Dempsey, A., Lavric, I. & Baumgärtner, W. (1999a), 'Bridge WIM Systems without Axle Detectors', in *Proceedings of the Final Symposium of the project WAVE*, Ed. B. Jacob, Hermes Science Publications, Paris, France, pp. 101-110.
- Žnidaric, A., Lavric, I. & Kalin, J. (1999b), 'Bridge WIM Measurements on Short Slab Bridges', in *Proceedings of the Final Symposium of the project WAVE*, Ed. B. Jacob, Hermes Science Publications, Paris, France, pp. 217-226.

➢ [1] Airsport Weigh-In-Motion Home Page <http://www.airport-corp.com/saepaper>. Accessed 1999 September.

➢ [2] Transportation Research Board. 2000 August 15. Long-term Pavement Performance. <http://www4.nationalacademies.org/trb/dive.nsf/web/ltpp_studies.htm>. Accessed 2000 October.

➢ [3] Žnidaric A. 2000 October 4. European Weigh-In-Motion Pages <http://www.zag.si/wim>. Accessed 2000 October.

➢ [4] Laboratoire Central des Ponts et Chaussées. 2000 May 7. WAVE. <http://www.lcpc.fr/LCPC/English/Collaboration/wave>. Accessed 2000 October.

- [5] COST – Transport. 1998 September 11. COST323 Publications. <http://www.cordis.lu/cost-transport/src/pub-323.htm>. Accessed 2000 October.
- [6] Žnidaric A. 1999 May 11. <http://www.zag.si/wim/general_WIM/photos>. Accessed 2000 October.
- [7] Žnidaric A. 2000 July 4. EUCO-COST/323/6/97 (WIM-LOAD) <http://www.zag.si/wim/reports/zurich>. Accessed 2000 October.
- [8] Jank. <http://www.zag.si/wimgloss>. Accessed 2000 October.
- [9] International Road Dynamics Inc. Home Page. 2000 October 18. <http://www.ird.ca>. Accessed 2000 October.
- [10] Australian Road Research Board Home Page. <http://www.arrb.org.au/products/culway.htm>. Accessed 2000 October.
- [11] Texas Measurements, Inc. Home Page. <http://www.straingage.com/strain>. Accessed 2000 October.
- [12] Golden River Traffic Home Page. <http://www.grt.co.uk>. Accessed 2000 October.
- [13] National Instruments Home Page. <http://www.ni.com/daq>. Accessed 2000 October.
- [14] National Instruments Home Page. <http://www.ni.com/labview>. Accessed 2000 October.
- [15] Borland Inprise Corporation Home Page. 2000 June 29. <http://www.borland.com/borlandcpp>. Accessed 2000 October.
- [16] Press W.H., Teukolsky S.A., Vetterling W.T. & Flannery B.P. 1992. Numerical Recipes in C, 2nd Edition. Published by the Press Syndicate of the University of Cambridge. <http://math1.unice.fr/~hassold/Mirror/recipes>. Accessed 2000 October.
- [17] Sayers M.W. & Karamihas S.M. 1998 September. The Little Book of Profiling. University of Michigan Transportation Research Institute. <http://www.umtri.umich.edu/erd/roughness/litbook.html>. Accessed 2000 October.
- [18] The MacNeal-Schwendler Corporation Home Page. MSc Software. Mechanical Solutions. <http://www.mechsolutions.com/products/nas4win>. Accessed 2000 October.